Probing amorphous and crystalline pharmaceuticals systems using NMR

Foumier, Romain

Probing amorphous and crystalline pharmaceuticals systems using NMR

By

Romain Fournier B.Sc. (Hons.), M.Sc., AMRSC

Ustinov College
University of Durham

A thesis submitted in partial fulfilment of the requirements for the degree of Doctor of Philosophy

Department of Chemistry
University of Durham

2006

Abstract

The ^{1}H and ^{13}C solution-state NMR spectra of the three studied drug molecules (indomethacin, nifedipine and carbamazepine) were fully assigned. This led to the characterisation and assignment of the ^{13}C CPMAS SSNMR spectra of the stable polymorphic forms of these molecules. The signal for the C-Cl carbon of indomethacin has been studied as a function of applied magnetic field, and the observed bandshapes have been simulated. A T_1^H and $T_{1\rho}^H$ study was undertaken on the crystalline materials, as well as on the quench-cooled amorphous and PVP/drug co-melts. This was done in order to fulfil the aim of this research, i.e. to understand the difference in stability of the amorphous compounds and also to investigate the effect of the presence of PVP on the stability and mobility of the drug. It was shown that, under the conditions of the experiments, amorphous indomethacin did not recrystallise until 110°C, whilst in the case of nifedipine and carbamazepine the recrystallisation occurred at 70°C and 75°C respectively. It was also shown that in the case of the co-melts a transition occurs consistently between 65°C and 85°C for the three materials and this seems to be due to the Tg of the co-melts. The comparison of the T_1^H and $T_{1\rho}^H$ data for the different states showed that amorphisation increased the mobility of the sample, this being more pronounced for carbamazepine and nifedipine than for indomethacin, and also that the co-melts were more stable and slightly more mobile than the amorphous compounds. The comparison of the relaxation data between the pure compounds showed that amorphous indomethacin was more stable than the other two amorphous drugs as slope changes occurred for the latter at a temperature below Tg, whilst this happens at or around Tg for amorphous indomethacin.

Memorandum

The research presented in this thesis has been carried out in the Department of Chemistry, University of Durham, and at GlaxoSmithKline R&D, Stevenage, between October 2001 and December 2004. Unless otherwise stated, it is the original work of the author. None of this work has been submitted for any other degree.

Acknowledgements

This is probably the trickiest bit of this thesis. Will I thank everybody, I hope so. If I forgot your name, I am truly sorry, it was not done on purpose.

I would like to thank my parents, without whom I would not be here today, for their help and support throughout my studies and especially my Ph.D. I would also like to thank my family for being there when I needed them to talk about anything but my Ph.D.

I would also like to thank my wife, Jenny, for her support in difficult times and helping me carry on when I thought that I should stop everything. My baby, Luke, is also to be thanked as he showed me that life is an important gift and that a smile can do a lot; you do not need to speak to help somebody during hard times, ask him.

I should not forget to thank my academic supervisors, Robin Harris and Paul Hodgkinson, my industrial supervisors, Bob Lancaster and Angus Forster, as well as David Apperley for their useful helps, tips, and discussions throughout my Ph.D. Obviously, there is also the group in which I worked during these three years to thank, to name but a few: Andy, Aom, Diane, Debbie, Gian Carlo, Matt, Phuong, and Veni.

Of course, the friends should be acknowledged. The ones in France: Adrien, Arnaud, Cyril, Laurent, Lilian, Tom, Yann, and all the others; the ones in England: Amel, Anna, Arnaud, Christophe, Damien, Didi, Manue, Marie-Paule, Nora, Pam, and Sarb. Without them, life as a Ph.D. student would have been missing the spices. There is the Graduate Society/Ustinov College pool club that should not be forgotten. I had a really good time with all of you guys.

There are also other people from the Chemistry department who helped me with some experiments: Alan, Catherine, and Ian for the solution-state NMR; Doug for the DSC and TGA; Jonathan Evans and his group for the XRPD and providing a hammer when needed. I also would like to give a big thank you to Gary for filling dewar after dewar of liquid nitrogen, without him my work will not have been done.

I also want to thank my sponsors, GlaxoSmithKline R&D, Stevenage, as well as the EPSRC for funding this experience.

I think that this is it. I still have a bit of space to give a special thanks to my wife and my baby, I love you both, thank you for being part of my life.

Abbreviations

1D: One-dimensional

2D: Two-dimensional

ATR: Attenuated total reflectance

BIRD: Bilinear rotation decoupling

CDS: Chemical database service

COSY: Correlation spectroscopy

CP: Cross-polarisation

CPMAS: Cross-polarisation with magic-angle spinning

CSA: Chemical shift anisotropy

DMSO: Dimethylsulphoxide

DP: Direct-polarisation

DSC: Differential scanning calorimetry

EFG: Electric field gradient

FID: Free induction decay

FTIR: Fourier-transform infra-red

HMBC: Heteronuclear multiple bond correlation

HSQC: Heteronuclear single quantum coherence

MAS: Magic-angle spinning

m.p.: Melting point

NMR: Nuclear magnetic resonance

NQS: Non-quaternary suppression

o.d.: Outer diameter

PDMSO: Poly(dimethylsiloxane)

PTFE: Polytetrafluoroethylene

PVP: Poly(vinylpyrrolidone)

r.f.: Radio frequency

R.T.: Room temperature

S/N: Signal to noise ratio

SCFH: Standard cubic feet per hour

SSNMR: Solid-state NMR

TGA: Thermo gravimetric analysis

TMS: Tetramethylsilane

VT: Variable temperature

XRPD: X-ray powder diffraction

Table of content

Chapter One: Introduction

1/ Solid-State Nuclear Magnetic Resonance (SSNMR)[1]

The main differences between SSNMR and solution-state NMR results from the general absence of rapid molecular motion. This lack of molecular motion implies the presence of two parameters that complicate the spectra. These two parameters are:

- Dipole-dipole interactions.
- Chemical Shift Anisotropy (CSA).

These parameters will be detailed in later sections.

In the presence of a liquid, we do not see the effects of these kinds of interaction directly because the molecules are tumbling rapidly. Therefore, these parameters, which are orientation dependent, are averaged to their isotropic values. Different techniques have been produced to help in reducing the broad lines created for solids by the above parameters. They are:

- Magic-Angle Spinning (MAS).
- High-power proton decoupling.

These techniques will be discussed in the following sections.

1.1/ Dipole-dipole interactions

This interaction involves pairs of nuclear spin dipoles, i.e. two spins, which interact through space. In solid-state NMR, this interaction is not generally averaged, and it can have values of tens to hundreds of kilohertz.

If one considers an isolated pair of different spins, AX, one will have an energy equation (to first order) of the form:

$$h^{-1}U = -\nu_A m_A - \nu_X m_X + R m_A m_X (1 - 3\cos^2\theta) \qquad \textbf{Equation 1.1}$$

where $\nu_A = \frac{\gamma_A B_0}{2\pi}$, $\nu_X = \frac{\gamma_X B_0}{2\pi}$ and $R = \frac{\mu_0}{4\pi}\gamma_A\gamma_X\frac{\hbar}{2\pi}r_{AX}^{-3}$ (in frequency units). ν_A and ν_X are the appropriate Larmor frequencies, m_A and m_X are the appropriate

quantum numbers, B_0 is the magnetic field of the spectrometer, γ_A and γ_X are the appropriate magnetogyric ratios and r is the distance between the two spins.

From equation 1.1, it is seen that the dipole-dipole interaction depends on the orientation of the system and also on the distance separating the two dipoles. Thence, the powder pattern (also known as a Pake doublet) of the system (figure 1.1) can be determined, i.e. the spectrum for a microcrystalline powder containing particles with all possible orientations of the inter-dipole distance.

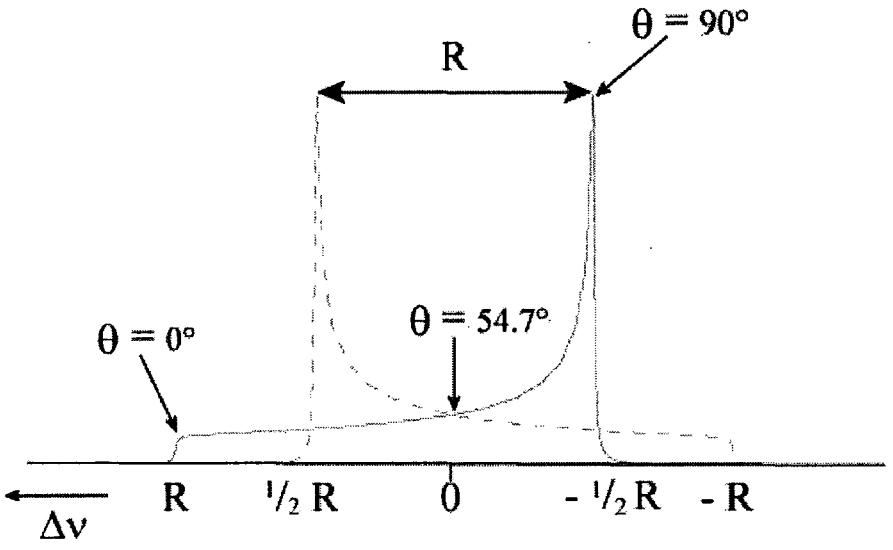

Figure 1.1: Representation of a heteronuclear dipolar powder pattern for an isolated AX system. Only the A part of the AX system is shown, the X part being identical.

1.2/ Chemical shift anisotropy

This interaction also depends on the orientation of the molecule. Therefore, it will not appear for a liquid sample because the rapid tumbling averages it to zero and so only the isotropic chemical shift affects the spectrum. This interaction works in the three dimensions, so we have three principal components to the shielding tensor (σ_{11}, σ_{22} and σ_{33}). Nevertheless, this interaction also depends on the symmetry of the studied molecule as shown in figure 1.2 which illustrates powder patterns for chemical shifts.

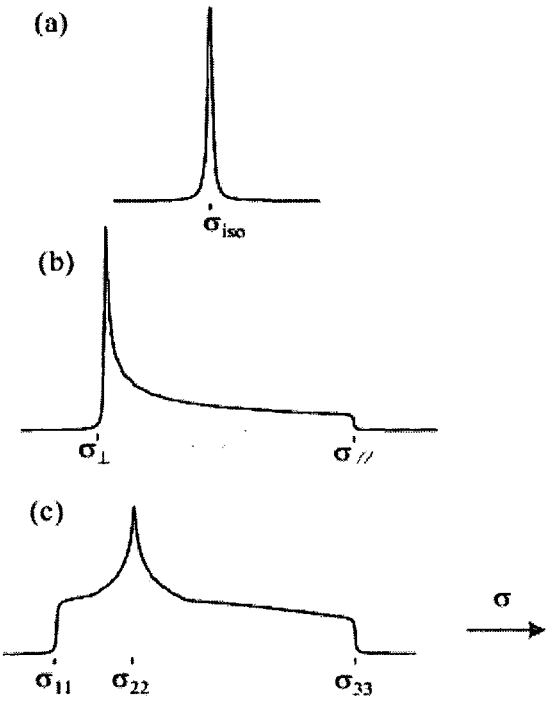

Figure 1.2: Schematic powder pattern caused by shielding anisotropy for isolated spins with site of (a) cubic symmetry (isotropic case) (b) axial symmetry, and (c) low symmetry.

For the case of cubic symmetry, e.g. ^{13}C in the molecule CH_4, all three shielding tensor components are equal:

$$\sigma_{11} = \sigma_{22} = \sigma_{33} = \sigma_{iso} \qquad \textbf{Equation 1.2}$$

For an axially symmetric case (e.g. ^{13}C in the molecule $CHCl_3$), we have two principal orientations, giving $\sigma_{\perp}$ and $\sigma_{//}$ as shown in figure 1.3.

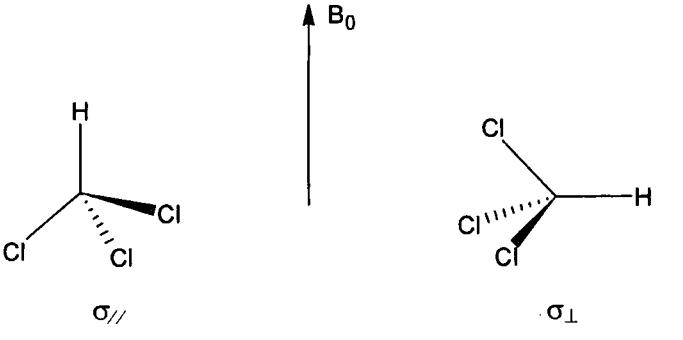

Figure 1.3: Axially symmetric case

In this case, the shielding anisotropy is defined as:

$$\Delta\sigma = (\sigma_{//} - \sigma_{\perp}) \qquad \textbf{Equation 1.3}$$

The isotropic shielding is:

$$\sigma_{iso} = \frac{2\sigma_{\perp} + \sigma_{//}}{3} \qquad \textbf{Equation 1.4}$$

This value will be slightly different between the solid and solution states. In the latter, only the isotropic shielding affects the spectrum.

For the general case, there are three tensor elements labelled:

$$|\sigma_{33} - \sigma_{iso}| \geq |\sigma_{11} - \sigma_{iso}| \geq |\sigma_{22} - \sigma_{iso}| \qquad \textbf{Equation 1.5}$$

where σ_{iso} is the isotropic chemical shift defined as follow:

$$\sigma_{iso} = \frac{1}{3}(\sigma_{11} + \sigma_{22} + \sigma_{33}) \qquad \textbf{Equation 1.6}$$

The shielding anisotropy is referred to as:

$$\Delta\sigma = \sigma_{33} - \frac{\sigma_{11} + \sigma_{22}}{2} \qquad \textbf{Equation 1.7}$$

Or, alternatively:

$$\zeta = \sigma_{33} - \sigma_{iso} \qquad \textbf{Equation 1.8}$$

Note that: $\Delta\sigma = \frac{3\zeta}{2}$

The shielding asymmetry, η, is defined as:

$$\eta = \frac{\sigma_{22} - \sigma_{11}}{\sigma_{33} - \sigma_{iso}} = \frac{\sigma_{22} - \sigma_{11}}{\zeta} \qquad \textbf{Equation 1.9}$$

1.3/ Magic-angle spinning and high-power proton decoupling

The shielding anisotropy and the dipole-dipole coupling interactions are dependent on the orientation of the molecule, expressed by the factor ($3\cos^2\theta$ - 1). Therefore, if it is possible to average this factor to zero, these interactions will not complicate the spectrum. In solution, this factor is averaged to zero by the rapid molecular tumbling of the molecule, which explains the very narrow peaks observed in solution-state NMR.

If one consider a solid sample spun at an angle β to B_0 (figure 1.4). For a single crystal the angle χ is fixed, which will not be true for a powder, where χ can take all

possible values. The average of $(3\cos^2\theta - 1)$ about the conical path, indicated for the internuclear vector "r" in equation 1.10, has to be found to be:

$$\langle 3\cos^2\theta - 1\rangle = \frac{1}{2}(3\cos^2\beta - 1)(3\cos^2\chi - 1) \qquad \textbf{Equation 1.10}$$

One can see that the function ½ $(3\cos^2\beta - 1)$ will scale the powder patterns.

One can also see that if β is 54.7°, then $\cos\beta = \frac{1}{\sqrt{3}}$, and $3\cos^2\beta - 1 = 0$. Therefore, $3\cos^2\theta - 1 = 0$ for all initial orientations of r in B_0.

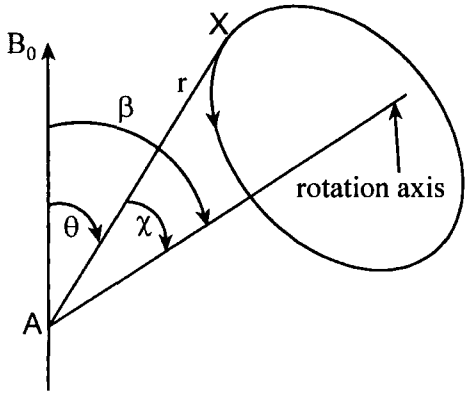

Figure 1.4: Spinning of a sample, represented by r, at an angle β in respect to B_0.

The speed at which the sample can be spun is also important because if the sample does not spin quickly enough to overcome totally the effect of the shielding anisotropy, spinning sidebands will appear at intervals of the spin rate from the isotropic chemical shift (which is referred to as the centreband). These spinning sidebands are useful when there is interest in the parameters of the shielding tensor, as they will enable information about these parameters to be found. The lower the spinning speed, the more spinning sidebands will be observed. It should be noted that the centreband can be located by varying the spin rate, if necessary.

However, one problem cannot be fully eliminated with this technique, which is the dipole-dipole interaction. In order to eliminate totally this kind of interaction, one would need to spin the sample at speed greater than the static bandwidth expressed in Hz. As this can be of the order of tens to hundreds of kHz for ^{13}C, it is not possible to be achieved. However, another technique has been developed called high-power proton decoupling. For the case of ^{13}C-^{1}H dipolar interactions, one just needs to

apply r.f. pulses on the proton channel, which should be equal to or greater than the dipole interaction, i.e. in the order of ten's of kHz, whilst acquiring on the carbon channel. This is quite different from solution-state NMR as one only needs to decouple J, which implies a lower power. The effect of the r.f. field will be to decouple the proton from the carbon. As a consequence, the spectrum will be greatly simplified.

1.4/ Relaxation times

Recently, NMR relaxation times have been shown to be particularly sensitive to changes around the glass transition. This led to some studies in which this technique is applied to amorphous compounds in order to investigate their molecular mobility[2-4]. For solids, the proton spin-lattice relaxation time and the proton spin-lattice relaxation time in the rotating frame of resonance (denoted T_1^H and $T_{1\rho}^H$ respectively) are generally measured. The relaxation time T_1^H reflects the molecular mobility on the timescale of the Larmor frequency (generally hundreds of MHz), while $T_{1\rho}^H$ represents the molecular mobility on the timescale of the nutation frequency of the experiment, which corresponds to the strengths of the applied radio frequency[5]. Some aspects of molecular mobility can also be investigated using differential scanning calorimetry[6].

As T_1^H relaxation times are in the order of seconds or tens of seconds, it is easily understood that the time required for measurement would be a limiting factor in obtaining a series of data over a wide range of temperatures. This explains why most of the studies done on T_1^H measurements do not show replicate measurements, or use only a narrow range of temperatures[3,4,7,8]. However, a few papers study T_1^H over a wide range of temperatures, but this is possible only because of a short T_1[9-11].

Another important point from the relaxation times is that the study of their variation over the temperature range allows one to retrieve the activation energies involved in the relaxation process.

In order to obtain the activation energy, one needs to refer to the equation 1.11[12]:

$$T^{-1} \propto \frac{\tau_c}{1+\omega^2\tau_c^2} \qquad \textbf{Equation 1.11}$$

where τ_c is the motional correlation time, i.e. the average time for a molecule with random molecular tumbling to progress through one radian, and ω is the spectrometer ^1H frequency for T_1 or the nutation frequency ($\gamma B_1/2\pi$) for $T_{1\rho}$. It should be noted that for an activated process one should use equation 1.12:

$$\tau_c = D\exp\left(\frac{-E_a}{RT}\right) \qquad \textbf{Equation 1.12}$$

where D is a constant.

For the rigid side of a relaxation minimum, τ_c is long, so we have $\omega^2\tau_c^2 >> 1$. Therefore, from equation 1.11, we can see that T_1^{-1} is proportional to $1/\omega^2\tau_c$, i.e. T_1 is proportional to τ_c. By applying this to equation 1.12, we get equation 1.13:

$$\ln(T_1) = A - \frac{E_a}{RT} \qquad \textbf{Equation 1.13}$$

where A is a constant.

Similarly, for the mobile side of the minimum, where τ_c is short, we have $1 >> \omega^2\tau_c^2$. Therefore, from equation 1.11 we can see that T_1^{-1} is proportional to τ_c. By applying this to equation 1.12, we get equation 1.14:

$$\ln(T_1) = B + \frac{E_a}{RT} \qquad \textbf{Equation 1.14}$$

where B is a constant.

One can then see that from the slope of the graph $\ln(T_1)$ vs. 1/T, and by using equations 1.13 and 1.14, it is possible to obtain the activation energy. Alternatively, one can fit the complete curve, but this may not be satisfactory if there is partial overlap between different minima.

By doing the differentiation of equation 1.11, one can see that the minimum will occur when:

$$\tau_c = \frac{1}{\omega} \qquad \textbf{Equation 1.15}$$

This is valid for crystalline materials as in such cases only a single specific type of motion appears to be involved. However, there are circumstances when meaningful activation energies cannot be retrieved from the slope. This can be due to the presence of several motions of similar activation energies. In the case of amorphous materials, it is likely that complications arise due to the fact that for any given motion, a range of activation energies is expected as the intermolecular interactions

will vary with the environment, which is variable throughout the amorphous sample. In both of these cases, the situation would involve overlapping minima, giving a broad and shallow minimum, if any minimum is visible at all. As a result, the slopes would not properly reflect the activation energies.

2/ Pulse sequences

2.1/ Solid-state NMR

2.1.1) Cross Polarisation (CP)

The cross polarisation is a pulse sequence that allows the magnetisation from an abundant spin, generally proton nuclei, to be transferred to a dilute spin, e.g. ^{13}C nuclei. The aim is to improve the sensitivity, which would otherwise be low, especially because of long relaxation times in solids. In order to achieve this, the system needs to fulfil the Hartmann-Hahn condition in the rotating frame of reference, that is:

$$\gamma_H B_{1H} = \gamma_C B_{1C} \qquad \textbf{Equation 1.16}$$

where B_{1H} and B_{1C} are the strengths of the ^{1}H and ^{13}C radiofrequency fields respectively.

This condition implies that both nuclei are precessing at the same frequency in their respective rotating frames of resonance.

The CP pulse sequence is shown in figure 1.5. At first, a 90° pulse is applied at the proton frequency in order to place the magnetisation in the xy plane, the rotating frame of resonance. Then, the proton magnetisation is spin locked in the y direction. The second step is to switch on the r.f. at the ^{13}C channel and to adjust B_{1C} in order to fulfil the Hartmann-Hahn condition. After a suitable time (the contact time), the r.f. at the ^{13}C channel is switched off and the FID recorded for this nucleus, but the r.f. is kept on at the ^{1}H channel in order to eliminate the effects of the ^{13}C-^{1}H dipolar and scalar interactions. Typically, a contact time of 1 to 5 ms is used for ^{13}C.

This pulse sequence is used because the magnitude of the ^{13}C signal will be determined by the magnetogyric ratio of the proton rather than that of the ^{13}C. This difference will, in theory, increase the magnitude of the ^{13}C signal by a factor of γ_H/γ_C, i.e. a factor of ca. four, compared to a normal $\pi/2$-acquire sequence on the ^{13}C.

Furthermore, as the magnetisation is coming from the protons, the delay between each pulse sequence is determined by the spin-lattice relaxation time of the protons (T_1^H), which is shorter than that of ^{13}C. As a consequence, the pulse delay will be greatly reduced and thus the experimental time.

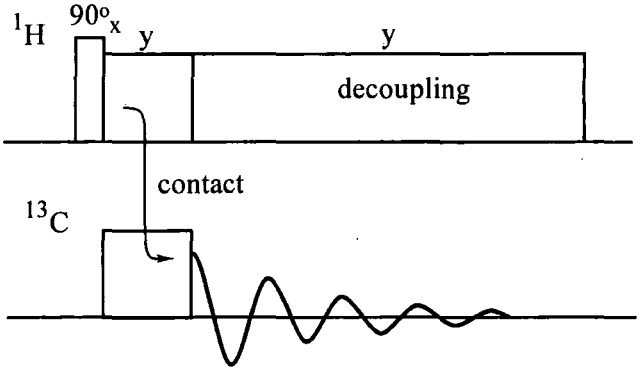

Figure 1.5: The pulse sequence for a CP experiment.

Generally, the CP pulse sequence is used with MAS, and the experiment is then called CPMAS. MAS is used to eliminate the shielding anisotropy and dipole-dipole interactions.

2.1.2) Non-Quaternary Suppression (NQS) – also known as dipolar dephasing

The NQS experiment works partly in the same way as the CP experiment. The difference between the two is the insertion of a decoupling window after the contact time (see figure 1.6). This decoupling window allows for the elimination of the signals coming from the non-quaternary carbons. A carbon attached to a proton will have a much stronger dipolar coupling than a quaternary one (in the absence of decoupling). A nucleus with a strong dipolar coupling will have a shorter FID than if it had a weak dipolar coupling. A short FID means that if a long enough time (about 40 to 60 μs), without applying a r.f. to the proton channel, is waited, then the signal from the non-quaternary carbons will not be seen and the signal from the quaternary carbons will still be present.

However, such an experiment still shows the CH_3 groups as these groups have long FIDs while the CH and CH_2 have short FIDs. This can be explained by the rapid

internal rotation of a methyl group which partially averages the dipolar coupling. As a consequence, the dipolar coupling is relatively weak and this means a long FID. Therefore, the CH_3 signal is also retained but with a lower intensity compared to a normal CP experiment.

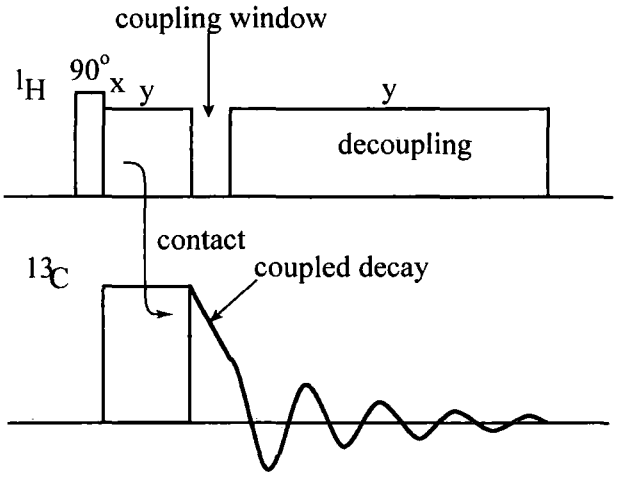

Figure 1.6: The pulse sequence for a NQS experiment.

2.1.3) T_1^H experiment

Measuring T_1^H for indomethacin and nifedipine was done using a saturation-recovery experiment (figure 1.7). This pulse sequence consists of a series of around one hundred 90° pulses, each of a few microsecond duration, which are separated by a typical time of around 100 μs; these pulses are used to saturate the signal. Then, a recovery time (τ) is waited in order to regain some of the magnetisation. This is then followed by a 90° pulse to put the magnetisation into the y direction so as to allow the acquisition of a signal. The time τ is arrayed in order to have a series of spectra that will provide data which can be fitted into equation 1.17.

$$y = amp \times \left[1 - \exp\left(\frac{-\tau}{T_1}\right)\right] \qquad \textbf{Equation 1.17}$$

where "amp" represents the intrinsic amplitude of the peak. However, some of the results were fitted to a double exponential: the equation is shown in equation 1.18.

$$y = amp_a \times \left[1 - \exp\left(\frac{-\tau}{T_{1a}}\right)\right] + amp_b \times \left[1 - \exp\left(\frac{-\tau}{T_{1b}}\right)\right] \qquad \textbf{Equation 1.18}$$

where "amp_a" and "amp_b" represent the intrinsic amplitudes of the first and second exponential respectively; and T_{1a} and T_{1b} represent the T_1 values of the first and

second exponential respectively. In the case of a double exponential fit, a population weighted average rate was used to derive an overall value of T_1.

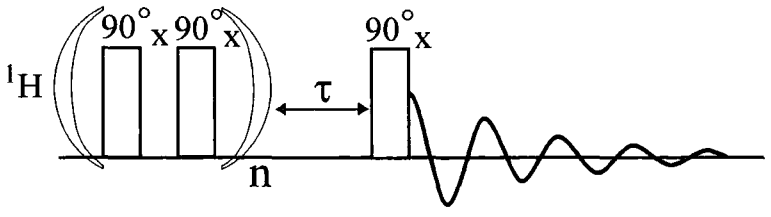

Figure 1.7: The pulse sequence for a saturation-recovery experiment.

2.1.4) $T_{1\rho}{}^{H}$ experiment

For indomethacin and nifedipine, the $T_{1\rho}{}^{H}$ measurements were done using a spin-lock experiment (figure 1.8). This consists of a 90° pulse to rotate the magnetisation to the y-axis, followed by a 90° phase change of B_1 to place it also in the y direction, thus "locking" it (i.e. slowing down its rate of decay). This situation is maintained for a variable time, τ (the spin-lock time), after which the spectrum is acquired. The spin-lock time is arrayed to get a series of spectra from which the data is recovered and fitted to equation 1.19.

$$y = amp \times \exp\left(\frac{-\tau}{T_{1\rho}}\right) \qquad \textbf{Equation 1.19}$$

where "amp" represents the intrinsic amplitude of the peak. However, some of the results were fitted to a double exponential: the equation is shown in equation 1.20.

$$y = amp_a \times \exp\left(\frac{-\tau}{T_{1\rho a}}\right) + amp_b \times \exp\left(\frac{-\tau}{T_{1\rho b}}\right) \qquad \textbf{Equation 1.20}$$

where "amp_a" and "amp_b" represent the intrinsic amplitudes of the first and second exponential respectively, and $T_{1\rho a}$ and $T_{1\rho b}$ represent the $T_{1\rho}$ values of the first and second exponential respectively. In the case of a double exponential fit, a population weighted average rate was used to determine the value of $T_{1\rho}$.

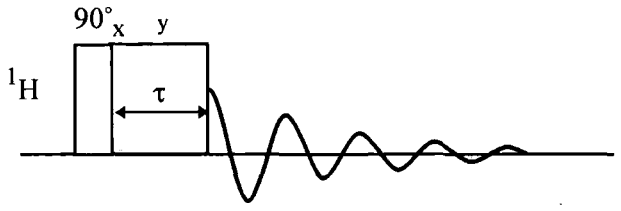

Figure 1.8: The pulse sequence for a spin-lock experiment.

However, for carbamazepine the value of T_1^H was so long (ca. 200 s) that it was decided to use a saturation-recovery with the spin-lock experiment (figure 1.9) in order to determine the value of $T_{1\rho}^H$. This experiment begins as a saturation-recovery one but τ is fixed to a value of about 20 % of T_1^H, then a spin-lock sequence is added. This version was used rather than the normal spin-lock experiment as this allows for a quicker recycle of the sequence and also the magnetisation is measured from a set point. The spin-lock time is then arrayed and the results obtained are fitted to equation 1.19 or equation 1.20.

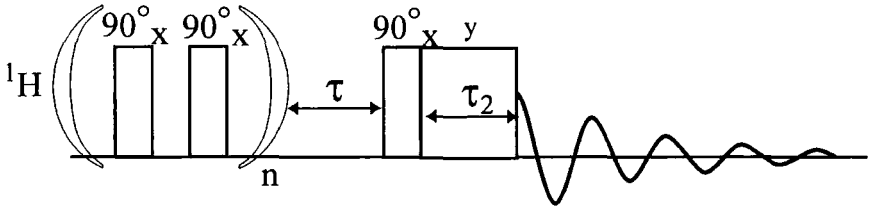

Figure 1.9: Pulse sequence for saturation-recovery with the spin-lock experiment.

2.2/ Solution-state NMR

The experiments described below are all 2D experiments. Such experiments require two waiting times, generally called t_1 and t_2. Thus, we are presented with a 2D matrix consisting of a series of FIDs, from which a set of 1D spectra is obtained by Fourier transformation with respect to t_2. Then, a second Fourier transformation, with respect to t_1, yields the final 2D spectrum with two frequency axes, namely F_1 and F_2.

2.2.1) COrrelation SpectroscopY (COSY)

This technique was first proposed by Jeener[13] and then published by Aue et al.[14]. The pulse sequence is shown in figure 1.10.

The COSY experiment consists of a 90° pulse to transfer the magnetisation into the y direction. This is followed by an evolution time, t_1, which is arrayed, during which the chemical shift and the spin-spin coupling develops. Then, a second 90° pulse is applied before acquisition, which transfers the magnetisation between spins that are coupled. The time t_1 gives the second dimension of the spectrum while the time t_2 give the first dimension.

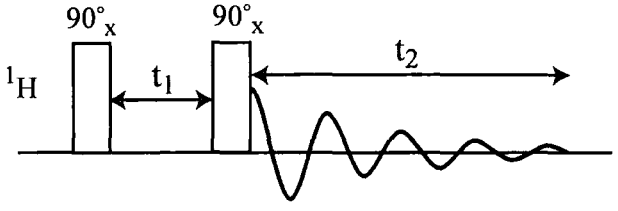

Figure 1.10: Pulse sequence for a COSY experiment.

The COSY experiment generates a 2D spectrum in which the cross-peaks appear if spin coupling is present. Thus, this sequence detects coupled pairs of protons.

2.2.2) Heteronuclear Single Quantum Coherence (HSQC)[15]

The sequence, shown in figure 1.11, starts with a transfer from ^1H to ^{13}C, by the 90°-d_2-180°-d_2-90° sequence on the proton channel and the 180°-d_2-90° sequence on the ^{13}C channel. This is followed by a t_1 period, which is arrayed, including a 180° pulse on the proton channel. During t_1 the ^{13}C chemical shift develops, and the 180° pulse on the proton channel is present to refocus the J(C,H) spin coupling that develops in the second dimension. The 90°-d_2-180° sequence is a transfer from ^{13}C to ^1H . The parameter d_2 is set to 1/[4J(C,H)].

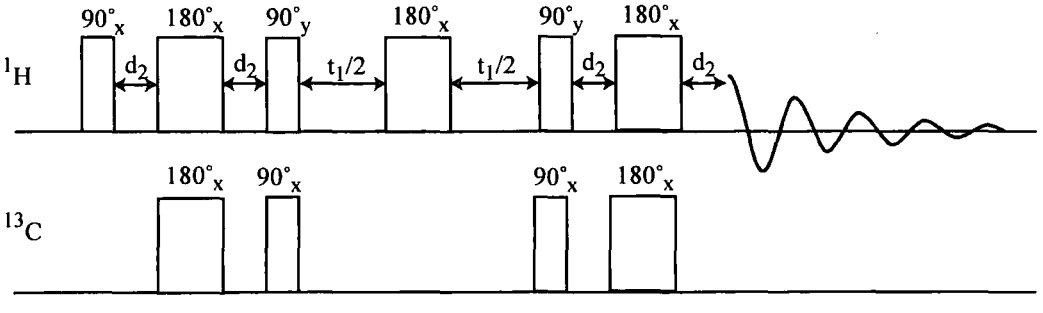

Figure 1.11: Pulse sequence for a HSQC experiment.

The HSQC experiments generates a 2D spectrum in which the peaks show protons directly bonded to ^{13}C atoms.

2.2.3) Heteronuclear Multiple Bond Correlation (HMBC)[16]

The pulse sequence is shown in figure 1.12.

The 90°-d_2-180°-d_2-90° sequence on the proton channel and the 180° pulse on the ^{13}C channel correspond to a BIRD filter, which allows rotation of the magnetisation of the proton attached to ^{12}C into the z direction, but leaves the magnetisation of the proton attached to ^{13}C unchanged. This allows one to observe only the proton attached to ^{13}C. The first 90° pulse on the ^{13}C channel acts as a low-pass filter to suppress the 1-bond correlations. The 90°-d_4+d_5-$t_{1/2}$-180°-$t_{1/2}$+d_2 sequence on the proton channel and the 90°-t_1-90° sequence on the ^{13}C channel correspond to an HMQC experiment, which allows the evolution of the ^{13}C chemical shifts, the C,H spin coupling, while suppressing the proton chemical shifts and the H,H spin coupling. The term d_2 is set to 50 ms, d_3 is the BIRD delay, which should be optimised for minimum FID, d_4 is set to 1/[2J(C,H)] and d_5 is equal to d_2-d_4.

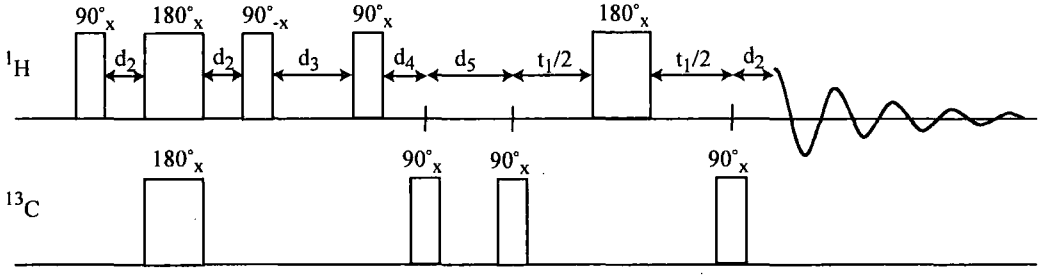

Figure 1.12: Pulse sequence for a HMBC experiment.

The HMBC experiments generates a 2D spectrum in which the peaks show protons bonded to ^{13}C atoms.

3/ Amorphous state

An amorphous solid may be obtained in four different main ways: vapour condensation, precipitation from solution (e.g. spray-drying), supercooling of melt, and milling. The supercooling of the melt is simply a rapid cooling of a liquid where the liquid goes through a supercooled liquid or rubbery state (i.e. an extremely

viscous liquid) before reaching Tg, the glass transition temperature. Below Tg, the material is "kinetically frozen" into a metastable glassy state, which is the amorphous state[17].

Amorphous compounds are of importance for pharmaceutical companies as they have increased solubility rate compared to their crystalline counterparts. Therefore, amorphous forms in a formulation could potentially improve the oral bioavailability of poorly water-soluble drugs, such as the ones studied here[18,19]. However, due to the metastable nature of the amorphous form, pharmaceutical companies tend not to formulate amorphous drug substances. A known exception is that of cefuroxime axetil; the amorphous form of this compound obtained by spray drying is physically and chemically stable without too rigorous storage conditions. In view of this, it is clear that it is of paramount importance to understand why some pharmaceutical drugs are stable in their amorphous form while others rapidly recrystallise, or require strenuous storage conditions, i.e. low temperature and humidity. Pharmaceutical companies are also interested in detecting and controlling small amounts of unwanted and unintentional amorphous materials which could be formed during the processing techniques.

The amorphous state has been the centre of quite a variety of research, from general information[20,21] to the differences between the amorphous and crystalline state[22-24], but more importantly on solubility[25] and molecular motions[26].

It is understood that changes in the molecular mobility of an amorphous drug could lead to recrystallisation of the material, e.g. in a formulated product, and this can change drastically the bioavailability of the drug. As a result, much research has been carried out in order to improve the stabilisation of the amorphous form of drugs or drug-carrier dispersions[27,28].

It is important to know that one should be careful in the preparation of the dispersion; Watanabe et al.[29] showed that the presence of silica decreased the recrystallisation rate of amorphous indomethacin on both co-grinding and quench-cooling and that the co-grinding technique gave slightly better results. However, if the co-grinding was incomplete the amorphous form obtained was quite unstable[29].

3.1/ Plasticiser and antiplasticiser effect

The plasticiser effect is a lowering of the Tg caused by the presence of water in the sample. Andronis et al.[30] showed that indomethacin, a poorly soluble drug, absorbed a large quantity of water when in the amorphous form. The presence of water increased the molecular mobility of the amorphous sample and thus increased its recrystallisation rate. Therefore, it is necessary to add some form of physical stabilisation to the amorphous sample to maintain the glassy state and to prevent recrystallisation. This is generally achieved by stringent conditions of storage. However, this is not really practical in many situations, and some level of residual water is difficult to avoid[31]. The other option is to stabilise the amorphous sample by the addition of an antiplasticiser, a compound with a high Tg, which will generally be a polymer. Aso et al.[32] showed that by mixing amorphous nifedipine with various compounds, the recrystallisation rate could be decreased due to the hygroscopic compounds preferentially taking up water. It was also shown by Gupta et al.[28] that the effect of grinding a sample with Neusilin (amorphous magnesium aluminosilicate) improved the amorphisation and also resulted in a more stable amorphous drug.

Bulk polymers such as PVP have been widely used to stabilise amorphous drugs. PVP was shown to improve the stability of an amorphous drug even when increasing the relative humidity[33]. It was also shown to inhibit the crystallisation of lactose for a significant period of time[34], whilst Forster et al.[35] showed that the presence of PVP increased the dissolution rate of indomethacin and nifedipine, more so as glass solutions than as physical mixtures.

4/ Indomethacin

Indomethacin is a nonsteroidal anti-inflammatory drug used in the relief of some pain problems, such as arthritis and tendonitis. Indomethacin has three recognised anhydrous polymorphs[36] generally referred to as the α-, β- and γ-forms[37]. Imaizumi et al.[38] refer to the α and γ polymorphs as forms I and II respectively. Kistenmacher et al.[39] determined the crystal structure of the γ-form, the stable form under ambient conditions[37], and its melting point is 158°C[37]. The crystal structure of the α-form is also known[40].

The crystallinity of indomethacin and the recrystallisation rate of its amorphous form has been studied as a function of temperature and also relative humidity using a variety of techniques[26,30,38,41-45]. Fukuoka et al.[46] showed that amorphous indomethacin has an increased dissolution rate compared to the crystalline form and also that, when kept intact, amorphous indomethacin was stable for up to 2 years at room temperature, but recrystallised rapidly when crushed. The effect of the addition of PVP to amorphous indomethacin was also studied[47] and it was shown that amorphous indomethacin was more stable when in dispersion with PVP than on its own or in a physical mixture.

Yoshioka et al.[48] showed that indomethacin could recrystallise rapidly when crushed and kept at temperature 30°C below Tg; they show evidence that the rotational mobility of indomethacin under these conditions is the reason why the recrystallisation occurs. They also showed that the method of preparation of the amorphous material was important as it could affect its physicochemical properties.

Crowley et al.[36] studied the effect of a specific method of grinding on the different polymorphs of indomethacin and showed that this technique did not necessarily produce an amorphous sample. Therefore, one should check the amorphous character of a sample after its preparation.

5/ Nifedipine

Nifedipine is a calcium channel blocker drug. This compound is used in the treatment of hypertension and coronary heart disease. Burger and Koller found that nifedipine had three anhydrous polymorphs and labelled them as modifications I, II and III[49] but earlier Hirayama et al.[50] used the letters A and B rather than I and II. The modification I, which is the stable form under ambient conditions, was also studied by Caira et al.[51]. The structure of this polymorph has been determined[52] and its melting point is 173°C[50].

Aso et al. studied amorphous nifedipine quite extensively[2,32,53-55]. They showed that the presence of moisture increased the crystallisation rate and mobility of nifedipine and also that nifedipine had a lower crystallisation rate when kept at low temperature. However, they observed that amorphous nifedipine showed considerable crystallisation within 4 months when kept at 40°C below its Tg. Nevertheless, they showed that the presence of PVP increased the stability of the

amorphous sample, which is due to a decrease in molecular mobility. One of Aso et al. articles[2] dealt with the study of T_1^H and $T_{1\rho}^H$ of amorphous nifedipine at a magnetic field of 25 MHz over a short range of temperatures (i.e. 5°C to 75°C). They showed that the relatively fast recrystallisation observed with amorphous nifedipine could be due to the high molecular mobility.

6/ Carbamazepine

Carbamazepine is an anticonvulsant. This molecule is used to treat certain types of seizures in the treatment of epilepsy. The polymorphism of carbamazepine has been widely studied, showing that this drug has four anhydrous polymorphs. These are generally labelled as forms I, II, III and IV[56], though Roberts et al.[57] used the symbols α and β instead of II and III. The crystal structure of form III, the stable form under ambient conditions, has been determined[58,59] and its melting point is 174°C[60]. Harris et al.[61] did an extensive structural study of the different polymorphs and pseudo polymorphs of carbamazepine using SSNMR and computational chemistry.

Amorphous carbamazepine, in comparison to the crystalline form, has been little studied. However, it was shown[62] that carbamazepine in dispersion with povidone was amorphous and that dispersions of carbamazepine in povidone and polyethylene glycol showed improved dissolution rate of the drug compared to the crystalline drug on its own.

7/ References

1. M. J. Duer. *Introduction to solid-state NMR spectroscopy*, Blackwell Publishing, Oxford, 2004.

2. Y. Aso, S. Yoshioka, and S. Kojima. Relationship between the crystallization rates of amorphous nifedipine, phenobarbital, and flopropione, and their molecular mobility as measured by their enthalpy relaxation and ^{1}H NMR relaxation times. *J. Pharm. Sci.* **89**: 408-416 (2000).

3. A. Koga, E. Yonemochi, M. Machida, Y. Aso, H. Ushio, and K. Terada. Microscopic molecular mobility of amorphous AG-041R measured by solid-state ^{13}C NMR. *Int. J. Pharm.* **275**: 73-83 (2004).

4. R. H. Tromp, D. van Dusschoten, R. Parker, and S. G. Ring. Carbon-13 nuclear magnetic relaxation in supercooled liquid and glassy maltose. *Phys. Chem. Chem. Phys.* **1**: 1927-1931 (1999).

5. J. K. M. Sanders and B. K. Hunter. *Modern NMR spectroscopy - a guide for chemists*, Oxford Univesity Press, Oxford, 1993.

6. B. C. Hancock and S. L. Shamblin. Molecular mobility of amorphous pharmaceuticals determined using differential scanning calorimetry. *Thermochim. Acta* **380**: 95-107 (2001).

7. K. Kimura, F. Hirayama, H. Arima, and K. Uekama. Solid-state ^{13}C nuclear magnetic resonance spectroscopy study on amorphous solid complexes of tolbutamide with 2-hydroxypropyl-α- and -β-cyclodextrins. *Pharm. Res.* **16**: 1729-1734 (1999).

8. C. A. Oksanen and G. Zografi. Molecular mobility in mixtures of absorbed water and solid poly(vinylpyrrolidone). *Pharm. Res.* **10**: 791-799 (1993).

9. N. Pislewski, J. Tritt-Goc, R. Goc, and R. Jakubas. Molecular motions in solid $[N(CH_3)_2H_2]_3Sb_2I_9$ studied by proton nuclear magnetic resonance spectroscopy. *Solid State Nucl. Magn. Reson.* **4**: 101-104 (1995).

10. E. R. Andrew and M. Kempka. Molecular motions in solid estradiol studied by nuclear magnetic resonance spectroscopy. *Solid State Nucl. Magn. Reson.* **4**: 249-253 (1995).

11. T. Grabias and N. Pislewski. Proton dynamics in solid noradrenaline hydrochloride. *Solid State Nucl. Magn. Reson.* **4**: 327-330 (1995).

12. R. K. Harris. *Nuclear Magnetic Resonance Spectroscopy*, Longman Scientific & Technical, Harlow, 1986, pp 85-88.

13. J. Jeener. *Ampère International Summer School*, Basko Polje, 1971.

14. W. P. Aue, E. Bartholdi, and R. R. Ernst. Two-dimensional spectroscopy. Application to nuclear magnetic resonance. *J. Chem. Phys.* **64**: 2229-2246 (1976).

15. G. Bodenhausen and D. J. Ruben. Natural abundance nitrogen-15 NMR by enhanced heteronuclear spectroscopy. *Chem. Phys. Lett.* **69**: 185-188 (1980).

16. A. Bax and M. F. Summers. ^{1}H and ^{13}C assignments from sensitivity-enhanced detection of heteronuclear multiple bond connectivity by 2D multiple quatum NMR. *J. Am. Chem. Soc.* **108**: 2093-2094 (1986).

17. B. C. Hancock and G. Zografi. Characteristics and significance of the amorphous state in pharmaceutical systems. *J. Pharm. Sci.* **86**: 1-12 (1997).

18. A. H. Forster, J. Hempenstall, and T. Rades. Characterisation of glass solutions of poorly water-soluble drugs produced by melt extrusion with hydrophilic amorphous polymers. *J. Pharm. Pharmacol.* **53**: 303-315 (2001).

19. C. Leuner and J. Dressman. Improving drug solubility for oral delivery using solid dispersions. *Eur. J. Pharm. Biopharm.* **50**: 47-60 (2000).

20. D. Q. M. Craig, P. G. Royall, V. L. Kett, and M. L. Hopton. The relevance of the amorphous state to pharmaceutical dosage forms: glassy drugs and freeze dried systems. *Int. J. Pharm.* **179**: 179-207 (1999).

21. L. Yu. Amorphous pharmaceutical solids: preparation, characterization and stabilization. *Adv. Drug Deliver. Rev.* **48**: 27-42 (2001).

22. X. C. Tang, M. J. Pikal, and L. S. Taylor. The effect of temperature on hydrogen bonding in crystalline and amorphous phases in dihydropyridine calcium channel blockers. *Pharm. Res.* **19**: 484-490 (2002).

23. X. C. Tang, M. J. Pikal, and L. S. Taylor. A spectroscopic investigation of hydrogen bond patterns in crystalline and amorphous phases in dihydropyridine calcium channel blockers. *Pharm. Res.* **19**: 477-483 (2002).

24. B. C. Hancock, G. T. Carlson, D. D. Ladipo, B. A. Langdon, and M. P. Mullarney. Comparison of the mechanical properties of the crystalline and amorphous forms of a drug substance. *Int. J. Pharm.* **241**: 73-85 (2002).

25. B. C. Hancock and M. Parks. What is the true solubility advantage for amorphous pharmaceuticals? *Pharm. Res.* **17**: 397-404 (2000).

26. S. L. Shamblin, X. Tang, L. Chang, B. C. Hancock, and M. J. Pikal. Characterization of the time scales of molecular motion in pharmaceutically important glasses. *J. Phys. Chem. B* **103**: 4113-4121 (1999).

27. B. C. Hancock, S. L. Shamblin, and G. Zografi. Molecular mobility of amorphous pharmaceutical solids below their glass transition temperatures. *Pharm. Res.* **12**: 799-806 (1995).

28. M. K. Gupta, A. Vanwert, and R. H. Bogner. Formation of physically stable amorphous drugs by milling with neusilin. *J. Pharm. Sci.* **92**: 536-551 (2003).

29. T. Watanabe, N. Wakiyama, F. Usui, M. Ikeda, T. Isobe, and M. Senna. Stability of amorphous indomethacin compounded with silica. *Int. J. Pharm.* **226**: 81-91 (2001).

30. V. Andronis, M. Yoshioka, and G. Zografi. Effects of sorbed water on the crystallisation of indomethacin from the amorphous state. *J. Pharm. Sci.* **86**: 346-351 (1997).

31. C. Ahlneck and G. Zografi. The molecular basis of moisture on the physical and chemical stability of drugs in the solid state. *Int. J. Pharm.* **62**: 87-95 (1990).

32. Y. Aso, S. Yoshioka, and S. Kojima. Relationship between water mobility, measured as nuclear magnetic relaxation time, and the crystallization rate of amorphous nifedipine in the presence of some pharmaceutical excipients. *Chem. Pharm. Bull.* **44**: 1065-1067 (1996).

33. A. H. Forster, J. Hempenstall, I. Tucker, and T. Rades. The potential of small-scale fusion experiments and the Gordon-Taylor equation to predict the suitability of drug/polymer blends for melt extrusion. *Drug Dev. Ind. Pharm.* **27**: 549-560 (2001).

34. J. Berggren and G. Alderborn. Long-term stabilisation potential of poly(vinylpyrrolidone) for amorphous lactose in spray-dried composites. *Eur. J. Pharm. Sci.* **21**: 209-215 (2004).

35. A. H. Forster, J. Hempenstall, and T. Rades. Investigation of drug / polymer interaction in glass solutions prepared by melt extrusion. *Internet J. Vib. Spectro.* **5**: 0 (2001).

36. K. J. Crowley and G. Zografi. Cryogenic grinding of indomethacin polymorphs and solvates: assessment of amorphous phase formation and amorphous phase physical stability. *J. Pharm. Sci.* **91**: 492-507 (2002).

37. N. Kaneniwa, M. Otsuka, and T. Hayashi. Physicochemical characterization of indomethacin polymorphs and the transformation kinetics in ethanol. *Chem. Pharm. Bull.* **33**: 3447-3455 (1985).

38. H. Imaizumi, N. Nambu, and T. Nagai. Stability and several physical properties of amorphous and crystalline forms of indomethacin. *Chem. Pharm. Bull.* **28**: 2565-2569 (1980).

39. T. J. Kistenmacher and R. E. Marsh. Crystal and molecular structure of an antiinflammatory agent, indomethacin, 1-(p-chlorobenzoyl)-5-methoxy-2-methylindole-3-acetic acid. *J. Am. Chem. Soc.* **94**: 1340-1345 (1972).

40. X. Chen, K. R. Morris, U. J. Griesser, S. R. Byrn, and J. G. Stowell. Reactivity difference of indomethacin solid forms with ammonia gas. *J. Am. Chem. Soc.* **124**: 15012-15019 (2002).

41. V. Andronis and G. Zografi. Crystal nucleation and growth of indomethacin polymorphs from the amorphous state. *J. Non-Cryst. Solids* **271**: 236-248 (2000).

42. L. S. Taylor and G. Zografi. Spectroscopic characterisation of interactions between PVP and indomethacin in amorphous molecular dispersions. *Pharm. Res.* **14**: 1691-1698 (1997).

43. L. S. Taylor and G. Zografi. The quantitative analysis of crystallinity using FT-Raman spectroscopy. *Pharm. Res.* **15**: 755-761 (1998).

44. A. H. Forster, D. C. Apperley, J. Hempenstall, R. W. Lancaster, and T. Rades. Investigation of the physical stability of amorphous drug and drug/polymer melts using variable temperature solid state NMR. *Pharmazie* **58**: 761-762 (2003).

45. V. Andronis and G. Zografi. The molecular mobility of supercooled amorphous indomethacin as a function of temperature and relative humidity. *Pharm. Res.* **15**: 835-842 (1998).

46. E. Fukuoka, M. Makita, and S. Yamamura. Some physicochemical properties of glassy indomethacin. *Chem. Pharm. Bull.* **34**: 4314-4321 (1986).

47. T. Matsumoto and G. Zografi. Physical properties of solid molecular dispersions of indomethacin with poly(vinylpyrrolidone) and poly(vinylpyrrolidone-co-vinyl-acetate) in relation to indomethacin crystallisation. *Pharm. Res.* **16**: 1722-1728 (1999).

48. M. Yoshioka, B. C. Hancock, and G. Zografi. Crystallisation of indomethacin from the amorphous state below and above its glass transition temperature. *J. Pharm. Sci.* **83**: 1700-1705 (1994).

49. A. Burger and K. T. Koller. Polymorphism and pseudopolymorphism on nifedipine. *Sci. Pharm.* **64**: 293-301 (1996).

50. F. Hirayama, Z. Wang, and K. Uekama. Effect of 2-hydroxypropyl-(β)-cyclodextrin on crystallization and polymorphic transition of nifedipine in solid state. *Pharm. Res.* **11**: 1766-1770 (1994).

51. M. R. Caira, Y. Robbertse, J. J. Bergh, M. Song, and M. M. De Villiers. Structural characterisation, physicochemical properties, and thermal stability of three crystal forms of nifedipine. *J. Pharm. Sci.* **92**: 2519-2533 (2003).

52. A. M. Triggle, E. Shefter, and D. J. Triggle. Crystal structure of calcium channel antagonists: 2,6-dimethyl-3,5-dicarbomethoxy-4-[2-nitro-, 3-cyano-, 4-(dimethylamino)-, and 2,3,4,5,6-pentafluorophenyl]-1,4-dihydropyridine. *J. Med. Chem.* **23**: 1442-1445 (1980).

53. Y. Aso, S. Yoshioka, and S. Kojima. Explanation of the crystallization rate of amorphous nifedipine and phenobarbital from their molecular mobility as measured by ^{13}C nuclear magnetic resonance relaxation time and the relaxation time obtained from the heating rate dependence of the glass transition temperature. *J. Pharm. Sci.* **90**: 798-806 (2001).

54. Y. Aso, S. Yoshioka, and S. Kojima. Molecular mobility-based estimation of the crystallization rates of amorphous nifedipine and phenobarbital in poly(vinylpyrrolidone) solid dispersions. *J. Pharm. Sci.* **93**: 384-391 (2004).

55. Y. Aso, S. Yoshioka, T. Otsuka, and S. Kojima. The physical stability of amorphous nifedipine determined by isothermal microcalorimetry. *Chem. Pharm. Bull.* **43**: 300-303 (1995).

56. A. L. Grzesiak, M. Lang, K. Kim, and A. J. Matzger. Comparison of the four anhydrous polymorphs of carbamazepine and the crystal structure of form I. *J. Pharm. Sci.* **92**: 2260-2271 (2003).

57. R. J. Roberts, R. S. Payne, and R. C. Rowe. Mechanical property predictions for polymorphs of sulphathiazole and carbamazepine. *Eur. J. Pharm. Sci.* **9**: 277-283 (2000).

58. J. P. Reboul, B. Cristau, J. C. Soyfer, and J. P. Astier. 5H-dibenz[b,f]azepinecarboxamide-5 (carbamazepine). *Acta Cryst.* **B37**: 1844-1848 (1981).

59. V. L. Himes, A. D. Mighell, and W. H. De Camp. Structure of carbamazepine: 5H-dibenz[b,f]azepine-5-carboxamide. *Acta Cryst.* **B37**: 2242-2245 (1981).

60. F. U. Krahn and J. B. Mielck. Relations between several polymorphic forms and the dihydrate of carbamazepine. *Pharm. Acta Helv.* **62**: 247-254 (1987).

61. R. K. Harris, P. Y. Ghi, H. Puschmann, D. C. Apperley, U. J. Griesser, R. B. Hammond, K. Ma, K. J. Roberts, G. J. Pearce, J. R. Yates, and C. J. Pickard. Structural study of the polymorphs of carbamazepine, its dihydrate, and two solvates. *Org. Process Res. Dev.* **9**: 902-910 (2005).

62. R. Nair, S. Gonen, and S. W. Hoag. Influence of polyethylene glycol and povidone on the polymorphic transformation and solubility of carbamazepine. *Int. J. Pharm.* **240**: 11-22 (2002).

Chapter Two: Experimental

1/ General information

The use of different characterisation techniques are likely to involve differences in the physical nature of the samples and the way they are handled in terms of the data obtained. Therefore, properties, such as rates of crystallisation and Tg itself, may depend on the sample preparation used.

1.1/ Materials

Samples of indomethacin (**I**), nifedipine (**II**) and carbamazepine (**III**) were provided by Sigma Aldrich (UK). Poly(vinylpyrrolidone) (PVP k30, average MW 50,000) (**IV**) was supplied by GlaxoSmithKline (UK). All sample were used without further purification. Nifedipine and carbamazepine were stored in the fridge and protected from light during storage and they were, as far as it was possible, protected from light during sample preparation and experimentation. The chemical stability of the compounds was checked by proton NMR of solutions in DMSO-d_6 following the procedures discussed below for TGA and variable-temperature solid-state NMR measurements. The numbering systems used for solid-state forms of compounds **I**, **II** and **III** were obtained from the papers by Kistenmacher & Marsh[1], Triggle et al.[2] and Himes et al.[3] respectively.

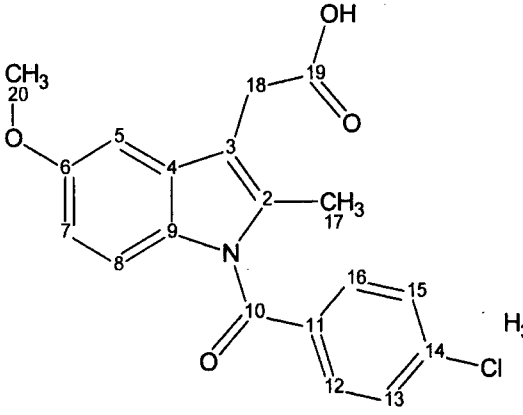

I. Indomethacin

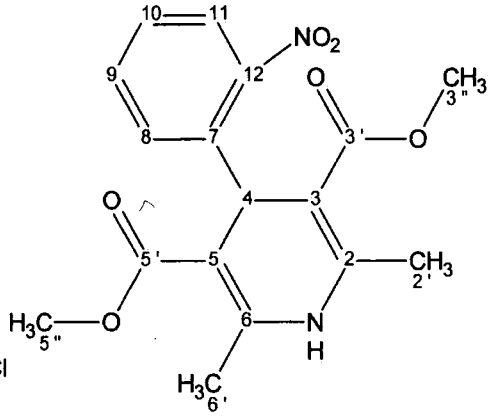

II. Nifedipine

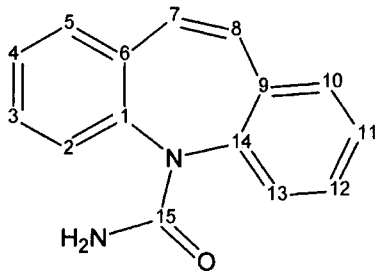

III. Carbamazepine

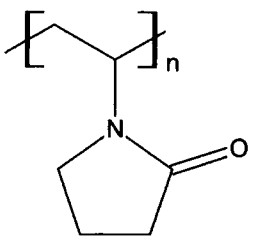

IV. PVP

1.2/ Preparation of amorphous samples

For the static ^{1}H spectra and relaxation experiments, approximately 500 mg of the crystalline drug was melted in an oven in glass tubes 1 cm in length. Nifedipine was melted at 180 °C for 5 minutes, indomethacin at 171 °C for 10 minutes and carbamazepine at 195 °C for 5 minutes. Then, the sample was put in a pre-cooled mortar and liquid nitrogen was added in this mortar after one minute for indomethacin and nifedipine, or straight away for carbamazepine. Amorphous indomethacin and nifedipine appeared as transparent yellow glasses straight after cooling, while amorphous carbamazepine appeared as a transparent amber glass. The thermal degradation of the compounds was investigated with thermo gravimetric analysis by holding the crystalline samples for an equivalent time, i.e. 5-10 minutes, and at the same temperature, i.e. 171 °C, 180 °C or 195 °C, as used during the sample preparation process. All samples showed less than 3 % weight loss, indicating satisfactory thermal stability. A solution-state NMR spectrum, obtained after a TGA experiment, was used to confirm this low level of degradation, ca. 1 %.

This approach of preparing the amorphous samples directly in the glass tubes was chosen to prevent the need for grinding solidified melts and to reduce the amount of water adsorbed by the sample following preparation. However, for the ^{13}C experiments it was decided to stop quench cooling the melt straight into the rotor in order to avoid stress on the rotor. Instead, the sample was melted, quench-cooled and ground in a beaker. In order to avoid recrystallisation, the grinding was done with the beaker placed in a bath of liquid nitrogen. The ^{13}C SSNMR spectra of the samples treated this way were the same as those obtained when quench-cooling in the rotor.

2/ Nuclear Magnetic Resonance (NMR)

2.1/ Solid-State NMR (SSNMR)

2.1.1) Spectrometers and probes

Two different spectrometers have been used primarily. One is a Varian InfinityPlus 500, used with a HX 7.5 mm MAS probe or a HX 2.5 mm MAS probe. This spectrometer operates at a proton frequency of 499.75 MHz and at a ^{13}C frequency of 125.68 MHz. The other spectrometer was a Chemagnetics CMX 200, used with a 7.5 mm MAS probe or a static probe fitted with a 10 mm o.d. coil. This spectrometer operates at a proton frequency of 200.13 MHz and a ^{13}C frequency of 50.32 MHz. For both spectrometers, the two channels were used for the MAS probes. One channel was used for observing ^{13}C signals and the other allowed cross-polarisation from and decoupling of protons, as well as direct ^{1}H observations. The static probe used only one channel for direct ^{1}H observations.

Some of the relaxation data have been previously acquired by D.C. Apperley on a Varian UnityPlus 300, which operates at a proton frequency of 299.946 MHz .

Another spectrometer has been used specifically for the study of quadrupolar effect for indomethacin. It was a Varian InfinityPlus 800, used with a 5 mm MAS probe, which was situated at the Rutherford-Appleton laboratory, Oxfordshire. This spectrometer operated at a proton frequency of 699.72 MHz at first, then at 799.76 MHz once the magnet reached full field. The spectra at 700 MHz and 800 MHz were obtained by P.Y. Ghi.

2.1.2) Experimental setup

2.1.2.1) Setting the magic-angle

Setting the magic-angle properly is an important task as, if the sample is not at the magic-angle, the CSA and heteronuclear dipole interactions will not be fully averaged. Therefore, they will complicate the spectra. The magic-angle should be set every 1 or 2 weeks. It is also good practice to set the angle again after a VT experiment, as the change of temperature can affect the angle.

In order to set this angle properly, a sample of potassium bromide is spun, and a ^{79}Br

spectrum is acquired with 32 to 64 acquisitions and a short pulse delay, i.e. 0.1 s. The number of acquisitions is chosen with the aim of obtaining a good signal to noise ratio to help with a fine adjustment. The next step is to move the transmitter to have the centreband on resonance. Then a FID is acquired to check the train of rotational echoes, which should be up to 10 ms in duration if the angle is set properly. If this is not the case, the angle needs adjustment until a satisfactory echo train is observed.

2.1.2.2) Setting the 90° pulse

The duration of the 90° pulse depends on the probe; in our case, it was mainly set to 5 μs, and is determined using adamantane. The sample is either spun at 2-3 kHz or static. The experiment is carried out by repetitively/continuously acquiring proton spectra whilst manually increasing or decreasing the amplifier power such that a null signal may be observed at twice the chosen 90° pulse duration for proton. At the point when a null signal is observed, it is assumed that the proton magnetisation has precessed through 180° and thus there is no component along the axis of observation. Then an array is done in order to confirm this and the 90° pulse value is the difference between 360° and 180° divided by two. This technique to get the value of the 90° pulse was used, as it is the technique employed by the manufacturer when giving the probe specifications. The same procedure is done for the carbon signal of adamantane and another 90° pulse value, normally the same as for protons, is determined.

2.1.2.3) Setting the Hartmann-Hahn condition (CP experiments only)

The previous section sets the Hartmann-Hahn condition. Nevertheless, we want this to be more accurate. Therefore, we change the value of the X CP power whilst observing adamantane. This value corresponds to the power used on the X channel during the contact time. One just needs to array the value in decreasing steps and from this experiment use the X CP value giving the highest intensity spectrum. In addition, one can also check that the H CP power, the power used on the proton channel during the contact time, is optimal by doing an analogous procedure. However, it is expected that the value for the H CP power should be equal to the maximum power used during the experiment, i.e. 90° pulse power.

2.1.2.4) Setting the recycle delay and the contact time

The recycle delay is the time between the end of the acquisition of one FID and the next sequence of radio frequency excitation. It is important to choose this time carefully as it determines the strength of signal that will be detected. It should not be too short, as this can result in a loss of the signal due to saturation, and could degrade the probe and/or the sample by heating effects. On the other hand, too long a recycle delay will result in a waste of spectrometer time.

The recycle delay is sample dependent, as it will directly derive from T_1^H for a CP experiment or T_1^X for a DP experiment on nucleus X. It should be about five times T_1 for the best signal intensity, or ~1.2 × T_1 for the best signal to noise ratio (S/N). However, it is not necessary to measure T_1 to determine the best recycle delay. It is possible to do an array on the recycle delay which will enable the experimentalist to determine the best time. This best time will depend on whether a quantitative experiment or a good S/N is wanted.

The contact time for a CP experiment has to be determined in order to have the best signal transferred between the abundant and the dilute spins. This is done by doing an array on the contact time. The time for which the signal has the strongest intensity will be the best contact time. It is important to note that the signal intensity varies across the spectrum, e.g. a quaternary carbon will usually need a longer contact time. This time should be long enough to allow maximum magnetisation to be transferred from one spin to another. It also should be short enough in order to avoid the magnetisation leaking to the lattice. This consideration depends on $T_{1\rho}^H$. In effect, the data from the contact time array can be fitted to equation 2.1, which is the equation for the intensity of the signal.

$$y = amp * \left[\exp\left(\frac{-\tau}{T_{1\rho}}\right) - \exp\left(\frac{-\tau}{T_{CP}}\right) \right] \qquad \textbf{Equation 2.1}$$

where "amp" represents the intrinsic amplitude of the peak, $T_{1\rho}^H$ is the spin-lattice relaxation time in the rotating frame of resonance, T_{CP} is the time constant of the CP experiment and τ is the contact time which is the arrayed parameter.

2.1.2.5) Referencing

In order to ensure comparability of results, it is necessary to reference the chemical

shifts in the spectra to a recognised standard. In our case, adamantane was used as a standard for ^{13}C and PDMSO was used for ^{1}H. The high-frequency ^{13}C peak of adamantane has a chemical shift of 38.4 ppm with respect to TMS, and PDMSO has a chemical shift of 0.1 ppm with respect to TMS. It is good to note that the referencing for proton is only important when a resolved spectrum is obtained.

2.1.3) Variable Temperature (VT) experiments

2.1.3.1) VT calibration

The VT calibration has to be done specifically for every probe, and at a specific spinning speed, as the speed influences the sample temperature. The aim of this calibration is to find the temperature in the rotor and to compare it to the value set by the spectrometer operator (this will be referred to as the reading temperature from now on). This will give a curve that will then be used, when doing a VT experiment, to find out the temperature in the rotor knowing the one recorded on the spectrometer.

The calibration is done in two steps. The first will be to find an absolute temperature. In order to achieve this, methanol is used and from the difference, in Hz, between the two proton peaks, a temperature is found, which will be the absolute temperature. This is generally done with a reading temperature of about 20°C to 25°C.

The second step is done using lead nitrate ($Pb(NO_3)_2$). The chemical shift of the ^{207}Pb signal is temperature dependent, and therefore will give information on the temperature in the rotor. This is done with equation 2.2[4]. The shape of the signal is interesting as it gives information on any temperature gradients that are present inside the rotor.

$$\delta = T \times 0.753 ppm/°C \qquad \textbf{Equation 2.2}$$

The VT calibration of the static probe used for this study is shown in appendix 1 and the precision of the calibrated temperature is ± 1.0°C.

2.1.3.2) VT method

The VT equipment was mainly used for the measurement of proton relaxation times. VT ^{13}C SSNMR of amorphous materials was also performed. The method used to do the VT experiments is as follows:

1. Insert a dewar of liquid nitrogen in the line.
2. Change the pipeline in order to use nitrogen gas as cooling/heating gas.
3. Set the purge and heater gas to the appropriate flow (ca. 90 SCFH for low temperature and ca. 110 SCFH for room temperature and above).
4. Start the experiment at the lowest temperature, in our case −70 °C.
5. Acquire a T_1^H saturation-recovery experiment followed by a $T_{1\rho}^H$ spin-lock experiment. Then increase the temperature.
6. When reaching 20 °C, it is good practice to reduce the temperature, down to ca. −20 °C, at the control before switching the controller off.
7. Remove the dewar of liquid nitrogen out of the line.
8. Carry on the rest of the experiments until the whole range of temperature is complete.

It is good to note that when the controller is switched off, the temperature inside the probe rises quite quickly due to compensation by the probe. This can cause some problems with temperature-dependent compounds, such as amorphous nifedipine. It is for this reason that the temperature is lowered before switching off the controller.

2.1.4) Carbon-13 SSNMR

Carbon-13 spectra were recorded with cross polarisation, magic-angle spinning and high-power proton decoupling using the Chemagnetics 200 spectrometer, operating at 50.32 MHz. A probe using 7.5 mm diameter rotors made of zirconia was employed. For all experiments, PTFE end caps were used. Typical operating conditions utilised a contact time of 3-5 ms, a recycle delay of 12-60 s, 512 transients and a spin rate of 4.5-5.5 kHz. For assignment purposes, spectra of non-protonated and protonated carbons were separately obtained using a dipolar dephasing pulse sequence[5]. Carbon-13 variable-temperature measurements were performed for amorphous indomethacin and nifedipine, from 22°C to 80°C for the former and from −40°C to 55°C for the latter. An analogous experiment was performed on crystalline indomethacin at −80 °C.

2.1.5) Proton SSNMR

The InfinityPlus 500 was used to do ^{1}H high-speed experiments on all three crystalline compounds and ^{13}C experiments on crystalline indomethacin. For the high-speed experiments, a HX 2.5 mm probe and a spinning speed of ca. 25 kHz were used. For the ^{13}C experiments, a HXY 7.5 mm probe and a spinning speed of ca. 5 kHz were used.

Proton wideline NMR spectra and relaxation times (T_1 and $T_{1\rho}$) for static samples were measured at 200.13 MHz using a Chemagnetics CMX 200 spectrometer and at 299.95 MHz using a Varian Unity Plus 300 spectrometer. Values of T_1 were derived from a saturation-recovery experiment with twelve delay times for each measurement. This experiment involves applying a series of one hundred 90° radio frequency pulses (duration 5 μs for the work at 200 MHz but 1.8 μs at 300 MHz) separated by a time of 100 μs, equalising the populations of the spin states which subsequently relax to their equilibrium situation. A series of delay times is then used prior to a 90° read pulse in order to map the relaxation rate[6]. This approach is particularly useful for systems with long T_1 values because a conventional inversion-recovery experiment may take a prohibitively long time. In the saturation-recovery case, only a short recycle delay (0.1 s) is required after data acquisition before a new series of saturation pulses can be applied. $T_{1\rho}$ measurements were performed by varying a spin-lock time (twelve different values) following a 90° radio frequency pulse (duration as for the T_1 measurements). The relaxation delay used in this case was equal to four times the measured T_1. For spin-locking, a radio frequency field equivalent to 50 kHz (200 MHz) or 70 kHz (300 MHz) was used.

Each decay curve (for both T_1 and $T_{1\rho}$ measurements) was fitted to a single or double exponential using the Origin 6.1 software. When a double exponential was used the value for T_1^H or $T_{1\rho}^H$ was obtained using the population weighted rate average. A series of such measurements was performed over a wide temperature range for all samples, including the drug/PVP co-melts but excluding PVP itself. The fitting to a double exponential was only done for high temperatures and principally for the $T_{1\rho}$ measurements. When a double exponential was needed one of the exponential represented at least 90% of the total, i.e. the other one did not influence much the stated results.

In order to obtain the decay curves, three methods were investigated: the peak height,

the peak integral and the first point of the FID. It was found that the most robust and easily reproducible was to use the first point of the FID. The reproducibility and easiness of use was managed by writing a simple macro.

As sample robustness is of particular interest, accurate time recording was performed beginning at the time of sample preparation for each set of measurements. The relaxation measurements for the three drugs were performed for two separately prepared quench-cooled melts.

The protocol used for proton NMR measurements was generally as follows:

1. The relevant sample was melted in an oven in a glass tube (10 mm o.d.) at 171 °C for 10 minutes, 180 °C for 10 minutes and 195 °C for 5 minutes, for indomethacin, nifedipine and carbamazepine respectively. It was kept in the tube throughout the experiments.
2. On removal from the oven, the tube was placed in a pre-chilled mortar and, after about 1 minute for indomethacin and nifedipine and straight away for carbamazepine, liquid nitrogen was poured over it, producing a clear yellow or amber glass. In the case of the PVP/drug mixtures, the sample was poured in a pre-chilled mortar and liquid nitrogen was poured directly over it, then crushed under liquid nitrogen and put into a tube.
3. The tube went straight into the spectrometer and was cooled to −70°C (as set using the software). Calibration shows that the actual sample temperatures are within 2 °C of those set.
4. The first NMR measurements were started half an hour after the sample went into the oven.
5. A T_1 measurement was followed by a $T_{1\rho}$ experiment, each with 12 delay times.
6. Each decay curve was fitted to a single exponential.
7. The temperature was then increased incrementally. The time allowed for equilibration at the new temperature was typically between 10 and 20 minutes, after which a new set of measurements was made.

The only difference for the co-melts was that PVP was dried at low pressure in an oven for a minimum of three hours. Then the sample of PVP was weighed and a similar mass of one of the drugs was added. This was followed by the above protocol.

The amorphous samples used for the ^{13}C experiments were prepared by melting the sample in a beaker for 10 minutes at the appropriate temperature. Then the sample

was poured and ground in liquid nitrogen. The preparation of an amorphous sample was checked using XRPD.

2.2/ Solution-state NMR

Solution-state NMR data were obtained for reference purposes. Spectra for indomethacin (in deuterated dimethylsulfoxide) were obtained at a 100.58 MHz for ^{13}C and at 399.97 MHz for ^{1}H, using a Varian Mercury 400 spectrometer at ambient probe temperature. Spectra for nifedipine and carbamazepine (in deuterated dimethylsulfoxide and in deuterated chloroform, respectively) were obtained at 125.70 MHz for ^{13}C and at 499.92 MHz for ^{1}H, using a Varian Inova 500 spectrometer at ambient probe temperature. All spectra were referenced to the solvent signal. For each compound, the full assignments were made using ^{1}H, ^{13}C, COSY, HSQC and HMBC experiments. Standard conditions for the COSY experiments are 1024 or 2048 data points with 256 increments in F_1 and 1 transient in F_2. For the HSQC experiments, these conditions are 1024 or 2048 data points with 2 x 256 increments in F_1 and 8 transients in F_2. For the HMBC experiments, these conditions are 1024 or 2048 data points with 400 increments in F_1 and 8 transients in F_2.

The solution-state indomethacin and nifedipine ^{13}C chemical shifts and assignments are consistent with the work of O'Brien et al.[7] and that of Ali[8] respectively, except that in the former case the assignments for C-2 and C-4 have been exchanged. The solution-state carbamazepine carbon chemical shifts and assignments were not found in the literature for comparison, whilst the proton chemical shifts and assignments are consistent with the work of Aboul-Enein & Al-Badr[9] with increased understanding of the aromatic region.

Solution-state NMR was also used to check the stability upon heating of all three compounds, as well as their stability after VT experiments. These spectra (in deuterated dimethylsulfoxide for indomethacin and nifedipine and in deuterated chloroform for carbamazepine) were obtained at 400.13 MHz for ^{1}H and at 100.61 MHz for ^{13}C, using a Bruker Avance 400 spectrometer at ambient probe temperature. All spectra were referenced to the solvent signal.

3/ X-Ray Powder Diffraction (XRPD)

XRPD was used to study the crystalline fomr, confirm that quench-cooling of the drugs resulted in the production of amorphous products and for VT investigation.

All samples were analysed with a Philips X'Pert MPD powder diffractometer (count time 1 second, step size 0.04 °2θ, Ni-filtered Cu-kα radiation, 45 kV, 50 mA, sample size: approx. 300 mg)

In the case of the crystalline form, a recessed silicon wafer holder front filled was used. In the case of the amorphous form, the samples were melted in an X-ray sample holder, TTK front fill holder, on a hot plate and then immediately immersed in liquid nitrogen. The powder diffractometer was fitted with an Anton-Parr TTK variable temperature camera for the VT experiments. The timescale of the VT experiment was similar to the timescale used for the VT SSNMR experiments as far as this was possible.

4/ Differential Scanning Calorimetry (DSC)

DSC was used to measure the Tg, to measure the melting point of the studied samples, to determine the crystalline form of the original samples and to check the feasibility of producing an amorphous material by melting and quench cooling it. Amorphous samples were prepared by melting the pure drug in lightly crimped aluminium pans (open-pan), using a TA Instruments 2920 DSC (Surrey, UK) at a heating rate of 10 K min^{-1} (nitrogen purge: 20 ml min^{-1}). The sample size was about 5 mg. Temperature and enthalpy calibrations were performed using indium. Quench-cooling of the samples was performed by placing a liquid nitrogen Dewar over the DSC cell. To determine Tg (onset value) the samples were then reheated in the DSC using the same conditions, interpretation of the data was done using Universal Analysis (TA instruments, Surrey, UK).

For amorphous nifedipine, a different experiment was carried out using a Perkin Elmer Pyris-1 apparatus using a water cooling system and non-hermetically sealed aluminium pans. A typical sample weight of 2 to 5 mg was used. In this case, the DSC was used in order to gain information on the recrystallisation process.

5/ Thermo Gravimetric Analysis (TGA)

TGA was used to determine the stability of the compounds by holding them 10 °C above the melting point for up to 10 min and measuring the weight loss. The samples were placed in open aluminium pans. The experiments were carried out using a TA instruments, Hi-Res. TGA 2950 Thermogravimetric Analyser, with a N_2 purge gas flowing at 100 ml/min. Typically, samples were about 20 mg.

6/ Microscopy techniques

Two different microscopy techniques were used:

- A polarised light microscope was used to determine if a sample was crystalline or amorphous. The instrument employed was a Zeiss polarised light microscope fitted with JVC digital video camera using Image Pro-plus software to capture the image. Powder samples were dispersed on a glass microscope slide using mineral oil.
- A hot-stage microscope was used to investigate the recrystallisation of amorphous samples upon heating. A Nikon polarised light microscope was used in combination with a Linkam LTS 350 hot-stage fitted with video image capture.

7/ Fourier-Transform Infra-Red (FTIR) spectroscopy

Samples were analysed by infra-red spectroscopy using an Attenuated Total Reflectance (ATR) accessory fitted with a germanium crystal on an Avatar FTIR model 360 instrument. Spectra (64 scans at 4 cm^{-1} resolution) were recorded over the 4000 – 700 cm^{-1} range and analysis was performed using Omnic ESP software.

8/ References

1. T. J. Kistenmacher and R. E. Marsh. Crystal and molecular structure of an antiinflammatory agent, indomethacin, 1-(p-chlorobenzoyl)-5-methoxy-2-methylindole-3-acetic acid. *J. Am. Chem. Soc.* **94**: 1340-1345 (1972).

2. A. M. Triggle, E. Shefter, and D. J. Triggle. Crystal structure of calcium channel antagonists: 2,6-dimethyl-3,5-dicarbomethoxy-4-[2-nitro-, 3-cyano-, 4-(dimethylamino)-, and 2,3,4,5,6-pentafluorophenyl]-1,4-dihydropyridine. *J. Med. Chem.* **23**: 1442-1445 (1980).

3. V. L. Himes, A. D. Mighell, and W. H. De Camp. Structure of carbamazepine: 5H-dibenz[b,f]azepine-5-carboxamide. *Acta Cryst.* **B37**: 2242-2245 (1981).

4. A. Bielecki and D. P. Burum. Temperature dependence of 207Pb MAS spectra of solid lead nitrate. An accurate, sensitive thermometer for variable-temperature MAS. *J. Magn. Reson. Ser. A* **116**: 215-220 (1995).

5. S. J. Opella and M. H. Frey. Selection of nonprotonated carbon resonances in solid-state nuclear magnetic resonance. *J. Am. Chem. Soc.* **101**: 5854-5856 (1979).

6. J. K. M. Sanders and B. K. Hunter. *Modern NMR spectroscopy - a guide for chemists*, Oxford Univesity Press, Oxford, 1993.

7. M. O'Brien, J. McCauley, and F. Cohen. Indomethacin. In K. Florey (ed), *Analytical profiles of drug substances*, Vol. 13 (K. Florey, ed), Academic Press, New York, 1984, pp. 211-238.

8. S. L. Ali. Nifedipine. In K. Florey (ed), *Analytical profiles of drug substances*, Vol. 18 (K. Florey, ed), Academic Press, New York, 1989, pp. 221-289.

9. H. Y. Aboul-Henein and A. A. Al-Badr. Carbamazepine. In K. Florey (ed), *Analytical profiles of drug substances*, Vol. 9 (K. Florey, ed), Academic Press, New York, 1980, pp. 87-106.

Chapter Three: Crystalline Materials

1/ Materials

This chapter will deal with the data acquired and the results obtained whilst dealing with the crystalline forms of the three studied drugs. It will detail to what extent the different techniques of analysis were used, and demonstrate how the techniques were utilised in order to help in the progression of this research.

Note that for the DSC traces there are two values around each of the peaks, the highest values correspond to the temperature at the maximum of the peak, while the lowest temperature corresponds to the onset temperature. The onset temperature is used when confirming the melting point.

1.1/ Indomethacin

The crystalline form studied was the γ-form, as determined by XRPD (figure 3.1) and DSC (figure 3.2). The results obtained are in agreement with the work of Kaneniwa et al.[1]. The FTIR of crystalline indomethacin is shown for reference in appendix 2.

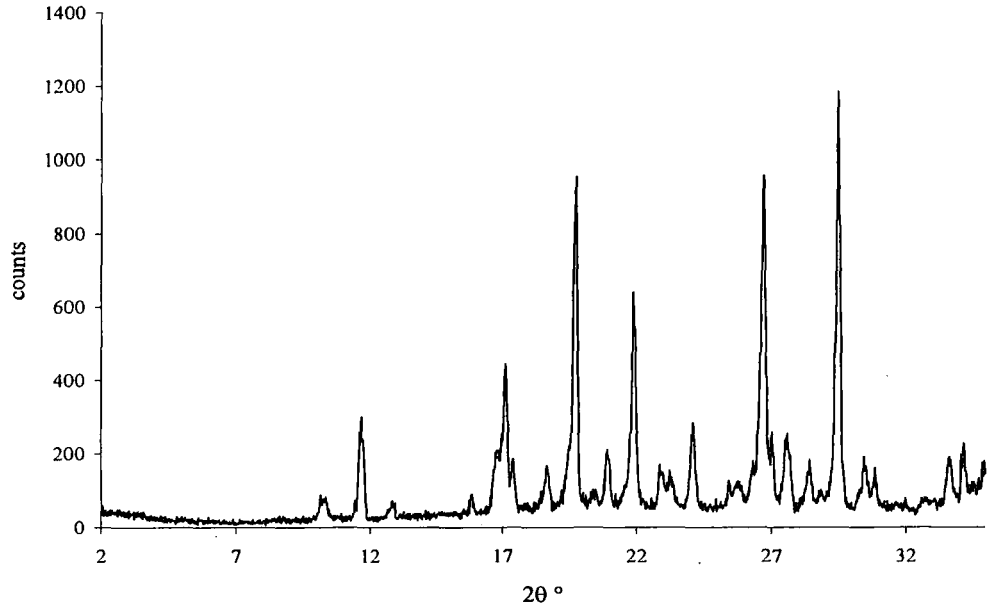

Figure 3.1: XRPD of the γ-form of crystalline indomethacin.

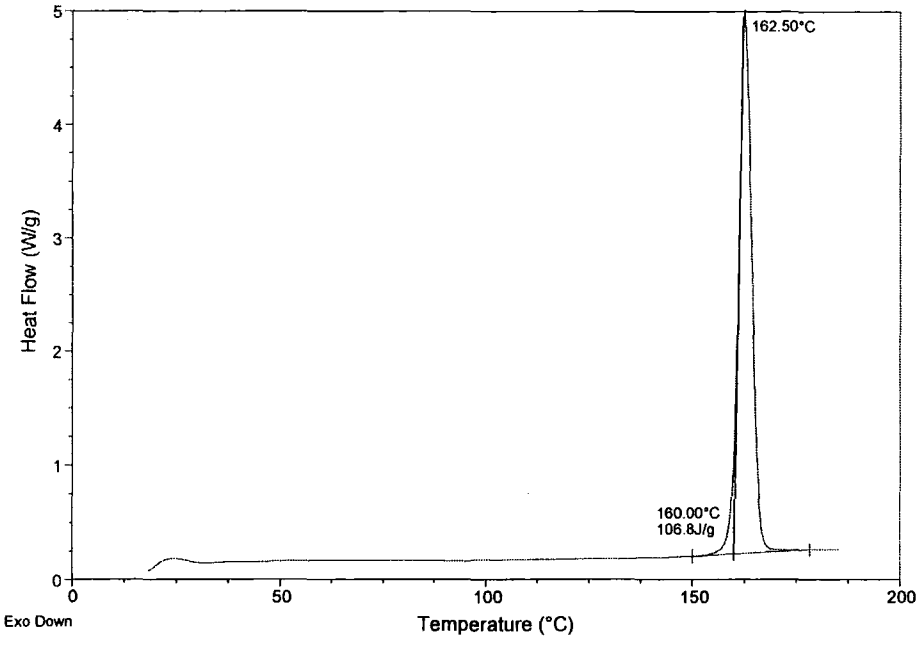

Figure 3.2: DSC of the γ-form of crystalline indomethacin showing T_m = 160°C.

The melting point (T_m) of the γ-form of indomethacin is 160°C[1]. The DSC (figure 3.2) was used to show that the studied form was the γ-form.

The solid-state phase relationship of this compound is shown in figure 3.3. This confirms that the crystalline form of indomethacin at room temperature is the same one as observed by XRPD (figure 3.1).

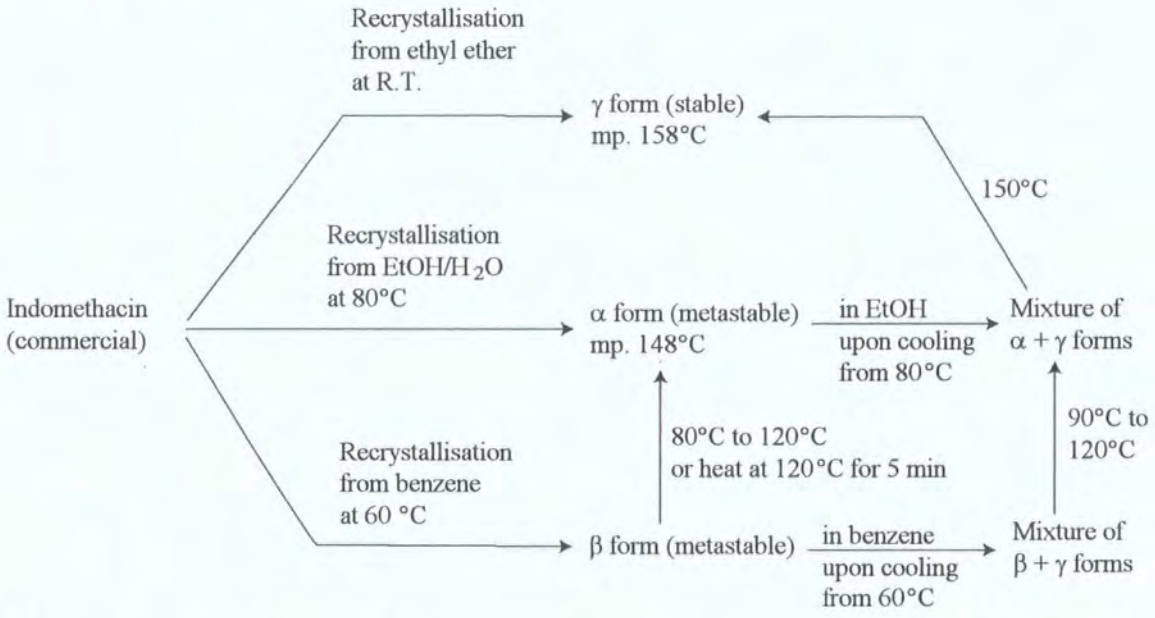

Figure 3.3: Phase relationship of indomethacin [1].

The conformation of the asymmetric unit of the γ-form of indomethacin is shown in figure 3.4 while figure 3.5 shows a unit cell.

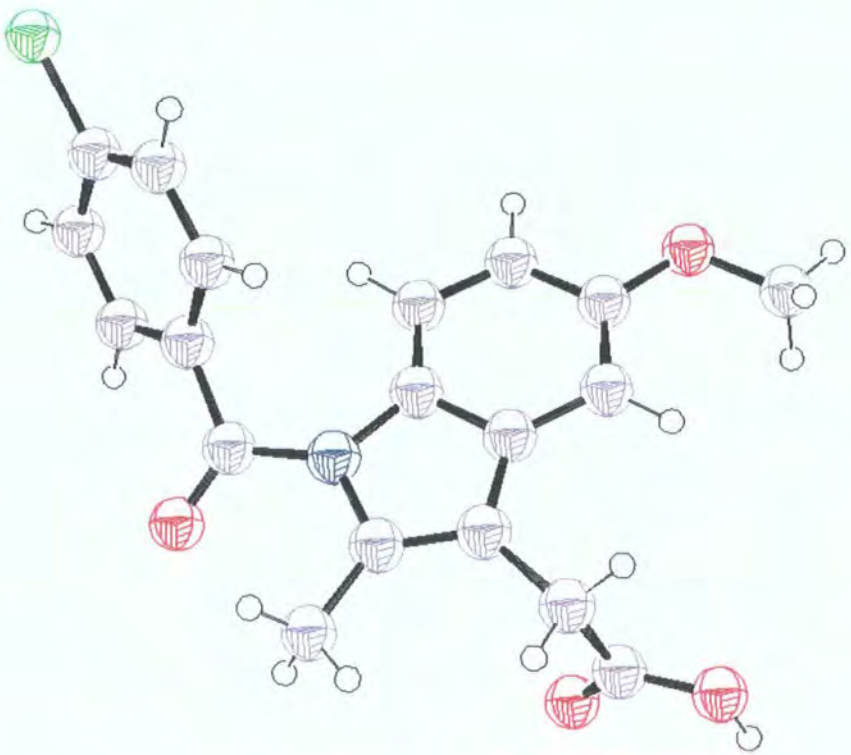

Figure 3.4: Conformation of the asymmetric unit of the γ-form of indomethacin. This crystal has one molecule per asymmetric unit and two molecules per unit cell[2].

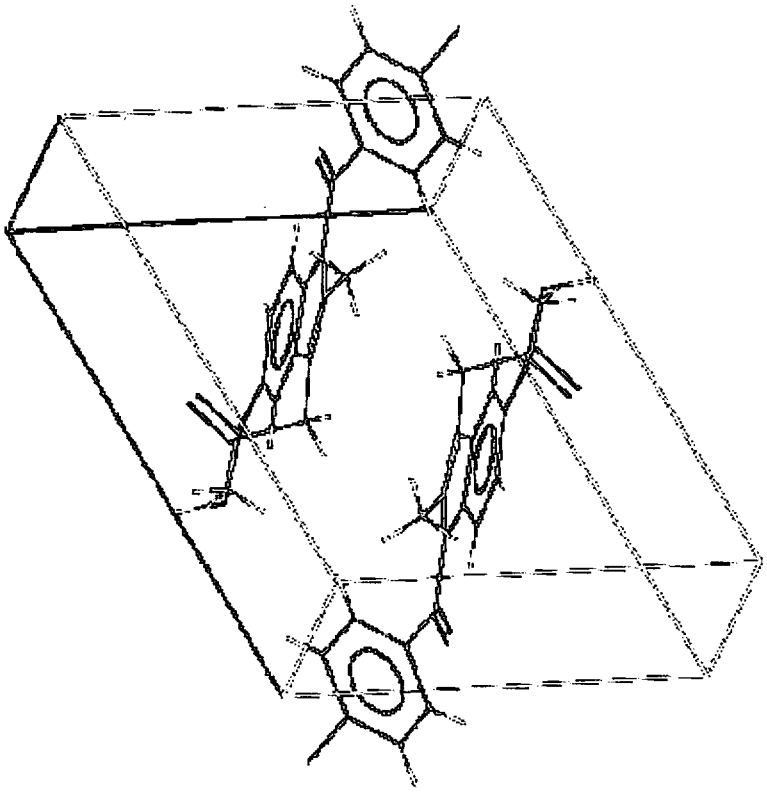

Figure 3.5: Unit cell of the γ-form of indomethacin.

1.2/ Nifedipine

The commercial sample provided is the polymorph modification I. This is shown by comparing the DSC (figure 3.6) and FTIR (figure 3.7), obtained experimentally, with the work of Burger and Koller[3]. The XRPD of crystalline nifedipine is shown for reference in appendix 3.

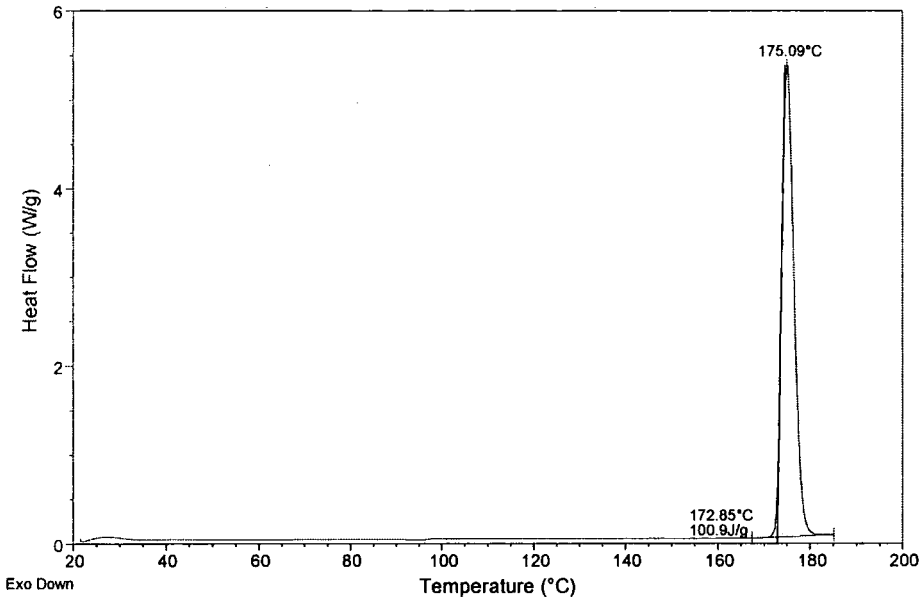

Figure 3.6: DSC of crystalline nifedipine showing T_m = 173°C.

The melting point (T_m) of the modification I of nifedipine is 171°C[4]. This was confirmed using DSC (figure 3.6).

The FTIR bands at 1689, 1649, 1619, 1192 and 746 cm^{-1} are characteristic of the modification I[3].

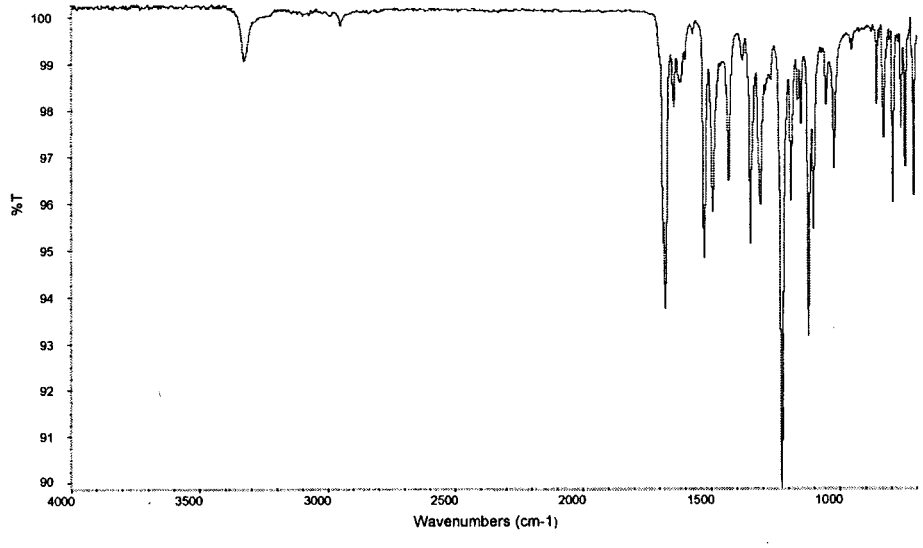

Figure 3.7: FTIR of crystalline nifedipine.

The conformation of the asymmetric unit of the modification I of nifedipine is shown in figure 3.8 while figure 3.9 shows its unit cell.

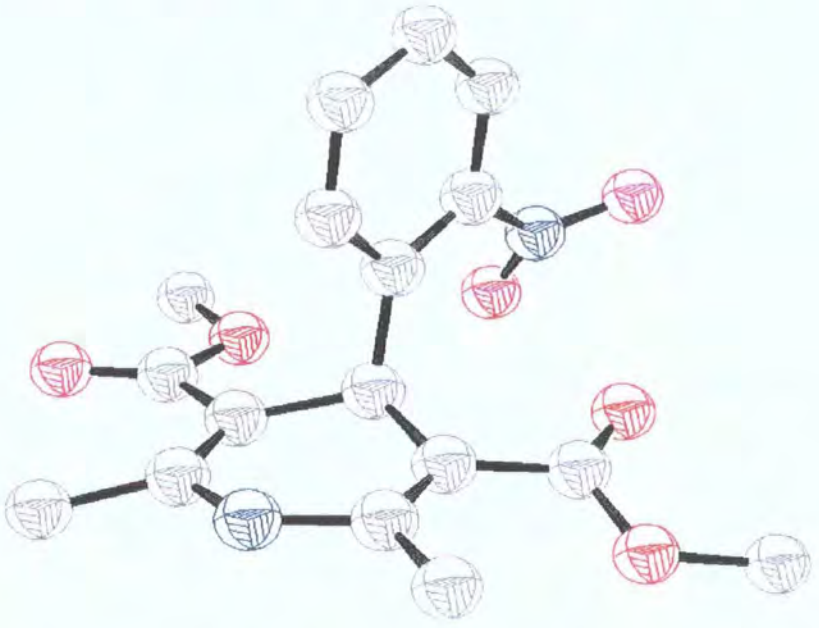

Figure 3.8: Conformation of the asymmetric unit of the modification I of nifedipine. This crystal has one molecule per asymmetric unit and four molecules per unit cell[5].

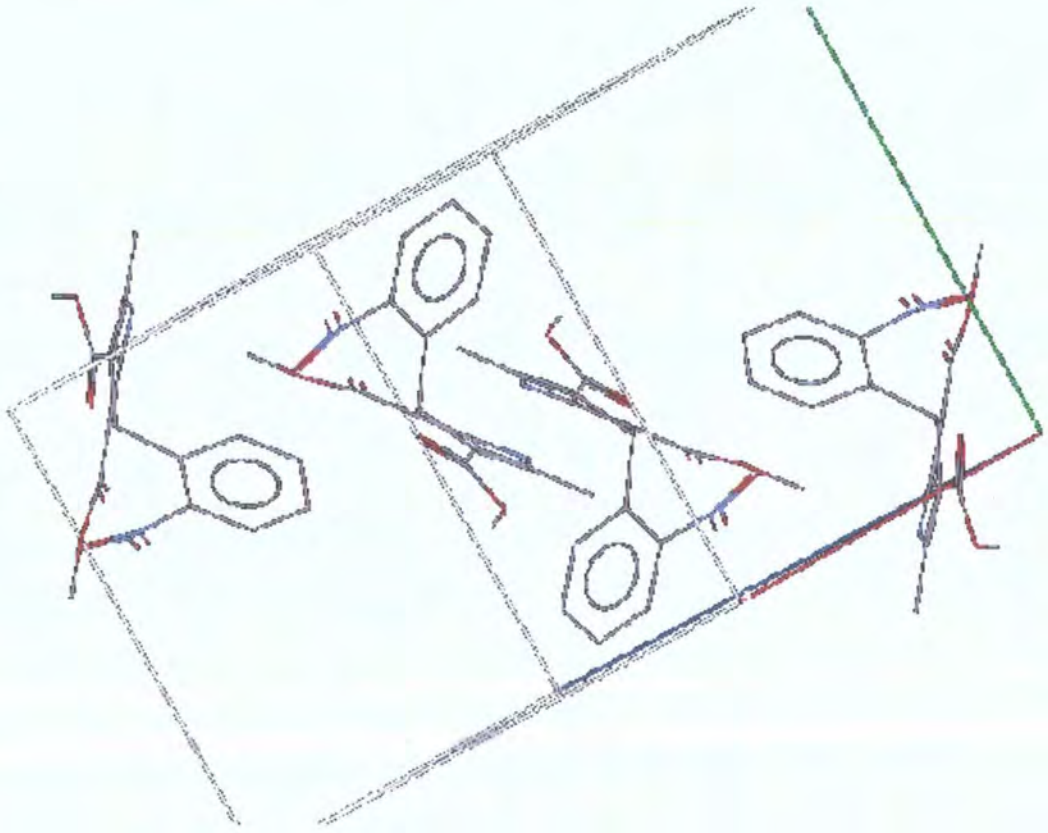

Figure 3.9: Unit cell of modification I of nifedipine.

1.3/ Carbamazepine

The commercial sample provided is the polymorph modification III as shown by comparing the work of Krahn and Mielck[6] with the DSC (figure 3.10) and XRPD (figure 3.11) obtained for this compound. The FTIR of crystalline carbamazepine is shown for reference in appendix 4.

The melting point (T_m) of the form III of carbamazepine is 174°C[6]. This was confirmed using DSC (figure 3.10). The DSC shows an endotherm at 175°C followed by an exotherm at 177°C corresponding to the melting of form III and the crystallisation of form I respectively. The endotherm at 192°C corresponds to the melting of form I.

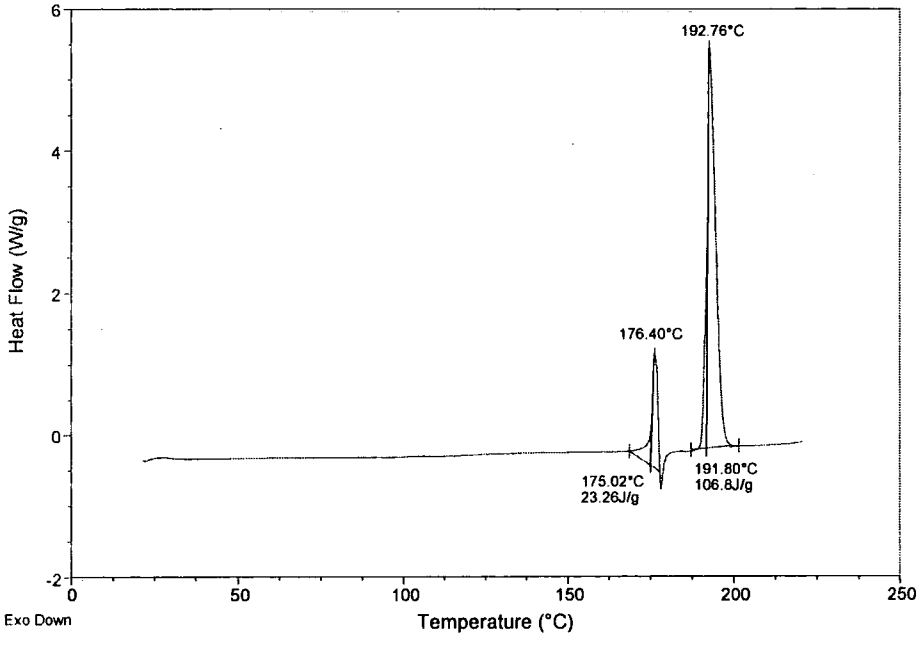

Figure 3.10: DSC of carbamazepine showing $T_{m\,III}$ = 175°C and $T_{m\,I}$ = 192°C.

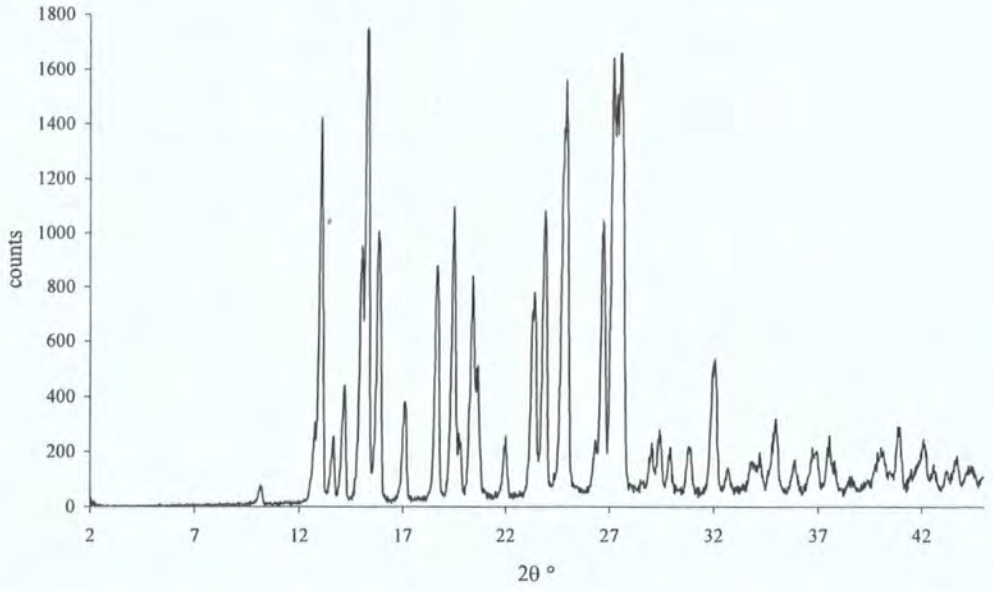

Figure 3.11: XRPD of the form III of crystalline carbamazepine.

The work of Grzesiak et al.[7] shows that the symmetry of the unit cell of modification III of carbamazepine, as referenced by Krahn and Mielck[6], is P-monoclinic. This was confirmed by comparing the work of Harris et al.[8], figure 3.12, with the ^{13}C SSNMR spectrum of carbamazepine obtained at 125 MHz, ^{13}C frequency (figure 3.13).

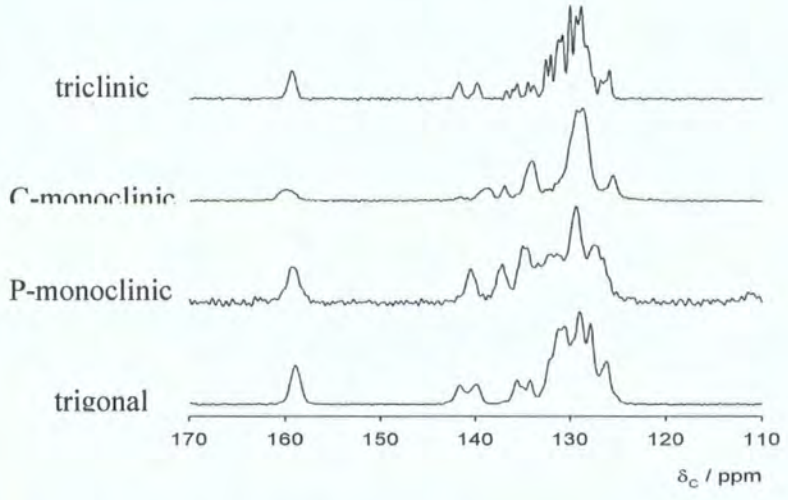

Figure 3.12: ^{13}C spectra of the four anhydrous forms of carbamazepine obtained at 125 MHz, ^{13}C frequency. The symmetry of the unit cell is specified for each spectra.

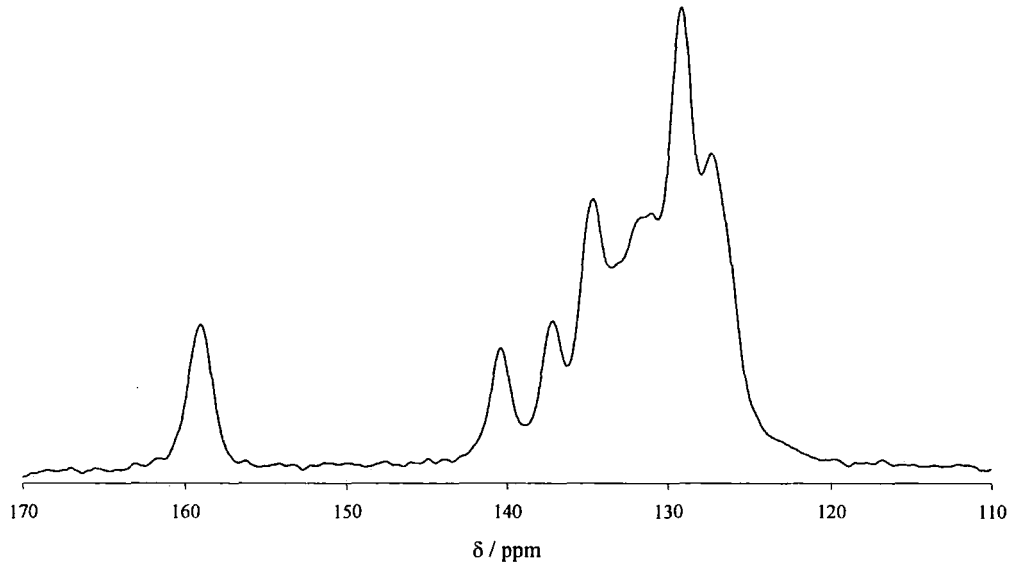

Figure 3.13: ^{13}C SSNMR spectrum of carbamazepine obtained at 125 MHz, ^{13}C frequency, showing only the high-frequency part of the spectrum.

The solid-state phase relationship of this compound is shown in figure 3.14. This confirms that the crystalline form of carbamazepine at room temperature is the same one as observed by XRPD.

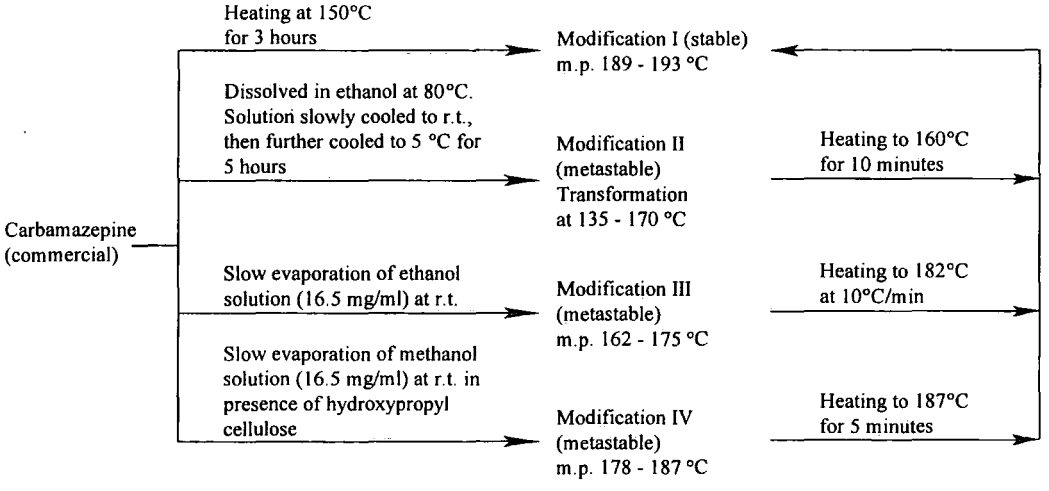

Figure 3.14: Phase relationship of carbamazepine[7].

The conformation of the asymmetric unit of the modification III of carbamazepine is shown in figure 3.15. The unit cell of this polymorph is shown in figure 3.16.

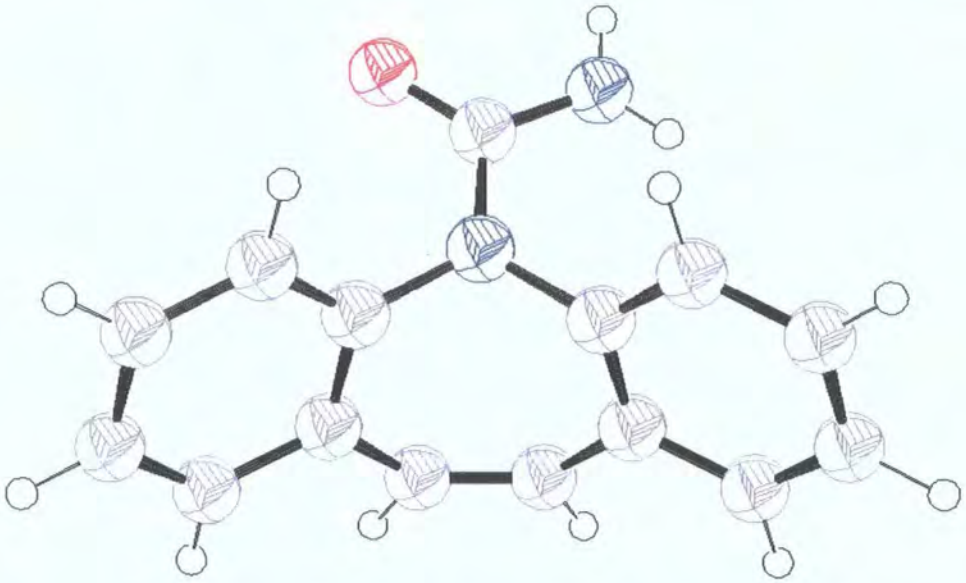

Figure 3.15: Conformation of the asymmetric unit of the modification III of carbamazepine. This crystal has one molecule per asymmetric unit and four molecules per unit cell[6].

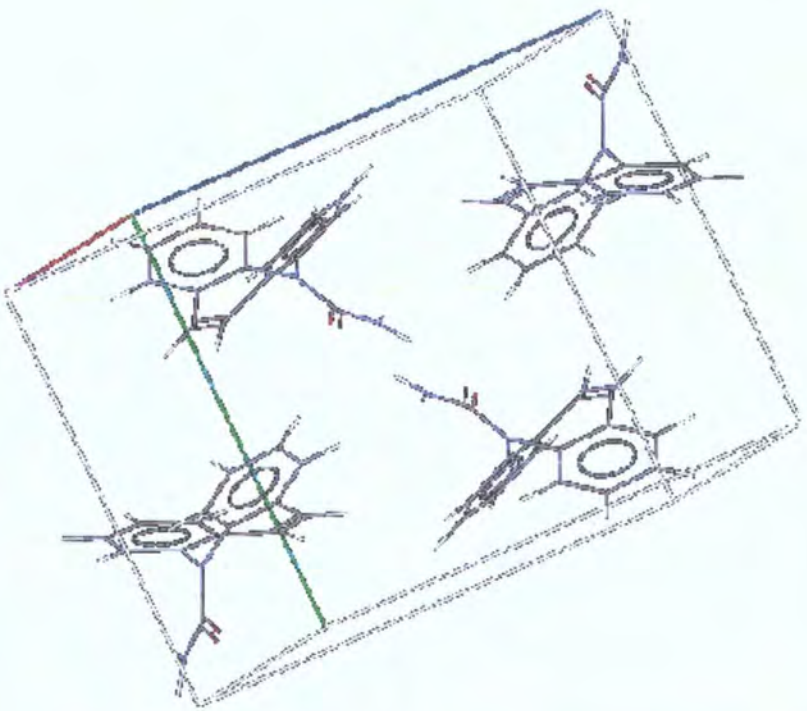

Figure 3.16: Unit cell of modification III of carbamazepine.

2/ Results

2.1/ Solution-state NMR

The second-order effect was investigated for the proton spectra using equation 3.1[9].

$$\nu_A - \nu_B = [(\nu_1 - \nu_4)(\nu_2 - \nu_3)]^{1/2} \qquad \textbf{Equation 3.1}$$

where, ν_A represents the true chemical shift of spin A, ν_B represents the true chemical shift of spin B and ν_1, ν_2, ν_3 and ν_4 are the four lines of the AB system from high frequency to low frequency. This is shown in figure 3.17:

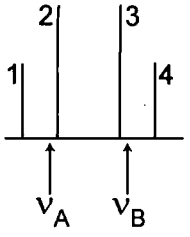

Figure 3.17: Representation of the second order effect on an AB spin system.

However, the deviations from first-order are so negligible in all three cases, ca. 0.2 Hz, that the results given in table 3.1, table 3.4 and table 3.5 show the centres of the doublets rather than the corrected value.

2.1.1) Indomethacin

The proton and carbon spectra are shown in figure 3.18 and figure 3.19 respectively. The assignments of these spectra are shown in table 3.1. The numbering is the same as that shown in chapter Two.

In order to do the assignment of the ^{13}C and ^{1}H spectra, the following procedure was used. First, the proton spectrum was assigned using tables[10], which allowed the assignment of the methyl and aromatic protons. Then, the COSY spectrum was used to assign the protons of the aromatic ring with the methoxy group attached to it, as shown in figure 3.20. Then, the carbon spectrum was assigned using tables[10] and the HSQC spectrum; this is illustrated in figure 3.21 and figure 3.22. Finally, the carbon spectrum was fully assigned using the HMBC spectrum, as shown in figure 3.23.

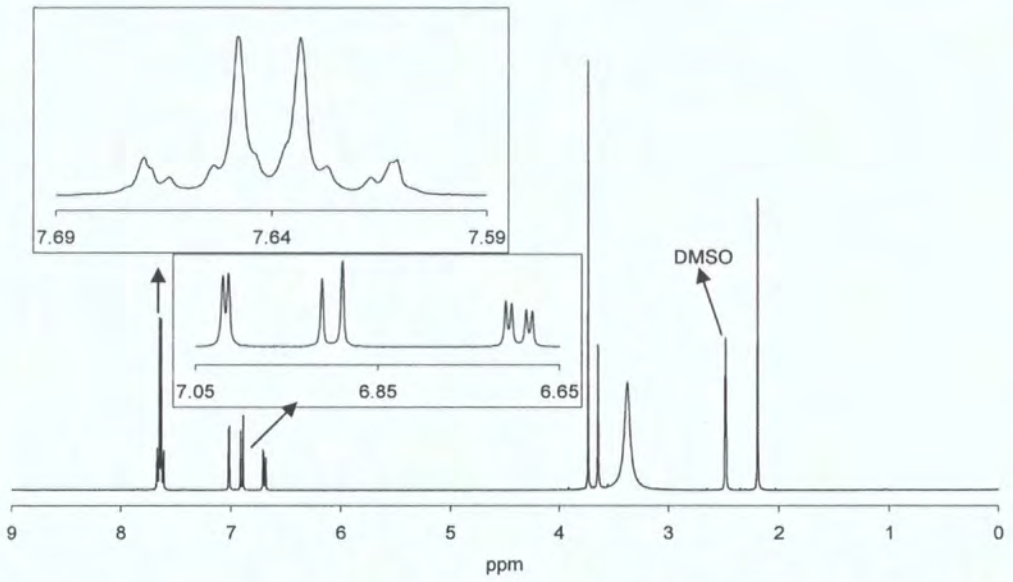

Figure 3.18: Indomethacin proton spectrum, in d_6-DMSO. The insets show the expansion of the aromatic protons. For a more detailed look at the 7.6-7.7 ppm region, see Table 3.3 and its preceding text.

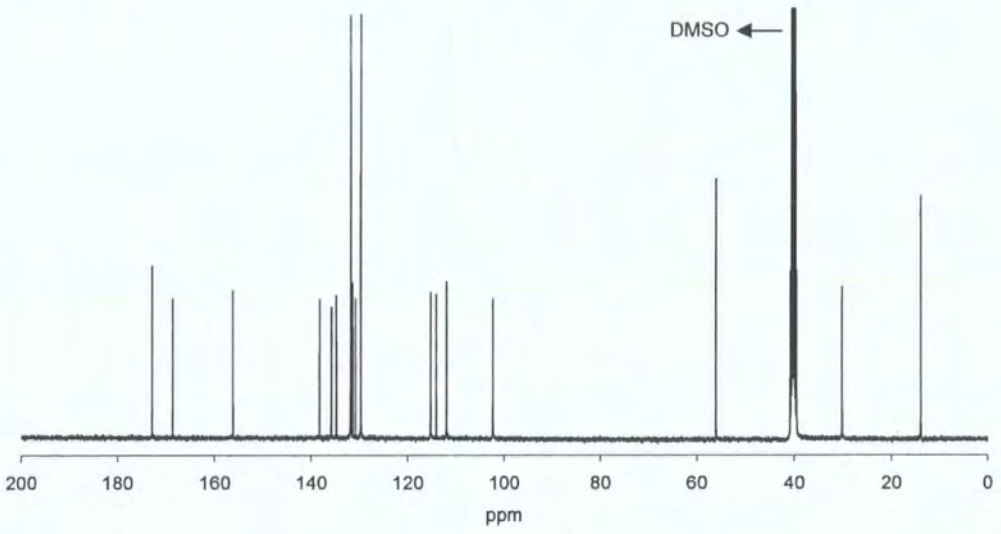

Figure 3.19: Indomethacin carbon spectrum, in d_6-DMSO.

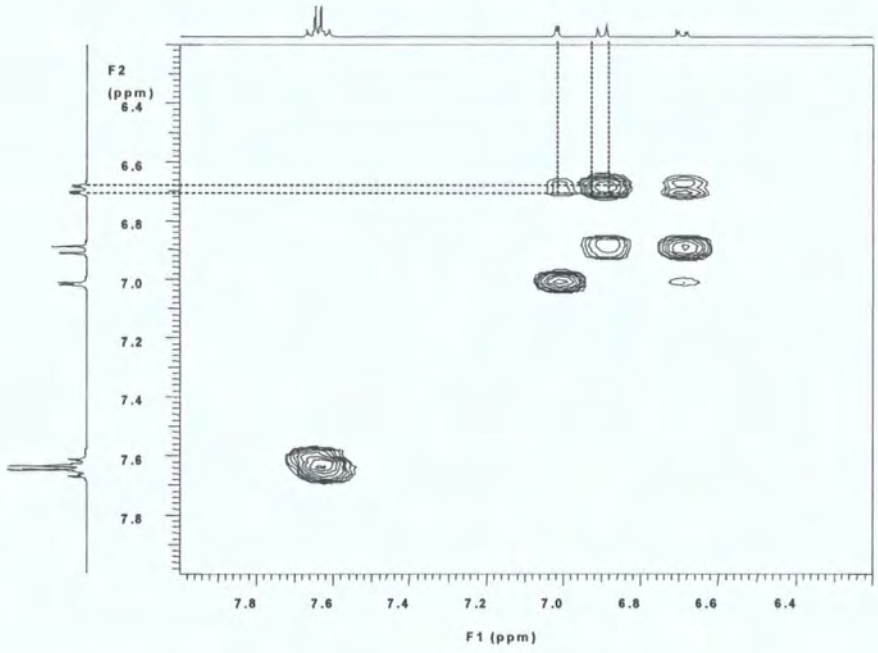

Figure 3.20: COSY spectrum of indomethacin, in d_6-DMSO, showing the high-frequency part.

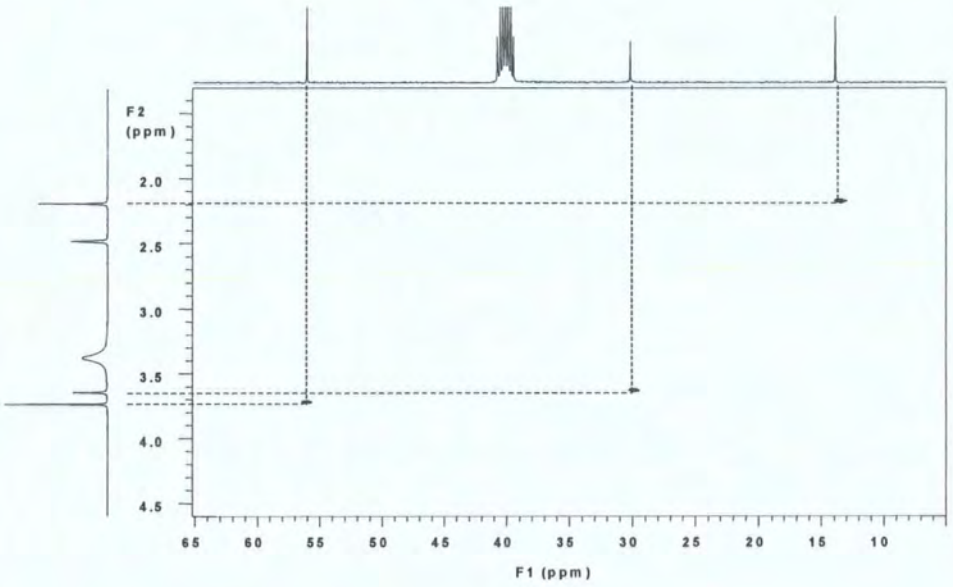

Figure 3.21: HSQC spectrum of indomethacin, in d_6-DMSO, showing the low-frequency part.

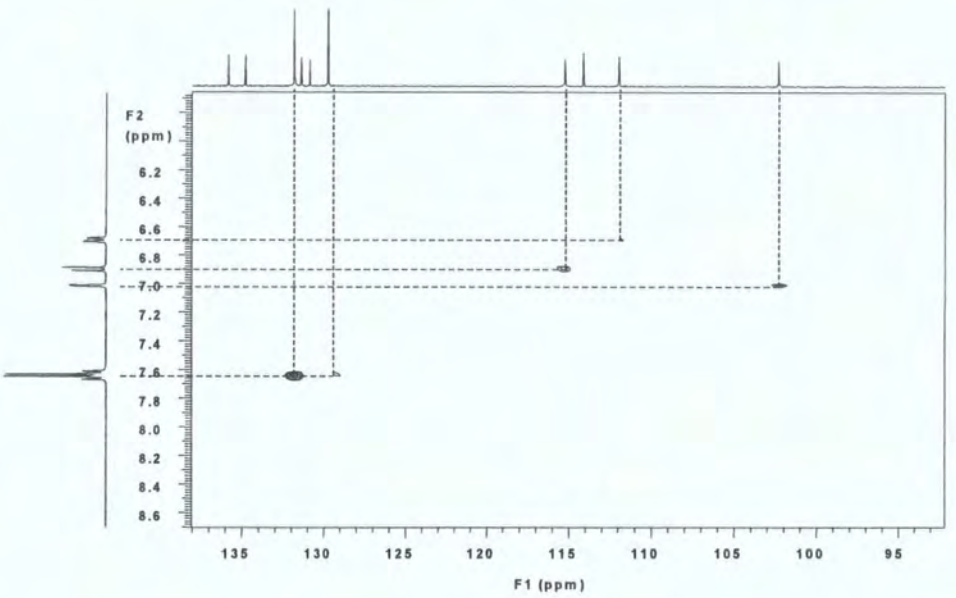

Figure 3.22: HSQC spectrum of indomethacin, in d_6-DMSO, showing the high-frequency part.

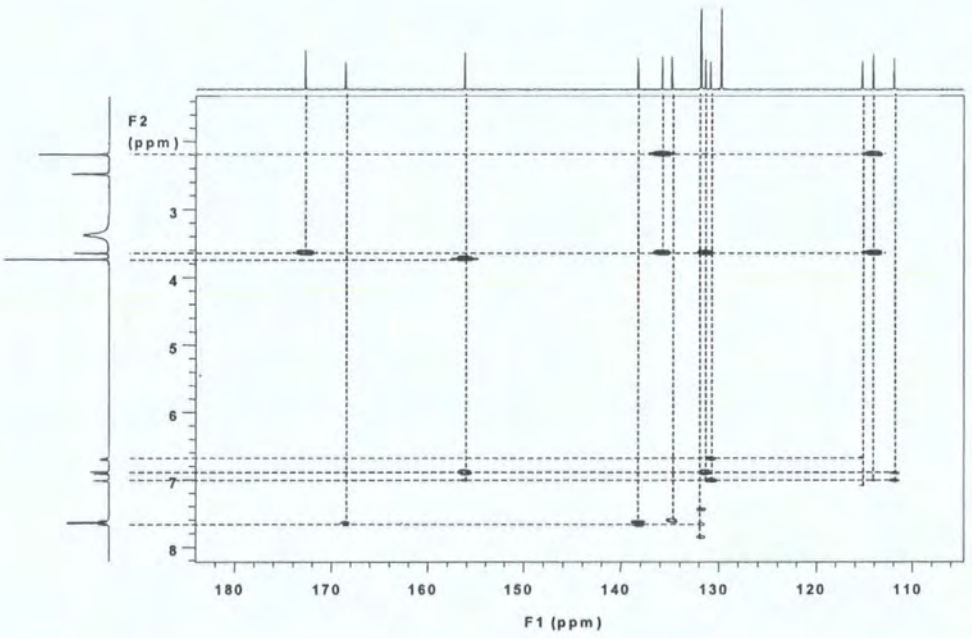

Figure 3.23: HMBC spectrum of indomethacin, in d_6-DMSO. F1: high-frequency only.

The broad singlet observed for indomethacin at 3.4 ppm is due to the acidic proton, but one would expect such a proton to show at around 10 ppm. However, the sample was prepared in DMSO and proton exchange can occur between the acidic proton and the protons of the residual water. Furthermore, if the amount of water present in the NMR tube, mainly associated with the solvent, is far higher than the amount of the acidic proton, then this proton will show a signal at a position near that for the water in DMSO.

^{1}H		
Multiplicity	Chemical shift / ppm	Atom number
singlet	2.20	17
broad singlet	3.38	Water in DMSO [a]
singlet	3.64	18
singlet	3.74	20
doublet of doublets	6.69	7
doublet	6.90	8
doublet	7.02	5
second order multiplet	7.61-7.67	12, 13, 15, 16

^{13}C		
Multiplicity	Chemical shift / ppm	Atom number
Singlet	13.3	17
Singlet	29.6	18
Singlet	55.4	20
Singlet	101.7	5
Singlet	111.4	7
Singlet	113.5	3
Singlet	114.6	8
Singlet	129.1	13, 15
Singlet	130.2	9
Singlet	130.8	4
Singlet	131.2	12, 16
Singlet	134.2	11
Singlet	135.2	2
Singlet	137.7	14
Singlet	155.6	6
Singlet	167.9	10
Singlet	172.2	19

J coupling [b]	
Chemical shift / ppm	J / Hz
6.69	$J_{7\text{-}8} = 8.8$
6.69	$J_{7\text{-}5} = 2.5$
6.90	$J_{8\text{-}7} = 8.8$
7.02	$J_{5\text{-}7} = 2.5$

[a] Note that the peak at 3.38 ppm includes the acidic proton, see text.

[b] Note that the value of J5-8 is too small and as such it cannot be resolved. The J couplings for the second order multiplet are shown in table 3.3.

Table 3.1: ^{1}H and ^{13}C chemical shifts with assignment and $J_{H\text{-}H}$ of indomethacin.

The Chemical Database Service (CDS) was checked in order to confirm the assignments. This showed a good agreement with the experimental, although some of the ^{1}H and/or ^{13}C assignments differed from "predicted" assignments. This was caused by the way the database looks for atoms with similar environments and for

some cases the number of matches is low. Therefore, the assignment was considered as inaccurate and the experimental assignment was used, see table 3.2 for the comparison on indomethacin. The comparisons for nifedipine and carbamazepine are shown in appendices 8 and 12 respectively. The difference between the database and the experimental values could also be due to the use of a different solvent.

^{1}H database[11]			^{1}H experimental	
Atom number	Chemical shift / ppm	Number of matches	Atom number	Chemical shift / ppm
17	2.45	1	17	2.19
18	3.68	4	OH	3.38
20	3.81	371	18	3.64
7	6.61	1	20	3.74
8	6.89	1	7	6.69
5	7.17	1	8	6.90
13, 15	7.45	8	5	7.02
12, 16	7.56	2	12, 13, 15, 16	7.61-7.67
OH	12.05	2		

^{13}C database[11]			^{13}C experimental	
Atom number	Chemical shift / ppm	Number of matches	Atom number	Chemical shift / ppm
17	18.9	3	17	13.3
18	39.3	1	18	29.6
20	55.2	13	20	55.4
5	100.3	3	5	101.7
3	103.2	2	7	111.4
7	111.4	2	3	113.5
8	124.2	2	8	114.6
4	127.6	33	13, 15	129.1
12, 16	128.2	10	9	130.2
13, 15	128.7	10	4	130.8
11	134.2	122	12, 16	131.2
14	137.6	37	11	134.2
			2	135.2
9	145.5	2	14	137.7
6	153.6	3	6	155.6
10	168.2	231	10	167.9
19	175.0	1	19	172.2

The author which to acknowledge the use of the EPSRC's Chemical Database Service (CDS) at Daresbury.

Table 3.2: Comparison between the experimental results and the database predictions for the assignment of ^{1}H and ^{13}C in the case of indomethacin.

Another problem occurs in the ^1H spectrum of indomethacin. The protons from the phenylene ring (attached to the chlorine) show a second-order multiplet centred at around 7.64 ppm that is difficult to interpret. In order to get more information, an experiment was done with indomethacin in d_6-acetone using the Varian Inova 500 spectrometer. This experiment shows an $[AB]_2$ pattern, see figure 3.24 (bottom). Abraham[12] gives a method to interpret such second-order patterns, which was used to gain a set of data for the different J couplings involved. These values were obtained on the assumptions that $J_{12\text{-}16}$ and $J_{13\text{-}15}$ are equal, and that $J_{12\text{-}15}$ and $J_{13\text{-}16}$ are negligible. Then this set of J coupling values was used to do a simulation, which was slightly different from the experimental. However, when looking at the simulation with a reduced linewidth, it was possible to see that $J_{12\text{-}16}$ and $J_{13\text{-}15}$ are slightly different. The results shown in table 3.3 give the final data used to do the simulation, and the comparison between simulation and experiment is shown in figure 3.24.

$J_{12\text{-}16} = 2.4$ Hz
$J_{12\text{-}13} = 8.5$ Hz
$J_{12\text{-}15} = 0$ Hz
$J_{16\text{-}13} = 0$ Hz
$J_{16\text{-}15} = 8.5$ Hz
$J_{13\text{-}15} = 2$ Hz
$\delta_{12} = \delta_{16} = 7.76$ ppm
$\delta_{13} = \delta_{15} = 7.66$ ppm

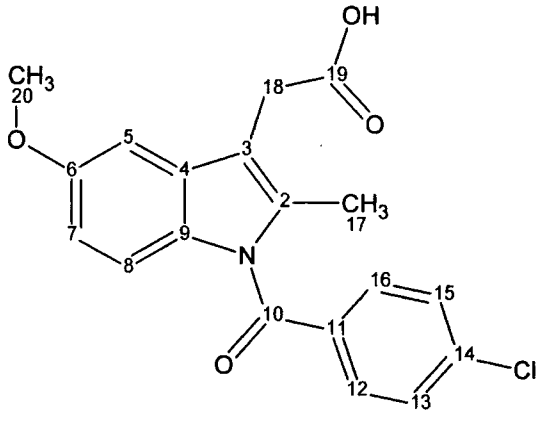

Table 3.3: This table shows the J coupling and the assignment of the protons attached to the para-substitued benzene ring.

It should be noted that the values of $J_{12\text{-}15}$ and $J_{13\text{-}16}$ used for the simulation were set to 0 Hz. This was because the effect of these couplings is too small to be resolved within the experimental linewidths, in this case about 1 Hz. However, for the experimental, these values should be mentioned as less than the linewidths.

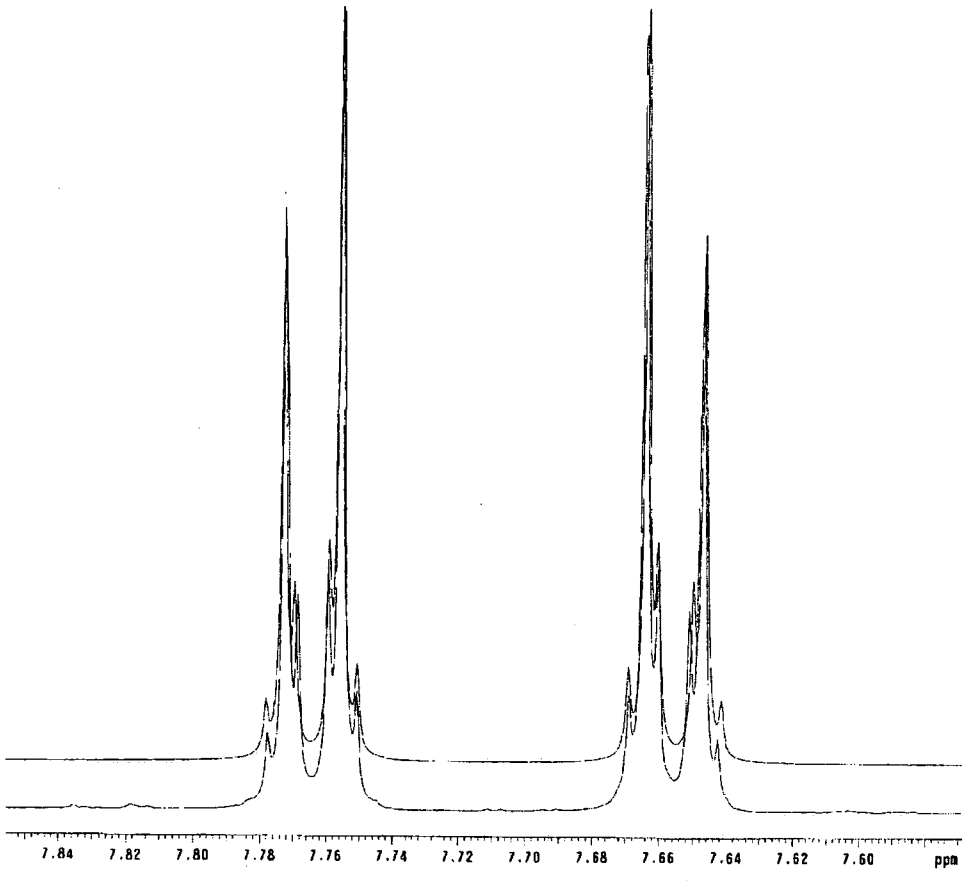

Figure 3.24: Comparison between experimental (bottom) and simulation (top) spectra of indomethacin in deuterated acetone, showing only the region of the para-substitued benzene protons.

2.1.2) Nifedipine

The ^{1}H and ^{13}C spectra of nifedipine are shown in figure 3.25 and figure 3.26 respectively. The assignment was carried out in the same manner as for indomethacin and the numbering is the same as that used in chapter Two. The COSY, HSQC and HMBC spectra are shown in appendices 5, 6 and 7 respectively. The assignments and J coupling are shown in table 3.4.

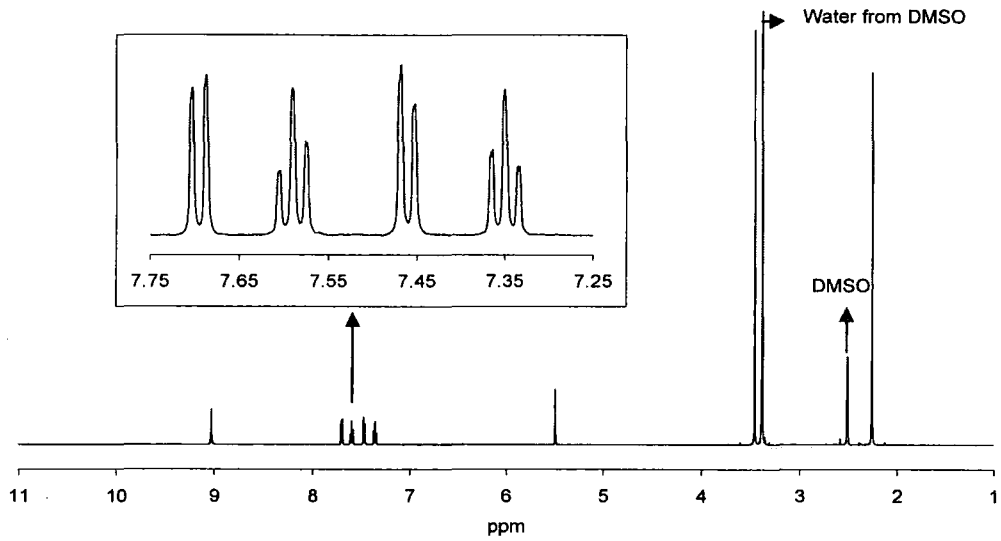

Figure 3.25: Nifedipine proton spectrum, in d_6-DMSO. The inset shows an expansion of the aromatic protons.

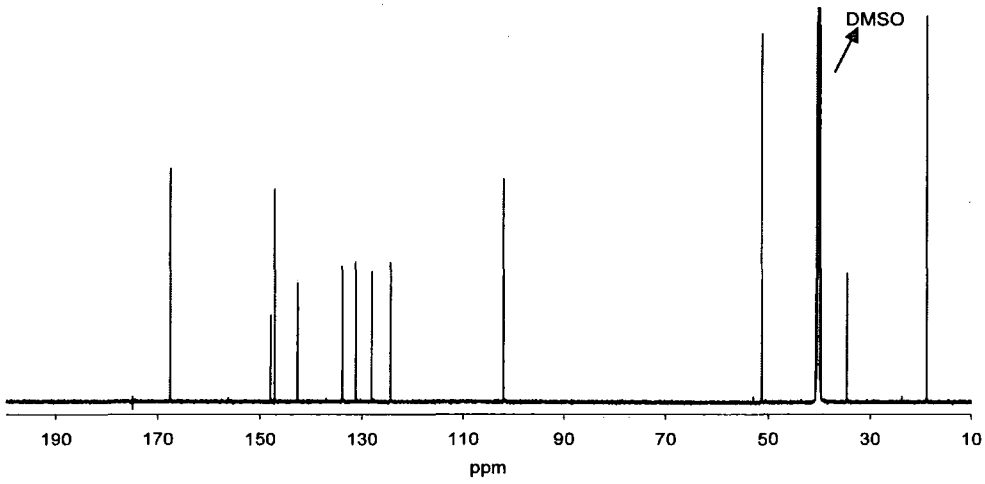

Figure 3.26: Nifedipine carbon spectrum, in d_6-DMSO.

^1H		
Multiplicity	Chemical shift / ppm	Atom number
singlet	2.25	2', 6'
singlet	3.45	3", 5"
singlet	5.49	4
triplet	7.35	10
doublet	7.46	8
triplet	7.59	9
doublet	7.70	11
singlet	9.03	NH

^{13}C		
Multiplicity	Chemical shift / ppm	Atom number
singlet	18.9	2', 6'
singlet	34.6	4
singlet	51.3	3", 5"
singlet	102.0	3, 5
singlet	124.3	11
singlet	128.1	10
singlet	131.3	8
singlet	133.9	9
singlet	142.7	7
singlet	147.2	2, 6
singlet	147.9	12
singlet	167.6	3', 5'

J coupling	
Chemical shift / ppm	J / Hz
7.35	$J_{10\text{-}11} = J_{10\text{-}9} = 7.5$
7.46	$J_{8\text{-}9} = 7.5$
7.59	$J_{9\text{-}10} = J_{9\text{-}8} = 7.5$
7.70	$J_{11\text{-}10} = 7.5$

Table 3.4: ^1H and ^{13}C chemical shifts with assignment and $J_{H\text{-}H}$ of nifedipine.

2.1.3) Carbamazepine

The ^1H and ^{13}C spectra of carbamazepine are shown in figure 3.27 and figure 3.28 respectively. The assignment was carried out in the same manner as for indomethacin and the numbering is the same as that used in chapter Two. The COSY, HSQC and HMBC spectra are shown in appendices 9, 10 and 11 respectively. The assignments and J coupling are shown in table 3.5.

The broad singlet observed at 4.8 ppm is probably due to proton exchange. This could also have been caused by rapid internal motion about the N-CO(NH_2) bond.

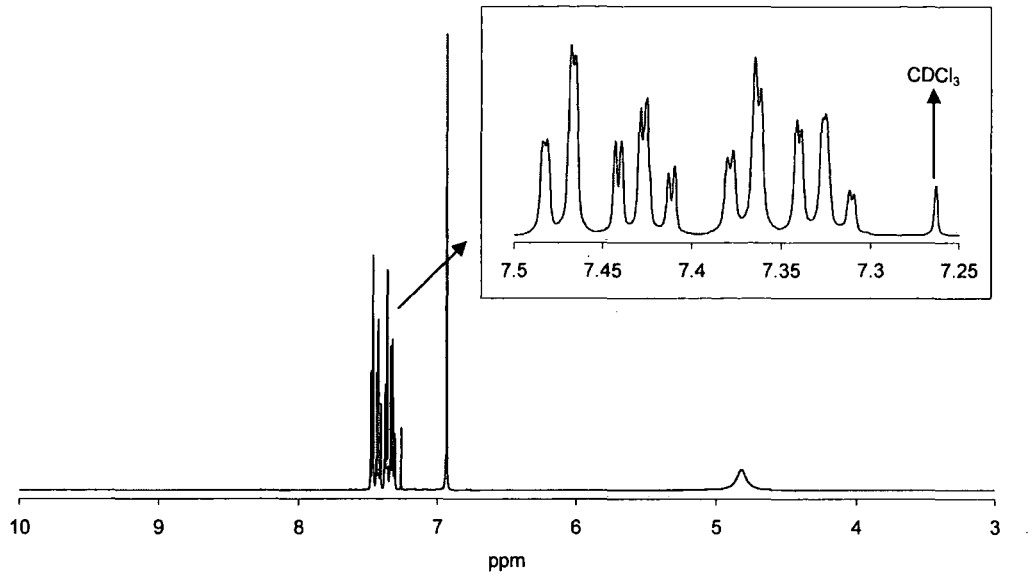

Figure 3.27: Carbamazepine proton spectrum, in $CDCl_3$. The inset shows an expansion of the aromatic protons.

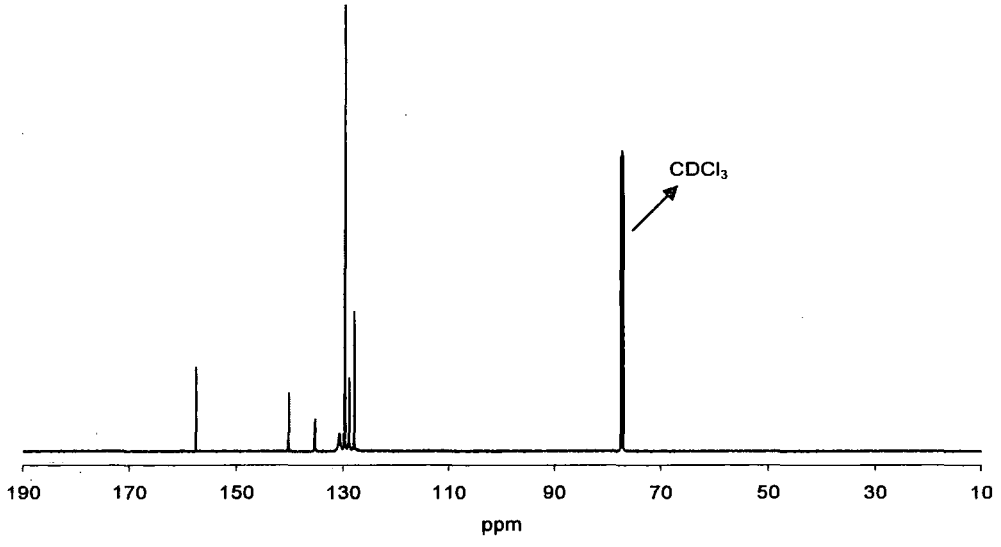

Figure 3.28: Carbamazepine carbon spectrum, in $CDCl_3$.

^{1}H		
Multiplicity	Chemical shift / ppm	Atom number
broad singlet	4.82	NH2
singlet	6.94	7, 8
doublet of triplets	7.33	4, 11
doublet of doublets	7.37	5, 10
doublet of triplets	7.43	3, 12
doublet of doublets	7.47	2, 13

^{13}C		
Multiplicity	Chemical shift / ppm	Atom number
singlet	128.0	4, 11
singlet	129.0	2, 13
singlet	129.7	3, 12
singlet	129.8	5, 10
broad singlet	130.7	7, 8
singlet	135.2	6, 9
singlet	140.2	1, 14
singlet	157.5	15

J coupling	
Chemical shift / ppm	J / Hz
7.33	$J_{4-2} = J_{11-13} = 0.75$
7.33	$J_{4-3} = J_{11-12} = 7.5$
7.33	$J_{4-5} = J_{11-10} = 7.5$
7.37	$J_{5-3} = J_{10-12} = 1.5$
7.37	$J_{5-4} = J_{10-11} = 7.5$
7.43	$J_{3-5} = J_{12-10} = 1.5$
7.43	$J_{3-4} = J_{12-11} = 7.5$
7.43	$J_{3-2} = J_{12-13} = 7.5$
7.47	$J_{2-3} = J_{13-12} = 7.5$
7.47	$J_{2-4} = J_{13-11} = 0.75$

Table 3.5: ^{1}H and ^{13}C chemical shifts with assignment and J_{H-H} of carbamazepine.

2.2/ SSNMR

2.2.1) Indomethacin

2.2.1.1) ^{1}H spectrum

A fast MAS ^{1}H spectrum was acquired using the HX 2.5 mm probe on the 500 MHz spectrometer, see figure 3.29. The peak at 12.6 ppm is due to the acidic proton and oxygen forming a hydrogen bond, the peak at 6.2 ppm is due to the aromatic protons and the peak at 2.3 ppm is due to the remaining protons.

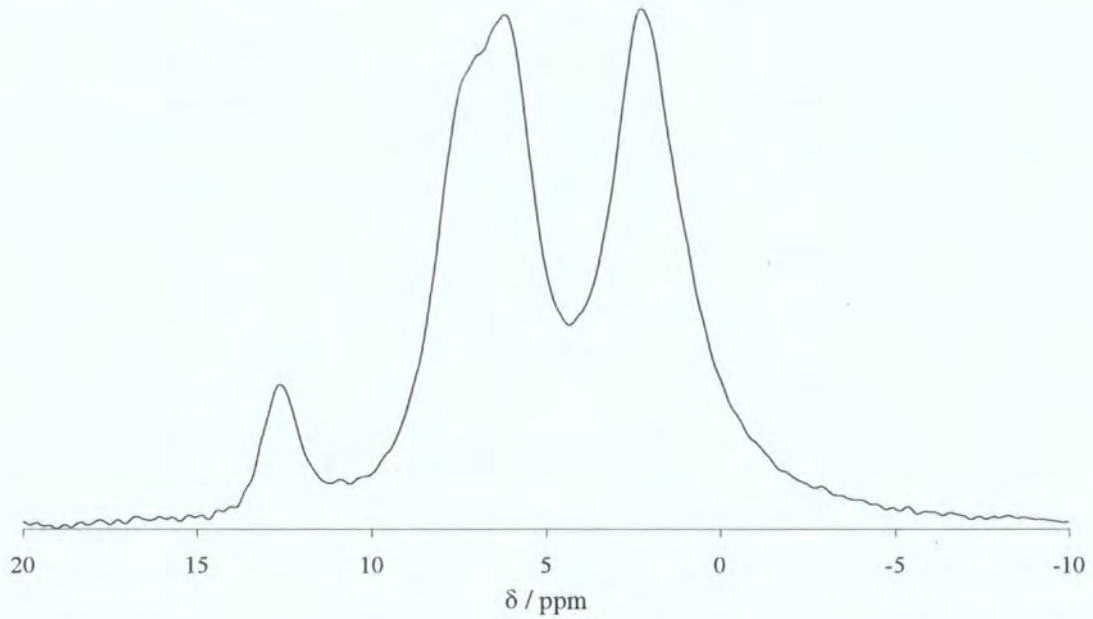

Figure 3.29: ^{1}H spectrum of crystalline indomethacin, acquired at 500 MHz ^{1}H frequency, spinning at 27 kHz.

2.2.1.2) ^{13}C spectra

The ^{13}C SSNMR spectrum of crystalline indomethacin was acquired using CPMAS and NQS (figure 3.30) techniques. The assignments, shown in table 3.6, were made using the solution-state results as well as the CPMAS and NQS spectra.

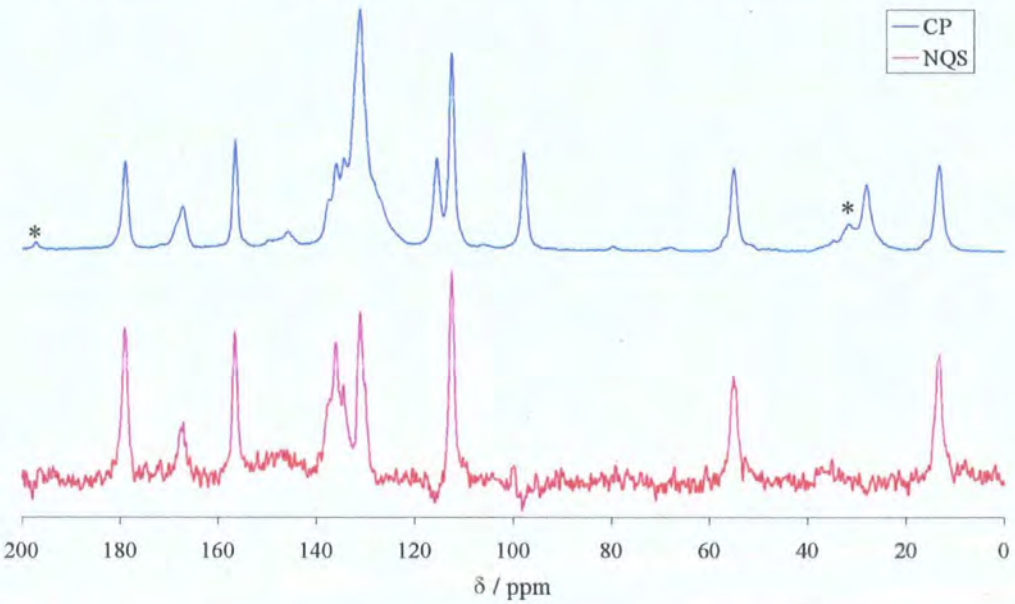

Figure 3.30: CP and NQS ^{13}C spectra of the γ-form of indomethacin obtained at 50.32 MHz, ^{13}C frequency. The asterisks show the spinning sidebands.

It would seem that signals from C-12, C-13, C-15 and C-16 of indomethacin cannot be resolved, which may indicate rapid internal rotation on the NMR timescale of the phenylene group about its axis, even in the solid state at ambient temperature (which would render these carbons equivalent in pairs: C-12/16 and C-13/15). However, spectra at –80°C are not significantly different from those at 25°C (data not shown).

Atom numbers	Solid-state NMR / ppm	Difference [a] / ppm
19	179.1	6.9
10	167.3	–0.6
6	156.7	1.1
14	139.0 [b]	1.3
2	131.2-137.4	-
11	131.2-137.4	-
12	131.2-137.4	-
16	131.2-137.4	-
4	131.2-137.4	-
9	131.2-137.4	-
13	131.2-137.4	-
15	131.2-137.4	-
8	115.6	1.0
3	112.6	–0.9
7	112.6	1.2
5	97.9	–3.8
20	55.2	–0.2
18	28.2	–1.4
17	13.4	0.1

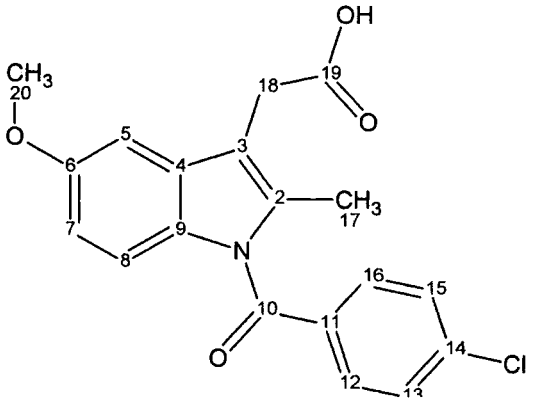

[a] For the solution-state NMR chemical shifts, see table 3.1. The difference is from solid to solution.

[b] Estimated to be at 139.0 ppm from a spectrum obtained using a Varian InfinityPlus 700 spectrometer.

Table 3.6: ^{13}C SSNMR assignments of the γ-form of indomethacin.

The two main differences observed between solution-state and solid-state are for the carbon atoms 19 and 5. The difference for the carbon 19 is explained by the presence of a hydrogen bond. The difference for the carbon 5 can be explained by the fact that the methoxy group is not freely rotating along the aromatic-oxygen bond. Therefore, it is "fixed" into the position shown in table 3.6. This, in turn, changes the chemical shift of the carbon 5.

VT ^{13}C SSNMR experiments have been carried out on crystalline indomethacin between 25°C and 150°C (data not shown). The spectra did not show any significant differences throughout the range of temperatures.

2.2.1.3) Quadrupolar effect - Introduction

When the ^{13}C spectrum of indomethacin was acquired at 50.3 MHz, it was noticed that the resonance of the carbon attached to the chlorine atom, i.e. atom 14, had a peculiar shape. This arises from dipolar coupling to the quadrupolar chlorine nuclei. Chlorine nuclei have a non-zero electric quadrupole moment in the ground state. Such nuclei have transition frequencies between energy levels in the order of MHz in the absence of a magnetic field (nuclear quadrupole resonance). These transition energies are dependent on the nuclear quadrupole moment and the Electric Field Gradient (EFG) tensor at the nucleus. In the solid state in the presence of a magnetic field, the quadrupolar coupling is not averaged out by motion of the sample. Thus, MAS cannot completely remove its effects, even if spinning is infinitely fast. Therefore, the spectrum of, for example, a carbon attached to a chlorine atom will be broadened compared to that of a carbon that is not attached. The shape of this peak is also complicated by the fact the chlorine has two isotopes with spin >½, i.e. ^{35}Cl and ^{37}Cl. It was understood that for indomethacin parts of the C-Cl bandshape were overlapped by other resonances. The same spectrum was acquired on the 300 MHz, 500 MHz, 700 MHz and 800 MHz spectrometers, to see if further information could be obtained. It was clearly visible from these spectra that the higher the field the more defined the band of this carbon atom becomes, as expected. Nevertheless, the true chemical shift of this carbon was needed and this was achieved by theoretical computation.

At high magnetic fields, when the quadrupolar interaction becomes less than the Zeeman interaction, perturbation theory may be invoked, and in the absence of scalar coupling a doublet splitting is predicted, as was indeed seen in the spectrum from the 800 MHz spectrometer (figure 3.31). However, in principle, each component of the doublet is a powder pattern. Moreover, isotropic scalar coupling leads to additional splittings. Such additional splitting is apparent in the high-frequency component of

the 700 MHz spectrum. At lower magnetic fields, perturbation theory is no longer applicable and the spectra become more complex, but they can still be computed.

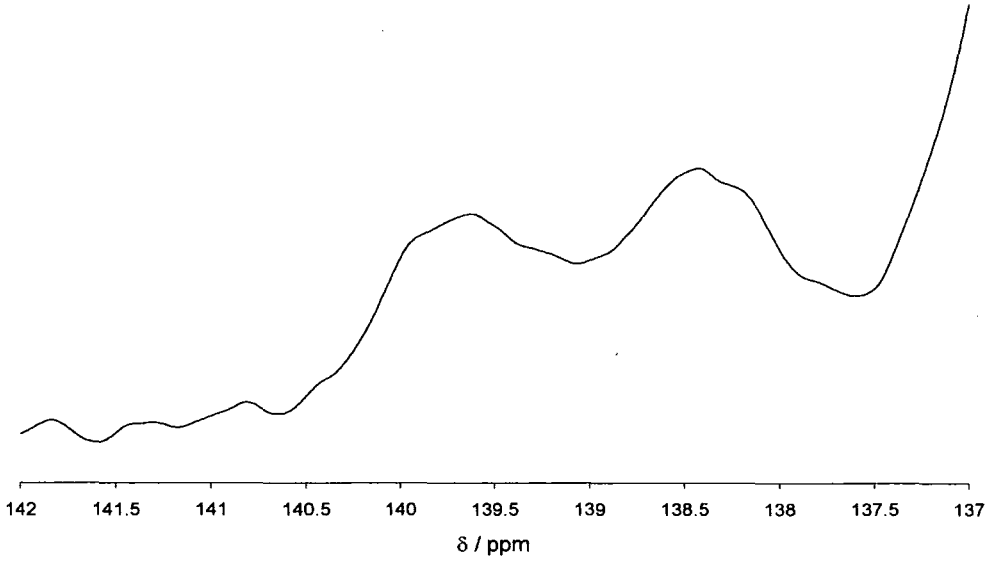

Figure 3.31: 800 MHz, ^{1}H frequency, spectrum of indomethacin showing the signals for the carbon attached to the chlorine.

2.2.1.4) Quadrupolar effect – Results

All the theoretical results show the weighted effect of ^{35}Cl and ^{37}Cl. This was done by adding both theoretical spectra at the correct percentage, i.e. 75.77 % for ^{35}Cl and 24.23 % for ^{37}Cl.

A program called "anychi-0", supplied by A.C. Olivieri, was used to find the theoretical shape of the peak representing the carbon atom attached to the chlorine. This program assumes that the EFG is axially symmetric (i.e. in the principal axis system the x and y components are identical) and that the quadrupolar and dipolar vectors are co-axial. In order to use this program some parameters need to be defined. They are:

- The quadrupolar coupling constant of the chlorine nuclei for this system (in MHz).
- The resonance frequency of the chlorine nuclei at the magnetic field used (in MHz).
- The isotropic coupling constant, J, (in units of D).
- The spectral width (in units of D).

– The Gaussian width to be used in the convolution (in units of D).

The dipolar coupling constant D between ^{13}C and ^{35}Cl (or ^{37}Cl) was calculated using equation 3.2:

$$D = \frac{\mu_0}{4\pi} h\gamma_C\gamma_{Cl} \frac{1}{4\pi^2 r^3} \qquad \textbf{Equation 3.2}$$

where μ_0 is the vacuum permeability, h is the Planck constant, γ_C is the magnetogyric ratio of ^{13}C, γ_{Cl} is the magnetogyric ratio of ^{35}Cl (or ^{37}Cl), and r is the distance between the carbon and chlorine atoms.

It is known that γ_C is 6.7282840 x 10^7 rad s^{-1} T^{-1}, γ_{Cl} is 2.624198 x 10^7 rad s^{-1} T^{-1} for ^{35}Cl and 2.184368 x 10^7 rad s^{-1} T^{-1} for ^{37}Cl, and r is 1.735 x 10^{-10} m. This gave D = 567 Hz for ^{35}Cl and D = 472 Hz for ^{37}Cl.

The quadrupolar coupling constant was first estimated using perturbation equation 3.3:

$$\chi = -\frac{10\Delta\nu_{Cl}}{3D} \qquad \textbf{Equation 3.3}$$

where Δ is half the splitting between the two peaks for the carbon attached to the chlorine (in Hz), ν_{Cl} is the frequency of ^{35}Cl (or ^{37}Cl) at a given magnetic field, and χ is the quadrupolar coupling constant of ^{35}Cl (or ^{37}Cl). It should be noted that in principle, D should be written D_{eff}, where $D_{eff} = D - \frac{\Delta J}{3}$. However, in this study it was considered that ΔJ was negligible (but see later). Therefore, $D_{eff} \approx D$.

It is known that the experimental value Δ at 700 MHz is 181Hz, measured between the maximum of the single peak and the highest-frequency part of the doublet, and ν_{Cl} is 68.66 MHz for ^{35}Cl, at 700 MHz proton frequency. This gave χ = –73 MHz, which is in reasonable accordance with the literature[13]. From χ, a value of R was calculated using the following equation: $R = \left|\frac{\chi}{\nu_s}\right|$ [14]. This gave a value of 1.06, which is slightly above that where perturbation theory applies (0<R<1). However, because the error is expected to be only ca. 1% the value of –73 MHz was used for further work.

The value of $J_{C\text{-}Cl}$ was needed. It was found in the literature[15] that this is –20 Hz for a chloroketosulfone. Therefore, this value was used in the computation before being optimised. A value of 5674 Hz was used for the spectrum width and the Gaussian

width was set to 100 Hz. These values needed to be in units of D, thus they were as follows for ^{35}Cl:

- J: –0.035 units of D for ^{35}Cl, or –0.042 units of D for ^{37}Cl.
- Spectrum width: 10 units of D for ^{35}Cl, or 12 units of D for ^{37}Cl.
- Gaussian width: 0.176 units of D for ^{35}Cl, or 0.212 units of D for ^{37}Cl.

This gave the theoretical spectrum shown in figure 3.32, but this did not fit well with the experimental spectrum. Therefore, the value of J was varied and, when using a value of –45 ± 5 Hz, the spectrum shown in figure 3.33 was simulated. It was then observed that the splitting between the singlet and the doublet was larger for the theory than the experiment. Therefore, the value of χ and so the value of Δ were revisited. It was then decided to measure Δ between the maximum of the low frequency peak and the middle of the doublet. This gave a value of Δ of 156 Hz, which in turn, using equation 3.3, gave a value of χ of –63 MHz, for which a value of R was calculated to be 0.916, which fits with perturbation theory. The result is shown in figure 3.34. It was then observed that the splitting of the low field peak was slightly larger for the theory than for the experiment and the value of J was optimised again and found to be –43 Hz ± 5 Hz, though this value may be greater in error because the fit is not good. The result is shown in figure 3.35.

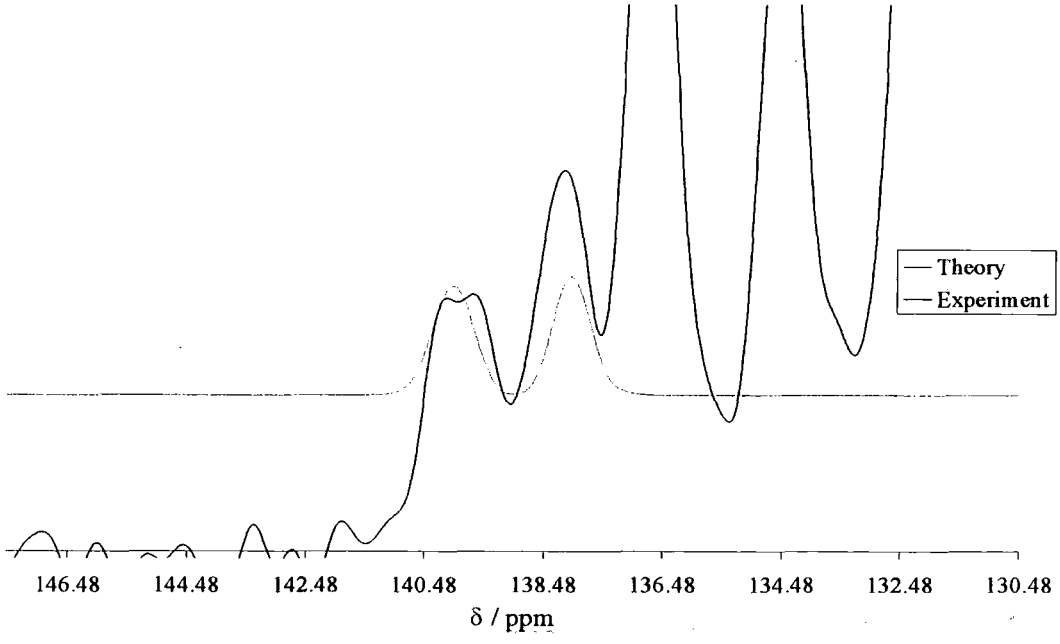

Figure 3.32: Theory versus experimental at 175.96 MHz, ^{13}C frequency, of C-14, J = –20 Hz and χ = –73 MHz.

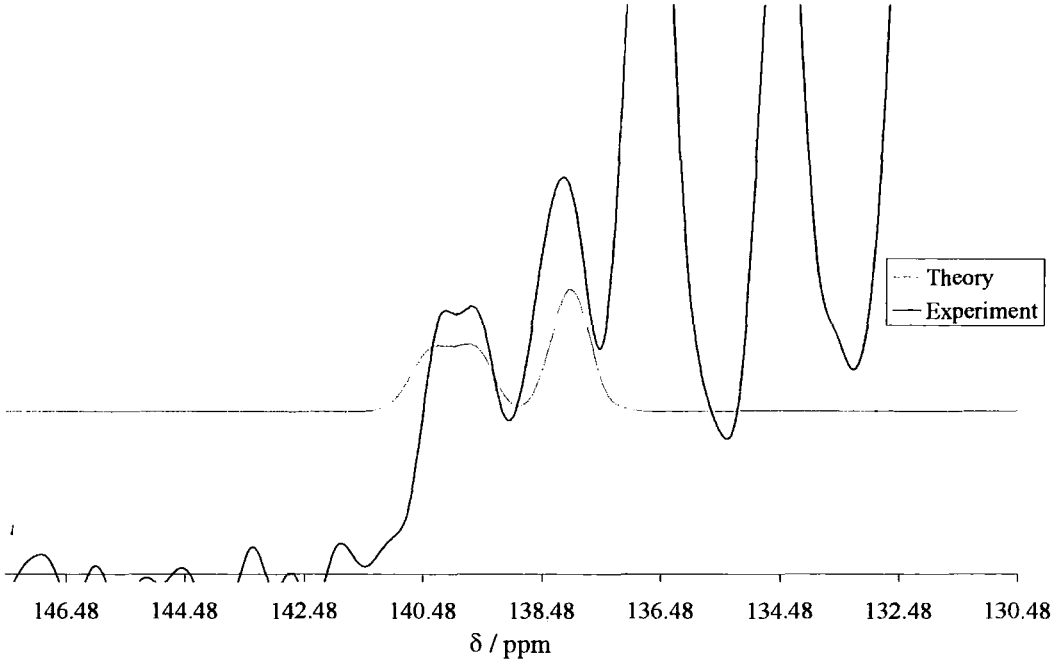

Figure 3.33: Theory versus experimental at 175.96 MHz, ^{13}C frequency, of C-14, J = –45 Hz and χ = –73 MHz.

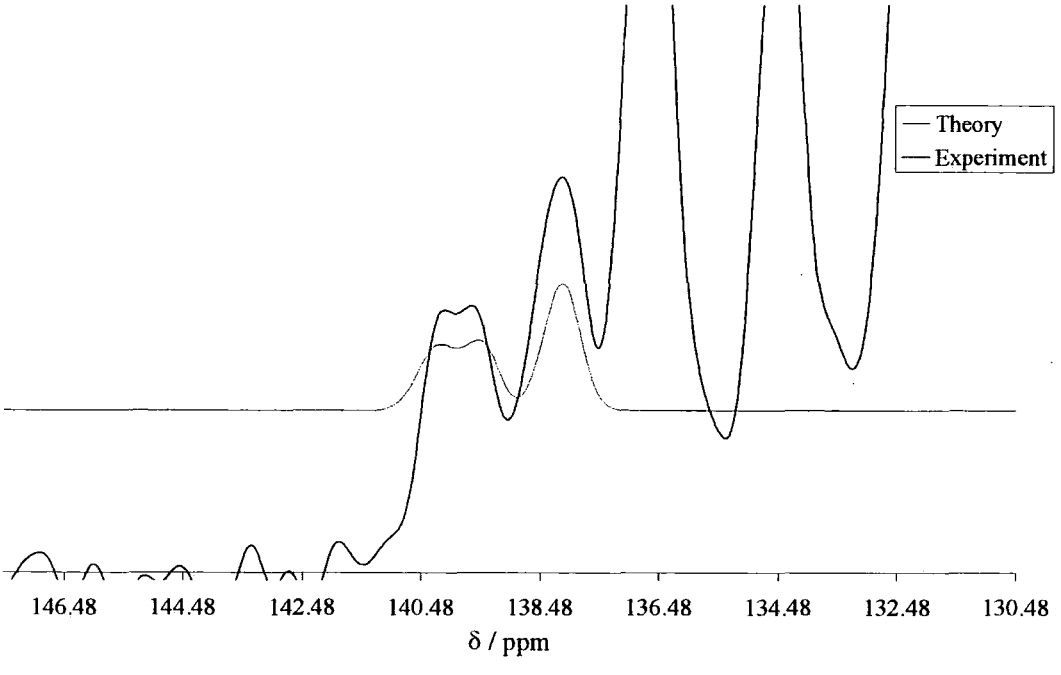

Figure 3.34: Theory versus experimental at 175.96 MHz, ^{13}C frequency, of C-14, J = –45 Hz and χ = –63 MHz.

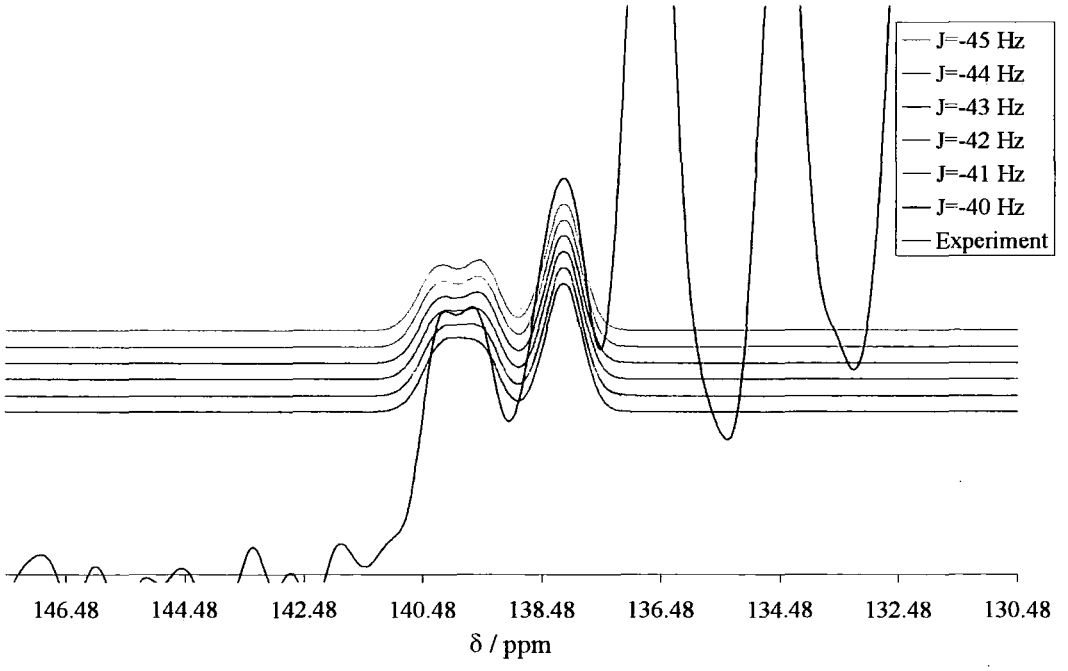

Figure 3.35: Theory versus experimental at 175.96 MHz, ^{13}C frequency, of C-14, $\chi = -63$ MHz.

The theory was then computed using the following values:

- $\chi = -63$ MHz
- $\nu_{Cl} = 68.66$ MHz for ^{35}Cl, or 57.16 MHz for ^{37}Cl.
- J: –0.076 units of D for ^{35}Cl, or -0.091 units of D, for ^{37}Cl.
- Spectrum width: 10 units of D for ^{35}Cl, or 12 units of D for ^{37}Cl.
- Gaussian width: 0.176 units of D, or 0.212 units of D for ^{37}Cl.

The final result is shown in figure 3.36. This fitted reasonably the experimental observation. Then, the same computation was repeated at 200 MHz, 300 MHz, 500 MHz and 800 MHz proton frequencies; the results are shown in figure 3.37. This is in good agreement with the experimental, see figure 3.38. The case-by-case comparison between the theory and the experimental at 200 MHz, 300 MHz, 500 MHz and 800 MHz is shown in appendices 13, 14, 15 and 16 respectively.
These calculations allowed to determine the true chemical shift of the carbon attach to the chlorine to be 139 ± 0.2 ppm.

It is possible that the splitting in the high-frequency doublet component at 700 MHz is an artefact arising from the relatively high noise level. A spectrum was obtained using an 800 MHz spectrometer (figure 3.31). Whilst this shows no such splitting, the available resolution is not good so the result is not definitive. Therefore, the main conclusion about scalar coupling is that its magnitude cannot be greater than 45 Hz, and the probable value is ca. –43 Hz.

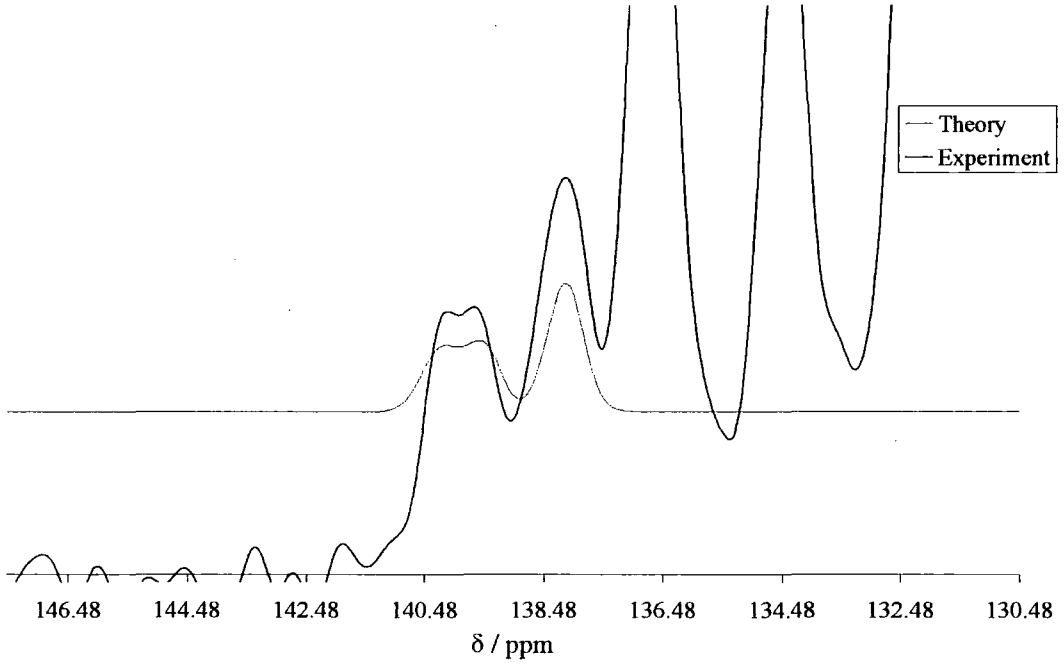

Figure 3.36: Theory versus experimental at 175.96 MHz, ^{13}C frequency, of C-14, J = –43 Hz and χ = –63 MHz.

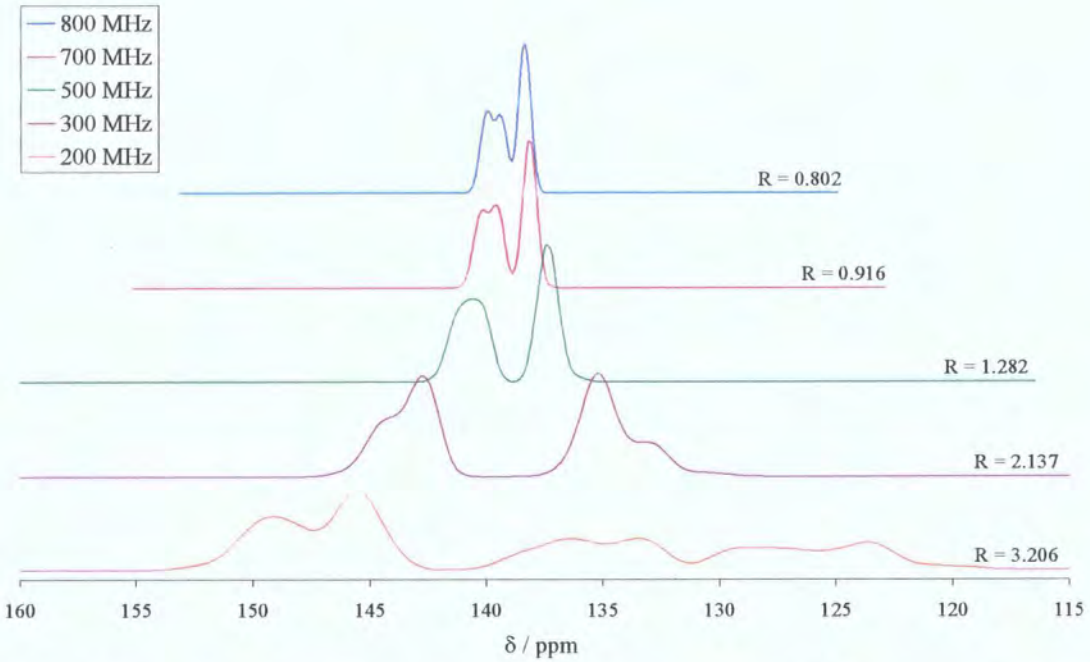

Figure 3.37: Theory at different magnetic fields, written as ^{1}H frequency, of C-14, J = –43 Hz and χ = –63 MHz.

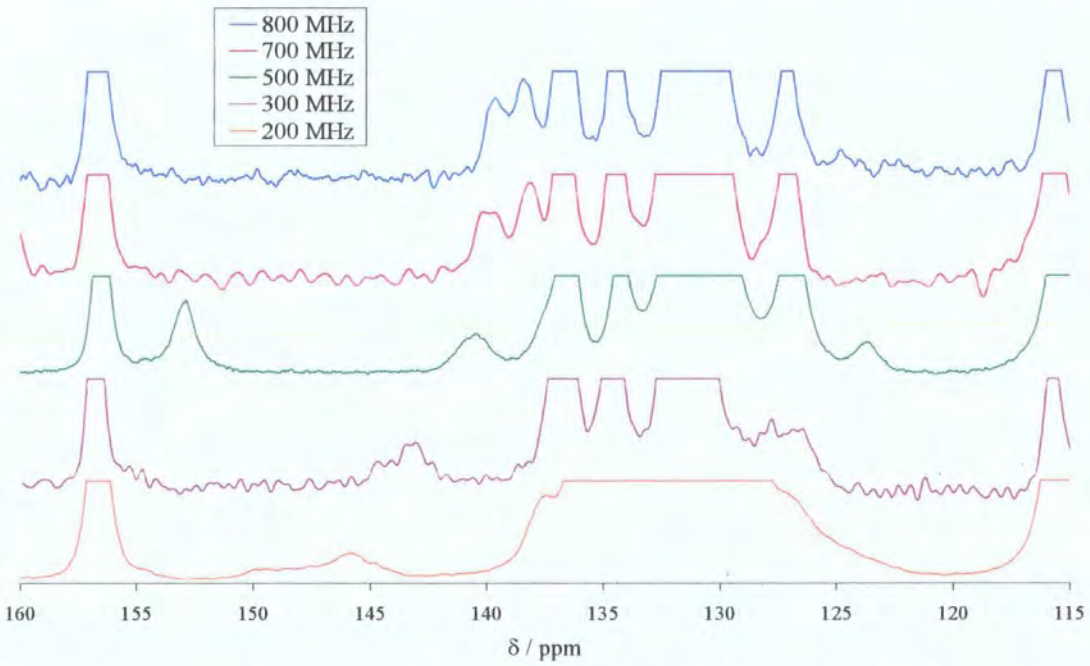

Figure 3.38: Experimental at different magnetic fields, written as ^{1}H frequency, of C-14.

In the theory so far, it has been considered that ΔJ was zero, in accordance to perturbation theory. However, if this value is not zero some changes will be

observed. In the perturbation theory case, Δ is used to measure the value for χD_{eff}, which is -36×10^9 Hz^2, which was calculated using equation 3.3, where Δ was taken from the experiment at 700 MHz (^1H frequency) for which ν_{Cl} was 68.66 MHz. For this purpose, it was assumed that the observed value of Δ is dominated by the effect of the more abundant isotope, ^{35}Cl.Note that in this study, D, rather than D_{eff}, was used to calculate χ. Therefore, if D_{eff} is less than D i.e. ΔJ is positive, χ will be bigger than 63 MHz, which is expected by comparison with the literature[13].

2.2.1.5) T_1^H and $T_{1\rho}^H$ measurements

The measurements have been carried out, in duplicate, as stated in chapter Two using crystalline drug. The plots are shown in figure 3.39 and figure 3.40, for T_1^H and $T_{1\rho}^H$ respectively. The raw data are shown in appendix 17.

The T_1^H measurements showed no minimum or maximum but a steady increase in the value of T_1^H with increasing temperature. This means that the measurements are on the high-temperature side of a T_1 minimum. The slope gave an activation energy of 12.1 kJ mol^{-1}. It is good to note that all values of activation energy stated in this work should be taken as having an error of ± 1 kJ.mol^{-1}.

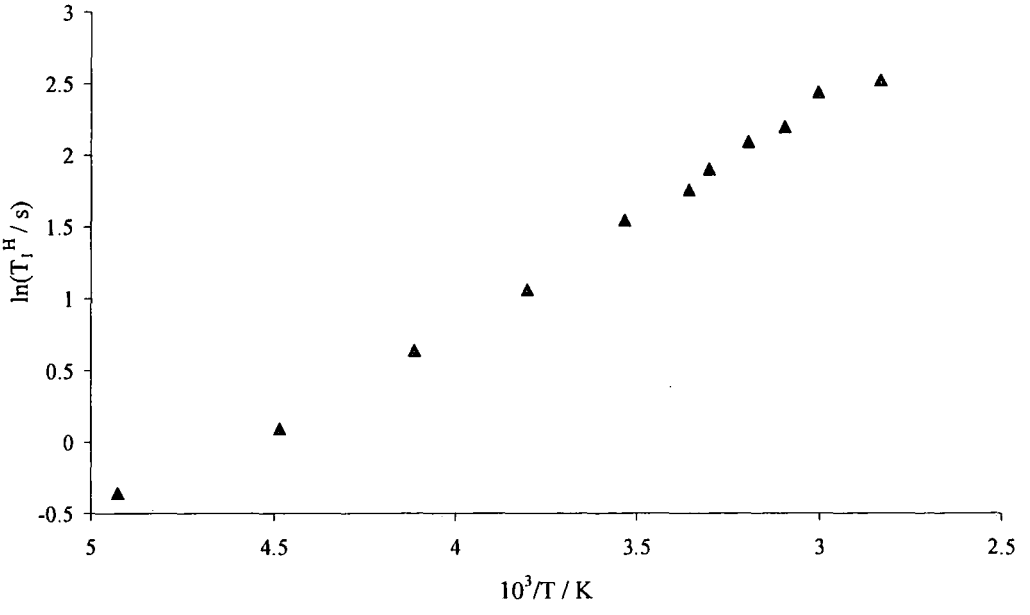

Figure 3.39: T_1^H measurements for crystalline indomethacin. The activation energy was calculated to be 12.1 kJ mol^{-1}.

The $T_{1\rho}^{H}$ measurements showed a minimum at 17.8°C. The slope gave an activation energy of 38.0 kJ mol^{-1}, between –30°C and 10°C, and 37.7 kJ mol^{-1}, between 25°C and 80°C. These activation energies are presumably associated with an internal rotation along a single bond, but it is not possible to precisely define which single bond this corresponds to.

In chapter One, it was seen that the minimum occurs when $\tau_c = 1/\omega$. In this case, it was calculated that τ_c = 20 ms, using ω_1 = 50 kHz. The values of E_a, τ_c and $T_{minimum}$ have now been calculated, and, by inserting these in equation 1.12, one can get the value for the pre-exponential factor, referred to as D. This value was calculated to be 125.9 s.

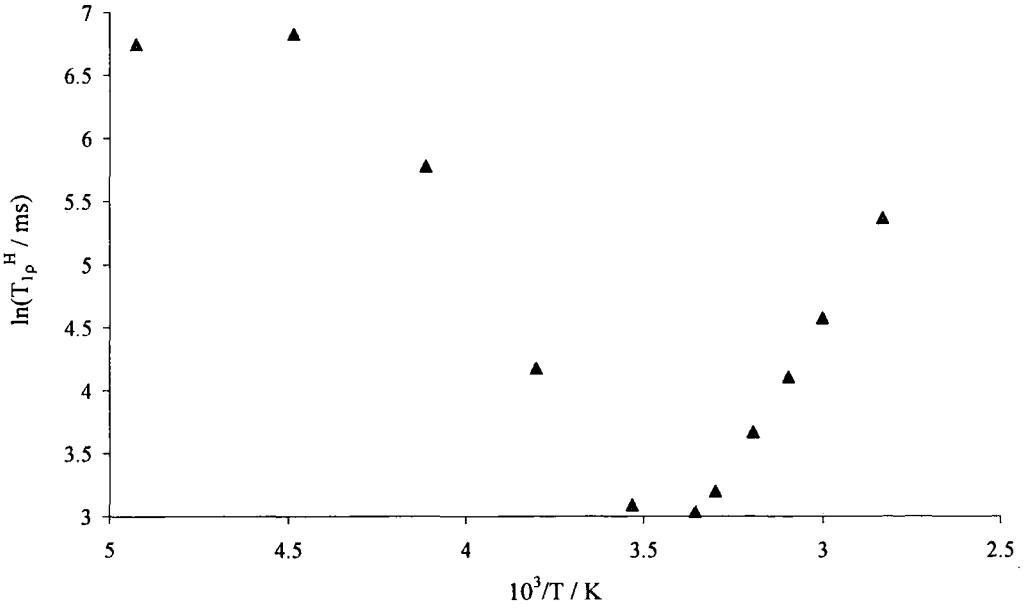

Figure 3.40: $T_{1\rho}^{H}$ measurements for crystalline indomethacin. The activation energy was calculated to be 38.0 kJ mol^{-1} for the low-temperature part, and 37.7 kJ mol^{-1} for the high-temperature part.

The difference in the activation energies between T_1 and $T_{1\rho}$ shows that two different motional processes are observed. It is, of course, expected that for a given motional process the T_1 minimum will occur at a significantly higher temperature than the $T_{1\rho}$ minimum. This is due to the fact that the minimum in $T_{1\rho}$ depends on the frequency

γB_1 rather then γB_0. Therefore, for a given temperature range, T_1 will reflect a lower-barrier motional process than $T_{1\rho}$, as observed.

2.2.2) Nifedipine

2.2.2.1) ^{1}H spectrum

A fast MAS ^{1}H spectrum was acquired using the HX 2.5 mm probe on the 500 MHz spectrometer, see figure 3.41. The peak at 8.3 ppm is due to the amine proton, the shoulder at 7.4 ppm is due to the aromatic protons, the peak at 5.5 ppm is due to the methyne proton, the peak at 2.4 ppm is due to the methyl-ester groups and the shoulder at 1.5 ppm is due to the remaining methyl groups.

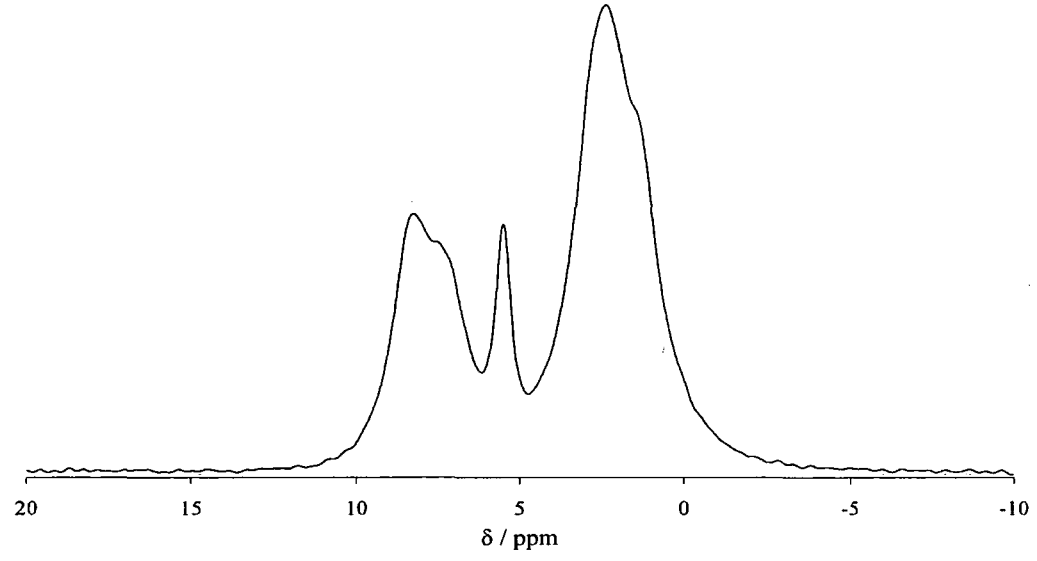

Figure 3.41: ^{1}H spectrum of crystalline nifedipine, acquired at 500 MHz ^{1}H frequency, spinning at 27 kHz.

2.2.2.2) ^{13}C spectra

The ^{13}C SSNMR spectrum of crystalline nifedipine was acquired using CPMAS and NQS (figure 3.43) techniques. The assignments, shown in table 3.7, were made using the solution-state results, as well as the CPMAS and NQS spectra.

In the solution-state, the molecules are tumbling rapidly. Therefore, there is an apparent symmetry in the ^{13}C spectrum. However, in the solid-state, this tumbling is

absent, so the symmetry is lost. This explains why the SSNMR spectrum looks more complicated than the solution-state one. Note that when this theory is considered one can confirm that there is only one molecule per asymmetric unit.

The differences observed for the carbon atoms 7, 8, 9 and 10 are probably due to the geometry of the asymmetric unit. The aromatic ring is positioned in such a way that it is above the other ring in the same molecule and carbon atom 8 is the closest to this second ring, see figure 3.42. Therefore, the shift observed for this atom could be due to steric effects.

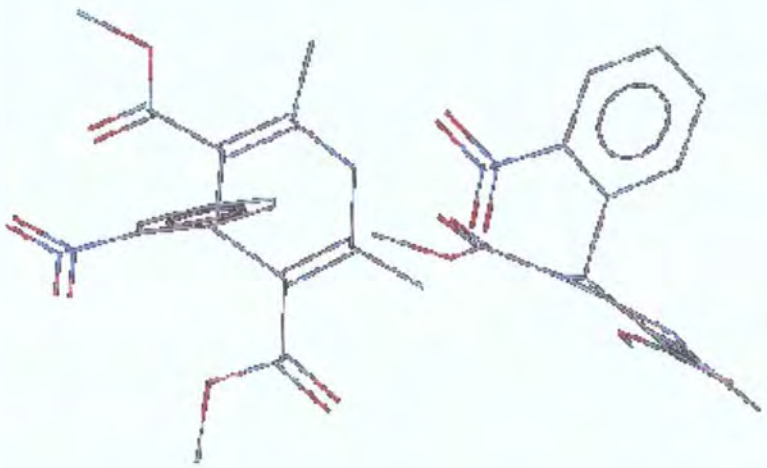

Figure 3.42: Crystal structure of nifedipine showing that C-8 is above the non-aromatic ring of the same molecule.

Atom numbers	Solid-state NMR / ppm	Difference [a] / ppm
3', 5'	169.9, 168.1	
12	148.4 [b]	0.5
2, 6	149.4, 144.8 [b]	
7	143.9 [b]	1.2
9	136.6	2.7
8	135.7	4.4
10	126.7	−1.4
11	124.1	−0.2
3, 5	103.1, 101.6	
3", 5"	51.1, 49.3	
4	35.4	0.8
2', 6'	19.2	0.3

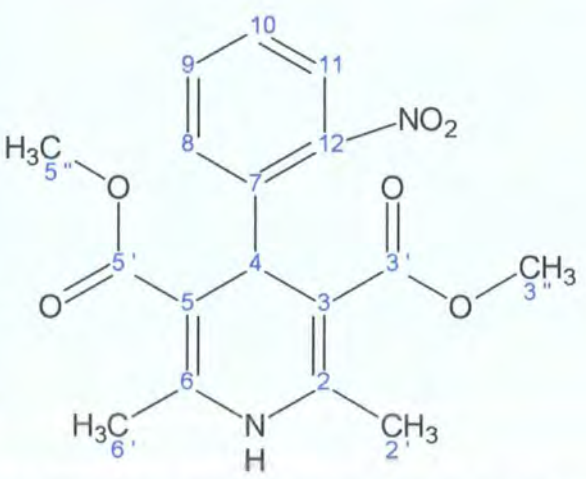

[a] For the solution-state NMR chemical shifts, see Table 3.4. The difference is from solid to solution.

[b] Estimated from a spectrum obtained using a 500 MHz spectrometer.

Table 3.7: ^{13}C SSNMR assignments of the modification I of nifedipine.

VT ^{13}C SSNMR experiments have been carried out on crystalline nifedipine between 25°C and 150°C (data not shown). The spectra did not show any significant differences throughout the range of temperatures.

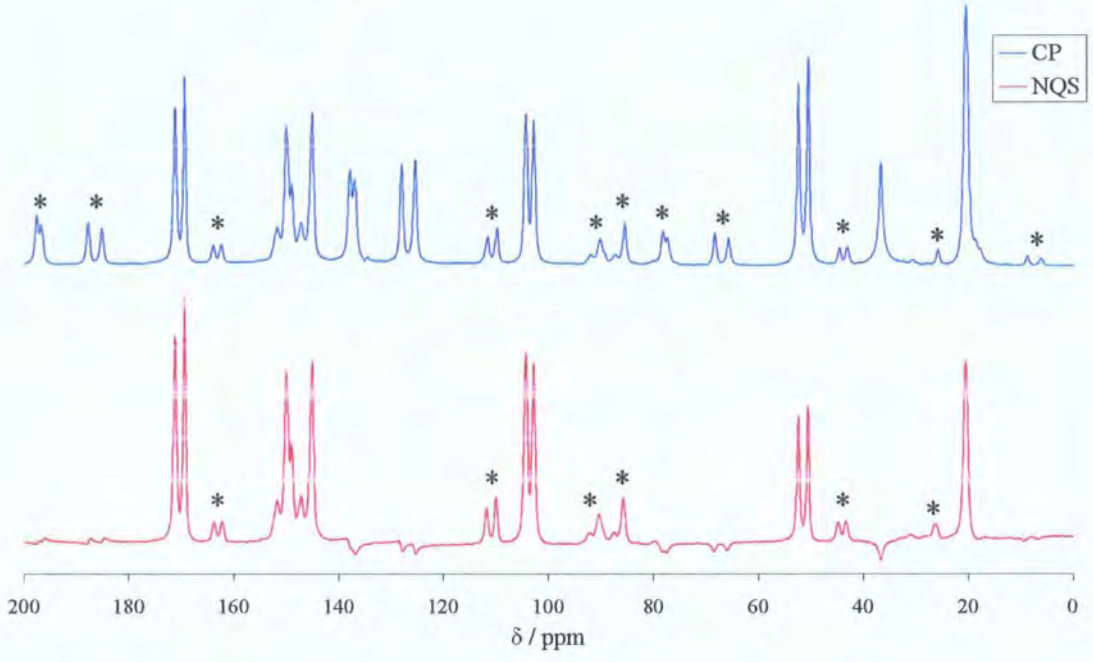

Figure 3.43: CP and NQS ^{13}C spectra of modification I of nifedipine obtained at 50.32 MHz, ^{13}C frequency. The asterisks show the spinning sidebands.

For the carbon atoms 3' and 5', 3 and 5, and 3'' and 5'', the solution-state chemical shift is at a lower-frequency, in the middle and at a higher-frequency than that of the doublet, respectively. This is probably due to hydrogen bonding between the carbonyl oxygen and the NH group.

One could see from figure 3.43 that the region from 130 ppm to 160 ppm is quite difficult to interpret. However, as stated in table 3.7, a 500 MHz spectrum was used to help the assignment. Figure 3.44 shows the spectra of crystalline nifedipine obtained at 125.68 MHz, 75.43 MHz and 50.32 MHz, ^{13}C frequencies, between 130 and 155 pm. It is easy to see the improvement in resolution as the strength of the magnetic field increases by looking at the doublet centred around 136 ppm. It is also visible that the group of peaks assigned to the carbons bonded to nitrogen atoms is getting easier to interpret. This could be explained by the fact that when a nitrogen

atom is bonded to a ^{13}C atom, the latter is subject to a 1:2 or 2:1 splitting. This influence of the nitrogen atom gets weaker as the magnetic field gets stronger, which can be observed in figure 3.44.

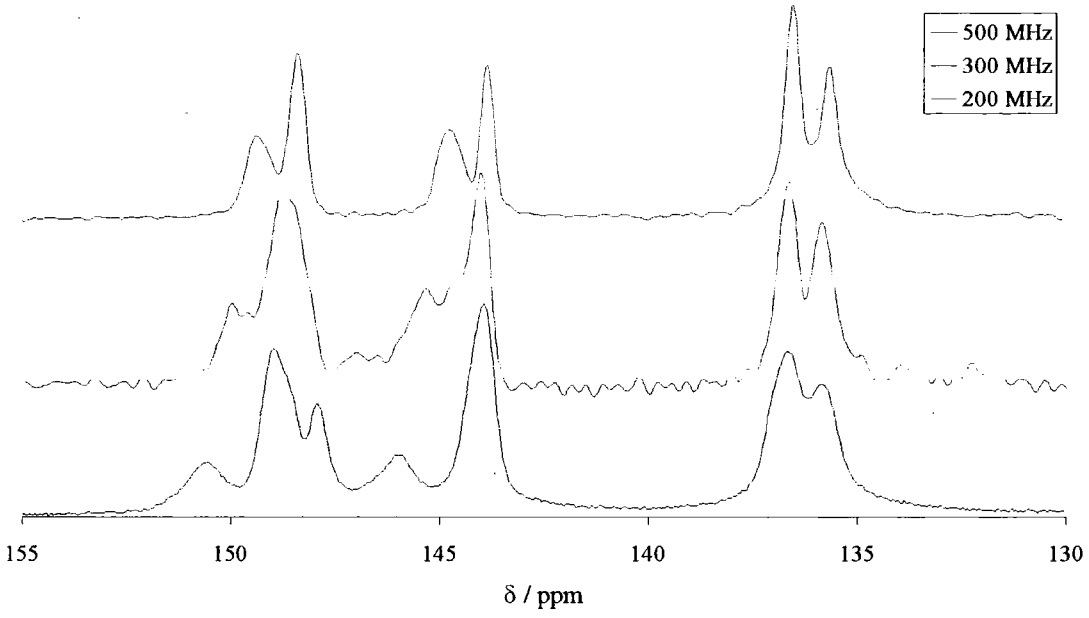

Figure 3.44: ^{13}C SSNMR spectra of crystalline nifedipine obtained at 125.68 MHz, 75.43 MHz and 50.32 MHz, ^{13}C frequencies, showing only the region between 155 ppm and 130 ppm.

2.2.2.3) T_1^H and $T_{1\rho}^H$ measurements

The measurements have been carried out the same way as for indomethacin. The plot of T_1^H is shown in figure 3.45. The $T_{1\rho}^H$ data were not obtained. This was due to the long $T_{1\rho}^H$ value and it was not possible to extend the spin-lock time array without damaging the probe; the array used went up to a value of 100 ms for the spin-lock time. The raw data are shown in appendix 18.

The T_1^H measurements nifedipine showed no minimum or maximum but a steady increase in the value of T_1^H with increasing temperature, which helped to draw the same conclusions as for indomethacin. The slope gave an activation energy of 3.4 kJ mol^{-1}.

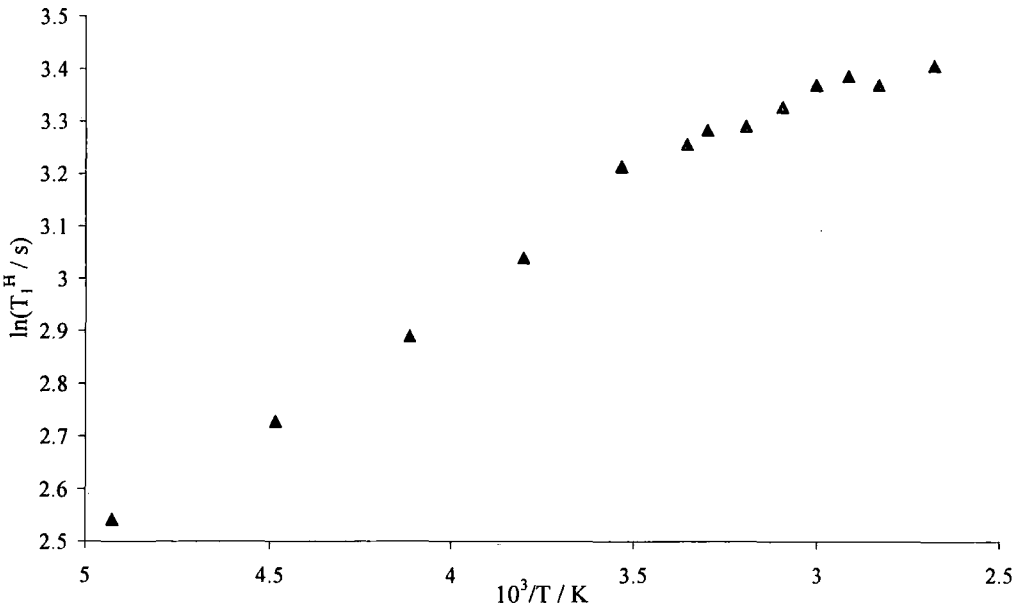

Figure 3.45: $T_1{}^H$ measurements for crystalline nifedipine. The activation energy was calculated to be 3.4 kJ mol^{-1}.

2.2.3) Carbamazepine

2.2.3.1) ^1H spectrum

A fast MAS ^1H spectrum was acquired using the HX 2.5 mm probe on the 500 MHz spectrometer, see figure 3.46.

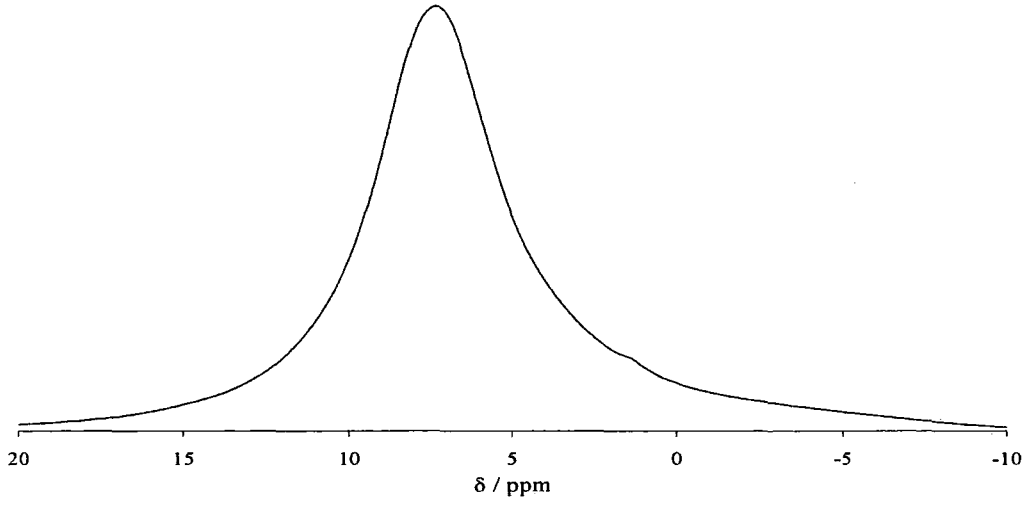

Figure 3.46: ^1H spectrum of crystalline carbamazepine, acquired at 500 MHz ^1H frequency, spinning at 27 kHz using a pulse delay of 60 s.

Figure 3.46 shows no resolved features and also shows that no hydrogen bond can be distinguished.

2.2.3.2) ^{13}C spectra

The ^{13}C SSNMR spectrum of crystalline carbamazepine was acquired using CPMAS and NQS (figure 3.47) techniques. The assignments, shown in table 3.8, were made using the solution-state results, as well as the CPMAS and NQS spectra.

Atom numbers	Solid-state NMR / ppm	Difference [a] / ppm
15	159.8	2.4
1, 14	141.7, 139.5	
6, 9	134.7	–0.5
7, 8	131.1	0.4
5, 10	129.3	–0.5
3, 12	129.3	–0.4
2, 13	129.3	0.3
4, 11	127.5	–0.5

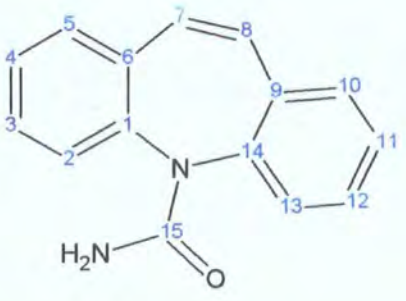

[a] For the solution-state NMR, see Table 3.5. The difference is from solid to solution.

Table 3.8: ^{13}C SSNMR assignments of modification III of carbamazepine.

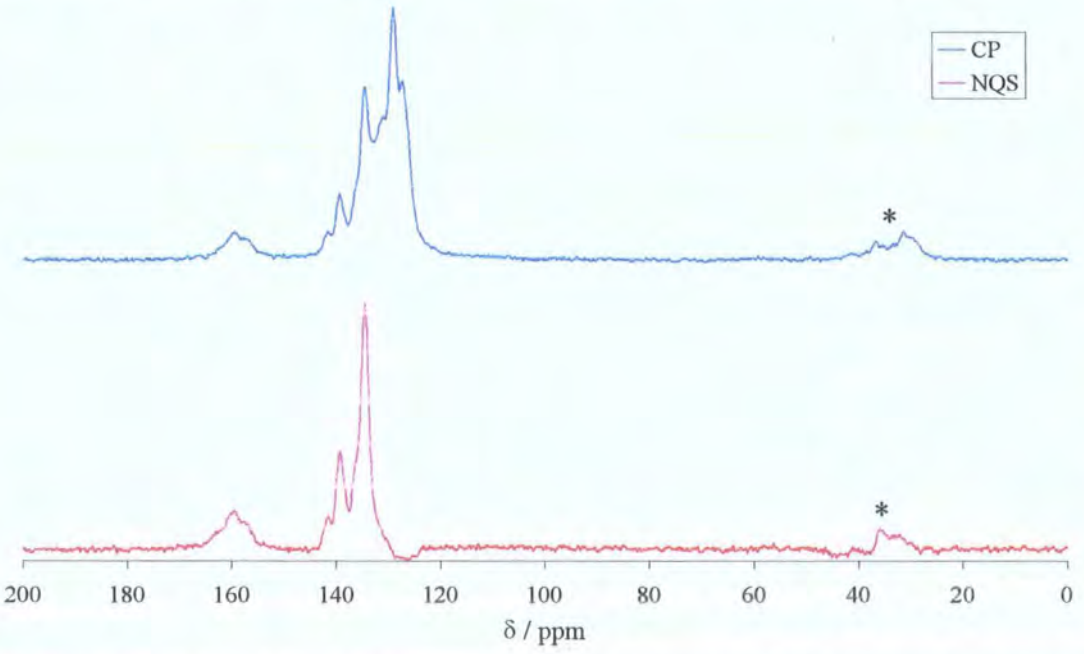

Figure 3.47: CP and NQS ^{13}C spectra of modification III of carbamazepine obtained at 50.32 MHz, ^{13}C frequency. The asterisks show the spinning sidebands.

The large difference observed in table 3.8 for the carbon atom 15 is probably due to the fact that the $CONH_2$ group is not freely rotating along the N-$CONH_2$ bond.

2.2.3.3) T_1^H and $T_{1\rho}^H$ measurements

The measurements have been carried out the same way as for indomethacin. The plot of T_1^H is shown in figure 3.48.

The T_1^H measurements for carbamazepine did not show any minimum or maximum. The rather small variation in the value of T_1^H could be explained by limited mobility, which is consistent with the lack of conformational flexibility. This also did not allow the activation energy to be retrieved from this set of measurements.

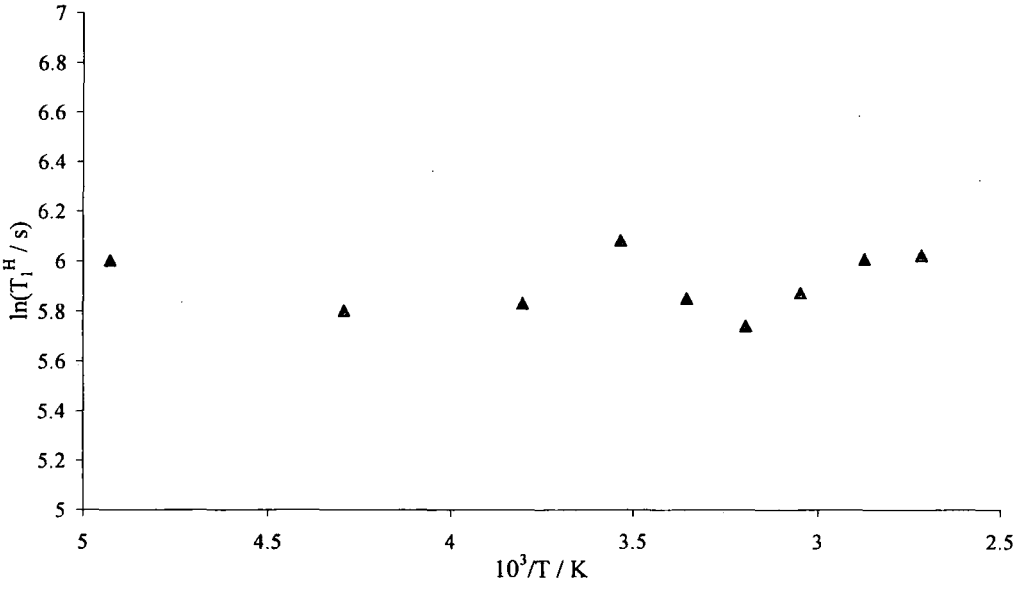

Figure 3.48: T_1^H measurements for crystalline carbamazepine. No activation energy could be retrieved from this set of data.

As for nifedipine, the $T_{1\rho}^H$ data were not obtained but this problem was not present at high-temperature, i.e. above 70°C. However, only two points were recorded passed this temperature and, as a consequence, the $T_{1\rho}^H$ graph was not plotted. The raw data of the T_1^H and $T_{1\rho}^H$ experiments are shown in appendix 19.

3/ Conclusions

3.1/ Materials

It has been confirmed, using different analytical techniques, that the studied compounds were of the γ-form, modification I and modification III for indomethacin, nifedipine and carbamazepine respectively.

3.2/ T_1^H and $T_{1\rho}^H$ measurements

The T_1^H measurements for indomethacin and nifedipine showed no minimum or maximum but a steady increase in the value of T_1^H with increasing temperature. This means that these measurements are on the high-temperature side of a T_1 minimum. The slope gave an activation energy of 12.1 kJ mol^{-1} and 3.4 kJ mol^{-1} for indomethacin and nifedipine respectively, which clearly corresponds to different motional processes. They are sufficiently low (especially the latter) that they probably reflect internal rotation of a methyl group.

The T_1^H measurements for carbamazepine did not show any minimum or maximum. The variation in the value of T_1^H is quite small and this could be explained by limited mobility, which is consistent with the lack of conformational flexibility. No activation energy can be retrieved from this set of measurements.

The $T_{1\rho}^H$ measurements for indomethacin showed a minimum at 17.8°C. The slope gave an activation energy of 38.0 kJ mol^{-1} between −30°C and 10°C, and 37.7 kJ mol^{-1} between 25°C and 80°C. These activation energies are presumably associated with an internal rotation along a single bond. However, it is not possible to precisely say which single bond this corresponds to.

The difference in the activation energies between T_1 and $T_{1\rho}$, for indomethacin, shows that two different motional processes are observed. It is, of course, expected that for a given motional process the T_1 minimum will occur at a significantly higher temperature than the $T_{1\rho}$ minimum, as the minimum in $T_{1\rho}$ depends on the frequency γB_1 rather then γB_0. Therefore, for a given temperature range, T_1 will reflect a lower-barrier motional process than $T_{1\rho}$, as observed.

3.3/ Quadrupolar effect

The investigation done for the quadrupolar effect of the chlorine atom in indomethacin allowed the following information to be obtained:

- The true ^{13}C chemical shift of C-14 is 139 ppm ± 0.2 ppm.
- The value of χD_{eff} is -36×10^9 Hz^2.
- J_{iso} = ca. –43 Hz, which should be taken as a maximum magnitude.
- $\chi = -63$ MHz, if it is considered that ΔJ is negligible.

The sign of χ should be given by the shape of low-field bands, but this is difficult to be certain of it given the problem of overlapping. However, the positions of the visible components at 200 and 300 MHz compare well with the theory in which the value of χ is negative. Therefore, it is safe to assume that χ is negative.

4/ References

1. N. Kaneniwa, M. Otsuka, and T. Hayashi. Physicochemical characterization of indomethacin polymorphs and the transformation kinetics in ethanol. *Chem. Pharm. Bull.* **33**: 3447-3455 (1985).

2. T. J. Kistenmacher and R. E. Marsh. Crystal and molecular structure of an antiinflammatory agent, indomethacin, 1-(p-chlorobenzoyl)-5-methoxy-2-methylindole-3-acetic acid. *J. Am. Chem. Soc.* **94**: 1340-1345 (1972).

3. A. Burger and K. T. Koller. Polymorphism and pseudopolymorphism on nifedipine. *Sci. Pharm.* **64**: 293-301 (1996).

4. F. Hirayama, Z. Wang, and K. Uekama. Effect of 2-hydroxypropyl-(β)-cyclodextrin on crystallization and polymorphic transition of nifedipine in solid state. *Pharm. Res.* **11**: 1766-1770 (1994).

5. A. M. Triggle, E. Shefter, and D. J. Triggle. Crystal structure of calcium channel antagonists: 2,6-dimethyl-3,5-dicarbomethoxy-4-[2-nitro-, 3-cyano-, 4-(dimethylamino)-, and 2,3,4,5,6-pentafluorophenyl]-1,4-dihydropyridine. *J. Med. Chem.* **23**: 1442-1445 (1980).

6. F. U. Krahn and J. B. Mielck. Relations between several polymorphic forms and the dihydrate of carbamazepine. *Pharm. Acta Helv.* **62**: 247-254 (1987).

7. A. L. Grzesiak, M. Lang, K. Kim, and A. J. Matzger. Comparison of the four anhydrous polymorphs of carbamazepine and the crystal structure of form I. *J. Pharm. Sci.* **92**: 2260-2271 (2003).

8. R. K. Harris, P. Y. Ghi, H. Puschmann, D. C. Apperley, U. J. Griesser, R. B. Hammond, K. Ma, K. J. Roberts, G. J. Pearce, J. R. Yates, and C. J. Pickard. Structural study of the polymorphs of carbamazepine, its dihydrate, and two solvates. *Org. Process Res. Dev.* **9**: 902-910 (2005).

9. W. Kemp. *NMR in Chemistry*, Macmillan, London, 1986, pp 76.

10. D. H. Williams and I. Fleming. *Spectroscopic methods in organic chemistry*, McGraw-hill, Maidenhead, 1995.

11. D. A. Fletcher, R. F. McMeeking, and D. Parkin. The United Kingdom chemical database service. *J. Chem. Inf. Comput. Sci.* **36**: 746-749 (1996).

12. R. J. Abraham. *The analysis of high resolution NMR spectra*, Elsevier, Amsterdam, 1971, pp 84-89.

13. G. K. Semin, T. A. Babushkina, and G. G. Yakobsen. *Applications of NQR in chemistry*, Khimiya, Leningrad, 1972.

14. S. H. Alarcón, A. C. Olivieri, S. A. Carss, R. K. Harris, M. J. Zuriaga, and G. A. Monti. Residual dipolar (^{35},^{37}Cl, ^{13}C) coupling in solid sodium chloroacetates. A combined variable-temperature ^{35}Cl NQR and variable-field ^{13}C MAS NMR study. *J. Magn. Reson. Ser. A* **116**: 244-250 (1995).

15. K. Eichele, R. E. Wasylishen, J. S. Grossert, and A. C. Olivieri. The influence of chlorine-carbon dipolar and indirect spin-spin interactions on high resolution carbon-13 NMR spectra of chloroketosulfones in the solid state. *J. Phys. Chem.* **99**: 10110-10113 (1995).

Chapter Four: Amorphous Materials – Confirmation

1/ Results

This chapter will look at the different methods used to produce amorphous materials and how it was checked that these materials were amorphous. This involved different analytical techniques, mainly XRPD and ^{13}C SSNMR, which allowed one to look at different properties of the amorphous materials, and also at the effect of different timescales, due to the different techniques, on the study of these materials. This chapter will also look at the influence of the timescale on the recrystallisation phenomenon.

1.1/ Indomethacin

1.1.1) DSC

The amorphous sample was prepared as specified in chapter Two. The observed value of Tg was 45°C, see figure 4.1, which is consistent with the work of Forster et al.[1]. This showed that amorphous indomethacin could be prepared using the melting and quench-cooling method. However, the amorphous phase was prepared using a small quantity of sample and it was necessary to see if the same preparation could be done on a bulk sample that would be needed for the SSNMR experiments. This experiment also showed that no recrystallisation occurs for amorphous indomethacin on the timescale of the DSC, and that no melting was observable, confirming the non recrystallisation of the sample.

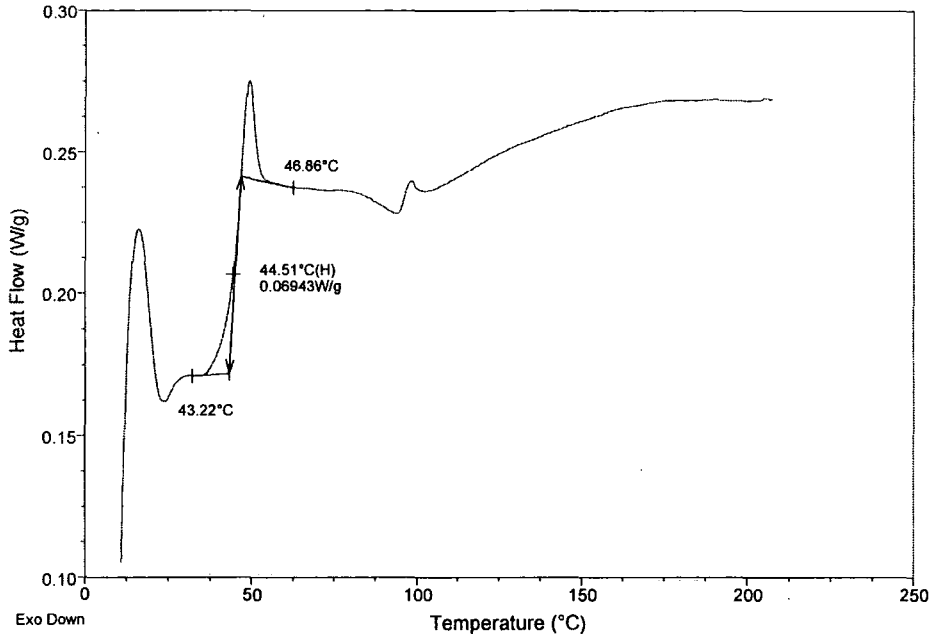

Figure 4.1: DSC of amorphous indomethacin showing Tg at 45°C.

1.1.2) FTIR

A sample from a large-batch preparation of quench-cooled amorphous indomethacin was prepared and studied using FTIR. The FTIR spectrum obtained is shown in figure 4.2.

It is observable that the FTIR of the crystalline and the amorphous forms (see figure 4.3) are different. This difference is observed mainly by a broadening of the peaks, where the crystalline FTIR spectrum had narrower peaks. It is also apparent that some peaks are not present in the amorphous spectrum, for some of these it is just due to the broadening. One can also see that the wavenumbers of some of the vibrations are changed. This experiment showed that the quench-cooled method on a bigger scale worked for indomethacin.

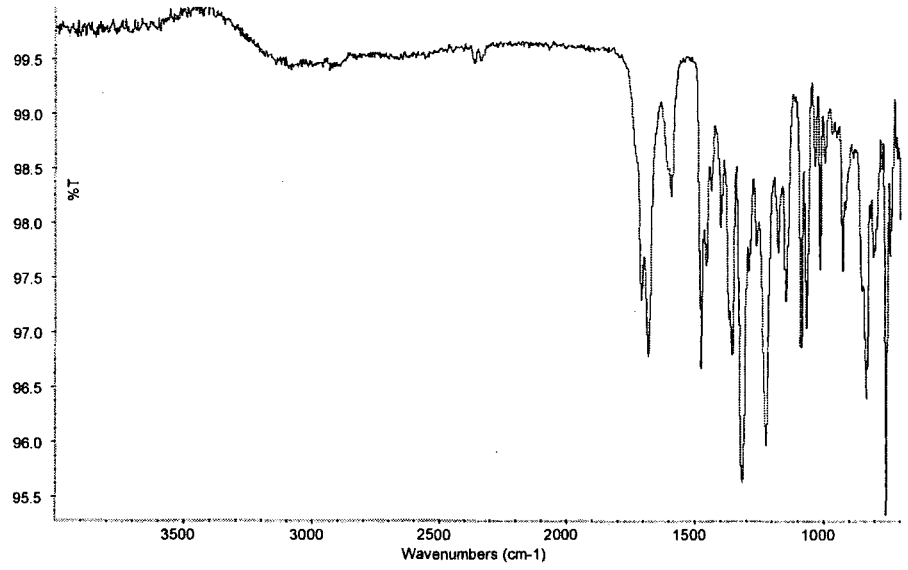

Figure 4.2: FTIR of amorphous indomethacin.

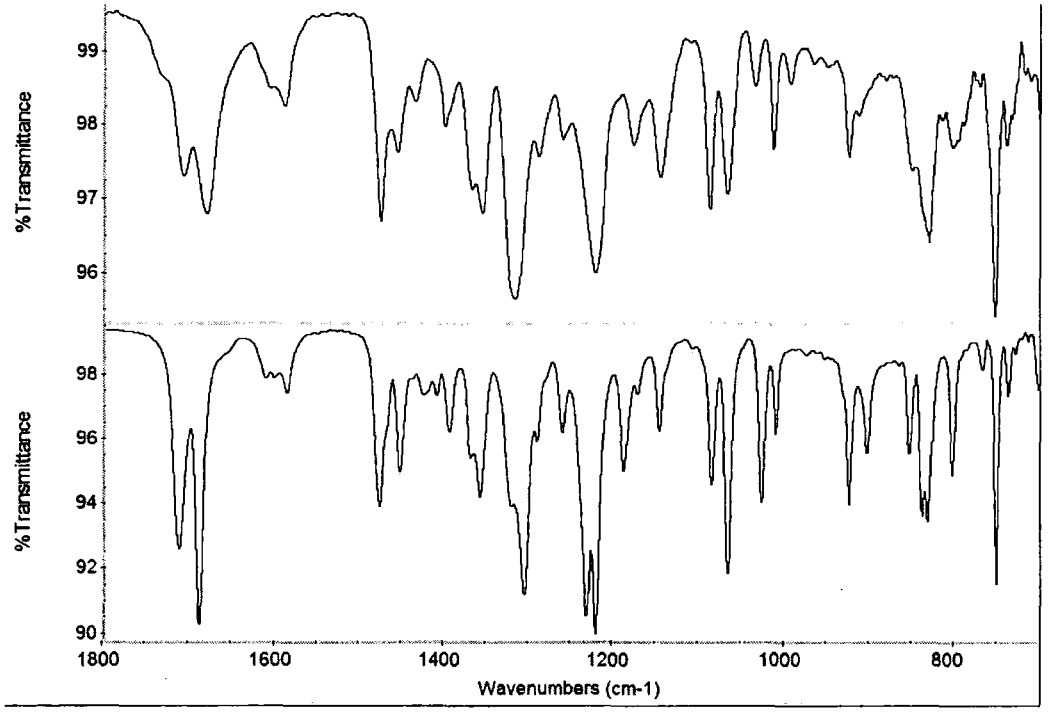

Figure 4.3: FTIR spectra of amorphous (top) and crystalline (bottom) indomethacin, showing only the 700-1800 cm^{-1} region.

1.1.3) Microscopy

For indomethacin, microscopy was solely used in order to determine if the prepared amorphous sample was truly amorphous. This was done by looking at the crystalline sample to observe the presence of any birefringence. Then, the same was done with the amorphous sample. It was observed that the crystalline sample showed birefringence, see figure 4.4, while the amorphous sample did not show any all through the sample; this was assuming that the sample had not change to a cubic system. Therefore, it was concluded that the prepared sample was amorphous. Nevertheless, due to the minute amount of sample under examination it was not possible to confirm that a large sample was amorphous throughout.

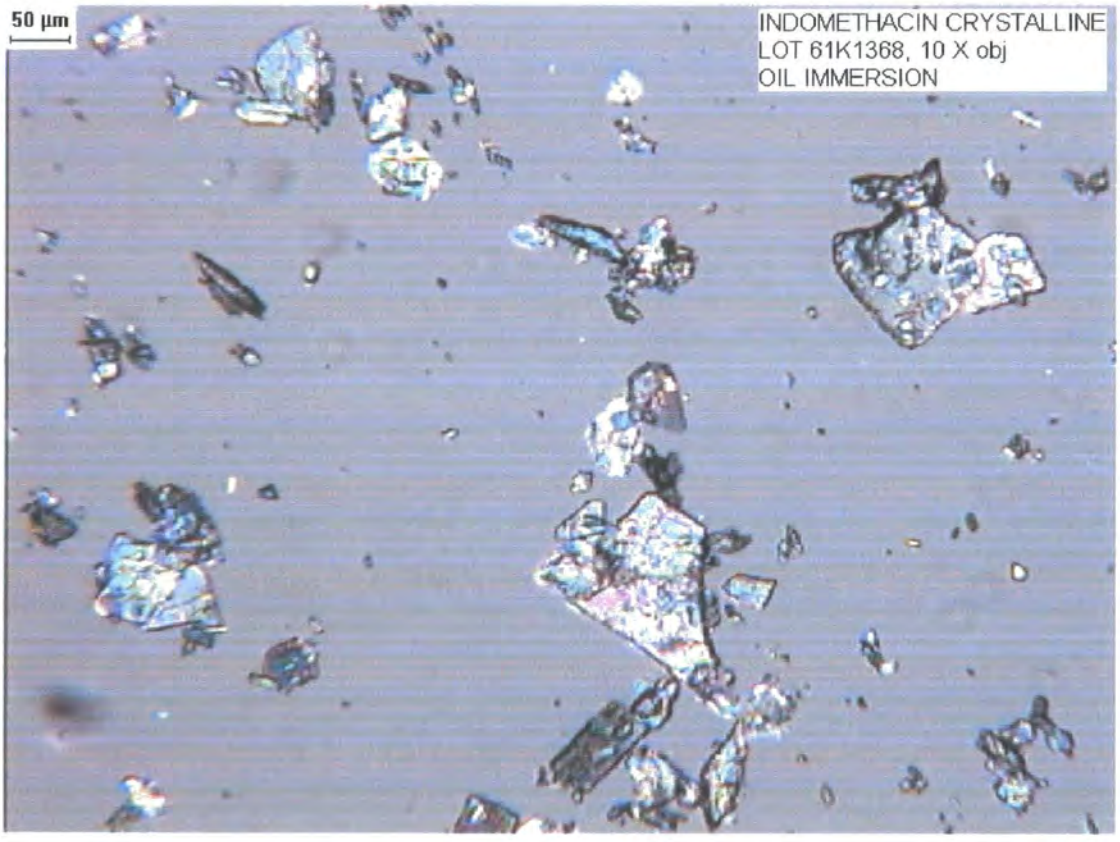

Figure 4.4: Polarised light microscopy snapshot of crystalline indomethacin, showing birefringence.

1.1.4)^{13}C SSNMR

^{13}C SSNMR was used to check the amorphous character of the sample obtained using the method described in chapter Two. The peaks obtained using this technique

on the prepared sample showed that the sample was indeed amorphous, see figure 4.5. This is shown by the much broader lines obtained with the spectrum of the amorphous sample, see table 4.1.

	Crystalline material	Amorphous material
Chemical shifts / ppm	Linewidths / Hz	
13.4	82	184
55.2	77	161
156.7	51	120

Table 4.1: Linewidths of different single peaks obtained from the crystalline and amorphous spectra of indomethacin.

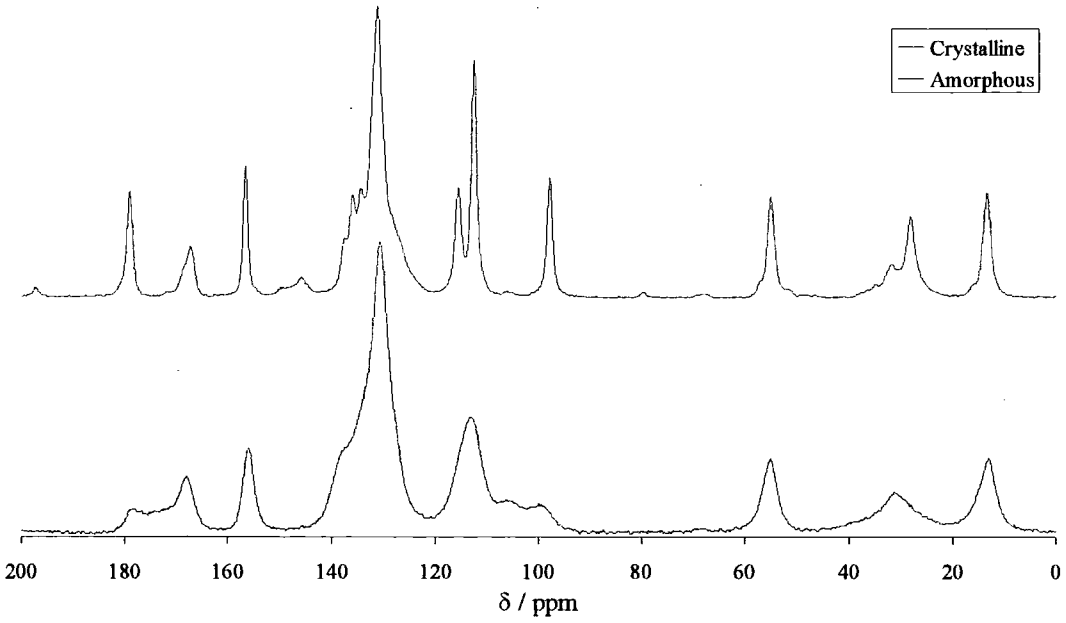

Figure 4.5: ^{13}C SSNMR of crystalline and amorphous indomethacin obtained at 50.32 MHz, ^{13}C frequency.

This technique was also used in order to check the effect of grinding on amorphous sample. Figure 4.6[2] shows the ^{13}C SSNMR spectra of intact and ground amorphous indomethacin and nifedipine; the crushed amorphous samples were obtained by gentle grinding under liquid nitrogen in a pestle and mortar. It can be seen from this figure that indomethacin does not seem to recrystallise immediately after grinding.

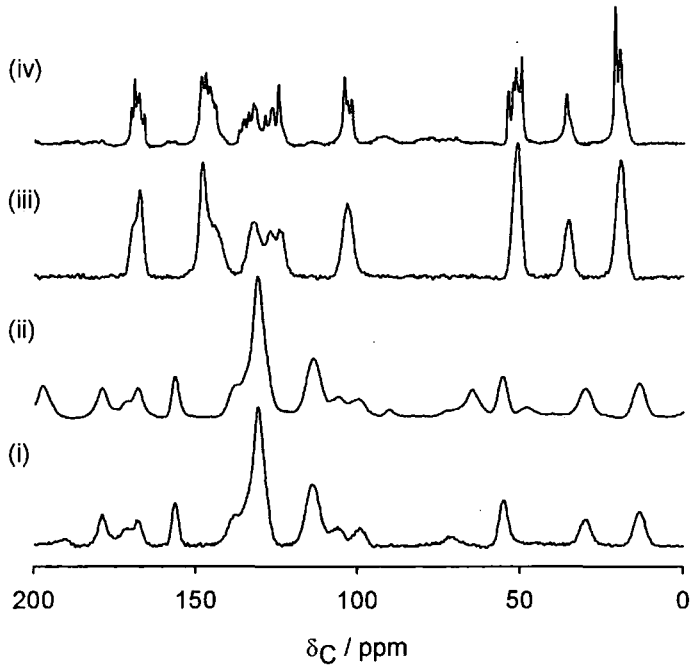

Figure 4.6: ^{13}C spectra at 74 MHz of indomethacin, (i) and (ii), and nifedipine, (iii) and (iv), quench-cooled melts at ambient probe temperature before, (i) and (iii), and after, (ii) and (iv), grinding.[2]

^{13}C SSNMR was also used in order to determine if amorphous indomethacin recrystallised on the timescale of an NMR experiment. From this experiment, see figure 4.7, it was observed that nothing occurred until a temperature of 90°C was reached, when the sample seems to recrystallise. However, this seemed to be a reversible effect because the recorded spectrum going back down to room temperature appeared more amorphous than crystalline. Therefore, it is possible to say that the sharpening is probably due to an increased molecular mobility rather than recrystallisation. The timing of the ^{13}C VT SSNMR experiment for amorphous indomethacin is shown in table 4.2.

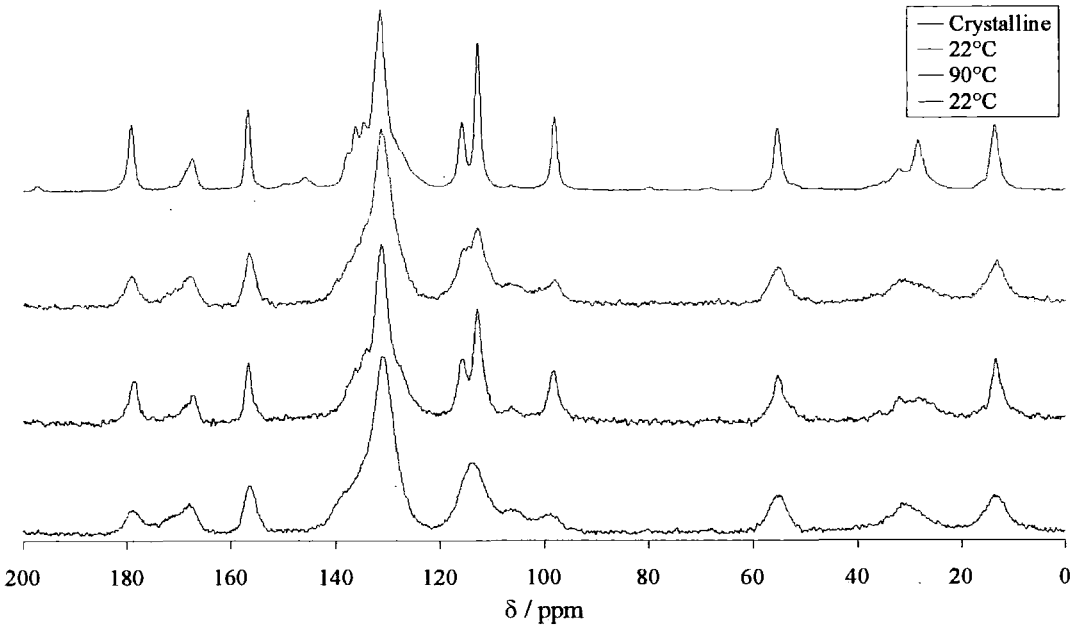

Figure 4.7: ^{13}C VT SSNMR of amorphous indomethacin obtained at 50.32 MHz, ^{13}C frequency. The crystalline spectrum is shown for reference.

Temperature / °C	Temperature reached at / hr:min	Experiment started at / hr:min	Experiment finished at / hr:min
22	0:00	0:10	0:23
30	0:28	0:38	0:51
35	0:56	1:06	1:27
40	1:32	1:42	2:03
45	2:08	2:18	2:31
50	2:36	2:46	3:07
55	3:12	3:22	3:43
60	3:48	3:58	4:19
70	4:24	4:34	4:55
80	5:00	5:10	5:52
90	5:57	6:07	6:49
22	6:54	7:14	7:35

Table 4.2: Timing used for the ^{13}C VT SSNMR experiment performed on amorphous indomethacin.

1.1.5) XRPD

At first, XRPD was used to determine the amorphous character of the prepared sample. Figure 4.8 shows that the prepared sample is definitely amorphous as only a halo of low counts value is visible, which is characteristic of an amorphous sample as a halo is due to a lack of long range order.

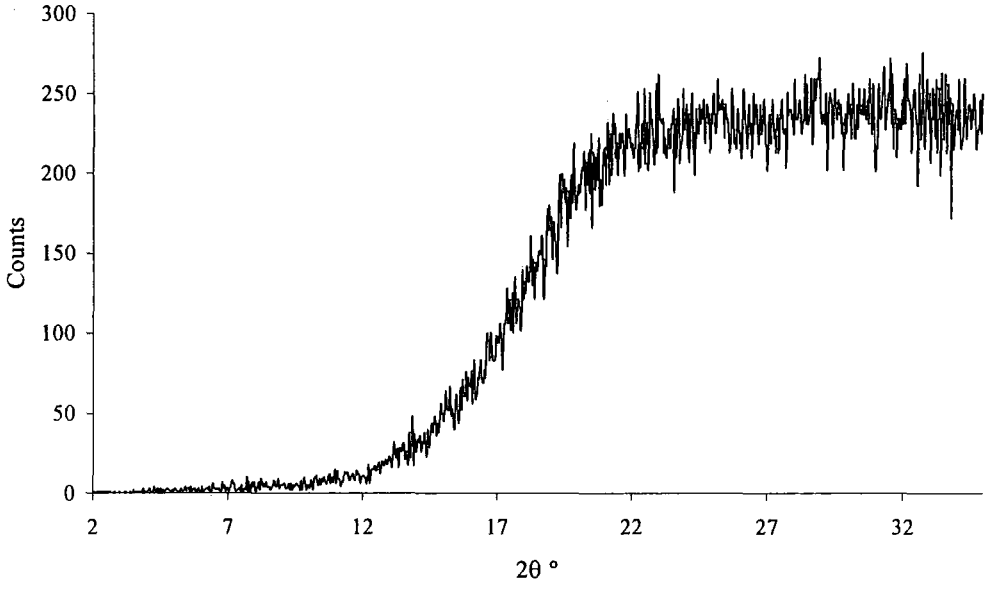

Figure 4.8: XRPD of amorphous indomethacin at room temperature.

XRPD was also used to study the physical stability of amorphous indomethacin (data not shown). This was done by looking at an intact and at a ground sample; each samples had two specimens one kept at room temperature, 20°C to 25°C, and one kept in the freezer, -15°C to -20°C. Both intact samples, as well as the ground sample kept in the freezer, showed no sign of recrystallisation after a week. However, the ground sample kept at room temperature started to recrystallise after a day, while it showed no sign of recrystallisation straight after the preparation; this is consistent with what was observed using SSNMR. This showed that in order to keep a sample of amorphous indomethacin from recrystallising, one should either keep it intact or ground and in the freezer. This is in agreement with the work of Fukuoka et al.[3] who observed the rapid recrystallisation of pulverised glassy indomethacin and also that intact glassy indomethacin was stable and recrystallisation did not occur for more than 2 years at room temperature.

This method was further used with VT equipment to see if any recrystallisation was appearing over a range of temperature similar to the one used for the ^{13}C VT SSNMR and following a similar time scale as for the relaxation times measurements, see chapter Five. Figure 4.9 shows the XRPD VT experiment. This experiment showed no recrystallisation throughout the range of temperature –70°C to 80°C, which is in agreement with the ^{13}C SSNMR VT experiment. Note that no real change is visible throughout the XRPD VT experiment, whilst there is an apparent change in mobility observed when looking at the ^{13}C SSNMR VT experiment. This difference can be explained by the fact that the mobility of amorphous samples will not be apparent in XRPD.

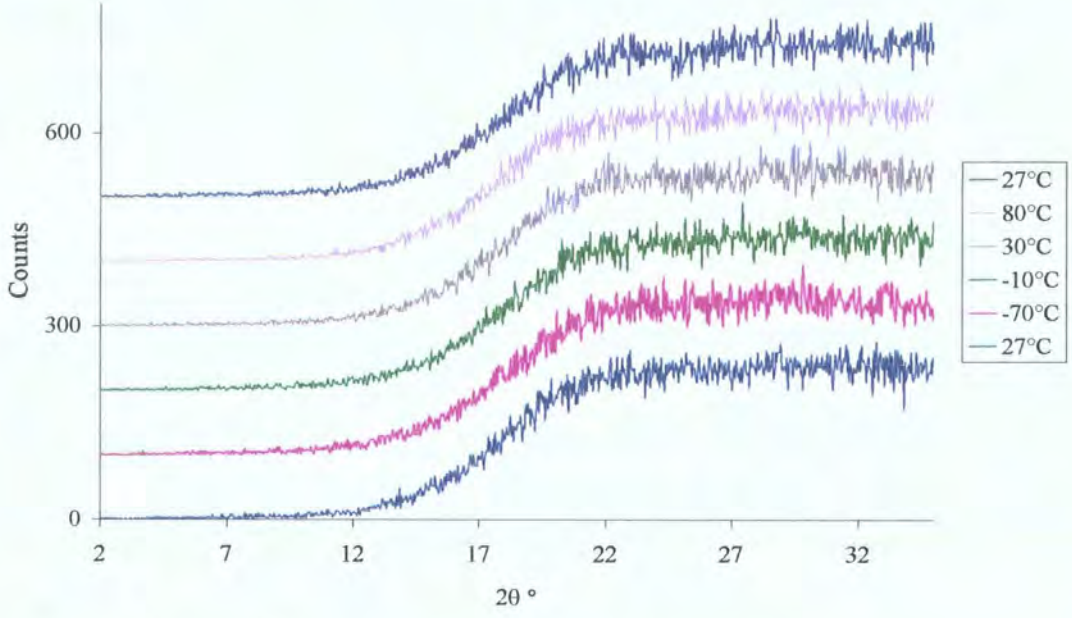

Figure 4.9: VT XRPD experiment of amorphous indomethacin.

1.2/ Nifedipine

1.2.1) DSC

The amorphous sample was prepared as specified in chapter Two. The value of Tg observed is 46°C, see figure 4.10, which is consistent with the work of Aso et al.[4]. The same conclusions as for indomethacin on the preparation of the amorphous sample apply for nifedipine. This experiment, see figure 4.10, also showed that recrystallisation occurs for amorphous nifedipine from 104°C and appears to go

through different phases. This was shown by Burger and Koller[5], and also by Keymolen et al.[6], to be the crystallisation of modifications III and II as well as the transition from modification III to modification II, followed by the transition from modification II to modification I and the melting of the rest of modification III. Burger and Koller[5] used thermomicroscopy to determine this, and in this study amorphous nifedipine was also examined using hot-stage microscopy, as shown in part 1.2.3 of this chapter.

The diffractogram ends by the recrystallisation of the sample into modification I, which then melts at 173°C. This is the same value as seen in figure 3.5.

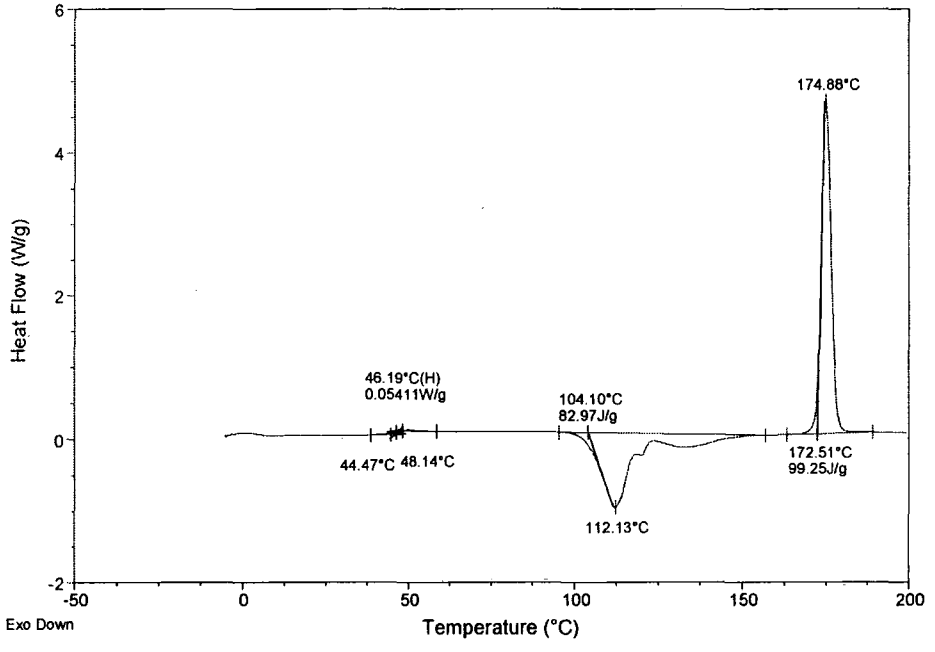

Figure 4.10: DSC of amorphous nifedipine, showing the Tg, at 46°C, the recrystallisation, at 104°C, and the melting, at 173°C.

Another DSC experiment was carried out using amorphous nifedipine in order to study the recrystallisation process. This experiment consisted of forming an amorphous sample and then reheating this sample at different speeds.

The following method was applied to the sample:

1. Heat from 20°C to 180°C at a rate of 40°C/min.
2. Hold at 180°C for 1 min.
3. Cool from 180°C to 20°C at a rate of 40°C/min.
4. Heat from 20°C to 180°C at a rate of x°C/min, where x was set to 10, 30, 50, 70, 100, 150, 200, 250 and 300.

This study showed that at a reheating rate of 10°C/min, the stable form of nifedipine was the major form present. But, when using a reheating rate of 30°C/min, the metastable form was also present in a significant quantity as the endothermic peaks of both forms were of similar area. At 50°C/min and 70°C/min, the metastable form was the major one. It was also observed that at a reheating rate of 100°C/min, and above, the recrystallisation did not occur. This gives a guide as how to prepare the metastable form of nifedipine. It also let one see that during the VT process, one should be careful about the temperature at which the sample is reheated. This is illustrated in figure 4.11.

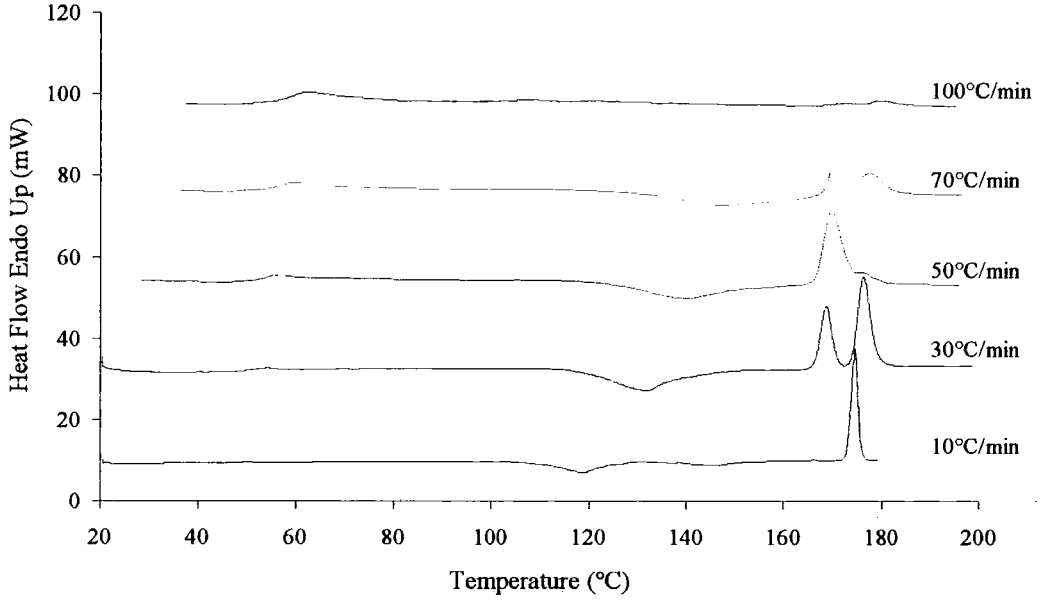

Figure 4.11: DSC of amorphous nifedipine, reheating rate of x°C/min, where x is 10, 30, 50, 70 and 100.

1.2.2) FTIR

A sample of quench-cooled amorphous nifedipine was prepared and studied using FTIR, see figure 4.12.

It is observable that the FTIR of the crystalline and amorphous forms (see figure 3.6 and figure 4.12 respectively) show similar differences when compared to those seen between crystalline and amorphous indomethacin, i.e. the crystalline sample shows sharp bands while the amorphous sample shows broad bands. This showed that the quench-cooled method worked on a bigger scale for this compound also.

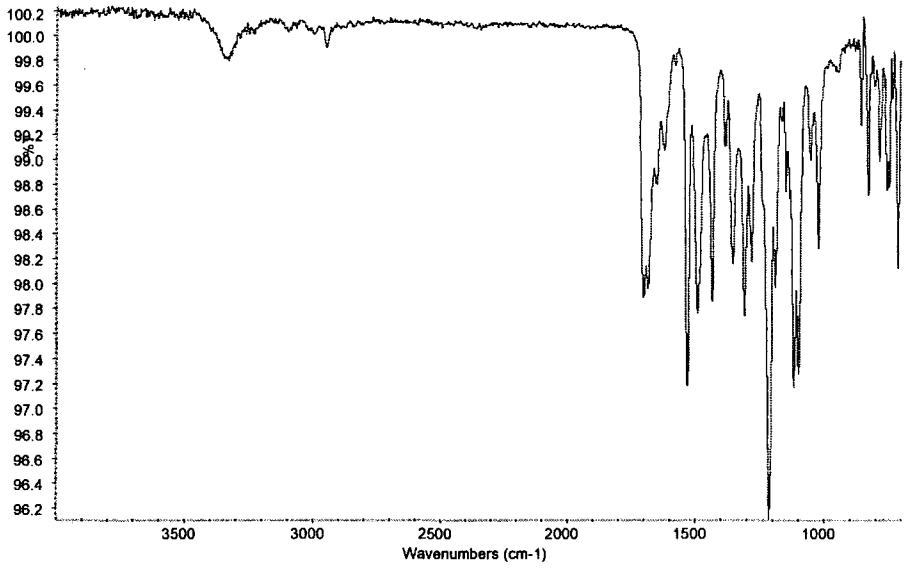

Figure 4.12: FTIR of amorphous nifedipine.

1.2.3) Microscopy

In the case of nifedipine, two kinds of microscopy were used. Polarised light microscopy was used in order to check the amorphous character of the prepared sample, see figure 4.13, and hot-stage microscopy, data not shown, was used in order to understand the process involved during the recrystallisation.

For the hot stage microscopy, the amorphous sample was heated from room temperature at a rate of 10°C / min until the start of the recrystallisation. At this point, the rate was lowered to 5°C / min. It was observed that the sample was going through different recrystallisation processes during the recrystallisation, which is in agreement with the work of Burger and Koller[5]. This could explain the complexity of the recrystallisation exotherm observed in figure 4.10.

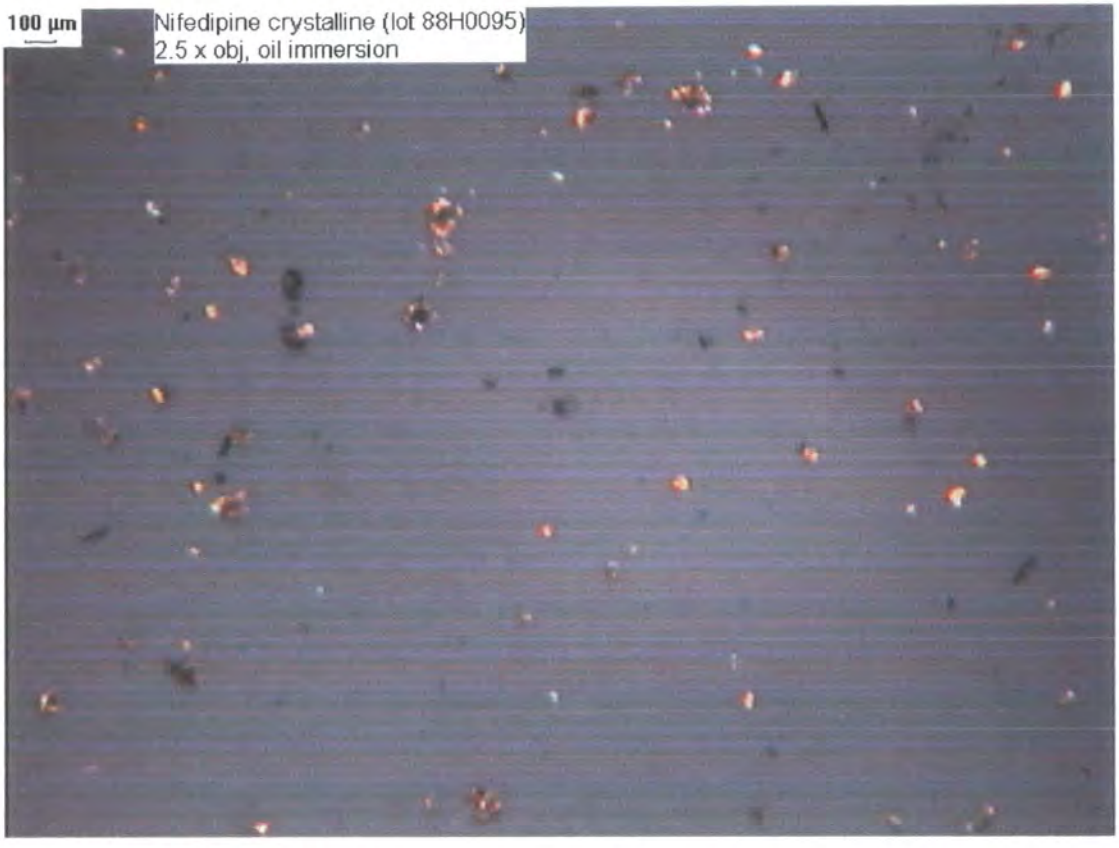

Figure 4.13: Polarised light microscopy snapshot of crystalline nifedipine showing birefringence.

Polarised light microscopy was used on both crystalline and amorphous samples, and both were checked for the presence of birefringence. As for indomethacin, only the crystalline sample showed birefringence, see figure 4.13. Therefore, it was concluded that the prepared sample was amorphous. Nevertheless, it was not possible to say that a bulk sample was amorphous throughout, as explained for indomethacin.

1.2.4) ^{13}C SSNMR

^{13}C SSNMR was used to check the amorphous character of the sample obtained using the method described in chapter Two. The ^{13}C SSNMR spectrum of this sample showed very broad peaks when compared to the crystalline form, see figure 4.14, which implies that the prepared sample was amorphous. Table 4.3 shows the comparison of the linewidths of some peaks between the crystalline and the amorphous spectra.

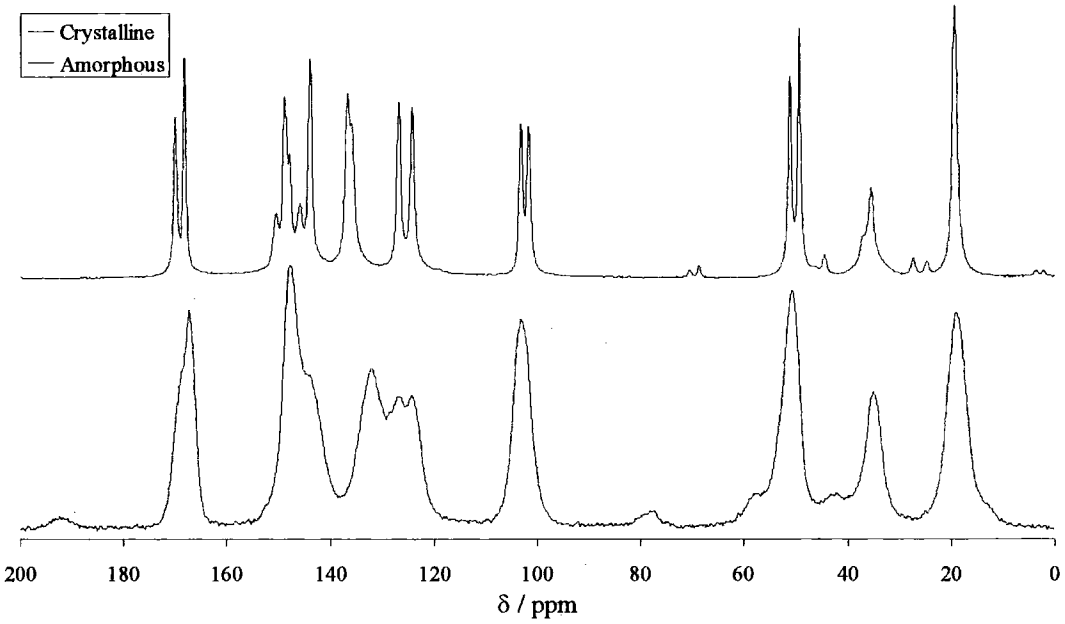

Figure 4.14: ^{13}C SSNMR of crystalline and amorphous nifedipine obtained at 50.32 MHz, ^{13}C frequency.

	Crystalline material	Amorphous material
Chemical shifts / ppm	Linewidths / Hz	
19.2	44	204
35.4	44	166

Table 4.3: Linewidths of different single peaks obtained from the crystalline and amorphous spectra of nifedipine.

Figure 4.6[2] shows the ^{13}C SSNMR spectra of intact and ground amorphous nifedipine. It can be observed from this figure that the ground sample is a mixture of broad lines (resembling the amorphous spectrum) and sharp resonances (resembling the crystalline spectrum) which indicate that grinding of glassy nifedipine causes recrystallisation.

This technique was also used to determine if amorphous nifedipine recrystallised on the timescale of an NMR experiment, see figure 4.15. The temperature was raised from room temperature to 65°C steadily. It was observed that some changes started to occur around this temperature. Therefore, a series of spectra was acquired at this temperature until no further change was observed. The obtained spectra were seen to

show recrystallisation into modification I. The temperature was then lowered back to room temperature in order to check for reversibility. However, the spectra obtained at 65°C and back at room temperature were similar and were comparable to that of a genuinely crystalline sample, proving a non-reversible phenomenon. The timing of the ^{13}C VT SSNMR experiment for amorphous nifedipine is shown in table 4.4.

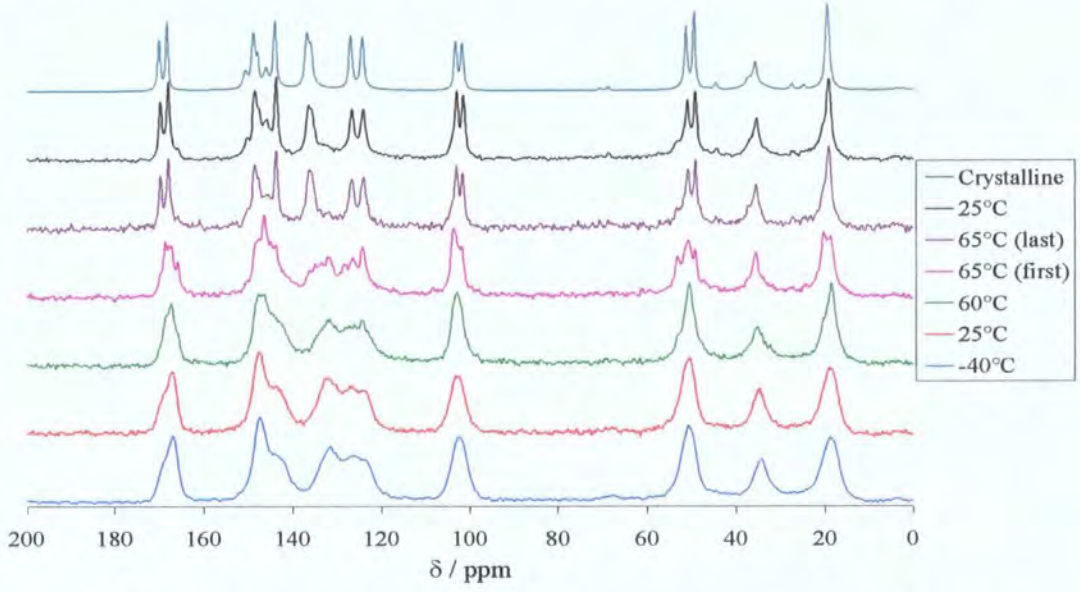

Figure 4.15: ^{13}C VT SSNMR of amorphous nifedipine obtained at 50.32 MHz, ^{13}C frequency. The crystalline spectrum is shown for reference.

Temperature / °C	Temperature reached at / hr:min	Experiment started at / hr:min	Experiment finished at / hr:min
-40	0:00	0:20	1:03
0	1:08	1:28	2:11
25	2:16	2:36	2:57
35	3:02	3:12	2:33
45	3:38	3:48	4:09
55	4:14	4:24	4:45
60	4:50	5:00	5:21
65 (first)	5:26	5:36	5:57
65 (last)	N/A	8:51	9:12
25	9:17	9:37	9:58

Table 4.4: Timing used for the ^{13}C VT SSNMR experiment performed on amorphous nifedipine.

1.2.5) XRPD

Figure 4.16 shows the XRPD diffractogram of amorphous nifedipine, which shows that the prepared sample is definitely amorphous as only a halo of low counts values is visible.

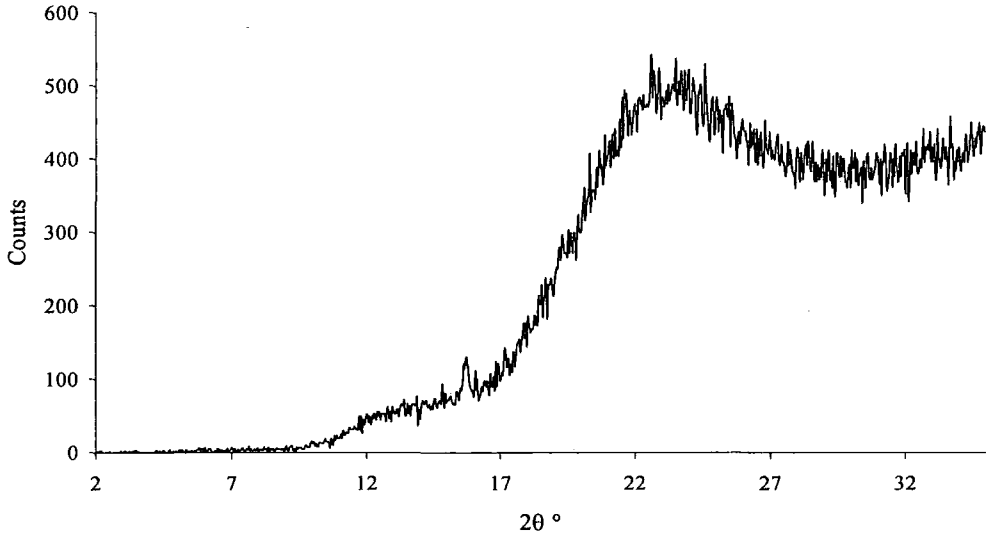

Figure 4.16: XRPD of amorphous nifedipine at room temperature.

This technique was also used in order to look at the stability of amorphous nifedipine under different conditions. This study consisted in acquiring the diffractograms (data not shown) of three samples of amorphous nifedipine; one intact kept in the freezer and two ground samples, kept in the same conditions as for indomethacin. It was observed than the ground samples showed sign of recrystallisation straight after preparation, supporting earlier XRPD[7] and SSNMR[2] findings. However, the intact sample showed no sign or recrystallisation after one week. Therefore, one should keep amorphous nifedipine intact and in the freezer.

XRPD was further used with VT equipment to see if any recrystallisation was appearing over a range of temperatures similar to the one used for the ^{13}C VT SSNMR, and using a similar timescale as for the relaxation times measurements, see chapter Five. The result of this experiment is shown on figure 4.17 and it can be seen that recrystallisation occurred between 60°C and 80°C and that it is a non-reversible phenomenon.

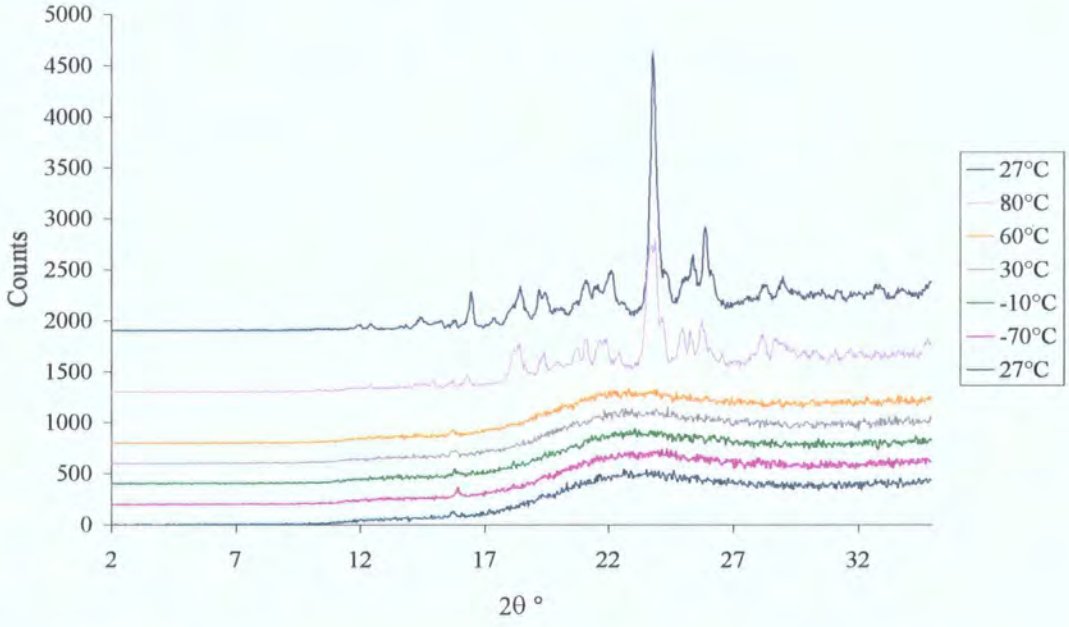

Figure 4.17: VT XRPD experiment of amorphous nifedipine.

Following the results of this experiment, it was decided to carry out a similar experiment using increments of 5°C, see figure 4.18, rather than following the temperatures used for the ^{13}C SSNMR experiment. The timing for this last experiment is shown in table 4.5.

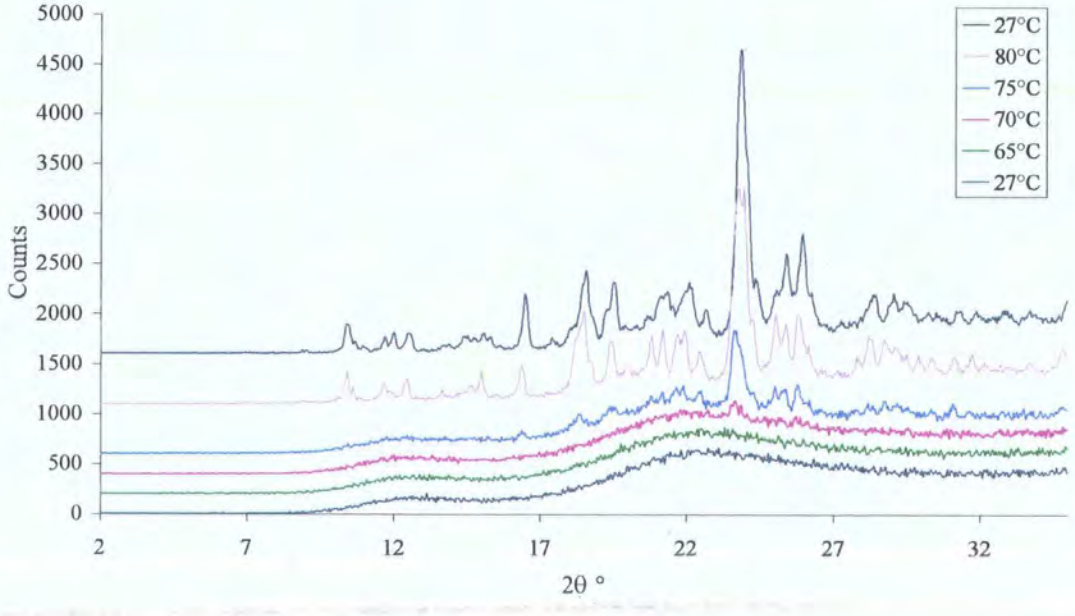

Figure 4.18: VT XRPD experiment of amorphous nifedipine.

Temperature / °C	Temperature reached at / hr:min	Experiment started at / hr:min	Experiment finished at / hr:min
27	0:00	0:10	0:24
15	0:25	0:35	0:49
20	0:50	1:00	1:14
25	1:15	1:25	1:39
30	1:40	1:50	2:04
35	2:05	2:15	2:29
40	2:30	2:40	2:54
45	2:55	3:05	3:19
50	3:20	3:30	3:44
55	3:45	3:55	4:09
60	4:10	4:20	4:34
65	4:35	4:45	4:59
70	5:00	5:10	5:24
75	5:25	5:35	5:49
80	5:50	6:00	6:14
27	6:19	6:39	6:53

Table 4.5: Timing used for the second VT XRPD experiment performed on amorphous nifedipine and amorphous carbamazepine.

1.3/ Carbamazepine

1.3.1) DSC

The amorphous sample was prepared as specified in chapter Two. The value of Tg observed is 57°C, see figure 4.19, which is in agreement with the work of Patterson et al.[8]. The same conclusions as for indomethacin on the preparation of the amorphous sample apply for carbamazepine. The DSC also showed that amorphous carbamazepine recrystallised to modification I from around 104°C, which then melts at around 186°C. It was understood that the amorphous form recrystallised predominantly to modification I as the endotherm/exotherm observed at around

175°C for the crystalline material is not present and also because modification I is the stable form at elevated temperature. However, the onset of the melting observed for the recrystallised amorphous form is lower, 186°C, than that expected for the crystalline form, 192°C (see figure 3.8). This could be explained by the presence of other polymorphic forms, impurities or incomplete recrystallisation.

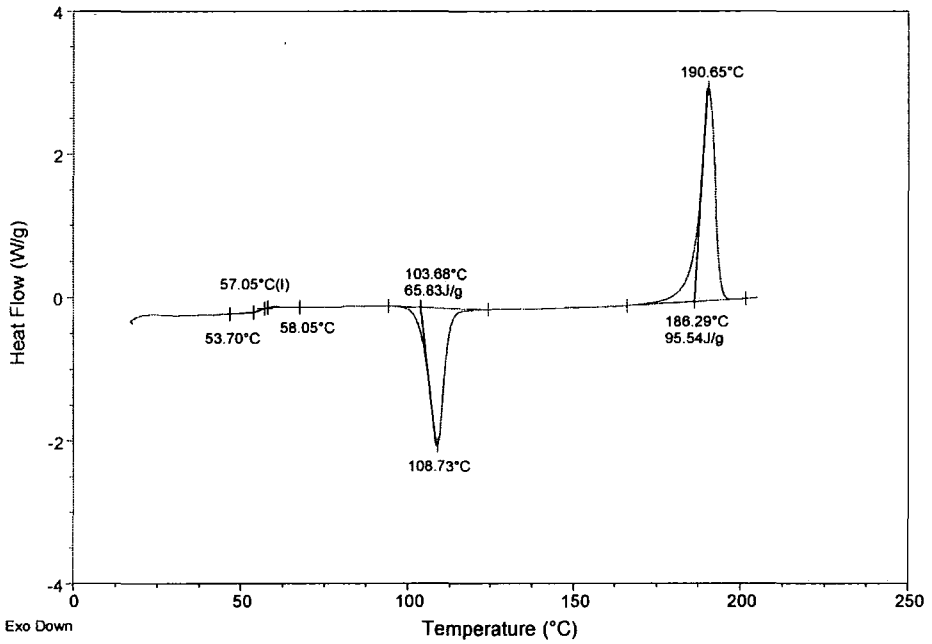

Figure 4.19: DSC of amorphous carbamazepine, showing the Tg at 57°C, recrystallisation at 104°C and melting at 186°C.

1.3.2) FTIR

A sample of quench-cooled amorphous carbamazepine was prepared and studied using FTIR, see figure 4.20.

It is observable that the FTIR of the crystalline form shows sharper bands than the amorphous forms (see appendix 4 and figure 4.20 respectively) and also that some differences are seen in the fingerprints. This showed that the quench-cooled method on a bigger scale worked for carbamazepine.

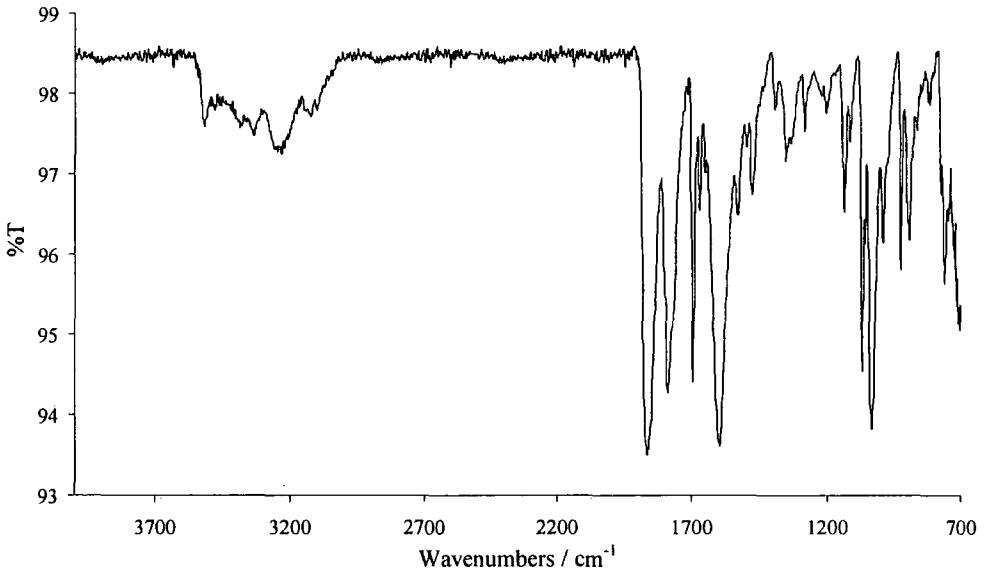

Figure 4.20: FTIR of amorphous carbamazepine.

1.3.3) ^{13}C SSNMR

The ^{13}C SSNMR was used in order to check the amorphous character of the sample obtained using the method described in chapter Two. The broadness of the peaks obtained for the amorphous form compared to the crystalline form showed that the sample was amorphous, see figure 4.21.

This technique was also used in order to determine if amorphous carbamazepine recrystallised on the timescale of an NMR experiment. It is observable that the peaks start to sharpen at 75°C and that this process is not reversible. Even though this sharpening does not lead to a truly crystalline phase, it still showed that carbamazepine started to recrystallise within the timescale of this experiment.
The timing of the ^{13}C VT SSNMR experiment for amorphous carbamazepine is shown in table 4.6

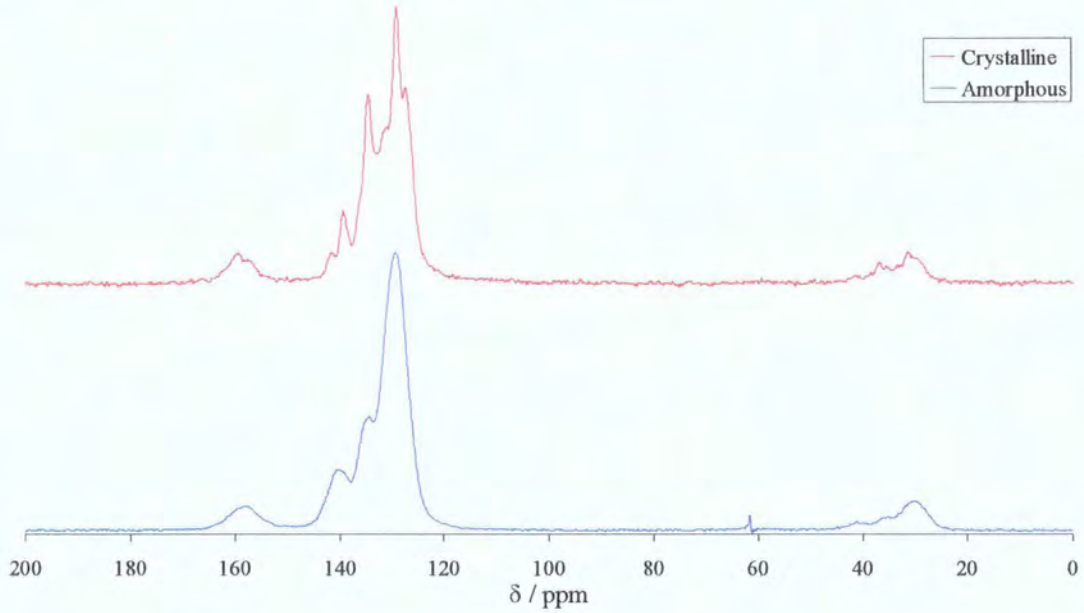

Figure 4.21: ^{13}C SSNMR of crystalline and amorphous carbamazepine obtained at 50.32 MHz, ^{13}C frequency.

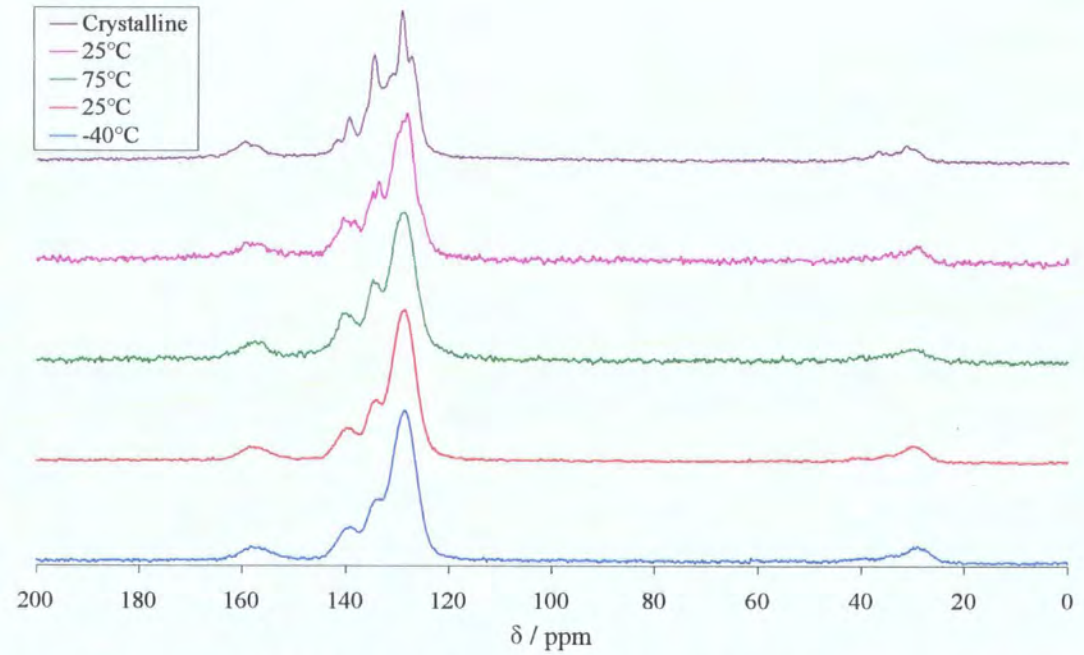

Figure 4.22: ^{13}C VT SSNMR of amorphous carbamazepine obtained at 50.32 MHz, ^{13}C frequency. The crystalline spectrum is shown for reference.

Temperature / °C	Temperature reached at / hr:min	Experiment started at / hr:min	Experiment finished at / hr:min
-40	0:00	0:20	0:31
0	0:36	0:56	1:07
25	1:12	1:32	1:43
35	1:48	1:58	2:09
45	2:14	2:24	2:35
55	2:40	2:50	3:01
65	3:06	3:16	3:27
75	3:32	3:42	3:53
25	3:58	4:18	4:29

Table 4.6: Timing used for the ^{13}C VT SSNMR experiment performed on amorphous carbamazepine.

1.3.4) XRPD

Figure 4.23 shows the XRPD diffractogram of amorphous carbamazepine. From this figure it is visible that the prepared sample is amorphous as only a halo of low counts values is visible.

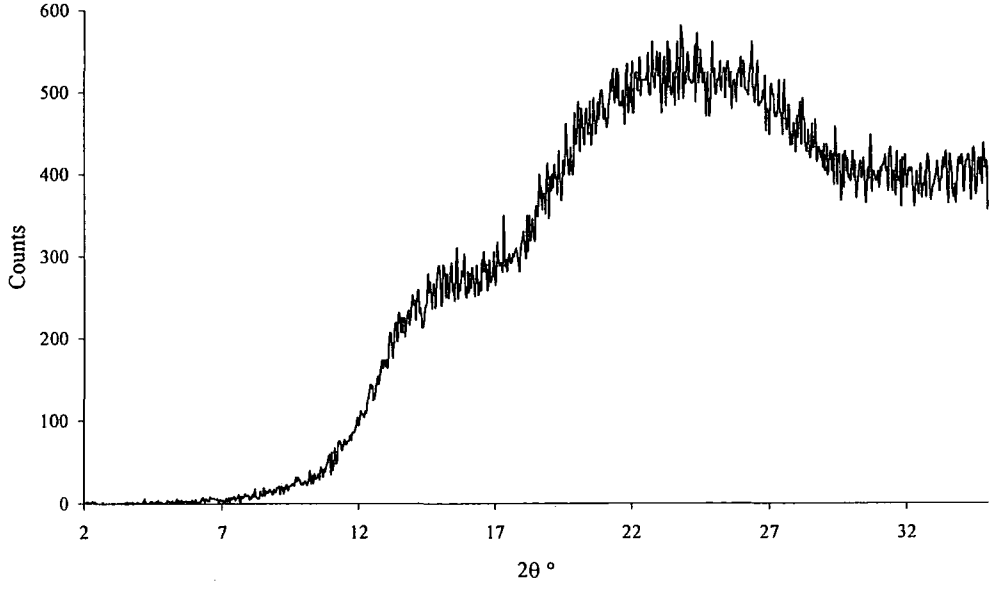

Figure 4.23: XRPD of amorphous carbamazepine at room temperature.

This method was further used with VT equipment to see if any recrystallisation was appearing over a range of temperatures similar to the one used for the ^{13}C VT SSNMR, and following a similar time scale to that shown in chapter Five for the relaxation times measurements. The result of this experiment is shown in figure 4.24 and it shows that recrystallisation occurred between 60°C and 80°C. Furthermore, it is possible to say that this phenomenon is non-reversible as the diffractogram obtained when going back down in temperature still shows substantial signs of crystallinity.

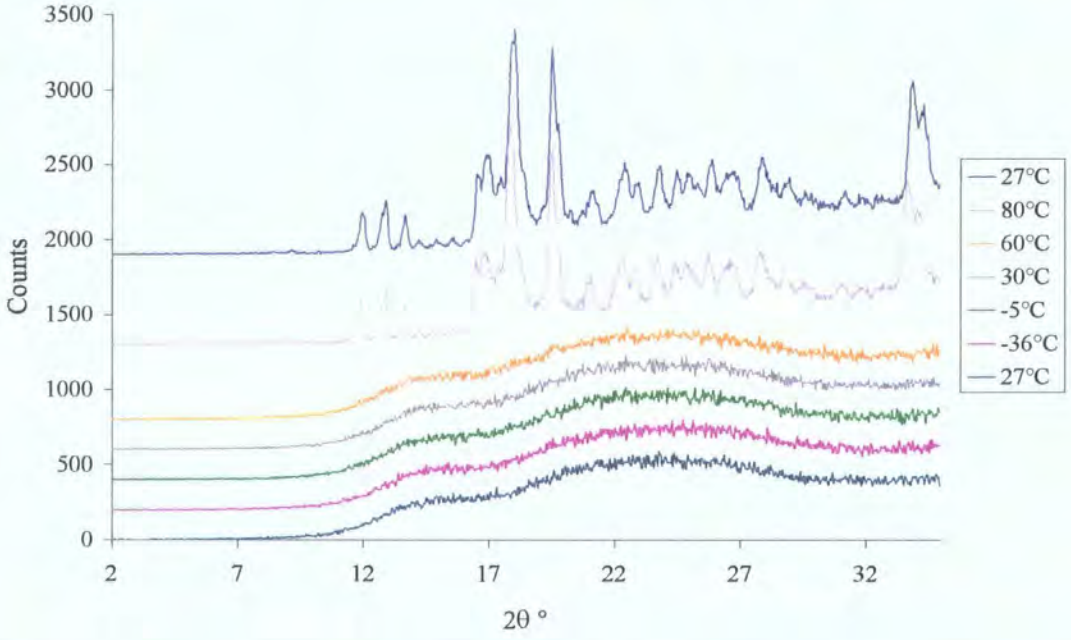

Figure 4.24: VT XRPD experiment of amorphous carbamazepine.

Following the results of this experiment it was decided to carry out a similar experiment using increments of 5°C, see figure 4.25, rather than following the temperatures used for the ^{13}C SSNMR experiment. The timing for this last experiment is shown in table 4.5. One can see that signs of recrystallisation are observable from 65°C and are more evident at 70°C and 75°C, at which point the process seems to be complete as no significant differences can be observed between the diffractograms at 75°C and 80°C. The temperature at which the recrystallisation starts to occur is consistent for both XRPD and ^{13}C SSNMR.

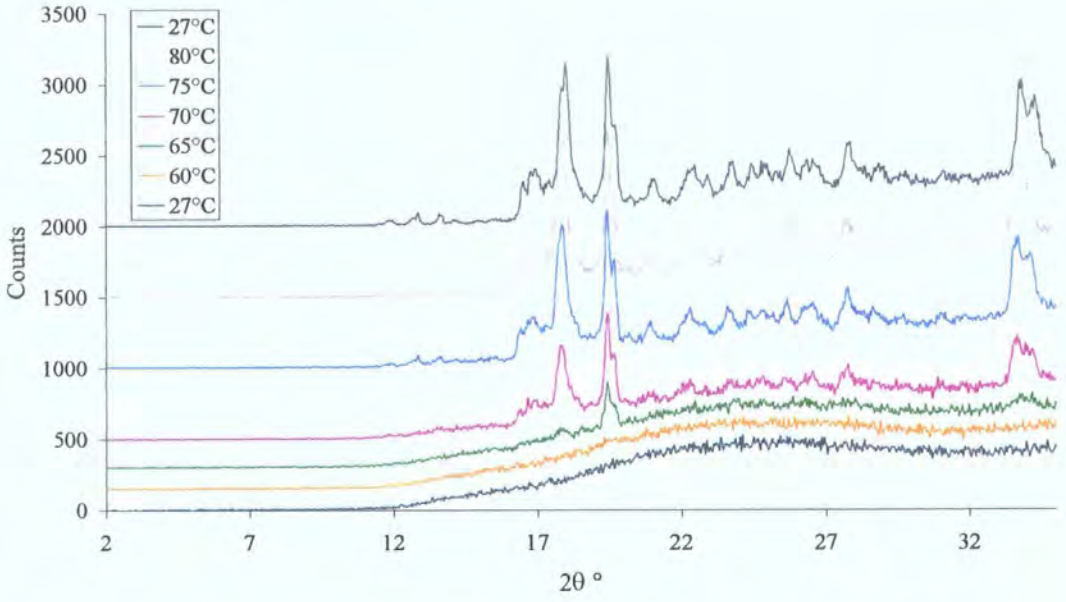

Figure 4.25: VT XRPD experiment of amorphous carbamazepine.

2/ Conclusions

It has been observed that all three compounds of interest can easily be made amorphous by a simple quench-cooling process. It was also shown that amorphous indomethacin could be kept either intact at room temperature or in the freezer, or ground and in the freezer, while amorphous nifedipine should be kept intact and in the freezer. Furthermore, it was seen that, once amorphous, these compounds behave in different ways. It was observed that amorphous indomethacin did not seem to recrystallise in the timescale of the SSNMR and XRPD experiments up to a temperature of 80°C but a reversible phenomenon, possibly due to an increase in molecular mobility, was observed, using ^{13}C SSNMR, at 90°C. However, both amorphous nifedipine and amorphous carbamazepine seem to recrystallise at a temperature of about 65°C. These observation were consistent between XRPD and ^{13}C SSNMR techniques.

3/ References

1. A. H. Forster, J. Hempenstall, and T. Rades. Characterisation of glass solutions of poorly water-soluble drugs produced by melt extrusion with hydrophilic amorphous polymers. *J. Pharm. Pharmacol.* **53**: 303-315 (2001).

2. D. C. Apperley and R. K. Harris. Unpublished work.

3. E. Fukuoka, M. Makita, and S. Yamamura. Some physicochemical properties of glassy indomethacin. *Chem. Pharm. Bull.* **34**: 4314-4321 (1986).

4. Y. Aso, S. Yoshioka, and S. Kojima. Relationship between the crystallization rates of amorphous nifedipine, phenobarbital, and flopropione, and their molecular mobility as measured by their enthalpy relaxation and ^{1}H NMR relaxation times. *J. Pharm. Sci.* **89**: 408-416 (2000).

5. A. Burger and K. T. Koller. Polymorphism and pseudopolymorphism on nifedipine. *Sci. Pharm.* **64**: 293-301 (1996).

6. B. Keymolen, J. L. Ford, M. W. Powell, and A. R. Rajabi-Siahboomi. Investigation of the polymorphic transformations from glassy nifedipine. *Thermochim. Acta* **397**: 103-117 (2003).

7. A. H. Forster. Ph.D. Thesis. School of Pharmacy. University of Otago (2001).

8. J. E. Patterson, M. B. James, A. H. Forster, R. W. Lancaster, J. M. Butler, and T. Rades. The influence of thermal and mechanical preparative techniques on the amorphous state of four poorly soluble compounds. *J. Pharm. Sci.* **94**: 1998-2012 (2005).

Chapter Five: Amorphous Materials – ^{1}H SSNMR

1/ Results

This chapter will look at the results obtained on the amorphous form of the studied drugs using ^{1}H SSNMR. This will involve studying the proton bandshapes as a function of temperature in order to gain more understanding of the recrystallisation process. It will also involve looking at the T_1^H and $T_{1\rho}^H$ values obtained over a wide range of temperature in order to gain information on the molecular-level motions.
The data obtained with the 300 MHz spectrometer was the work of D.C. Apperley[1] and is shown here for comparative purposes.

1.1/ Proton bandshapes

The proton bandshapes of the amorphous samples were studied over a range of temperatures past the Tg in order to obtain information about the recrystallisation phenomenon at high temperatures. The spectra were recorded using a one-pulse-and-acquire pulse sequence.
The proton bandshapes were also recovered, as secondary information, from the T_1^H and $T_{1\rho}^H$ experiments, more precisely from the last spectrum of the array for T_1^H and the first spectrum of the array for $T_{1\rho}^H$. They were then analysed in order to obtain more information on the way the sample behaves over a wider range of temperature.
The last spectrum of the array for the T_1^H measurements was used as this is the spectrum where the recovery time allowed the system to be back to complete equilibrium. Therefore, after this recovery time, one is actually in the presence of a simple one-pulse-and-acquire pulse sequence on a sample at equilibrium. Furthermore, the first spectrum of the array for the $T_{1\rho}^H$ experiment was also used as this is the spectrum where the spin-lock time is the shortest. Thus, the spectrum acquired is as close as possible to one that would have been obtained using a pulse-and-acquire pulse sequence.
In this chapter, only the proton bandshapes obtained from the T_1^H are shown since the T_1^H and $T_{1\rho}^H$ experiments, as expected, yielded similar spectra.

1.1.1) Indomethacin

The static ^{1}H VT SSNMR spectra of amorphous indomethacin obtained by pulse-and-acquire are shown in figure 5.1. The timing for this experiment is shown in table 5.1. Figure 5.1 shows that, when heating from ambient temperature up to 70°C, only a sharpening of the peak is visible. However, from 90°C upwards a very sharp set of peaks is visible without any other broad peaks. This shows that there is rapid motion in the amorphous solid, probably due to some amorphous sample having not yet recrystallised.

The spectra at 120°C and 150°C are similar, and were compared to the high-speed MAS ^{1}H SSNMR spectra obtained for the crystalline material (see figure 3.29).

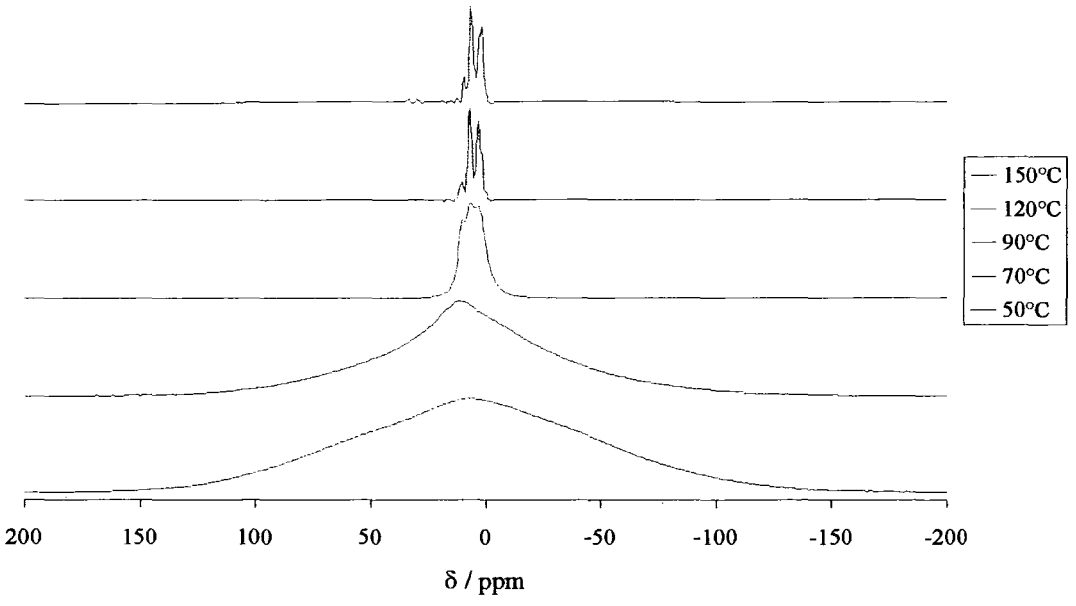

Figure 5.1: Static ^{1}H VT SSNMR spectra of amorphous indomethacin obtained by single-pulse-and-acquire at 200.13 MHz, ^{1}H frequency.

Figure 5.2 shows the proton bandshapes obtained from the last spectrum of the T_1^H array at different temperatures for amorphous indomethacin. The timing for the experiment is shown in table 5.2. The timing was matched to within two hours between the different series of experiments.

Temperature / °C	Temperature reached at / hr:min	Experiment started at / hr:min	Experiment finished at / hr:min
50	0:00	0:20	0:23
70	0:28	0:48	0:51
90	0:57	1:17	1:20
120	1:25	1:45	1:48
150	1:54	2:14	2:17

Table 5.1: Timing used for the ^{1}H VT SSNMR experiment performed on amorphous indomethacin.

It is seen from figure 5.2 that no real changes, apart from a slight sharpening, occurs for the proton bandshape for temperatures between –70°C and 50°C, apart from a slight sharpening at 50°C, i.e. past Tg. However, at 60°C the sharpening is increased and from 80°C only a single, relatively sharp peak is visible. This shows a change in mobility, probably arising from non-recrystallised amorphous parts in the sample, which is in accordance with that observed in figure 5.1. Note that the splitting of the sharp peak was observable in figure 5.1 but does not seem to appear in figure 5.2. This is explained by the change in the scale of the x-axis between the two figures.

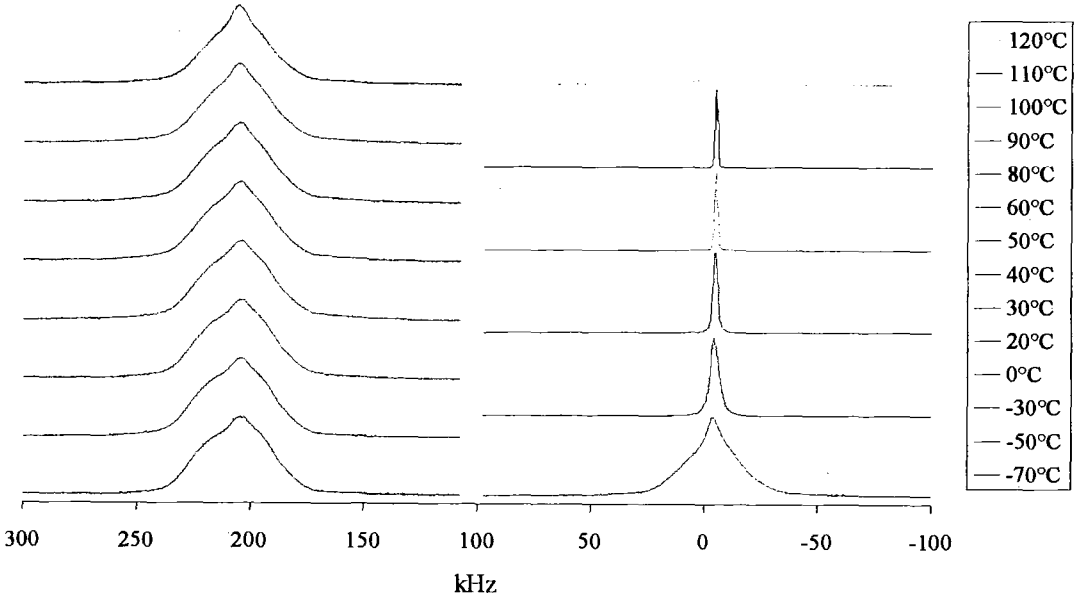

Figure 5.2: Proton bandshapes obtained from the last spectrum of the T_1^H array at different temperatures for amorphous indomethacin. The horizontal scale is for reference only.

At the highest temperature, a very broad signal can be seen underlying the sharp peak. This may be ascribed to recrystallised indomethacin, which is relatively rigid. Such a spectrum was also obtained, earlier, by Dr. Apperley[1]. The broad underlying signal is not visible in figure 5.1, probably because the total time taken for the pulse-and-acquire spectra is significantly less than that for the T_1^H experiment.

Temperature / °C	Temperature reached at / hr:min	Experiment started at / hr:min	Experiment finished at / hr:min
-70	0:00	0:20	0:28
-50	0:33	0:48	0:54
-30	0:59	1:14	1:25
0	1:30	1:45	2:00
20	2:05	2:20	2:43
30	2:48	2:58	3:24
40	3:29	3:39	4:05
50	4:10	4:20	4:42
60	4:47	4:57	5:21
80	5:26	5:41	6:02
90	6:07	6:17	6:30
100	6:35	6:45	6:55
110	7:00	7:10	7:42
120	7:47	7:57	8:41

Table 5.2: Timing used for the T_1^H and $T_{1\rho}^H$ experiments performed on amorphous indomethacin. The experiment times include both experiments.

1.1.2) Nifedipine

The static ^{1}H VT SSNMR spectra of amorphous nifedipine obtained by pulse-and-acquire are shown in figure 5.3. The timings for this experiment is shown in table 5.3. The figure shows that the peak is sharpening a lot between 50°C and 70°C, probably due to more mobility in the amorphous phase. However, at 90°C significantly broader peak with a sharp peak on top of it appears. This could be explained by a two-phase system where both the amorphous and the crystalline phases are present. It is clear that the recrystallisation is significantly easier (and occurs at a lower temperature) for nifedipine than for indomethacin. This phenomenon was described briefly in chapter Four and in more detail by Burger and

Koller[2]. The sharp peak is more and more defined as the temperature rises form 90°C to 150°C. This sharp peak might be due to residual amorphous domains that are difficult to recrystallise.

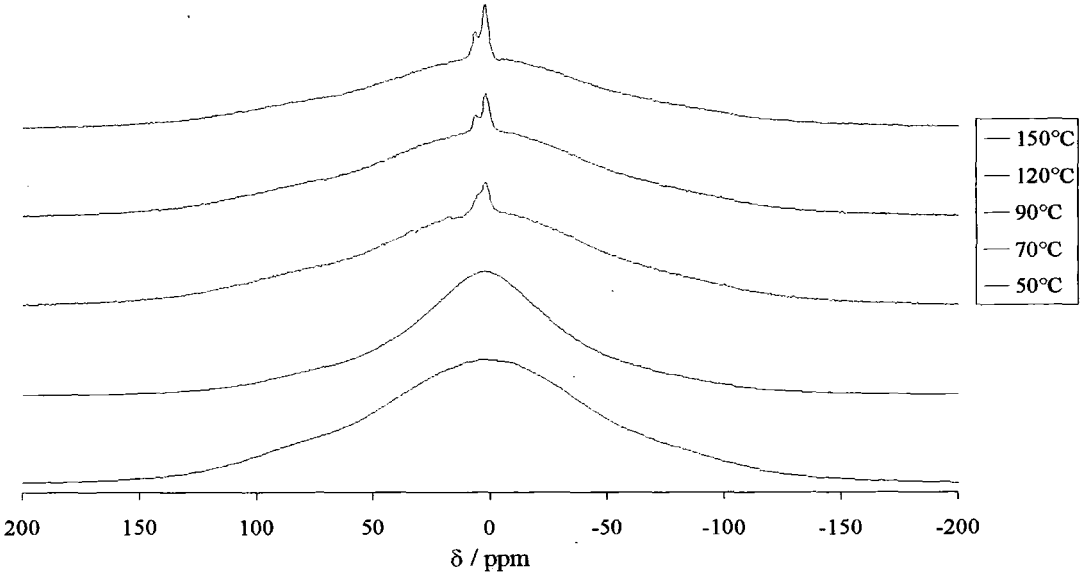

Figure 5.3: Static ^{1}H VT SSNMR spectra of amorphous nifedipine obtained by single-pulse-and-acquire at 200.13 MHz, ^{1}H frequency.

Temperature / °C	Temperature reached at / hr:min	Experiment started at / hr:min	Experiment finished at / hr:min
50	0:00	0:20	0:28
70	0:33	0:53	1:01
90	1:06	1:26	1:34
120	1:39	1:59	2:07
150	2:12	2:32	2:38

Table 5.3: Timing used for the ^{1}H VT SSNMR experiment performed on amorphous nifedipine.

Figure 5.4 shows the proton bandshapes obtained from the last spectrum of the T_1^H array at different temperatures for amorphous nifedipine. The timing for the experiment is shown in table 5.4. The timing was matched to within two hours between the different series of experiments. The difference observed in the shape of the peak between figure 5.3 and figure 5.4 is due to the fact that the total time taken for the pulse-and-acquire spectra is significantly less than that for the T_1^H experiment.

Figure 5.4 shows that there is little change until 80°C is reached when a sharp peak, with a broad peak under it, is visible. It would seem that recrystallisation has not occurred up to 60°C. It may have done so to some extent at 80°C, but this is hard to see, the sharp peak presumably arising from increased mobility in amorphous domains.

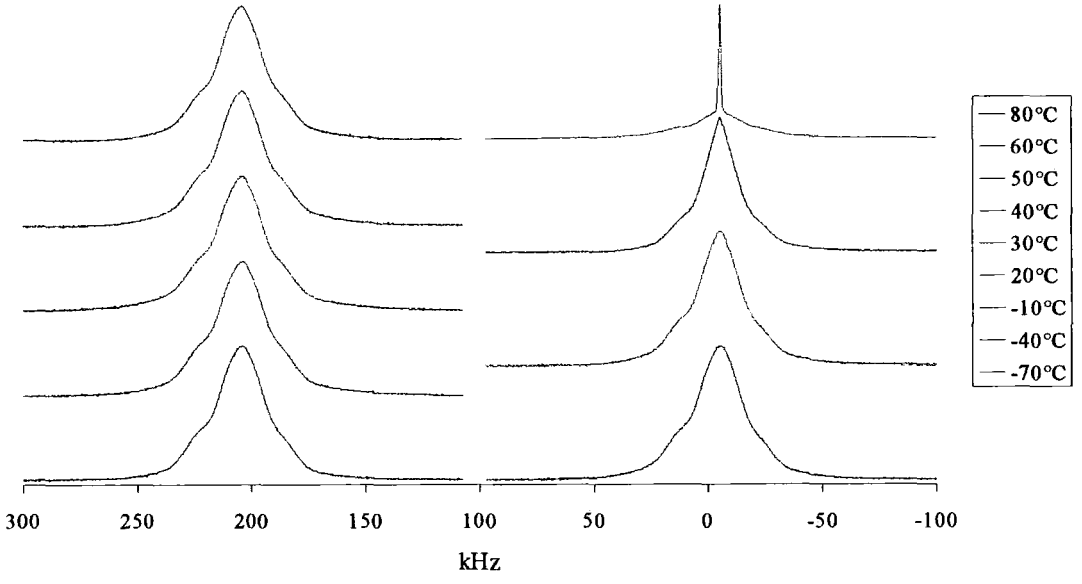

Figure 5.4: Proton bandshapes obtained from the last spectrum of the T_1^H array at different temperatures for amorphous nifedipine. The horizontal scale is for reference only.

Temperature / °C	Temperature reached at / hr:min	Experiment started at / hr:min	Experiment finished at / hr:min
-70	0:00	0:20	0:33
-40	0:38	0:58	1:10
-10	1:15	1:35	1:48
10	1:53	2:13	2:27
25	2:32	2:52	3:07
30	3:12	3:22	3:37
40	3:42	3:52	4:07
50	4:12	4:22	4:38
60	4:43	4:53	5:09
80	5:14	5:34	5:48

Table 5.4: Timing used for the T_1^H and $T_{1\rho}^H$ experiments performed on amorphous nifedipine. The experiment times include both experiments.

1.1.3) Carbamazepine

The one-pulse-and-acquire pulse sequence was not used to obtain information on the proton bandshape as this compound has a very long T_1^H value (more than 300 s), as discussed in chapter One. However, the bandshape could still be recovered from the T_1^H and $T_{1\rho}^H$ experiments and the series of spectra obtained from the T_1^H case is shown in figure 5.5. The timing for this experiment is shown in table 5.5. The timing was matched to within two hours between the different series of experiments.

The proton bandshapes shown in figure 5.5 seem to be composed of a peak surrounded by two "wings". These "wings" resemble a Pake doublet and from this doublet it is possible to see that $\frac{3}{2}D$ is 38.4 kHz yielding a proton to proton radius of 0.167 nm. This value does not fit with any of the proton-proton distances observed for carbamazepine. However, it does fall between the H-H value for the amino group and that of the two protons on the 7-atoms ring, 0.156 nm and 0.229 nm respectively. The fact that the calculated value is "in between" is expected as both distances are present in the molecule.

Figure 5.5 shows that the proton bandshape of amorphous carbamazepine does not change much between –70°C and 55°C. However, a sharpening is observable from 65°C, which is consistent with the VT XRPD study shown in figure 4.20, and is consistent with expectations as the sample is heated above Tg. The sharpening is more pronounced at 75°C, even more at 85°C and finally a really sharp peak is observed at 105°C.

As for indomethacin and nifedipine, the sharp peak is associated with amorphous domains that have not yet recrystallised, while the underlying broad peak at 85°C and 105°C probably arises from the recrystallised sample. One can also see that the area of the sharp peak gets smaller as the temperature rises. This is probably due to the fact that the recrystallisation is more and more complete, i.e. that the non-recrystallised amorphous is becoming crystalline. This seems to be in accordance with what was observed in chapter Four, i.e. that amorphous carbamazepine starts to recrystallise around 65°C and this phenomenon is still going on at 80°C. From this study, it can be seen that the recrystallisation phenomenon is still being under way at 105°C when using the timing shown below.

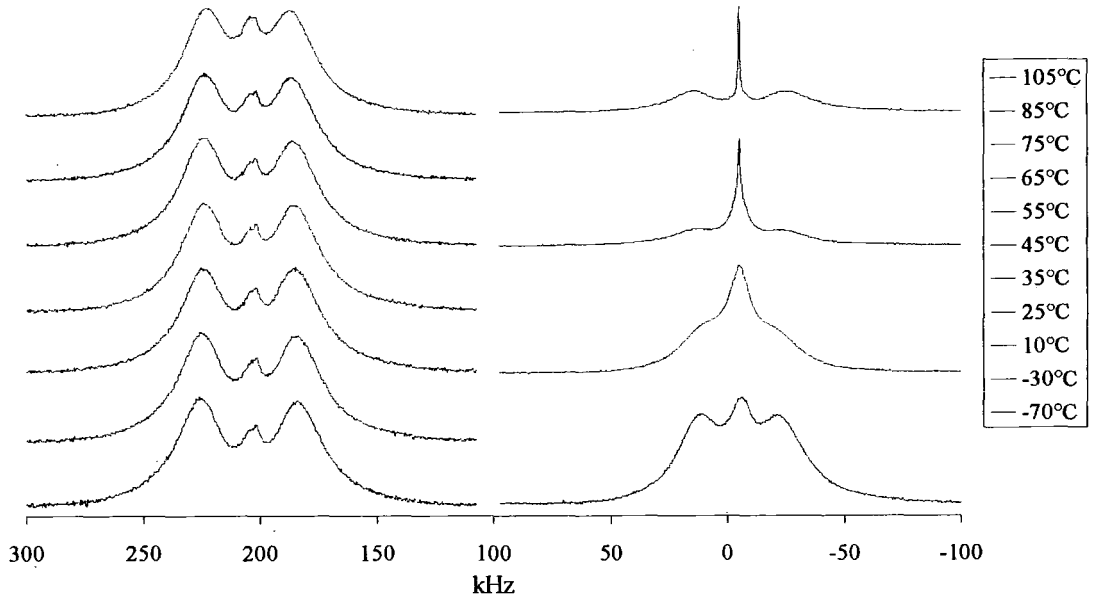

Figure 5.5: Proton bandshapes obtained from the last spectrum of the T_1^H array at different temperatures for amorphous carbamazepine. The horizontal scale is for reference only.

Temperature / °C	Temperature reached at / hr:min	Experiment started at / hr:min	Experiment finished at / hr:min
-70	0:00	0:20	0:59
-30	1:04	1:24	1:54
10	1:59	2:19	2:53
25	2:58	3:18	3:50
35	3:55	4:05	4:39
45	4:43	4:53	5:27
55	5:32	5:42	6:16
65	6:21	6:31	7:04
75	7:09	7:19	7:49
85	7:54	8:04	8:28
105	8:33	8:53	9:56

Table 5.5: Timing used for the T_1^H and $T_{1\rho}^H$ experiments performed on amorphous carbamazepine. The experiment times include both experiments.

1.2/ T_1^H and $T_{1\rho}^H$ measurements

The measurements have been carried out, at the miniumum, in duplicate using the amorphous drug which was prepared according to the protocol shown in chapter Two.

In the case of the crystalline materials, the activation energies were retrieved from the slopes of the T_1^H and $T_{1\rho}^H$ curves because in such a case only a single specific type of motion appears to be involved. However, there are circumstances when meaningful activation energies cannot be retrieved from the slope. This can be due to the presence of several motions of similar activation energies. In the case of amorphous materials, it is likely that complications arise due to the fact that for any given motion a range of activation energies is expected as the intermolecular interactions will vary with the local environment which is variable throughout an amorphous sample. In both of these cases, the situation would involve overlapping minima, giving a broad and shallow minimum, if any minimum is visible at all. As a result, the slopes would not properly reflect the activation energies.

Srcic et al.[3] showed that SSNMR could be used to confirm the amorphous nature of a sample by looking at T_1 for both the crystalline and amorphous materials; it appears that the closer the sample gets to its melting point the greater the difference in T_1 between the crystalline and amorphous materials becomes. They used this as a proof that they had formed glassy felodipine. However, the relaxation time study in this thesis was well below the melting point of the drugs, and as such it is difficult to assess the amorphous character of any of the compounds using SSNMR.

1.2.1) Indomethacin

Figure 5.6 shows the T_1^H curve, as a function of the temperature, obtained for amorphous indomethacin. The raw data are given in appendix 20. It is clearly visible from the figure that the trends in T_1^H have similar behaviour at different magnetic fields, as one could expect. However, as T_1^H is dependent on the Larmor frequency, the change of strength of the magnetic field influences its value, as demonstrated in figure 5.6.

From this figure, it can be seen that a maximum appears around Tg at ca. 45°C (Tg was measured, using DSC, to be 45°C for amorphous indomethacin, see figure 4.1).

The maximum appears after a steady increase in the T_1^H value from -70°C which could indicate recovery from a T_1^H minimum at or below -70°C. If one compares the slopes obtained from the crystalline material to those obtained from the amorphous material, it can be seen that they follow a similar trend before Tg. It is also noticeable that the T_1^H value is slightly lower for the amorphous than for the crystalline, which is expected as the former is likely to be somewhat more mobile than the latter. Above Tg, the values of T_1^H drop sharply as generalised motion occurs. This observation is consistent with the linewidth decreases mentioned above, but is apparent at lower temperatures.

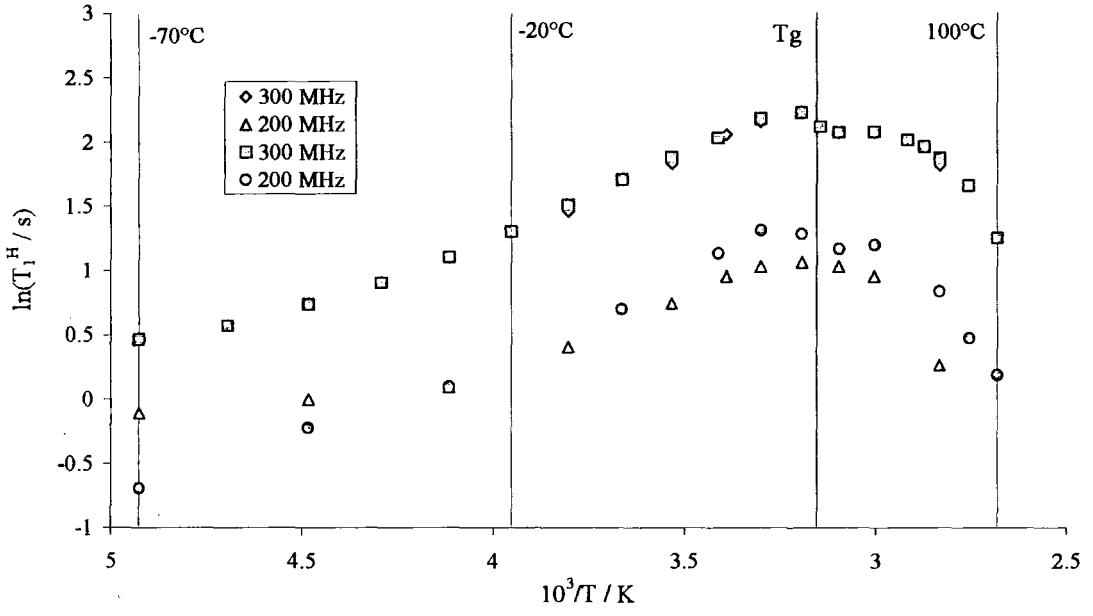

Figure 5.6: T_1^H measurements for amorphous indomethacin. The maximum is observed at Tg (45°C).

Figure 5.7 shows the $T_{1\rho}^H$ curve, as a function of the temperature, obtained for amorphous indomethacin. The raw data are given in appendix 20.

It is clearly visible from the figure that $T_{1\rho}^H$ behaves similarly at different magnetic fields. This is fortuitous, as the nutation frequency was set to different values (50 kHz and 70 kHz at 200 MHz and 300 MHz, respectively). This anomaly could be due to sample history.

Figure 5.7 shows two distinctive changes in slope through the studied range of temperature. The first change occurs around Tg, at around 45°C, which indicates a increase in mobility, as expected. The second change, which appears to involve a

minimum, happens at around 80°C and could be caused by the start of the recrystallisation. However, if recrystallisation occurs then it is expected that the value of T_1^H would begin to increase, which is not seen in figure 5.6. This is consistent with what was observed by ^{13}C VT SSNMR in chapter Four; that is to say that this change could be due to an increased molecular mobility. One can also see that below Tg the slope of $T_{1\rho}^H$ is slightly negative while that for T_1^H is positive, clearly showing a difference in the motion process monitored by the two relaxations, which is expected and explained in chapter Three.

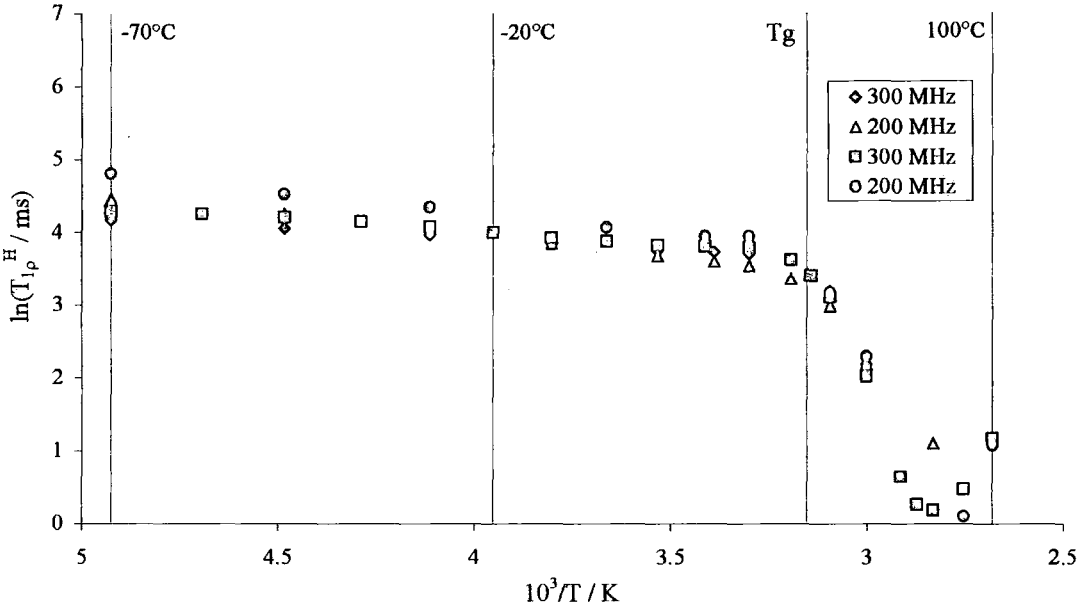

Figure 5.7: $T_{1\rho}^H$ measurements for amorphous indomethacin. The change of slope is observed at Tg (45°C).

As for the T_1^H study, it is possible to see that the relaxation times are lower for the amorphous phase, even though they are complicated by the minimum for the crystalline form. This suggests that amorphisation increases the mobility of the sample, as expected.

1.2.2) Nifedipine

The first experiments done on amorphous nifedipine showed a rather abnormal, and irreproducible, jump in T_1^H at around 20°C (data not shown). As stated in chapter Two, one needs to be careful when dealing with temperature-dependent

measurements as the temperature inside the probe rises quite quickly in order to compensate when the VT controller is switched off. As amorphous nifedipine involved temperature-dependent NMR properties, this explains the phenomenon observed which was solved by following the protocol described in chapter Two.

Figure 5.8 shows the T_1^H curve, as a function of the temperature, obtained for amorphous nifedipine. The raw data are given in appendix 21.

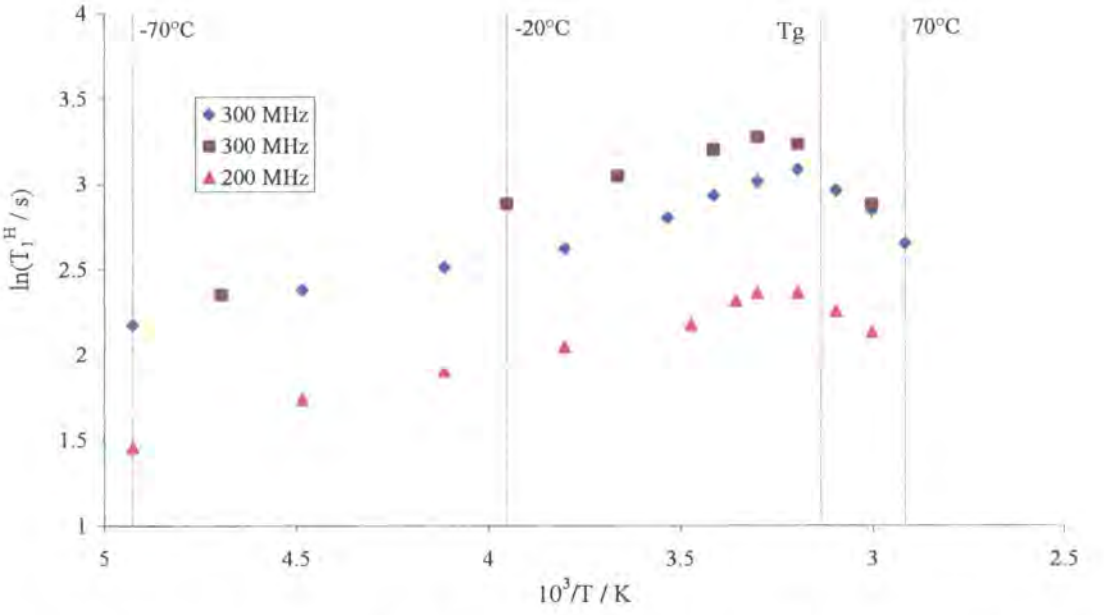

Figure 5.8: T_1^H measurements for amorphous nifedipine. The maximum is observed to be at ca. 40°C.

From figure 5.8, it can be seen that a maximum is observed to be at ca. 40°C which is significantly lower than Tg (measured to be 46°C using DSC, see figure 4.9). This maximum indicates a change in mobility happening before Tg; this could be a reason why amorphous nifedipine is not as stable as amorphous indomethacin.

When comparing the crystalline and amorphous relaxation times data, one can see that, as for indomethacin, the T_1^H slopes run parallel until Tg. Furthermore, the crystalline T_1^H values are higher than for the amorphous, showing more mobility for the amorphous material, as for indomethacin. However, the difference observed between the two phases of the sample for nifedipine is larger than for indomethacin, perhaps also helping to explain the tendency of nifedipine to recrystallise.

Figure 5.9 shows the $T_{1\rho}^{H}$ curve, as a function of the temperature, obtained for amorphous nifedipine. The raw data are given in appendix 22.

From this figure it is again visible that a change in the slope happens at a temperature 5-8°C lower than Tg, which is in agreement with what was observed for T_1^{H} and also with the work of Aso et al.[4]. This confirms that there is something happening to amorphous nifedipine before it reaches Tg. However, it is not possible to determine what is exactly happening, though one could say that this is probably related to the lack of stability for amorphous nifedipine.

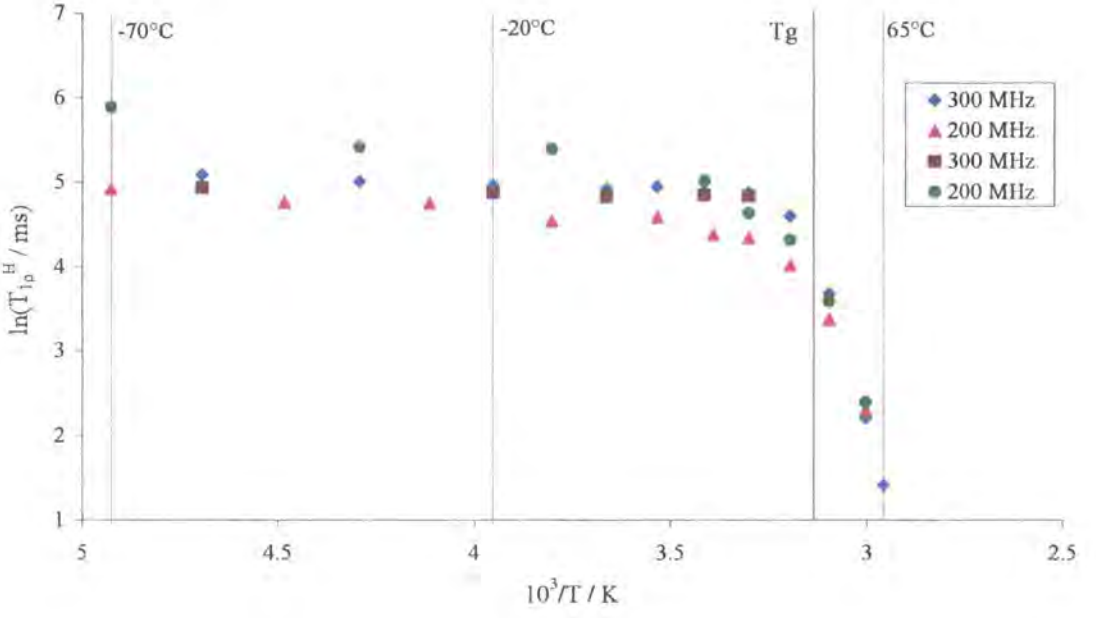

Figure 5.9: $T_{1\rho}^{H}$ measurements for amorphous nifedipine. The change in slope is observed at ca. 40°C.

As for indomethacin, the $T_{1\rho}^{H}$ values for amorphous nifedipine are smaller than for the crystalline counterpart, though in this case, $T_{1\rho}^{H}$ is too long for the crystalline material to be measured. Clearly, the difference in $T_{1\rho}^{H}$ values between the two phases is far greater for nifedipine than for indomethacin, as was observed for T_1^{H}. This supports the idea that the amorphisation of the sample makes it more mobile. Furthermore, the larger difference in $T_{1\rho}^{H}$ values indicates that nifedipine is relatively more mobile than indomethacin, which could explain why nifedipine has a greater tendency to recrystallise than indomethacin.

1.2.3) Carbamazepine

Figure 5.10 shows the T_1^H curve, as a function of temperature, obtained for amorphous carbamazepine. The raw data is given in appendix 23.

From this figure it can be seen that a maximum appears at ca. 55°C, which is close to Tg (Tg was found to be 57°C for amorphous carbamazepine, see figure 4.14). This maximum appears to be the recovery of the system after a minimum that seems to be around -30°C. This minimum is broad and shallow, as would be expected for an amorphous system (see the discussion at the beginning of part 1.2).

In chapter Three, it was noted that no information could be retrieved from the T_1^H measurements on crystalline carbamazepine. This was linked to the lack of conformational flexibility of the molecule. Moreover, if one compares the crystalline and amorphous T_1^H behaviour over this range of temperature, it is clearly visible that the T_1^H values are lower for the amorphous form than for the crystalline form. This demonstrate that amorphisation is making carbamazepine, as for the other two samples, somewhat more mobile.

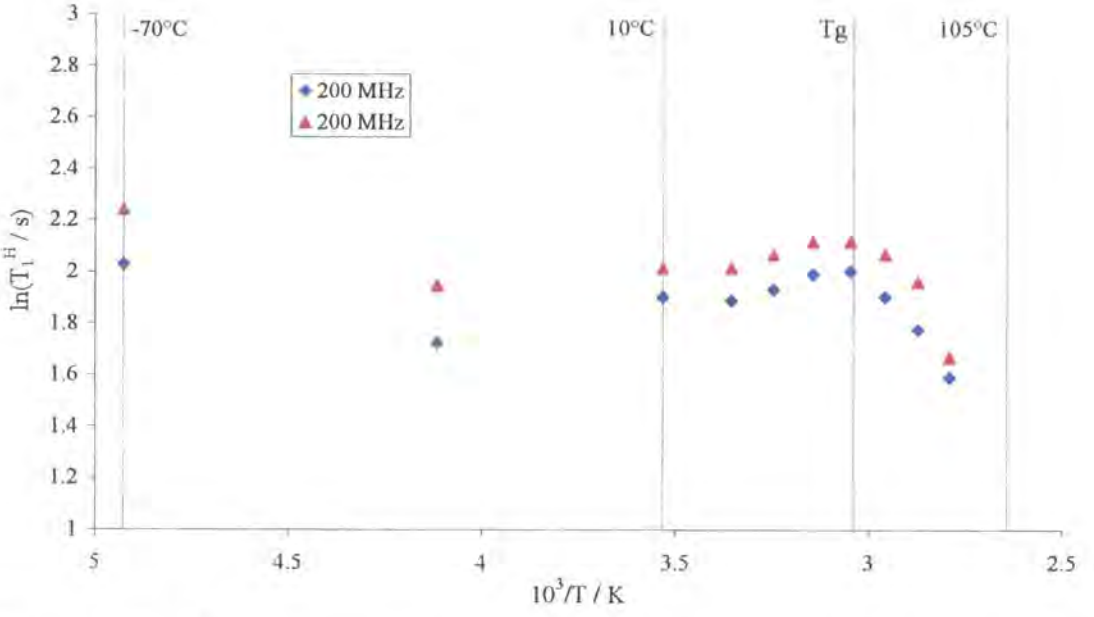

Figure 5.10: T_1^H measurements for amorphous carbamazepine. A maximum is observed at ca. 55°C.

From figure 5.6 and figure 5.10, one can see that amorphous indomethacin and amorphous carbamazepine are quite similar in their behaviour, that is to say that they both go through a maximum around their Tg and also that they appear to go through

a broad minimum at low temperature. If one also considers figure 5.8, it is visible that amorphous nifedipine is different from the other two drugs because the maximum happens before Tg. This is probably a reason for the poor stability of amorphous nifedipine. One could suggest from the similarity between indomethacin and carbamazepine that carbamazepine is stable when amorphous. However, as seen earlier, the big difference in T_1^H values from crystalline to amorphous for carbamazepine seems to point to a relatively unstable amorphous material, as observed experimentally.

Figure 5.11 shows the $T_{1\rho}^H$ curve, as a function of temperature, obtained for amorphous carbamazepine. The raw data is given in appendix 23.

From this figure, a visible change in slope happens between 35°C and 45°C, i.e. before Tg. This change in slope shows that something happens to the motional process of the molecule which could be causing some disturbances, and as such may be related to the lower stability of amorphous carbamazepine.

From figure 5.11, it can be observed that the $T_{1\rho}^H$ curve goes through a minimum between 75°C and 85°C. This change in the value of $T_{1\rho}^H$ is probably due to the recrystallisation of the material. This was confirmed by the proton bandshapes study where it was visible, see figure 5.5, that the recrystallisation probably starts between 75°C and 85°C.

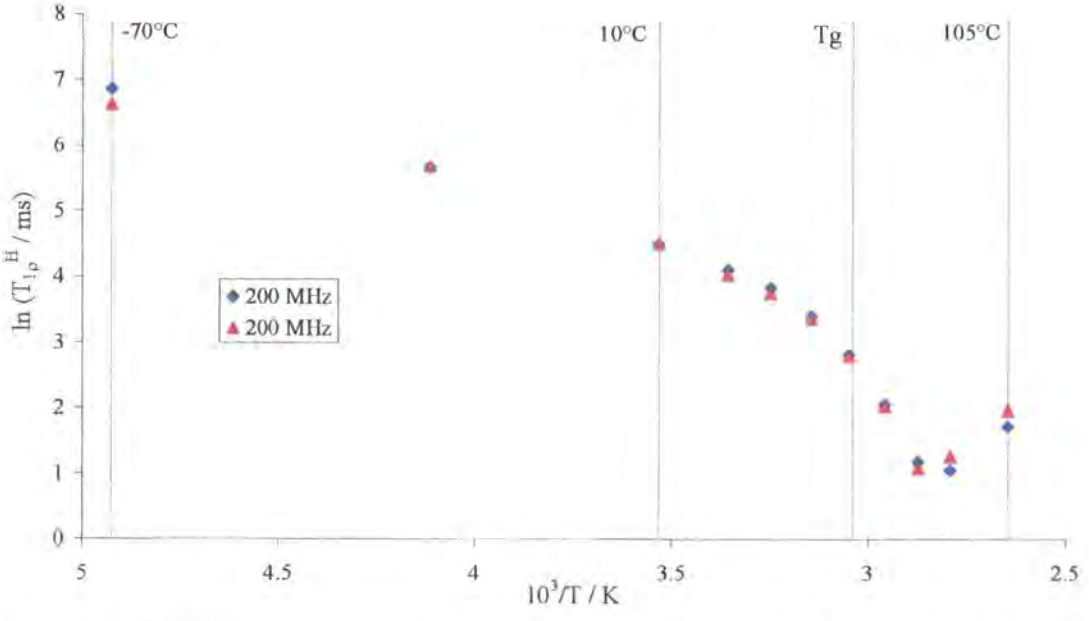

Figure 5.11: $T_{1\rho}^H$ measurements for amorphous carbamazepine. A change in slope is observed between 35°C and 45°C and a minimum between 75°C and 85°C.

As for the other two compounds, the $T_{1\rho}^H$ values for amorphous carbamazepine are smaller than for the crystalline counterpart; the $T_{1\rho}^H$ values being too long for the crystalline material to be measured. Much as for nifedipine, the difference in $T_{1\rho}^H$ values between the two phases is clearly far greater for carbamazepine than for indomethacin. This strengthens the fact that the amorphisation of the sample makes it more mobile, but also that amorphisation gives carbamazepine a greater tendency to recrystallise than indomethacin.

When comparing figure 5.7, figure 5.9 and figure 5.11, one can see that all three compounds go through a change in slope around or before Tg. It was also seen that indomethacin and carbamazepine go through a minimum at high temperature. However, this minimum may be caused by an increase in molecular mobility for indomethacin while it might be caused by recrystallisation for carbamazepine . It was observed through these three figures that a change in slope before Tg could possibly be linked to a compound being more prone to recrystallisation.

2/ Conclusions

2.1/ Proton bandshape

It has been seen that indomethacin recrystallises above 100°C in the time scale of the SSNMR experiments.

In the case of nifedipine, the recrystallisation process started at around 70°C and a two-phase system seemed to be present during this recrystallisation. This could explain what was observed with the DSC and hot-stage microscopy experiments.

For carbamazepine, the recrystallisation process may have started around 75°C, although this is not clear. However, due to the long pulse delay necessary for amorphous carbamazepine, information at higher temperatures than 105°C using the pulse-and-acquire pulse sequence could not be obtained.

2.2/ T_1^H and $T_{1\rho}^H$ measurements

It was seen from the T_1^H experiments on the three amorphous samples that the amorphisation process seemed to increase the mobility of the sample. However, this increase in mobility was larger for carbamazepine and nifedipine than for

indomethacin. This could possibly explain the fact that the two former samples are more prone to recrystallisation than the latter. It was also seen that indomethacin and carbamazepine behave similarly as they both show a change in slope around Tg. Although this seemed to indicate that amorphous carbamazepine, like amorphous indomethacin, is relatively stable, the change in T_1^H value from crystalline to amorphous seems to indicate the opposite, which is consistent with the experimental data. This difference seemed to show that one should look at the results from both phases, not just from the amorphous material, in order to understand the stability of the amorphous phase.

The results obtained from the $T_{1\rho}^H$ experiments seemed to confirm that amorphisation increases the mobility of the sample. These experiments also showed that all three compounds go through a change in slope. This change in slope happened around Tg for indomethacin and before Tg for the other two compounds and it seemed that a change in slope before Tg could be linked to a compound being more prone to recrystallisation. It was also seen that indomethacin and carbamazepine go through a minimum at high temperature. However, this minimum seemed to be caused by a different phenomenon for each compound, i.e. increased molecular mobility for indomethacin and recrystallisation for carbamazepine. Therefore, the presence of a minimum is not particularly indicative of any particular phenomenon and should be investigated using other experiments, such as ^{13}C SSNMR and XRPD.

3/ References

1. D. C. Apperley. Glaxo - Amorphous drug project, Unpublished.

2. A. Burger and K. T. Koller. Polymorphism and pseudopolymorphism on nifedipine. *Sci. Pharm.* **64**: 293-301 (1996).

3. S. Srcic, J. Kerc, U. Urleb, I. Ziupancic, G. Lahajnar, B. Kofler, and J. Smid-Korbar. Investigation of felodipine polymorphism and its glassy state. *Int. J. Pharm.* **87**: 1-10 (1992).

4. Y. Aso, S. Yoshioka, and S. Kojima. Relationship between the crystallization rates of amorphous nifedipine, phenobarbital, and flopropione, and their molecular mobility as measured by their enthalpy relaxation and ^{1}H NMR relaxation times. *J. Pharm. Sci.* **89**: 408-416 (2000).

Chapter Six: PVP work

1/ Results

This chapter will look at the results obtained on the PVP/drug co-melts using ^{13}C and ^{1}H SSNMR. This will involve studying the ^{13}C spectra of the co-melts in order to check their amorphous character. This will also involve the study of the proton bandshapes as a function of temperature in order to obtain information about the effect of PVP on the system. It will also involve looking at the T_1^H and $T_{1\rho}^H$ values obtained over a wide range of temperatures in order to gain some information on the effect of PVP on the motional processes.

1.1/ PVP

Amorphous drugs in formulation are often associated with a polymeric compound acting as an antiplasticiser. In the case of this study, PVP was used because it has a high Tg when dry, i.e. 165°C. However, this polymer is really hygroscopic, which implies that its' Tg will decrease rapidly in the presence of humidity. Nevertheless, the mix of the amorphous drug and such a polymer will have a higher Tg than the amorphous drug itself. Therefore, the formulation will probably have a greater stability than the amorphous drug alone. In order to minimise the amount of moisture going into the sample, a sufficient portion of PVP was dried under vacuum for a minimum of 3 hours before every experiment. Moreover, the drug and PVP portions were weighed quickly after the removal of the PVP sample from the oven and put straight into the oven in order to obtain the co-melt.

The CPMAS ^{13}C SSNMR spectrum of PVP itself was acquired and is shown in figure 6.1. The assignment of PVP is the work of Zheng et al.[1]

Figure 6.2 shows the proton bandshapes obtained from the last spectrum of the T_1^H array at different temperatures for PVP. The timing for the experiment is shown in table 6.1. This figure shows that two components are present from the beginning of the experiment and also that the intensity in the narrow signal starts to be lost at 80°C and has practically gone by 90°C.

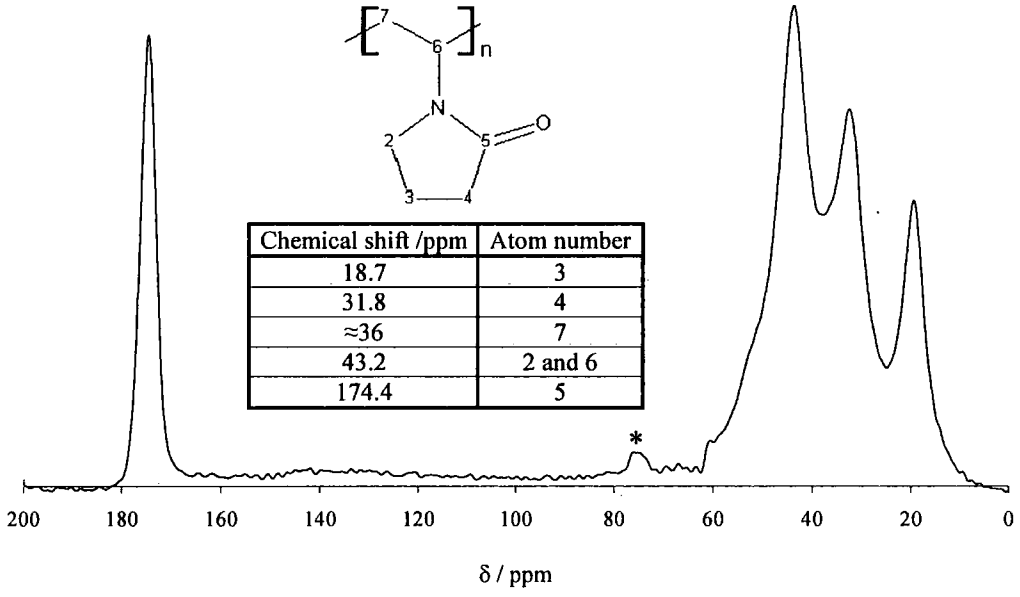

Chemical shift /ppm	Atom number
18.7	3
31.8	4
≈36	7
43.2	2 and 6
174.4	5

Figure 6.1: ^{13}C CPMAS spectra of PVP obtained at 50.32 MHz, ^{13}C frequency. The asterisk shows the spinning sideband.

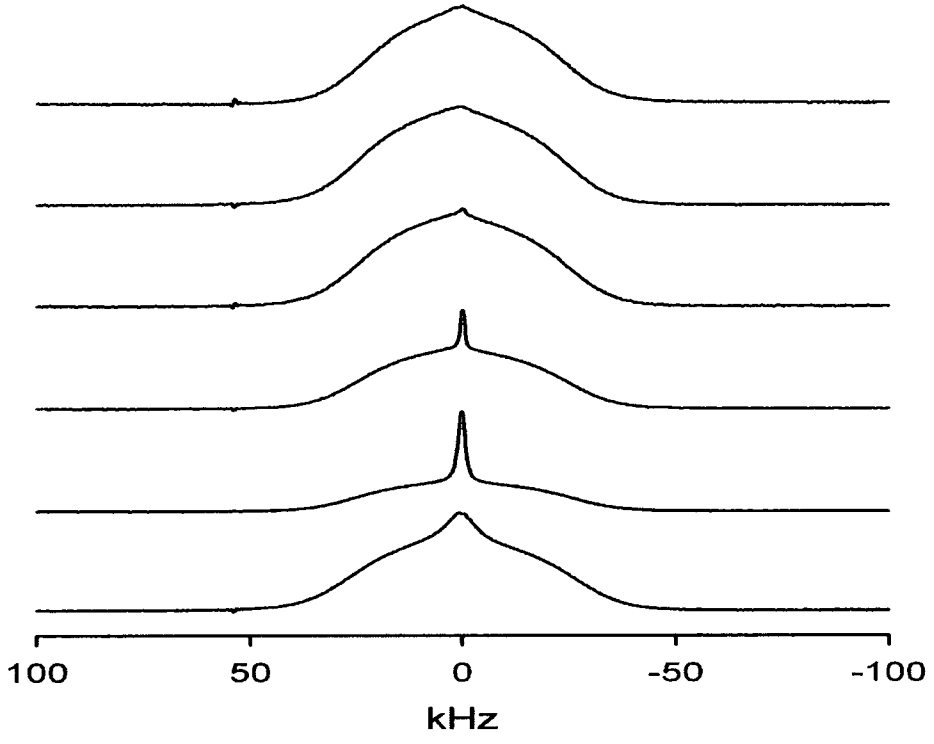

Figure 6.2: Proton bandshapes obtained from the last spectrum of the T_1^H array at different temperatures for PVP[2]. Bottom to top, the temperature values are -20, 20, 80, 90, 100 and 140°C.

The study of T_1^H and $T_{1\rho}^H$ of quench-cooled PVP over a range of temperature was done by Dr. D.C. Apperley using a 300 MHz spectrometer[2]. The results obtained are shown in figure 6.3 and figure 6.4, with the raw data given in appendix 24. The timing for this experiment is shown in table 6.1.

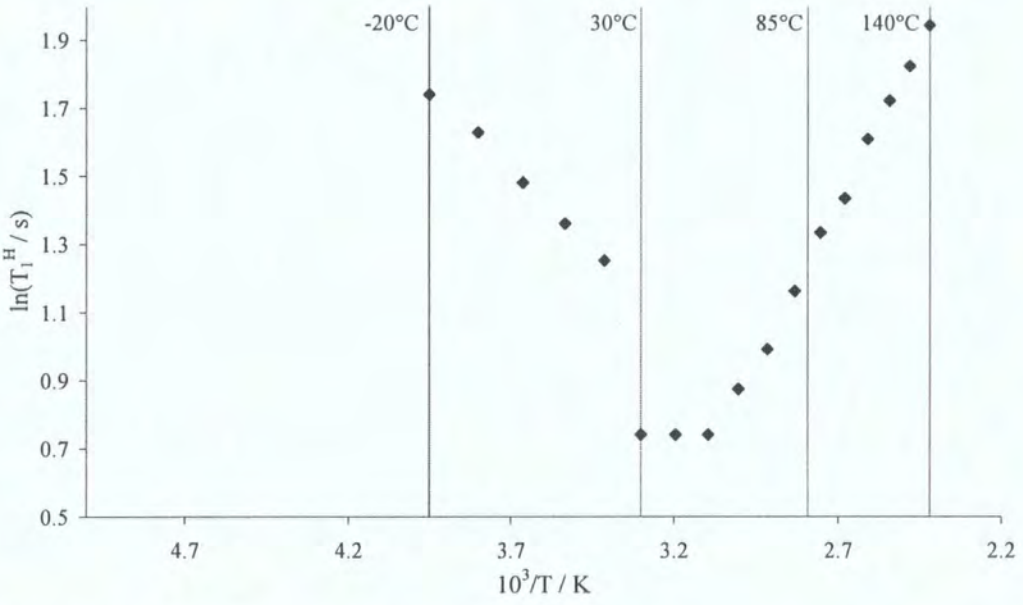

Figure 6.3: T_1^H measurements for quench-cooled PVP.

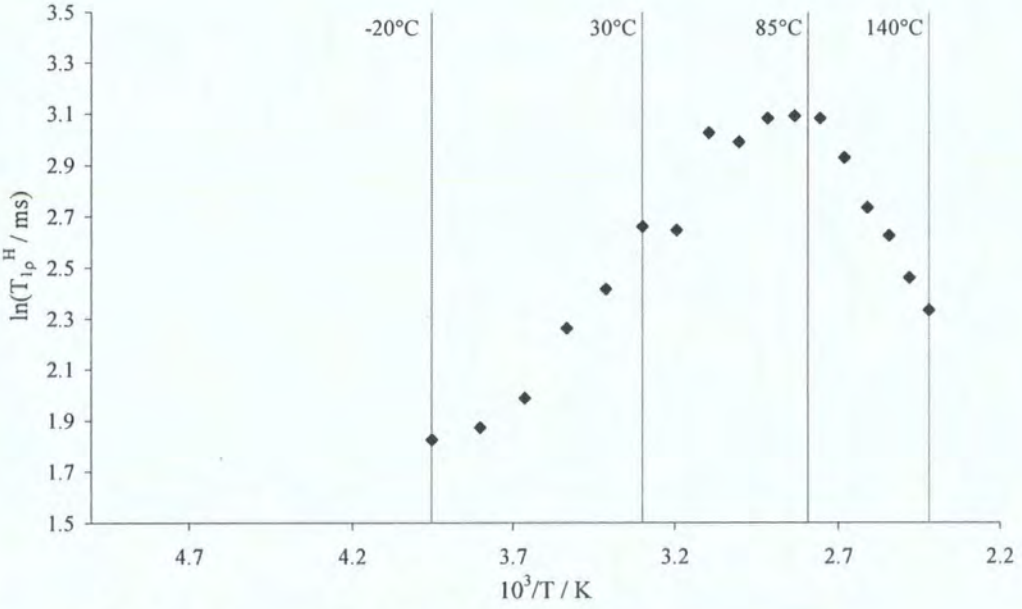

Figure 6.4: $T_{1\rho}^H$ measurements for quench-cooled PVP.

Temperature / °C	Temperature reached at / hr:min	Experiment started at / hr:min	Experiment finished at / hr:min
-20	0:00	0:12	0:35
-10	0:40	0:43	1:02
0	1:07	1:10	1:23
10	1:28	1:31	1:42
20	1:47	1:51	2:02
30	2:07	2:16	2:27
40	2:32	2:43	2:52
50	2:57	3:02	3:15
60	3:20	3:29	3:40
70	3:45	3:50	4:01
80	4:06	4:15	4:28
90	4:33	4:57	5:17
100	5:22	5:31	5:55
110	6:00	6:14	6:37
120	6:42	6:56	7:22
130	7:27	7:36	7:59
140	8:04	8:20	8:48

Table 6.1: Timing used for the T_1^H and $T_{1\rho}^H$ experiments performed on pure PVP. The experiment times include both experiments.

These experiments are important as they help in determining if the T_1^H and $T_{1\rho}^H$ measurements of the PVP/drug co-melts are dominated by the behaviour of PVP.
The mixtures prior to being melted are physical mixtures with a 1:1 ratio in mass; this corresponds to a percentage of hydrogen atoms, from the drug, in the mixture of 35.6%, 39.1% and 38.6%, for PVP/indomethacin, PVP/nifedipine and PVP/carbamazepine co-melts respectively. The co-melts were obtained using the protocol shown in chapter Two. In order to check the amorphous character of the PVP/drug co-melts, a ^{13}C CPMAS SSNMR spectrum was obtained and compared to those of the crystalline and amorphous forms of the drug on their own.

1.2/^{13}C SSNMR

1.2.1) PVP/indomethacin

The ^{13}C CPMAS SSNMR spectra of crystalline and amorphous indomethacin, and of the PVP/drug co-melt are shown in figure 6.5. The spectrum of PVP on its own is shown for reference.

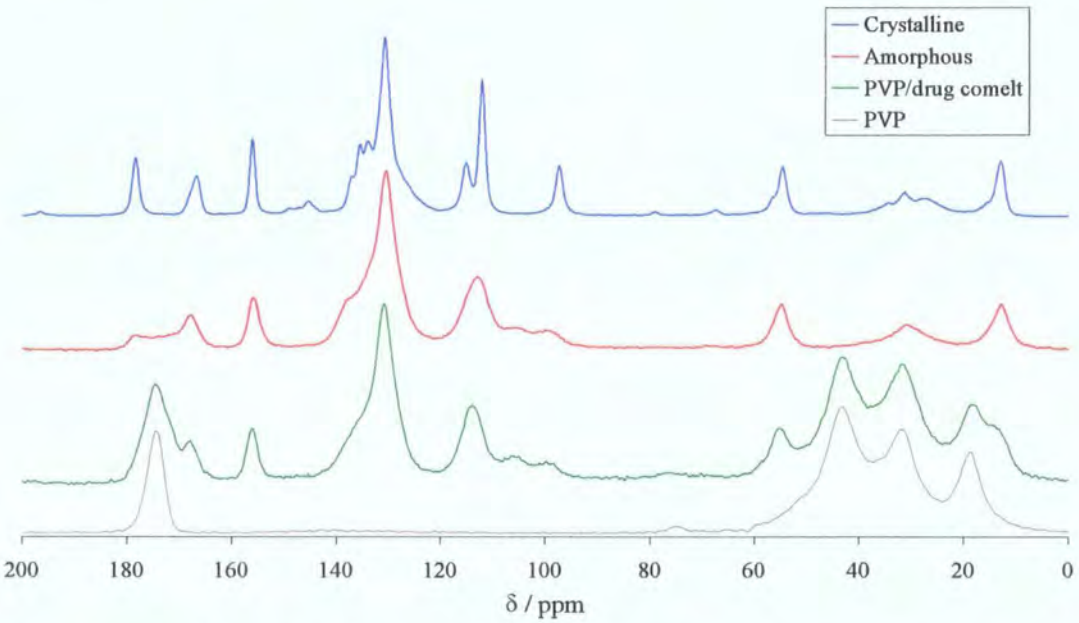

Figure 6.5: ^{13}C CPMAS SSNMR spectra of crystalline and amorphous indomethacin, PVP/indomethacin co-melt and PVP alone obtained at 50.32 MHz, ^{13}C frequency.

One can see from figure 6.5 that the peaks, not overlapped by PVP peaks, of the PVP/drug co-melt are really similar to those of the amorphous indomethacin, but not as well defined as for the crystalline case. This shows that the PVP/drug co-melt is actually amorphous. The differences in chemical shifts between the pure amorphous drug and the PVP/drug co-melt are shown in table 6.2. It is important to consider the likely errors occurring when obtaining these chemical shifts: there could be a difference in the referencing from one experiment to the other, or the peak peaking could be not exactly at the centre of the peaks.

200 MHz			300 MHz[2]		
Chemical shift / ppm			Chemical shift / ppm		
Amorphous	Co-melt	Difference	Amorphous	Co-melt	Difference
55.1	55.2	-0.1	54.8	54.9	-0.1
113.1	113.9	-0.8	113.9	114.1	-0.2
130.7	131.1	-0.4	130.9	131.6	-0.7
156.0	156.1	-0.1	156.4	156.6	-0.2

Table 6.2: Differences of chemical shifts between the pure amorphous form and the co-melt for indomethacin.

From table 6.2 it can be seen that the chemical shifts of the pure amorphous drug and the one of the co-melt are similar, and, as such, do not provide any evidence of any strong specific chemical interactions between the two compounds. This is consistent with the work of Taylor and Zografi[3]. This similarity was observed at two magnetic fields. Note that all the calculated differences are negative, which could arise from instrumental effects or non-specific interactions.

1.2.2) PVP/nifedipine

The ^{13}C CPMAS SSNMR spectra of crystalline and amorphous nifedipine, and of the PVP/drug co-melt are shown in figure 6.6. The spectrum of PVP on its own is shown for reference.

200 MHz			300 MHz[2]		
Chemical shift / ppm			Chemical shift / ppm		
Amorphous	Co-melt	Difference	Amorphous	Co-melt	Difference
50.8	50.4	0.4	51.1	50.7	0.4
103.1	102.9	0.2	124.2	124.0	0.2
132.1	131.7	0.4	126.8	127.0	-0.2
147.9	147.8	0.1	132.3	132.0	0.3
167.4	167.5	-0.1	147.0	147.0	0.0

Table 6.3: Differences of chemical shifts between the pure amorphous form and the co-melt for nifedipine.

As for indomethacin, it can be seen that the PVP/drug mixture is amorphous by comparing its spectrum to that of the crystalline and amorphous drugs. The differences in chemical shifts between the pure amorphous drug and the PVP/drug co-melt are shown in table 6.3.

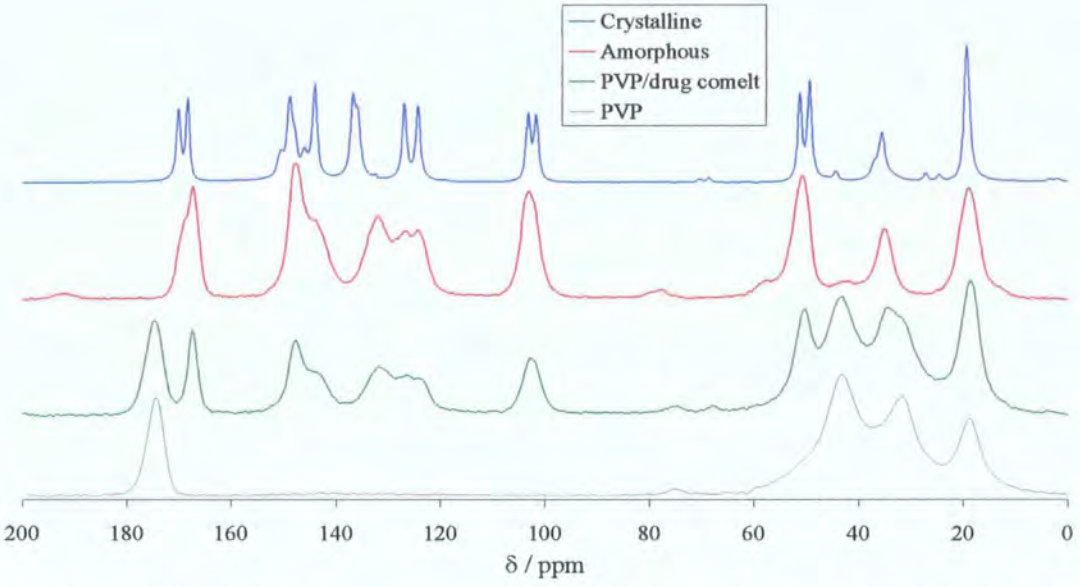

Figure 6.6: ^{13}C CPMAS SSNMR spectra of crystalline and amorphous nifedipine, PVP/nifedipine co-melt and PVP alone obtained at 50.32 MHz, ^{13}C frequency.

From table 6.3 it can be seen that the chemical shifts of the pure amorphous drug and the one of the co-melt are similar and as such do not provide any evidence of any strong specific chemical interactions between the two compounds. This similarity was observed at two magnetic fields.

1.2.3) PVP/carbamazepine

The ^{13}C CPMAS SSNMR spectra of crystalline and amorphous carbamazepine, and of the PVP/drug co-melt are shown in figure 6.7. The spectrum of PVP on its own is shown for reference. As for indomethacin and nifedipine, it is visible that the PVP/drug mixture is amorphous by comparing its spectrum to that of the crystalline and amorphous drugs. The differences in chemical shifts between the pure amorphous drug and the PVP/drug co-melt are shown in table 6.4.

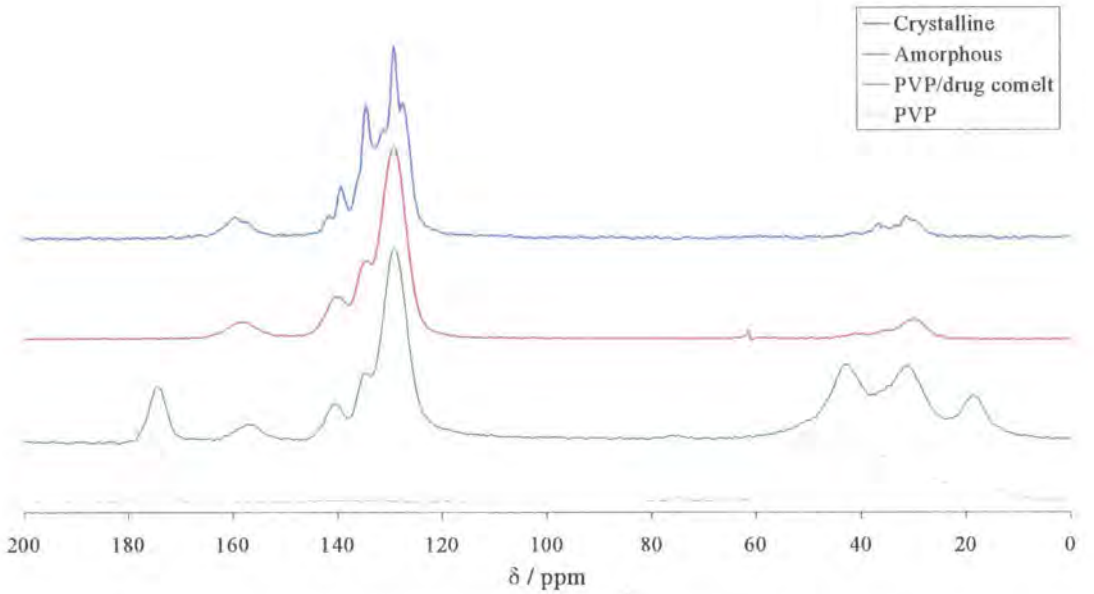

Figure 6.7: ^{13}C CPMAS SSNMR spectra of crystalline and amorphous carbamazepine, PVP/carbamazepine co-melt and PVP alone obtained at 50.32 MHz, ^{13}C frequency.

200 MHz		
Chemical shift / ppm		
Amorphous	Co-melt	Difference
129.2	129.4	-0.2
134.4	134.7	-0.3
140.4	140.7	-0.3
158.0	157.2	0.8

Table 6.4: Differences of chemical shifts between the pure amorphous form and the co-melt for carbamazepine.

Table 6.4 shows that there are no significant differences between the chemical shifts obtained for the pure amorphous drug and those of the co-melt. This seems to show that there is no strong chemical interactions between the two components of the co-melt.

1.3/ Proton bandshapes

The proton bandshapes of PVP[2] and of the PVP/drug co-melts were recovered, as secondary information, from the T_1^H and $T_{1\rho}^H$ experiments, more precisely from the

last spectrum of the array for T_1^H and the first spectrum of the array for $T_{1\rho}^H$, as stated in chapter Five. They were then analysed in order to get some information on the way the samples behaved over a wide range of temperatures. This helps to understand the effect on mobility caused by the addition of a polymer to the system. As for chapter Five, only the proton bandshapes obtained from the T_1^H are shown since the T_1^H and $T_{1\rho}^H$ experiments, as expected, yielded similar spectra.

1.3.1) PVP/indomethacin

Figure 6.8 shows the proton bandshapes obtained from the last spectrum of the T_1^H array at different temperatures for the PVP/indomethacin co-melt. The timing for the experiment is shown in table 6.5. The timing was matched to within two hours between the different series of experiments studied.
When comparing the proton bandshapes of PVP and of the PVP/indomethacin co-melt, one can see that PVP does not seem to have influence on the co-melt.

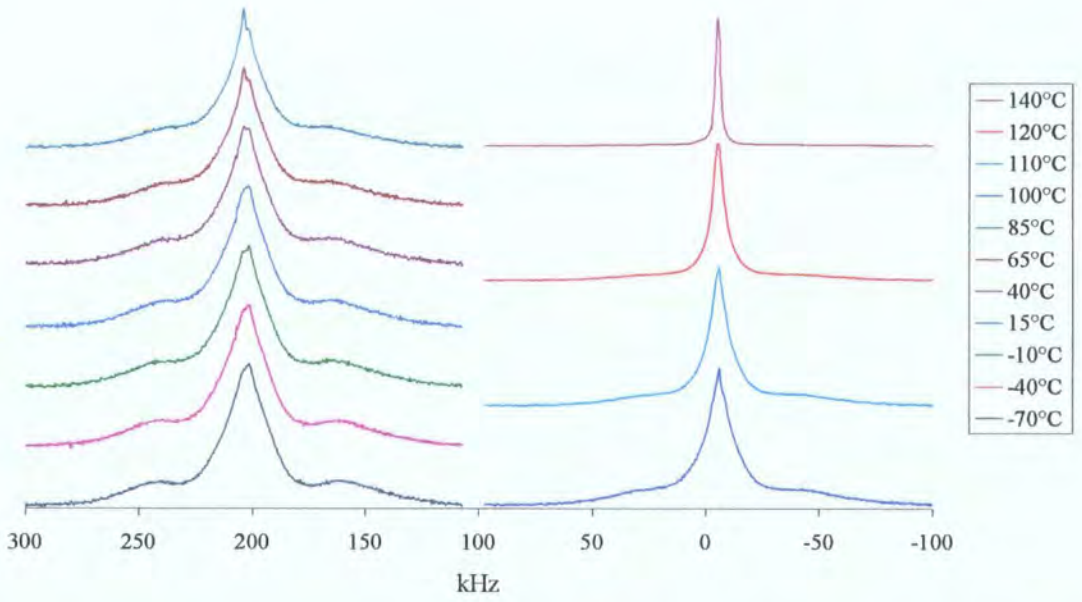

Figure 6.8: Proton bandshapes obtained from the last spectrum of the T_1^H array at different temperatures for the PVP/indomethacin co-melt. The horizontal scale is for reference only.

If one looks at figure 6.8, it can be seen that there is no real change, apart from a slight sharpening, in the proton bandshape for temperatures between –70°C and

65°C. However, at 85°C the sharpening seems to be more pronounced and this is definite from 100°C. At the same time, the broad underlying peak seems to be decreasing. This shows that that there is an increase in mobility which is probably due to the co-melt going through a transition related to the Tg of the co-melt. It should be noted that when two compounds are mixed at a molecular level, the Tg of the mixture should be the average of the Tg of the separate components. It is then possible to calculate the theoretical Tg of PVP/indomethacin co-melt to be at 105°C. The fact that the transition happens at a lower temperature may indicate that the PVP sample was not totally dry, and, as such, its' Tg would have been lower due to the plasticising effect of water.

Temperature / °C	Temperature reached at / hr:min	Experiment started at / hr:min	Experiment finished at / hr:min
-70	0:00	0:20	0:34
-40	0:39	0:59	1:15
-10	1:20	1:40	1:57
15	2:02	2:22	2:42
40	2:47	3:07	3:31
65	3:36	3:56	4:23
85	4:28	4:48	5:14
100	5:19	5:39	6:07
110	6:12	6:22	6:49
120	6:54	7:04	7:28
140	7:33	7:53	8:14

Table 6.5: Timing used for the T_1^H and $T_{1\rho}^H$ experiments performed on the PVP/indomethacin co-melt. The experiment times include both experiments.

1.3.2) PVP/nifedipine

Figure 6.9 shows the proton bandshapes obtained from the last spectrum of the T_1^H array at different temperatures for the PVP/nifedipine co-melt. The timing for the T_1^H and $T_{1\rho}^H$ experiments is shown in table 6.6. This timing was matched to within two hours between the different series of experiments.

The proton bandshapes obtained for the PVP/nifedipine co-melt, figure 6.9, show a very similar behaviour to those obtained for the PVP/indomethacin co-melt, figure

6.8. Therefore, it is possible to say that a change of mobility is happening at some point between 65°C and 100°C and that this change in mobility is probably due to a the PVP/nifedipine co-melt going through its Tg.

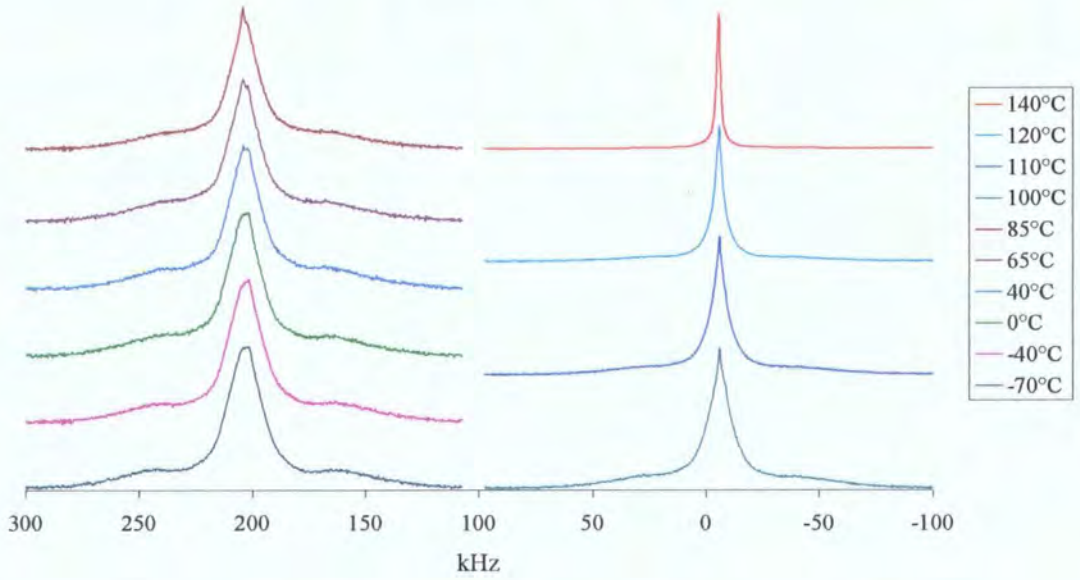

Figure 6.9: Proton bandshapes obtained from the last spectrum of the T_1^H array at different temperatures for the PVP/nifedipine co-melt. The horizontal scale is for reference only.

Temperature / °C	Temperature reached at / hr:min	Experiment started at / hr:min	Experiment finished at / hr:min
-70	0:00	0:20	0:38
-40	0:43	1:03	1:21
0	1:26	1:46	2:04
40	2:09	2:29	2:51
65	2:56	3:16	3:42
85	3:47	4:07	4:33
100	4:38	4:58	5:25
110	5:30	5:40	6:05
120	6:10	6:20	6:44
140	6:49	7:19	7:39

Table 6.6: Timing used for the T_1^H and $T_{1\rho}^H$ experiments performed on the PVP/nifedipine co-melt. The experiment times include both experiments.

The comparison between the proton bandshapes of PVP and the PVP/nifedipine co-melt seems to indicate that PVP does not influence strongly the co-melt.

1.3.3) PVP/carbamazepine

Figure 6.10 shows the proton bandshapes obtained from the last spectrum of the T_1^H array at different temperatures for the PVP/carbamazepine co-melt. The timing for the experiment is shown in table 6.7. The timing was matched to within two hours between the different series of experiments.

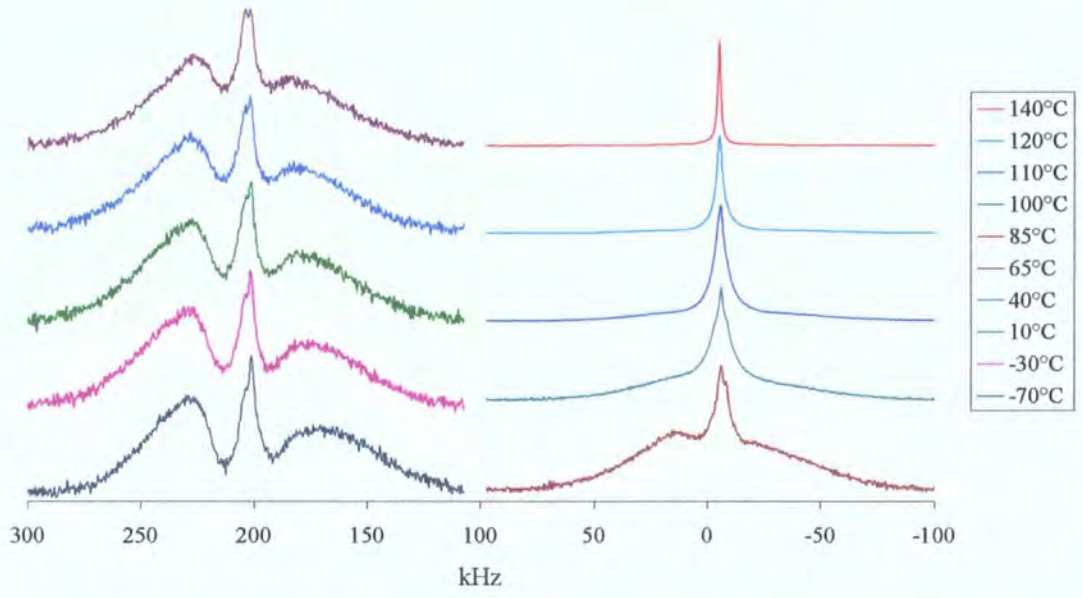

Figure 6.10: Proton bandshapes obtained from the last spectrum of the T_1^H array at different temperatures for the PVP/carbamazepine co-melt. The horizontal scale is for reference only.

The proton bandshapes shown in figure 6.10 seem to be composed of a peak surrounded by two "wings". This is very similar to what was observed for the pure amorphous drug. However, the main peak is not centred as was the case for the pure amorphous system; this could be due to the presence of PVP in the co-melt.

The same conclusion as for the other two co-melts can been drawn from these bandshapes; that is to say that a change of mobility is observed, which is probably due to the Tg of the co-melt. However, in this case it is easier to pinpoint the temperature at which the mobility seems to change which occurs between 85°C and 100°C. It can also been seen, by comparing figure 6.2 and figure 6.10, that PVP does not seem to have much influence in the behaviour of the PVP/carbamazepine co-melt.

Temperature / °C	Temperature reached at / hr:min	Experiment started at / hr:min	Experiment finished at / hr:min
-70	0:00	0:20	0:46
-30	0:51	1:11	1:36
10	1:41	2:01	2:25
40	2:30	2:50	3:16
65	3:21	3:41	4:14
85	4:19	4:39	5:11
100	5:16	5:36	6:07
110	6:12	6:22	6:50
120	6:55	7:05	7:31
140	7:36	7:56	8:16

Table 6.7: Timing used for the T_1^H and $T_{1\rho}^H$ experiments performed on the PVP/carbamazepine co-melt. The experiment times include both experiments.

1.4/ T_1^H and $T_{1\rho}^H$ measurements

The measurements have been carried out at least in duplicate using the PVP/drug co-melt samples which were prepared according to the protocol shown in chapter Two.

As the co-melts are mixtures of a polymer and an amorphous drug, the statement on activation energies applies in this case, i.e. it would be meaningless to retrieve activation energies from the slope of the T_1^H and $T_{1\rho}^H$ experiments. Furthermore, the presence of the polymer in the mixture will complicate the phenomenon and it would be equally meaningless to relate the measurements to barriers to rotation. It is also important to note that the relaxation times of the co-melts measure an average for the drug and PVP. If the PVP/drug mixing occurs essentially at the molecular level, as expected from the co-melting procedure, spin diffusion should be efficient between the components.

1.4.1) PVP/indomethacin

Figure 6.11 shows the T_1^H curve, as a function of the temperature, obtained for the PVP/indomethacin co-melt. The raw data are given in appendix 25. Figure 6.12 shows the comparison of the T_1^H curves, as a function of temperature, of the

crystalline form, the pure amorphous drug, the PVP/drug co-melt and pure PVP (note that only one set of measurements is shown for simplicity).

From figure 6.11, it can be seen that the mixture appears to behave somewhat differently at different magnetic fields. It actually seems that the data acquired at a proton frequency of 300 MHz are relatively erratic compared to that obtained at 200 MHz. Comparison between figure 6.3 and figure 6.11 shows that the erratic character of the measurements observed at 300 MHz could be due to the presence of PVP. However, the presence of the polymer does not seem to influence the T_1^H measured at 200 MHz, see figure 6.12.

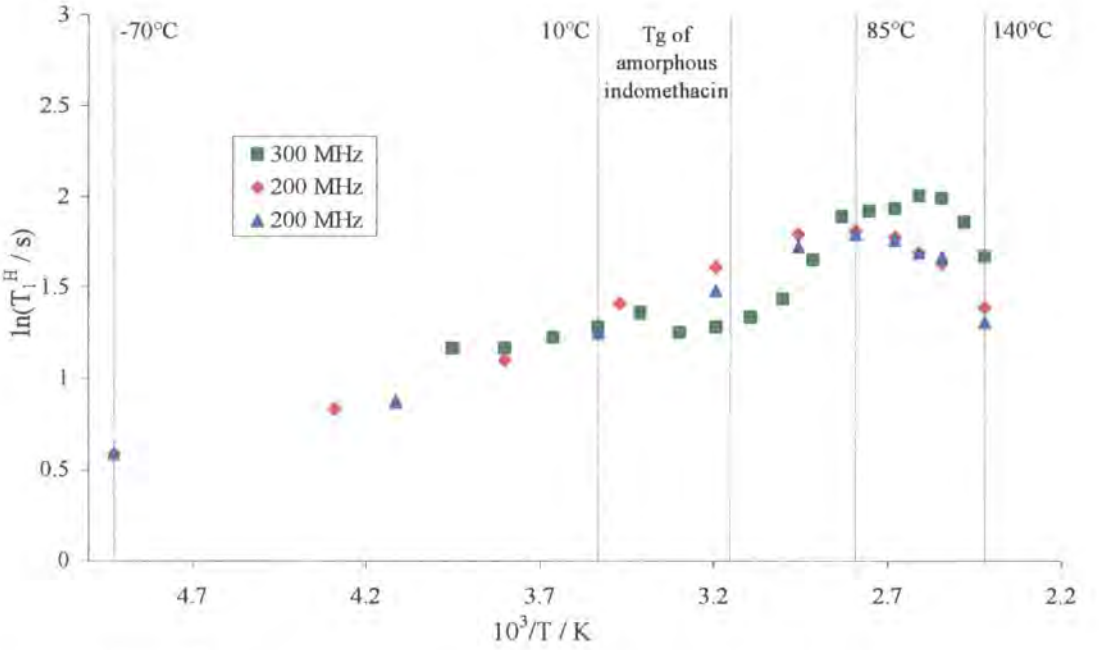

Figure 6.11: T_1^H measurements for the PVP/indomethacin co-melt.

One can see from figure 6.11 that a definite maximum is visible well above the Tg of amorphous indomethacin, which seems to show that the sample is less prone to changes until higher temperatures. Therefore, the co-melt seems to be more stable, as expected due to the presence of the polymer. The maximum observed from the 200 MHz data is at ca. 85°C, whilst it is at ca. 110°C from the 300 MHz data. The maximum for the 200 MHz data appears after a steady increase in the T_1^H value from -70°C which could indicate recovery from a T_1^H minimum at or below -70°C. The difference in the temperature at which the maximum is observed between the two magnetic fields could be due to the amount of water present in the sample; it has

been said that water was a plasticiser and, as such, could influence the value of Tg. As a consequence, it could be assumed that the transition observed at 85°C is probably due to the Tg of the co-melt.

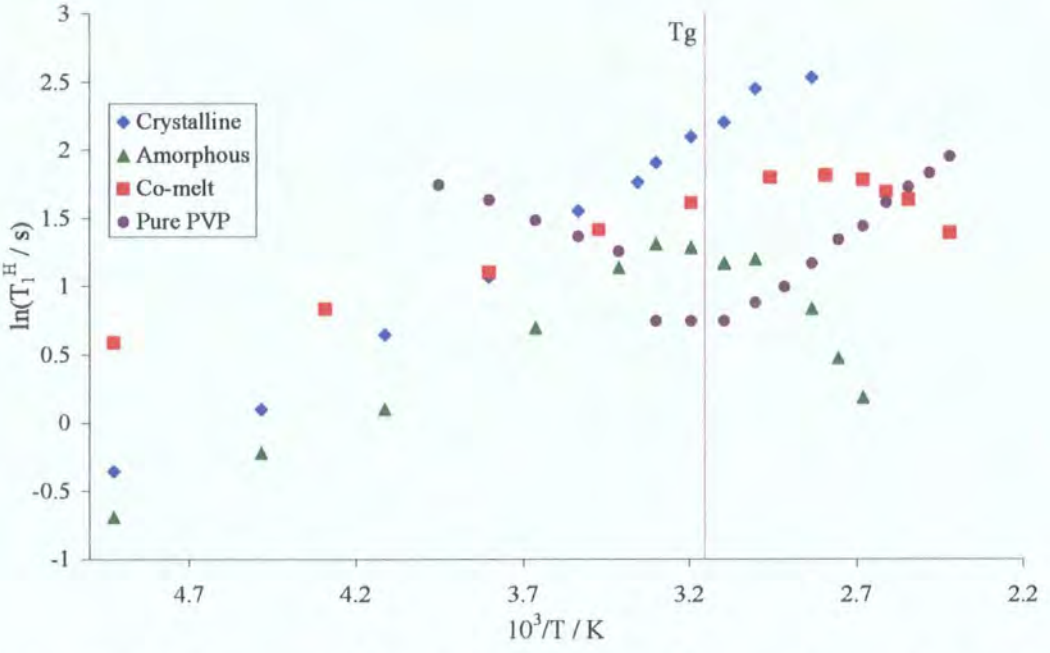

Figure 6.12: Comparison of the T_1^H curves obtained for crystalline and amorphous indomethacin, PVP/indomethacin co-melt and pure PVP[2].

If one compares the slopes obtained form the crystalline and amorphous materials to those obtained from the co-melt, see figure 6.12, it can be seen that the co-melt has a smaller slope than the other two states of the sample. It is also noticeable that the T_1^H value is slightly higher for the co-melt than for the other states when observing below 10°C, but this value is changing to become between the values of the other states above this temperature. This shows that the co-melt is more rigid than the other states below 10°C. However, this somehow changes past this temperature as the co-melt seems to be more mobile than the crystalline material, but more rigid than the amorphous sample. This seems to reinforce the statement of the previous chapter which suggested that amorphisation increases molecular mobility, whilst the higher maximum value seems to show that the co-melt is somewhat more stable that the amorphous drug on its own.

Figure 6.13 shows the $T_{1\rho}^{H}$ curve, as a function of temperature, obtained for the PVP/indomethacin co-melt. The raw data is given in appendix 25.

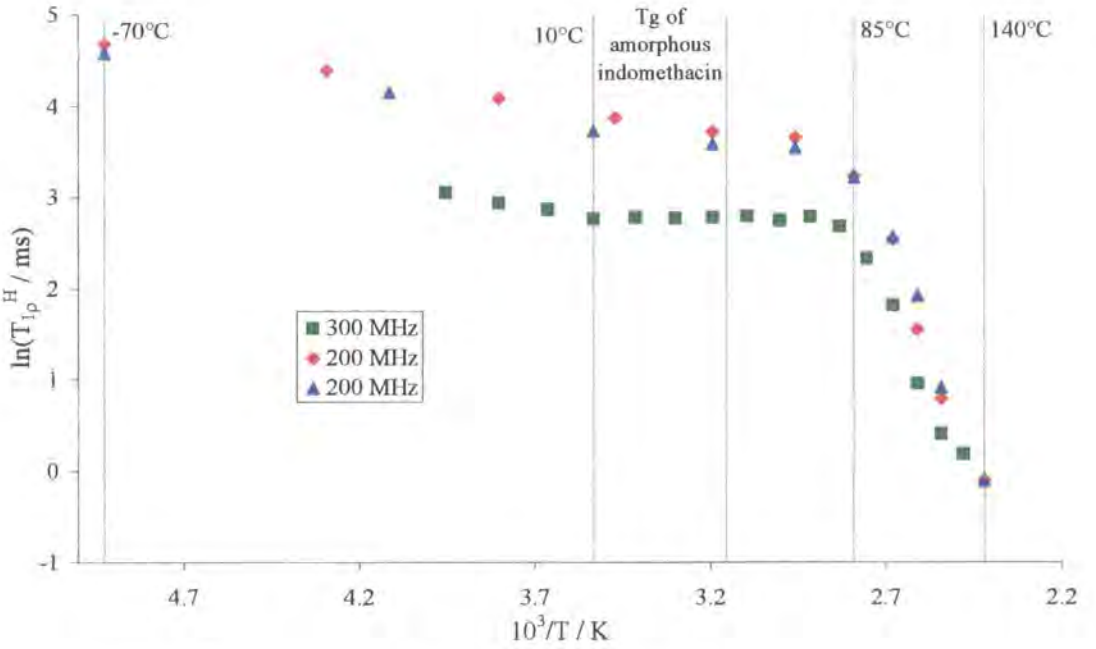

Figure 6.13: $T_{1\rho}^{H}$ measurements for the PVP/indomethacin co-melt.

This figure shows similar behaviour between the two different magnetic fields with a small, but consistent, difference in the magnitude of $T_{1\rho}^{H}$ which was expected as B_1 was set to 70 kHz and 50 kHz for the 300 MHz and 200 MHz spectrometers, respectively. It is visible that, for both magnetic fields, the slopes change at ca. 85°C, and that the data from the 300 MHz spectrometer shows a broad shallow minimum at ca. 130°C which is not present within the data from the 200 MHz spectrometer.

Figure 6.14 shows the comparison of the $T_{1\rho}^{H}$ curves, as a function of temperature, of the crystalline form, the pure amorphous drug, the PVP/drug co-melt and pure PVP (note that only one set of measurements is shown for simplicity).

If one compares the data obtained for the amorphous sample to those from the co-melt, one can see that they have a very similar slopes and $T_{1\rho}^{H}$ values below Tg, see figure 6.14. However, the change of slope occurs around Tg for the amorphous sample, whilst it occurs around 85°C for the co-melt, and this change in slope is probably due to Tg. This seems to indicate that the co-melt is more stable than the amorphous material. As stated in the previous chapter, it is possible to see that the

relaxation times are lower for the amorphous phase than for crystalline indomethacin, even though complicated by the minimum for the crystalline form. Furthermore, as both the co-melt and amorphous states have similar values of $T_{1\rho}^{H}$ this conclusion also holds for the co-melt, indicating a more mobile state than that of the crystalline material. This, again, suggests that amorphisation leads to a more mobile system.

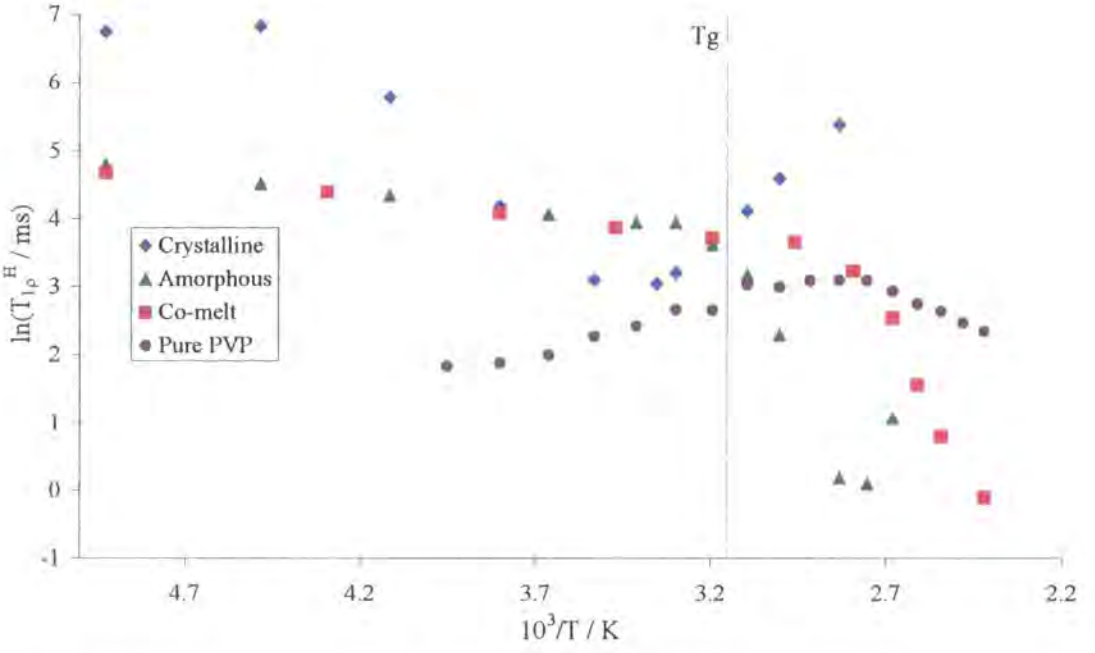

Figure 6.14: Comparison of the $T_{1\rho}^{H}$ curves obtained for crystalline and amorphous indomethacin, PVP/indomethacin co-melt and pure PVP.

Figure 6.14 seems to indicate that the relaxation of PVP is not dominating the relaxation of the co-melt. However, the $T_{1\rho}^{H}$ curves for both PVP and PVP/indomethacin co-melt go through a transition at 85°C, this transition seems to be due to the Tg of the co-melt for the latter but is not explainable for PVP.

1.4.2) PVP/nifedipine

Figure 6.15 shows the T_1^{H} curve, as a function of temperature, obtained for the PVP/nifedipine co-melt. The raw data are given in appendix 26.

Figure 6.16 shows the comparison of the T_1^H curves, as a function of temperature, of the crystalline form, the pure amorphous drug, the PVP/drug co-melt and pure PVP (note that only one set of measurements is shown for simplicity).

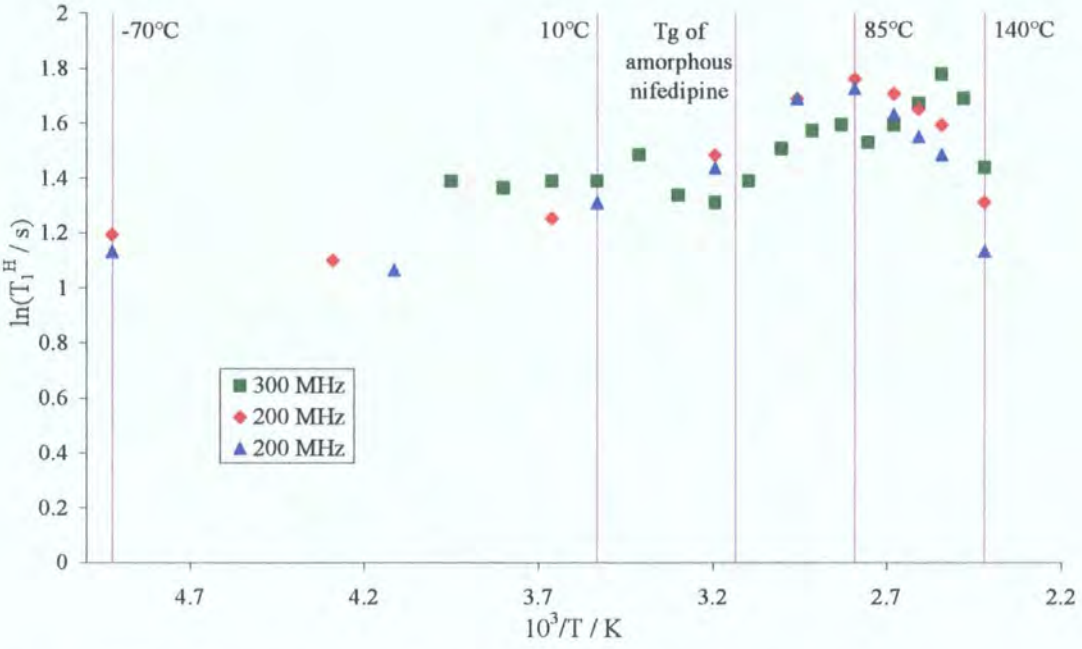

Figure 6.15: T_1^H measurements for the PVP/nifedipine co-melt.

As for the PVP/indomethacin co-melt, it is visible, from figure 6.15, that the data obtained at a proton frequency of 300 MHz are more erratic than the ones obtained at a proton frequency of 200 MHz; this could be due to the presence of PVP. This figure also shows that for both magnetic fields a maximum is reached at a temperature above the Tg of the amorphous drug on its own, i.e. at ca. 85°C with the 200 MHz data and at ca. 120°C with the 300 MHz data. This leads to the same conclusion as for the PVP/indomethacin co-melt; that is to say that the co-melt seems more stable than the amorphous drug on its own. The maximum observed from the 200 MHz data appears to be coming from the recovery of a shallow T_1^H minimum happening between -40°C and -30°C. The higher temperature observed for the maximum for the co-melt compared to that for the amorphous drug seems to indicate that the co-melt is more stable that the amorphous drug on its own, as observed in the case of indomethacin. The difference in the temperature when the maximum is observed is probably due to a difference in water content between the two samples;

thus confirming that the transition observed at 85°C at 200 MHz is due to the Tg of the co-melt.

If one compares the slopes obtained form the crystalline and amorphous materials to the ones obtained from the co-melt (figure 6.16), it is visible that all three states have similar slopes until Tg. It is also noticeable that the co-melt T_1^H value are the smallest of those for the three states, showing that the co-melt is more mobile than the crystalline or amorphous materials. This again seems to reinforce the statement of the previous chapter, which suggested that amorphisation increased molecular mobility.

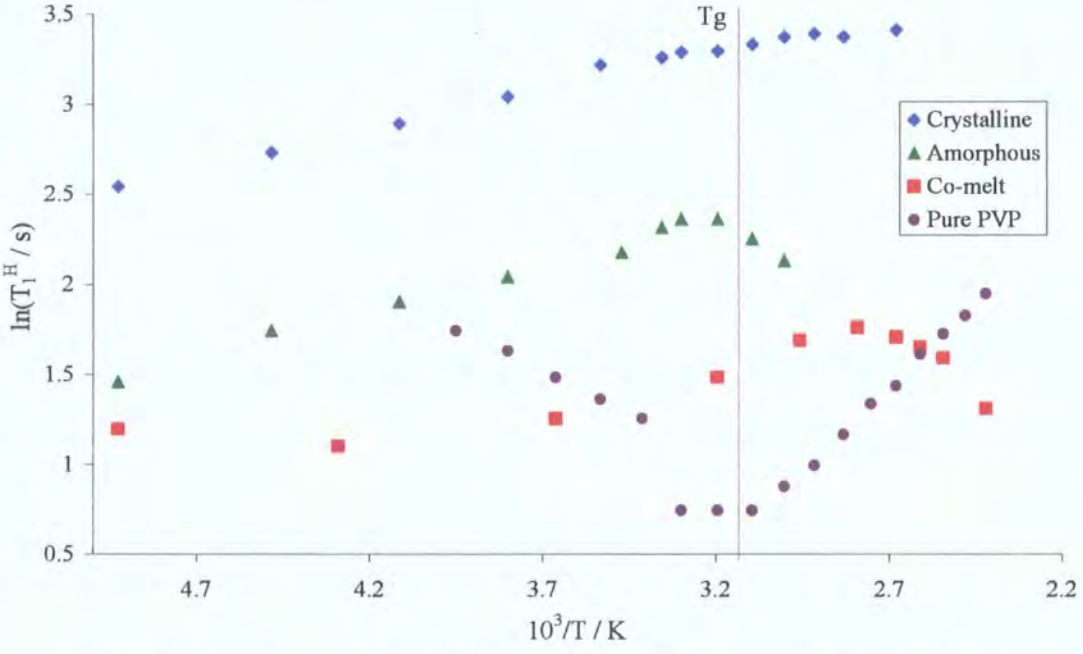

Figure 6.16: Comparison of the T_1^H curves obtained for crystalline and amorphous nifedipine, PVP/nifedipine co-melt and pure PVP[2].

When comparing figure 6.11 and figure 6.15, it is visible that both co-melts go through a maximum in T_1^H value at around 85°C. However, the PVP/nifedipine co-melt also shows a possible minimum at around -30°C, whilst this minimum seems to be at a lower temperature for indomethacin. Nevertheless, both co-melts seem to be more stable than their respective amorphous form.

Figure 6.17 shows the $T_{1\rho}^H$ curve, as a function of temperature, obtained for the PVP/nifedipine co-melt. The raw data is given in appendix 26.

Figure 6.17 shows a very similar behaviour to that which was observed for indomethacin, see figure 6.13; that is to say that a slight difference is observed in the values of $T_{1\rho}^{H}$ between the different magnetic fields and that a shallow minimum is observed from the 300 MHz data and not from the 200 MHz data. However, in this case the slopes behave differently between the two magnetic fields as the slope changes at a lower temperature when considering the 300 MHz data, at ca. 50°C, compared to the 200 MHz data, at ca. 65°C. Nevertheless, in both cases, this change in slope is occurring at a higher temperature than for the amorphous drug on its own, which again seems to indicate that the co-melt is somewhat more stable that the amorphous material.

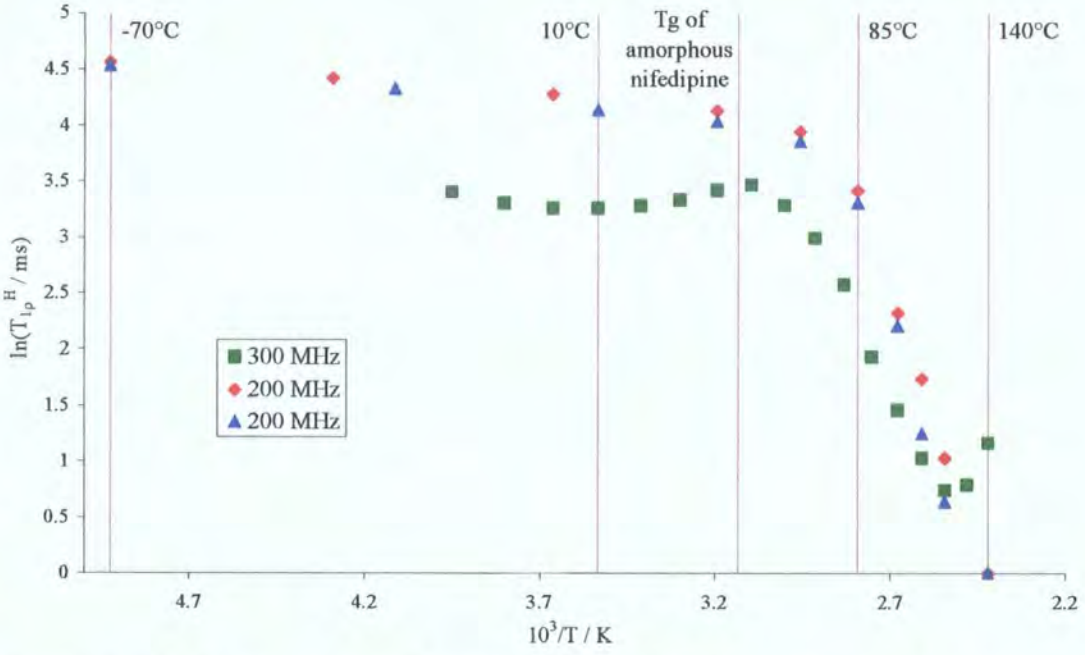

Figure 6.17: $T_{1\rho}^{H}$ measurements for the PVP/nifedipine co-melt.

Figure 6.18 shows the comparison of the $T_{1\rho}^{H}$ curves, as a function of temperature, of the pure amorphous drug, the PVP/drug co-melt and pure PVP (note that only one set of measurements is shown for simplicity).

If one compares the data obtained for the amorphous sample to the ones from the co-melt, see figure 6.18, one can see that they have very similar slopes and $T_{1\rho}^{H}$ values, up to the change of slope. This change of slope is observed for the amorphous sample at ca. 40°C, which is at a lower temperature than for the co-melt, as stated previously. It was shown in the previous chapter that the $T_{1\rho}^{H}$ values were not

obtained for the crystalline material as they were too long to be measured. Therefore, the amorphous and co-melt have smaller $T_{1\rho}^{H}$ values than the crystalline material and, as such, are probably more mobile. This strengthens again the fact that amorphisation seems to render the sample more mobile and that the presence of PVP make a more stable sample than the amorphous drug on its own.

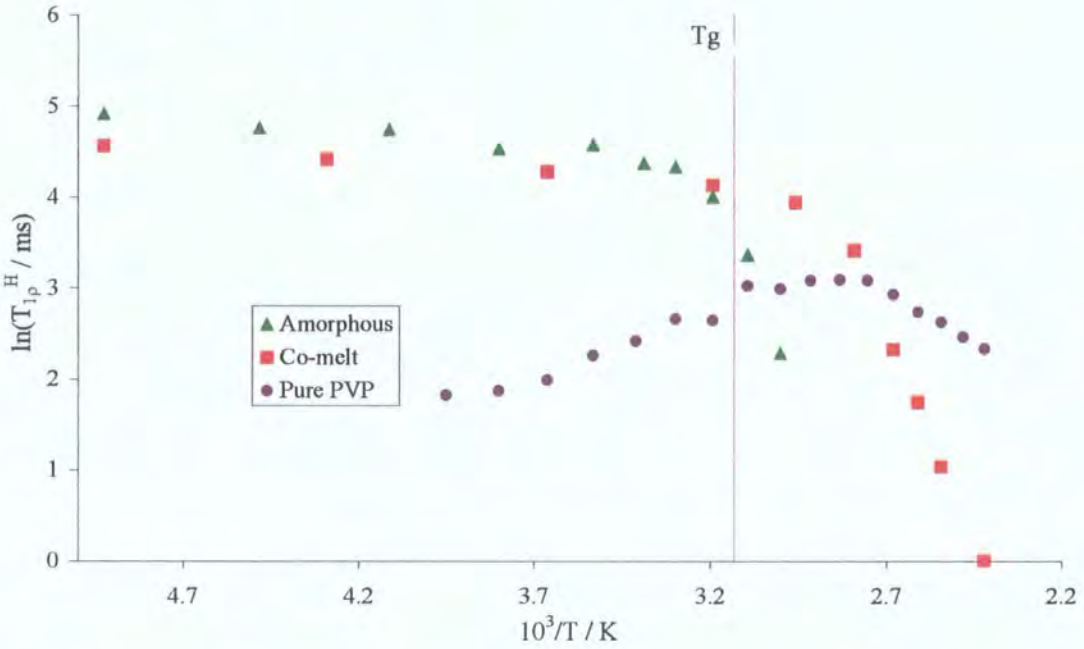

Figure 6.18: Comparison of the $T_{1\rho}^{H}$ curves obtained for amorphous nifedipine, PVP/nifedipine co-melt and pure PVP.

The comparison of figure 6.4 and figure 6.17 seems to indicate that the relaxation of PVP is not dominating the relaxation of the co-melt.

As observed for indomethacin and in the previous chapter, the slopes obtained with the $T_{1\rho}^{H}$ data are negative below the change of slopes, whilst they are positive for T_1^{H}. Furthermore, this change of slope happens at a lower temperature for $T_{1\rho}^{H}$ than for T_1^{H}. These two points clearly show a difference in the motional process, which is expected, as explained in chapter Three.

Figure 6.13 and figure 6.17 show that the $T_{1\rho}^{H}$ values for those two co-melts behave in a similar way and follow similar slopes apart from the fact that PVP/nifedipine goes through a change of slope at a lower temperature than PVP/indomethacin, when looking at the 300 MHz data. This could indicate a less stable sample. However, both co-melts seem to be more stable than their amorphous counterparts.

1.4.3) PVP/carbamazepine

Figure 6.19 shows the T_1^H curve, as a function of temperature, obtained for the PVP/carbamazepine co-melt. The raw data is given in appendix 27.

Figure 6.19 shows that a maximum happens at ca. 85°C and that this maximum appears to be the recovery of the system after a minimum that seems to occur around -30°C. It is also visible that this maximum happens at a temperature above the Tg of the amorphous drug on its own, which probably indicates a more stable system.

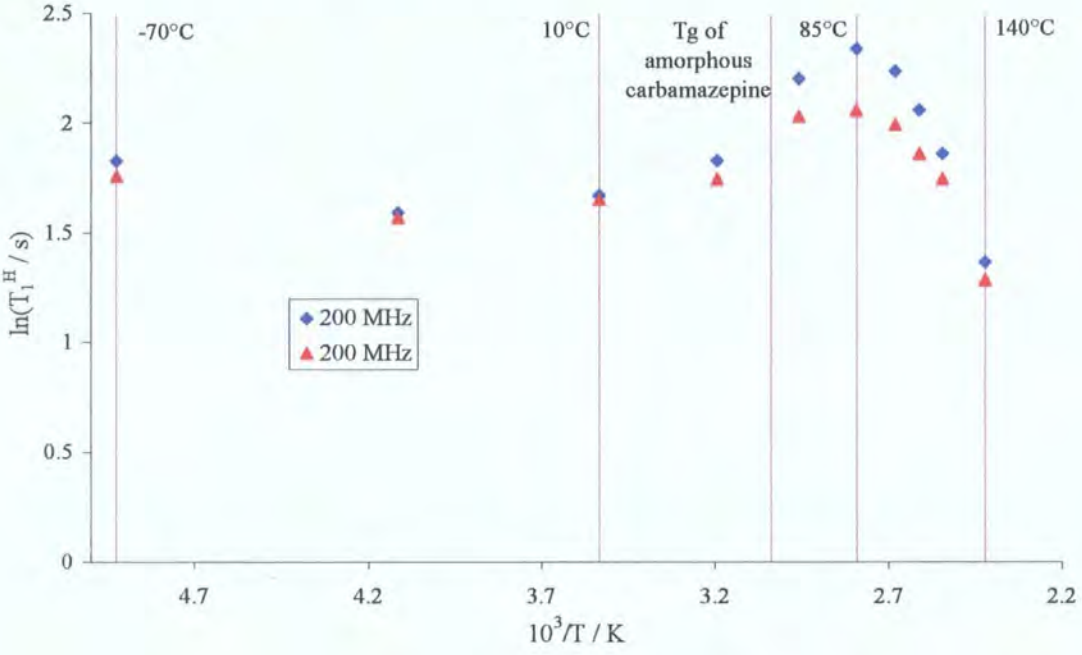

Figure 6.19: T_1^H measurements for the PVP/carbamazepine co-melt.

Figure 6.20 shows the comparison of the T_1^H curves, as a function of temperature, of the pure amorphous drug, the PVP/drug co-melt and pure PVP (note that only one set of measurements is shown for simplicity).

When comparing the T_1^H values obtained from the different states, i.e. co-melt, amorphous and crystalline (see figure 6.20), one can see that the ones for the amorphous and the co-melt systems are lower than those for the crystalline system. This probably shows that the amorphous and co-melt systems are more mobile than their crystalline counterpart. It is also possible to see that up to Tg the T_1^H values are slightly higher for the amorphous drug than for the co-melt, and that their slopes are similar up to this temperature. Moreover, as said earlier, the maximum in T_1^H

happens at a higher temperature for the co-melt. This seems to show that the co-melt is more stable and slightly more mobile than the amorphous drug.

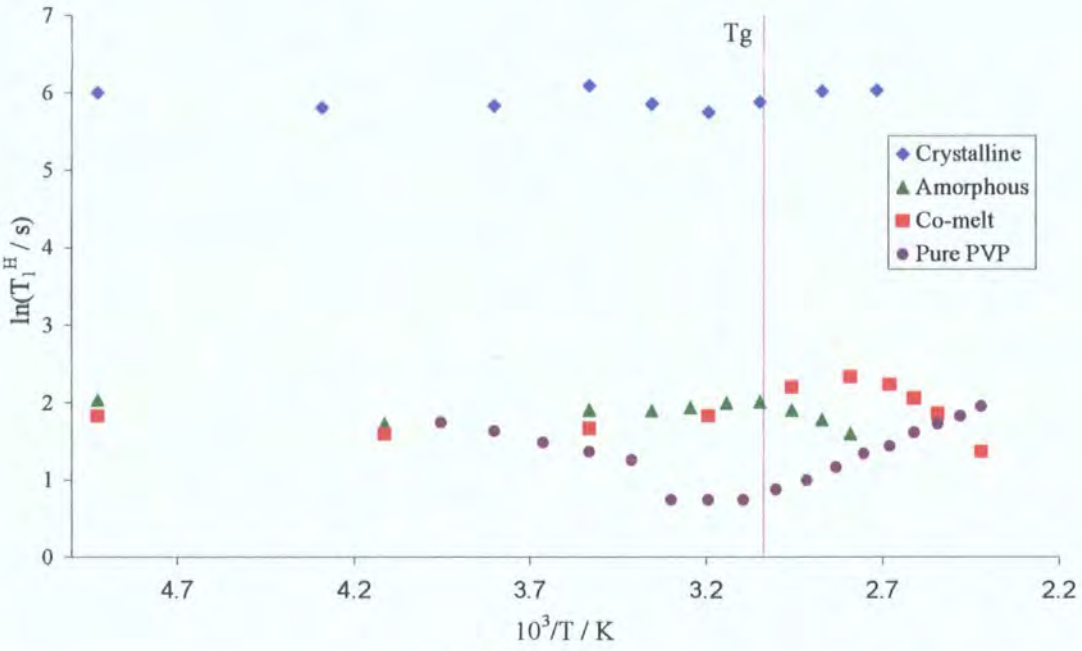

Figure 6.20: Comparison of the T_1^H curves obtained for crystalline and amorphous carbamazepine, PVP/carbamazepine co-melt and pure PVP[2].

The comparison between figure 6.19, figure 6.11 and figure 6.15 shows that PVP/carbamazepine behaves in a similar way to the other two co-melts, having a maximum at around 85°C. This co-melt also shows a minimum in T_1^H around -30°C, which is similar to what was observed for PVP/nifedipine. As for the other co-melts, PVP/carbamazepine seems to be more stable than amorphous carbamazepine without PVP, and it also seems that the relaxation of PVP is not dominating the relaxation of the co-melt.

Figure 6.21 shows the $T_{1\rho}^H$ curve, as a function of temperature, obtained for the PVP/carbamazepine co-melt. The raw data is given in appendix 27.
From this figure, it can be seen that a change in slope happens around 85°C. This is similar to what is seen with the T_1^H values. However, this change happening at the same temperature for both T_1 and $T_{1\rho}$ is probably fortuitous as these properties are dependent on different parameters.

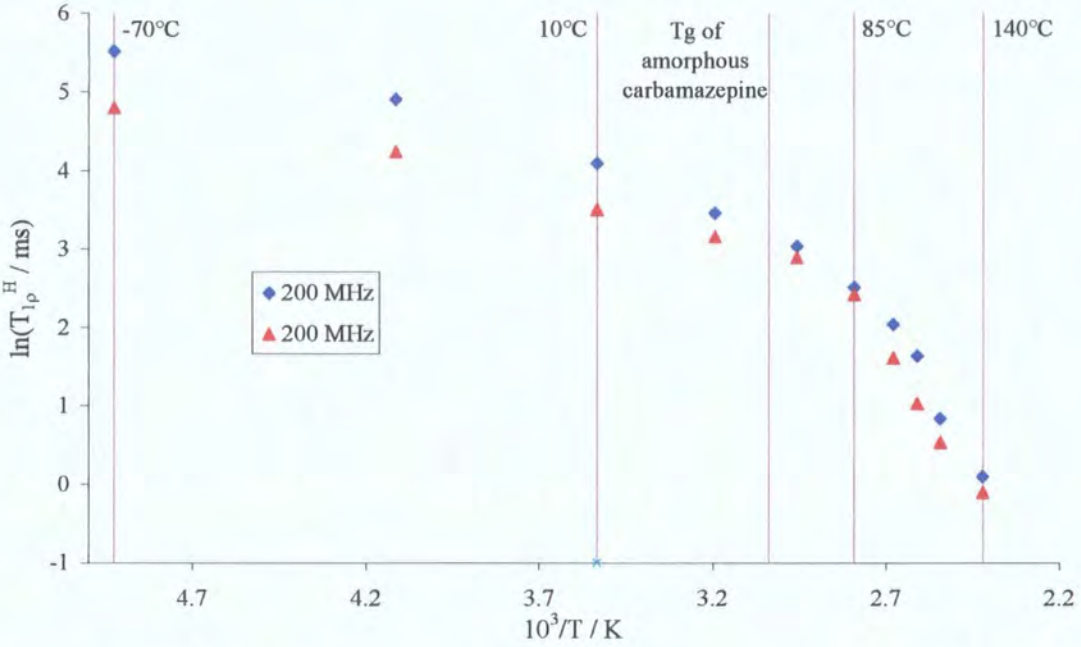

Figure 6.21: $T_{1\rho}^{H}$ measurements for the PVP/carbamazepine co-melt.

Figure 6.22 shows the comparison of the T_1^{H} curves, as a function of temperature, of the pure amorphous drug, the PVP/drug co-melt and pure PVP (note that only one set of measurements is shown for simplicity).

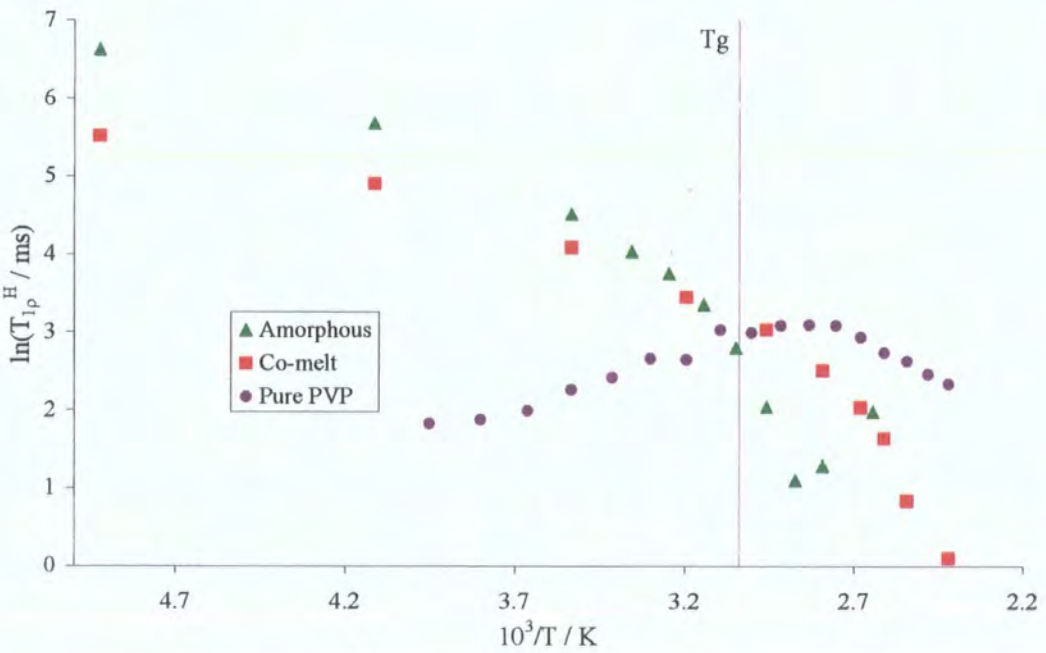

Figure 6.22: Comparison of the $T_{1\rho}^{H}$ curves obtained for amorphous carbamazepine, PVP/carbamazepine co-melt and pure PVP.

From figure 6.22 one can see that PVP/carbamazepine has lower $T_{1\rho}^{H}$ values than the crystalline sample, indicating a more mobile system. It can also be seen that the $T_{1\rho}^{H}$ values are lower for the co-melt than for the amorphous, up to the change of slope observed for the amorphous drug. At this point, the co-melt has higher $T_{1\rho}^{H}$ values, which seems to indicate a more stable system. It is also interesting to note that the change of slope observed for the co-melt happens at the same temperature as the minimum observed for the amorphous sample; this is probably just fortuitous, but it emphasises the fact that the co-melt is more stable than the amorphous drug on its own.

When looking at the $T_{1\rho}^{H}$ behaviour of the three co-melts, see figure 6.13, figure 6.17 and figure 6.21, it is visible that there are some similarities as the three co-melts show negative slopes and go through a change of slope between 65°C and 85°C. However, the slope observed for PVP/carbamazepine is more pronounced than those for the other two co-melts, though it is not possible to assign this difference to any particular phenomenon. The comparison between the $T_{1\rho}^{H}$ measurements of pure PVP, figure 6.4, and that of the PVP/carbamazepine co-melt, figure 6.21, shows that the relaxation of this co-melt is not dominated by the relaxation behaviour of PVP.

2/ Conclusions

2.1/ Proton bandshape

It has been seen that all three co-melts seemed to go through a transition between 65°C and 105°C. The change in mobility observed seemed to be due to the PVP/drug co-melt going through its Tg.

2.2/ T_1^{H} and $T_{1\rho}^{H}$ measurements

It was seen, from the T_1^{H} and $T_{1\rho}^{H}$ experiments on the three co-melts, that the amorphisation process seemed to increase the mobility of the samples compared to that for the crystalline samples. These experiments also showed that the presence of PVP seemed to slightly increase the mobility of the co-melt compared to that of the amorphous drug.

The T_1^H and $T_{1\rho}^H$ measurements of the three co-melts did not seem to be dominated by the relaxation of pure PVP. A similar result, i.e. no evidence of an interaction for a drug/polymer physical mixture, was also observed by Di Martino et al.[4] in their study of a physical mixture of PVP and ketoprofen.

When looking at the T_1^H experiments, it was observed that the three co-melts behaved similarly in the fact that they all went through a maximum in T_1^H at around 85°C. Nevertheless, in the case of the nifedipine and carbamazepine co-melts this maximum seemed to be a recovery from a broad minimum at about -30°C, whilst for PVP/indomethacin this minimum was around or below -70°C. The main point from the T_1^H study was that the maximum observed was at a higher temperature for the co-melts than for the amorphous drugs, probably showing a greater stability of the former.

The results obtained from the $T_{1\rho}^H$ experiments showed that all three compounds went through a change in slope. This change happened around the same temperature for all three co-melts, and also at a higher temperature than the change in slope observed for their respective amorphous drugs. This seemed to indicate, as with the T_1^H study, that the co-melts were more stable than their respective amorphous drugs.

3/ References

1. S. Zheng, Q. Guo, and Y. Mi. Characterisation of blends of poly(vinyl chloride) and poly(N-vinyl pyrrolidone) by FTIR and ^{13}C CP/MAS NMR spectroscopy. *J. Polym. Sci. Part B* **37**: 2412-2419 (1999).

2. D. C. Apperley. GlaxoWellcome - Amorphous drug project, Unpublished.

3. L. S. Taylor and G. Zografi. Spectroscopic characterisation of interactions between PVP and indomethacin in amorphous molecular dispersions. *Pharm. Res.* **14**: 1691-1698 (1997).

4. P. Di Martino, E. Joiris, R. Gobetto, A. Masic, G. F. Palmieri, and S. Martelli. Ketoprofen-poly(vinylpyrrolidone) physical interaction. *J. Cryst. Growth* **265**: 302-308 (2004).

Chapter Seven: Conclusions

1/ Crystalline material

The ^{1}H and ^{13}C solution-state NMR spectra of indomethacin, nifedipine and carbamazepine have been fully interpreted and this interpretation was in general agreement with the literature, except that, in the case of indomethacin, the assignments for C-2 and C-4 have been exchanged, and also gave a more detailed understanding for the aromatic region of carbamazepine.

The crystalline forms of the studied molecules were confirmed to be of the γ-form, modification I and modification III for indomethacin, nifedipine and carbamazepine respectively.

The T_1^H measurements showed that indomethacin and nifedipine had different motional processes and confirmed a lack of conformational flexibility for carbamazepine. The $T_{1\rho}^H$ measurements showed that for indomethacin some internal motion was in place over the studied range of temperatures, i.e. -70°C to 80°C. In the case of nifedipine and carbamazepine it was not possible to obtain the $T_{1\rho}^H$ values as they were too long to be measured without damage to the probe.

The ^{13}C SSNMR spectrum of indomethacin was slightly complicated by the quadrupolar effect caused by the chlorine atom present in the molecule and, from the investigation done on the effect, the following parameters were retrieved:

- The true ^{13}C chemical shift of C-14 is 139 ppm ± 0.2 ppm.
- J_{iso} = ca. –43 Hz, which should be taken as a maximum magnitude.
- χ = –63 MHz, if ΔJ is considered negligible.

It was also shown that it was safe to assume that χ is negative.

2/ Amorphous material

2.1/ Primary studies

The three studied compounds could easily be made amorphous by a simple quench-cooling process. It was observed that amorphous indomethacin was somewhat more stable than amorphous nifedipine and carbamazepine, as the former did not show

signs of recrystallisation up to a temperature of 80°C, whilst the other two compounds seem to recrystallise from a temperature of 65°C. However, some reversible process happened for indomethacin at 90°C. This process seemed to be related to an increased molecular mobility. All these results were obtained on the timescales of both XRPD and ^{13}C SSNMR experiments, apart from the reversible phenomenon at 90°C where only ^{13}C SSNMR was used.

2.2/ ^{1}H SSNMR

It was observed, using the proton bandshapes, that indomethacin started to recrystallise above 100°C, whilst for nifedipine this started around 70°C and around 75°C for carbamazepine.

The T_1^H experiments showed that the amorphisation process seemed to increase the mobility of the sample. It was also noticed that this increase in mobility was larger for carbamazepine and nifedipine than for indomethacin, and that this probably caused the lower stability for the two former samples. The similarity in the T_1^H plots for indomethacin and carbamazepine, as well as the previous conclusion, seemed to show that comparison between the crystalline and amorphous materials should also be taken into account when trying to understand the stability of a given sample. The $T_{1\rho}^H$ experiments confirmed the more mobile character of the amorphous forms compared to their crystalline counterparts. It was also seen that nifedipine and carbamazepine seemed more prone to recrystallisation than indomethacin, confirming the observations made with the T_1^H experiments.

3/ PVP/drug co-melts

The ^{13}C SSNMR spectra of the crystalline and amorphous forms and of the solidified co-melts were compared. This showed that the method used to prepare the co-melts gave amorphous samples.

The proton bandshape study showed that all three co-melts went through a transition between 65°C and 85°C, which was probably due to the Tg of the mixture.

The T_1^H and $T_{1\rho}^H$ experiments further confirmed the fact that amorphisation increased the mobility of a sample. It was also noticed from these experiments that the presence of PVP seemed to slightly increase the mobility of the co-melt

compared to the amorphous drug, and that the relaxation of PVP was not dominating the relaxation of the co-melts. Both relaxation experiments showed that the co-melts were more stable than the amorphous samples as the temperature at which noticeable change occurred was higher for the former.

4/ Future work

It would be interesting to develop a database of compounds establishing the way their mobility is influenced by their form: crystalline, amorphous or co-melt. It would also be interesting to look at the effect on the mobility of amorphous materials depending on the method used to prepare them. This would obviously have limits, depending upon how easy it would be to make a given compound amorphous using a specific method. One could also look at the effect of the polymer used in the co-melts, as well as different ways to prepare the drug/polymer mixtures.

This database should help deriving general principles which could be of great interest for pharmaceutical companies because, as stated in the introduction, amorphous compounds are generally more bioavailable than their crystalline counterparts.

Appendices

Appendix 1: Temperature calibration of the static probe

During the experiments (on the CMX200), the VT and purge gases were at 90 SCFH with nitrogen, and 110 SCFH with air. It is good to note that the purge gas has a very limited effect on the temperature as only the VT gas goes into the sample chamber. Therefore, it can be considered that the purge gas is having no effect on the temperature, and its value could be changed if needed.

The temperature measurements were done using a sample of methanol put in a glass holder of 10 mm outer diameter. The spectra were acquired on a static sample. The actual temperature was calculated using the difference in peak positions ($|\Delta\delta|$) for each spectrum, using the following relation [1]:

$$T = 403K - (29.46K.ppm^{-1}) * |\Delta\delta| - (23.83K.ppm^{-2}) * |\Delta\delta|^2$$

The plot of readout temperature versus sample temperature, figure 1, confirms that the two temperatures are indistinguishable (within experimental error). This shows that the thermocouple used to measure the temperature is well calibrated over the temperature range examined. The standard deviation of the difference between the reading and "real" temperature is 0.96. This means that the readout temperature can be taken as the actual sample temperature ± 1.0°C when using this probe. The raw data are shown in table 1.

[1] Bielecki A., Burum D.P., *J. Magn. Reson. Ser. A*, 1995, **116**, p. 215

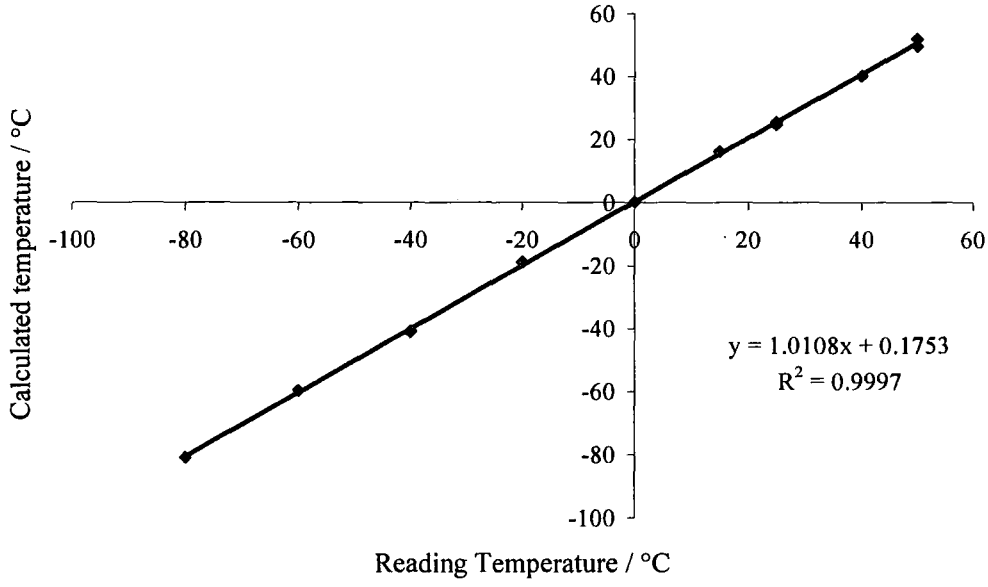

Figure 1: Reading versus calculated temperature plot of the VT calibration of the static probe, mounted with the 10 mm coil, on the CMX 200.

$\|\Delta\delta\|$ / ppm	Reading Temperature / °C	Calculated Temperature /°C
1.565	25	25.53
1.653	15	16.19
1.796	0	0.22
1.957	-20	-18.92
2.131	-40	-41.00
2.270	-60	-59.67
2.420	-80	-80.85
2.133	-40	-41.26
1.573	25	24.70
1.420	40	40.12
1.294	50	51.98
1.319	50	49.68

Table 1: Raw data for the VT calibration of the static probe, mounted with the 10 mm coil, on the CMX 200.

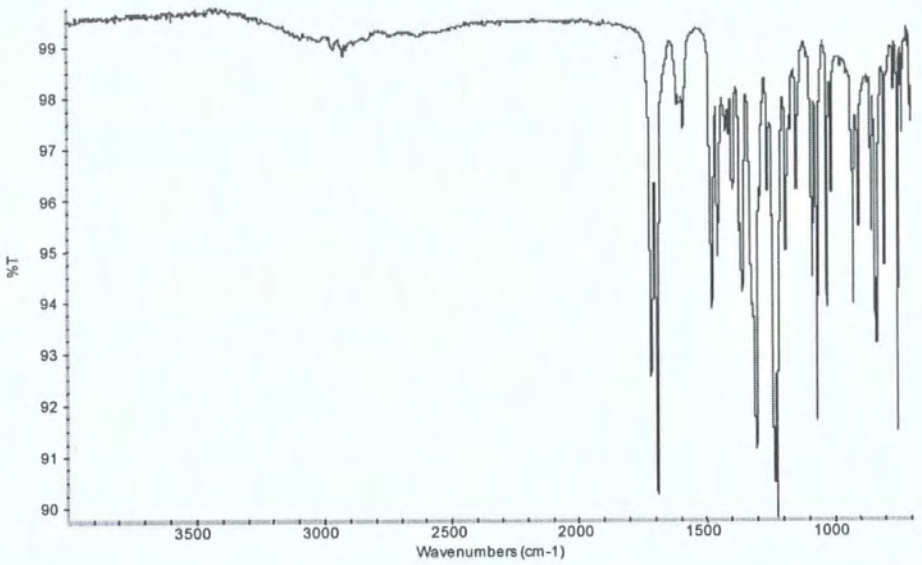

Appendix 2: FTIR of crystalline indomethacin.

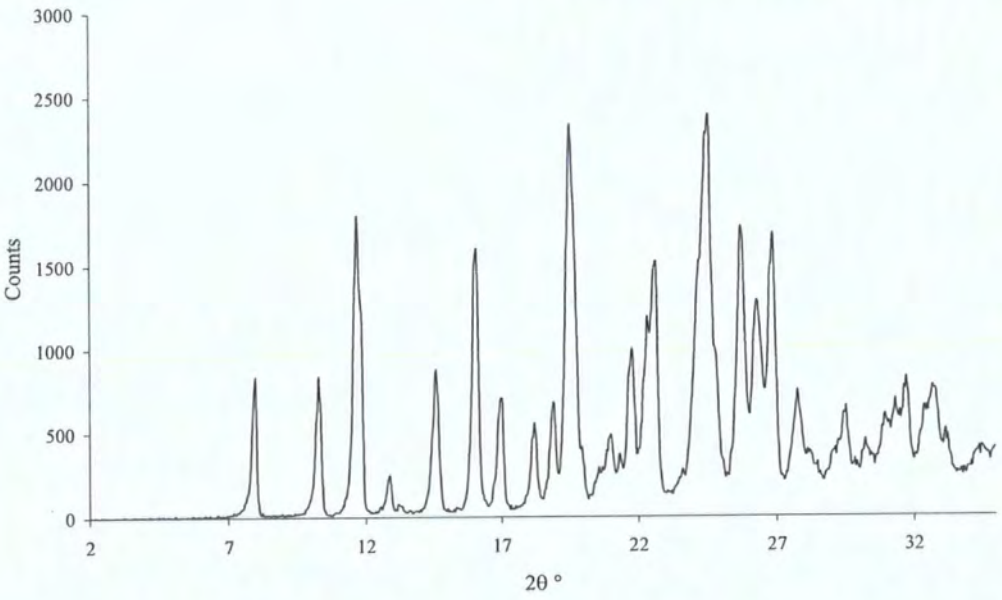

Appendix 3: XRPD of crystalline nifedipine.

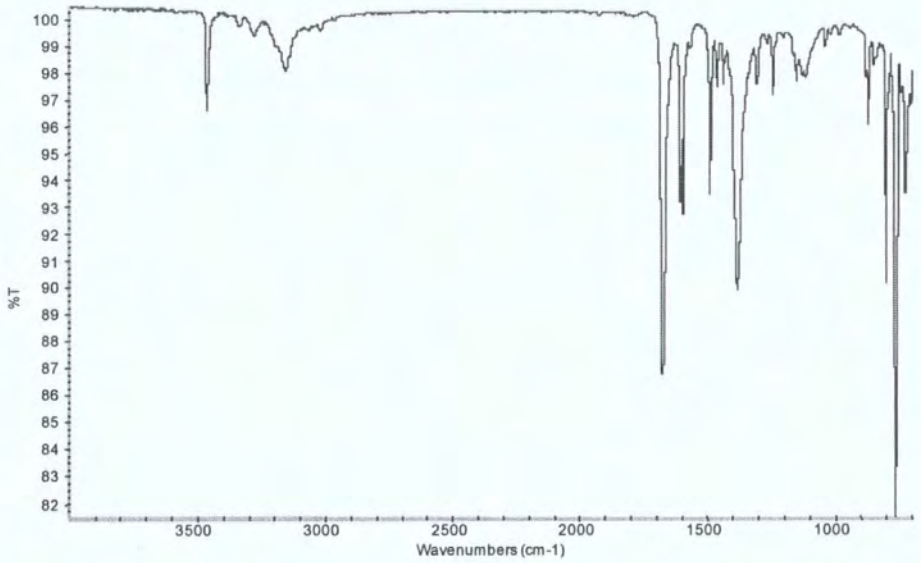

Appendix 4: FTIR of crystalline carbamazepine.

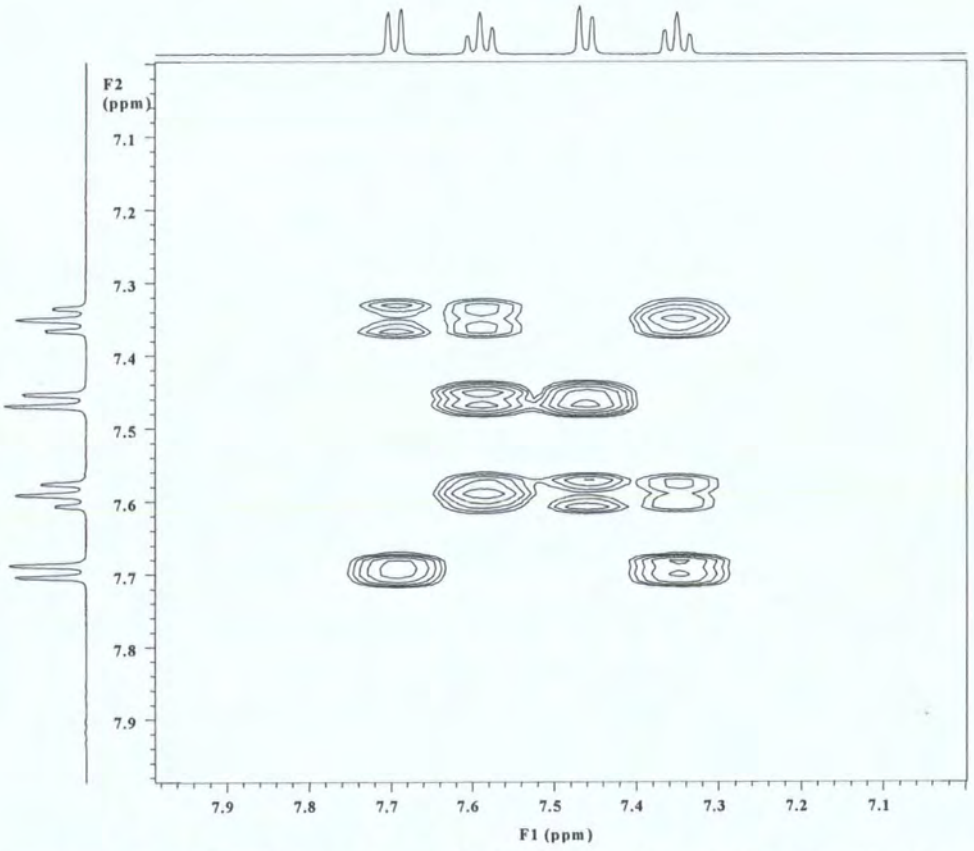

Appendix 5: COSY spectrum of nifedipine, in d_6-DMSO, showing the high-frequency part.

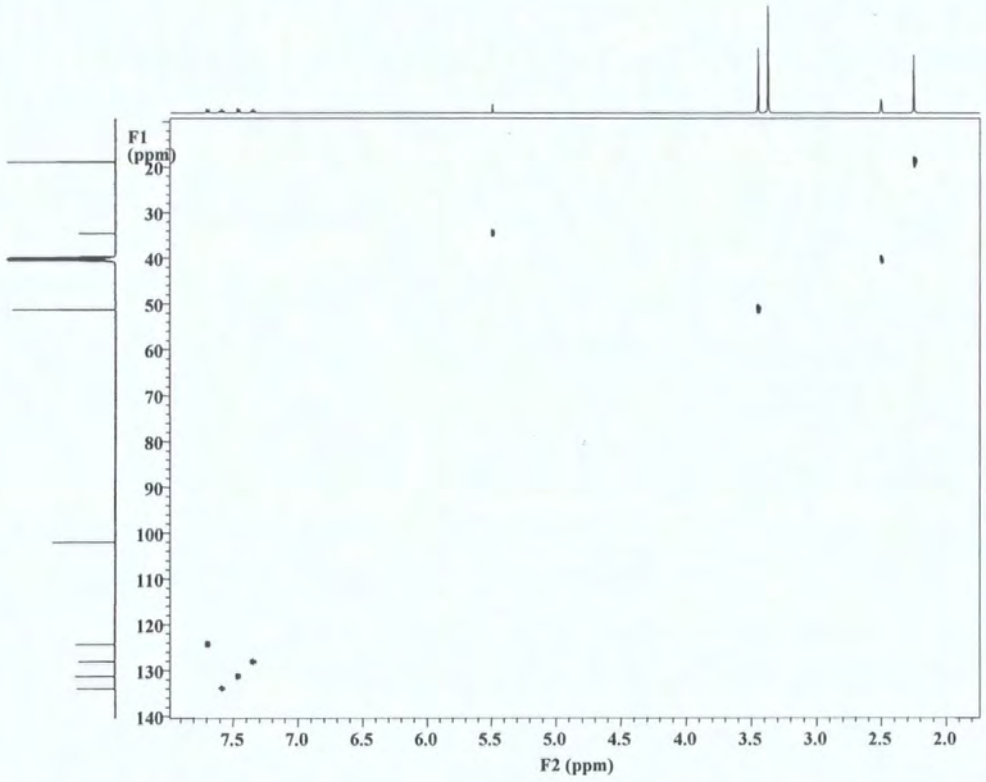

Appendix 6: HSQC spectrum of nifedipine, in d_6-DMSO.

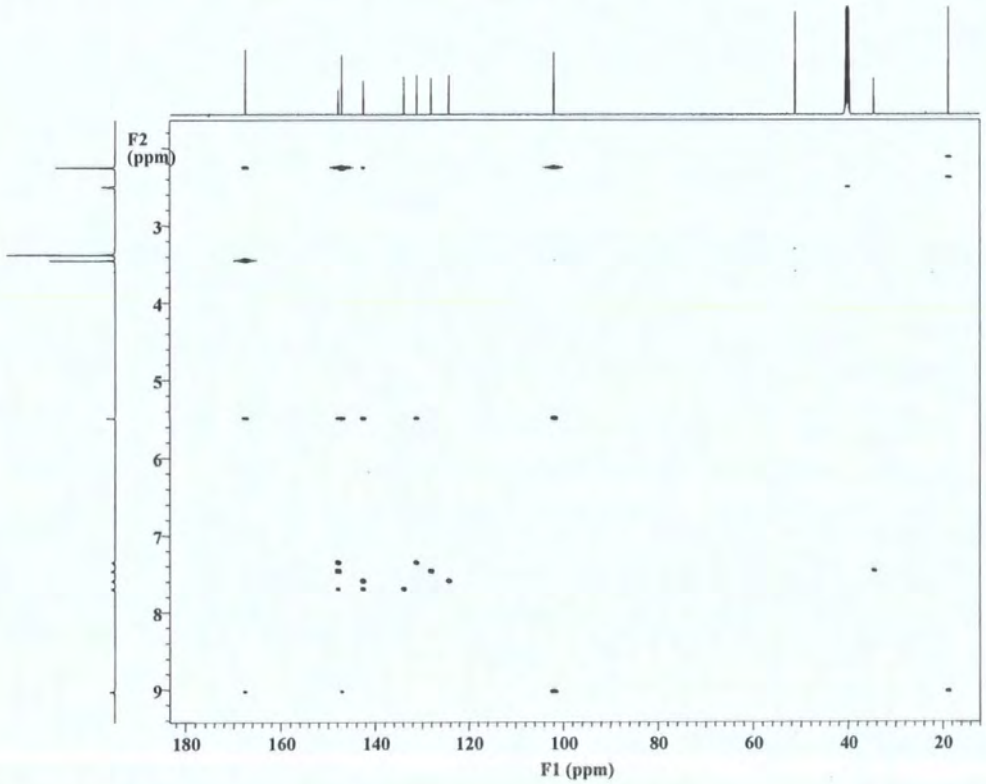

Appendix 7: HMBC spectrum of nifedipine, in d_6-DMSO.

^{1}H database			^{1}H experimental	
Atom number	Chemical shift / ppm	Number of matches	Atom number	Chemical shift / ppm
2', 6'	2.25	13	2', 6'	2.25
3", 5"	3.63	15	3", 5"	3.45
4	4.98	85	4	5.49
9	7.34	13958	10	7.35
8	7.53	45102	8	7.46
10	7.62	6	9	7.59
11	8.04	11	11	7.70
NH	8.53	13	NH	9.03

^{13}C database			^{13}C experimental	
Atom number	Chemical shift / ppm	Number of matches	Atom number	Chemical shift / ppm
2', 6'	19.4	2	2', 6'	18.9
4	34.9	16	4	34.6
3", 5"	50.8	1	3", 5"	51.3
3, 5	104.4	2	3, 5	102.0
11	123.5	88	11	124.3
8	126.7	1009	10	128.1
9	127.2	213	8	131.3
10	129.5	51	9	133.9
7	137.9	2	7	142.7
2, 6	143.9	2	2, 6	147.2
12	148.8	2	12	147.9
3', 5'	168.1	1	3', 5'	167.6

Appendix 8: Comparison between the experimental results and the database predictions for the assignment of ^{1}H and ^{13}C in the case of nifedipine.

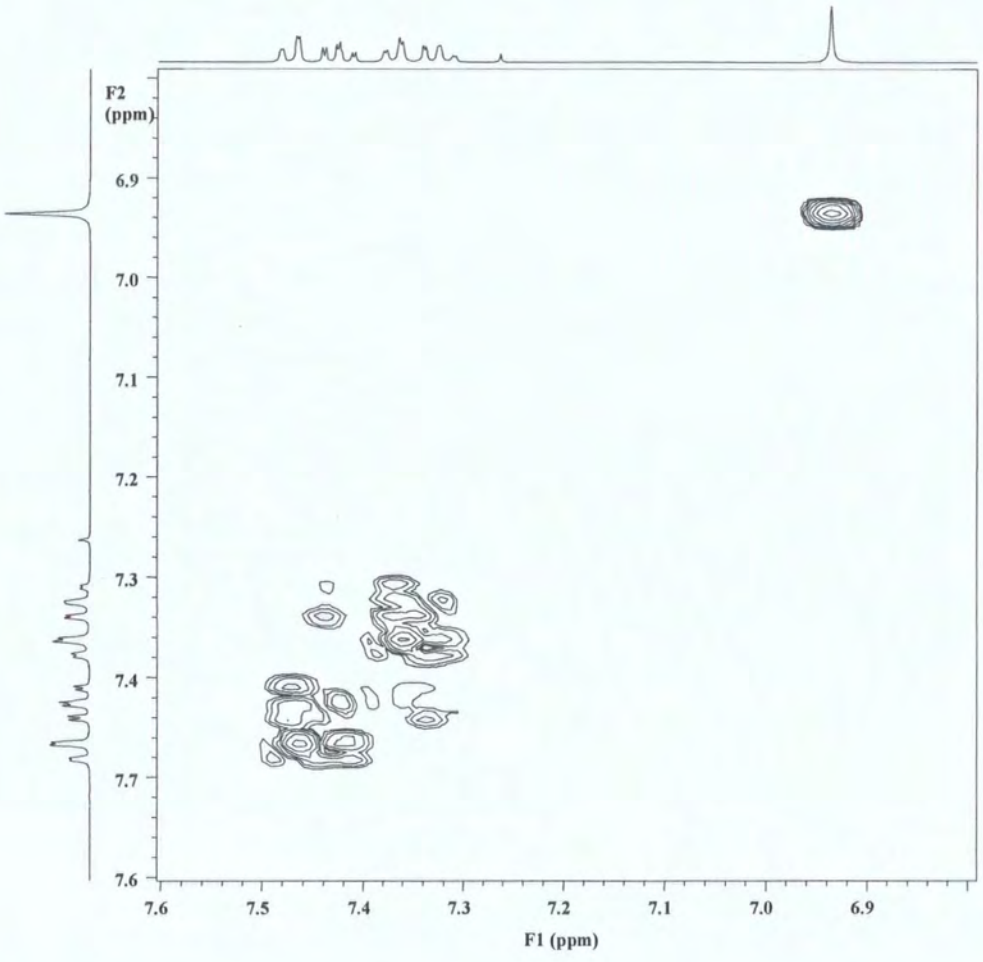

Appendix 9: COSY spectrum of carbamazepine, in $CDCl_3$, showing the high-frequency part.

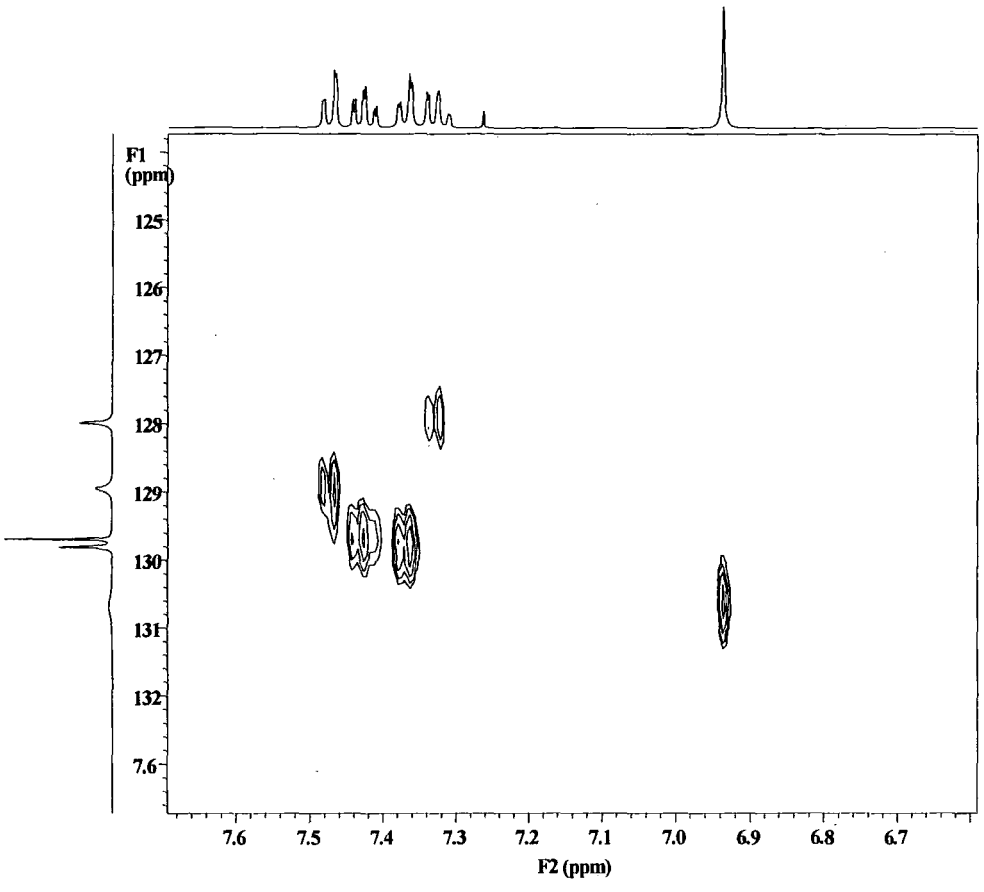

Appendix 10: HSQC spectrum of carbamazepine, in $CDCl_3$, showing the high-frequency part.

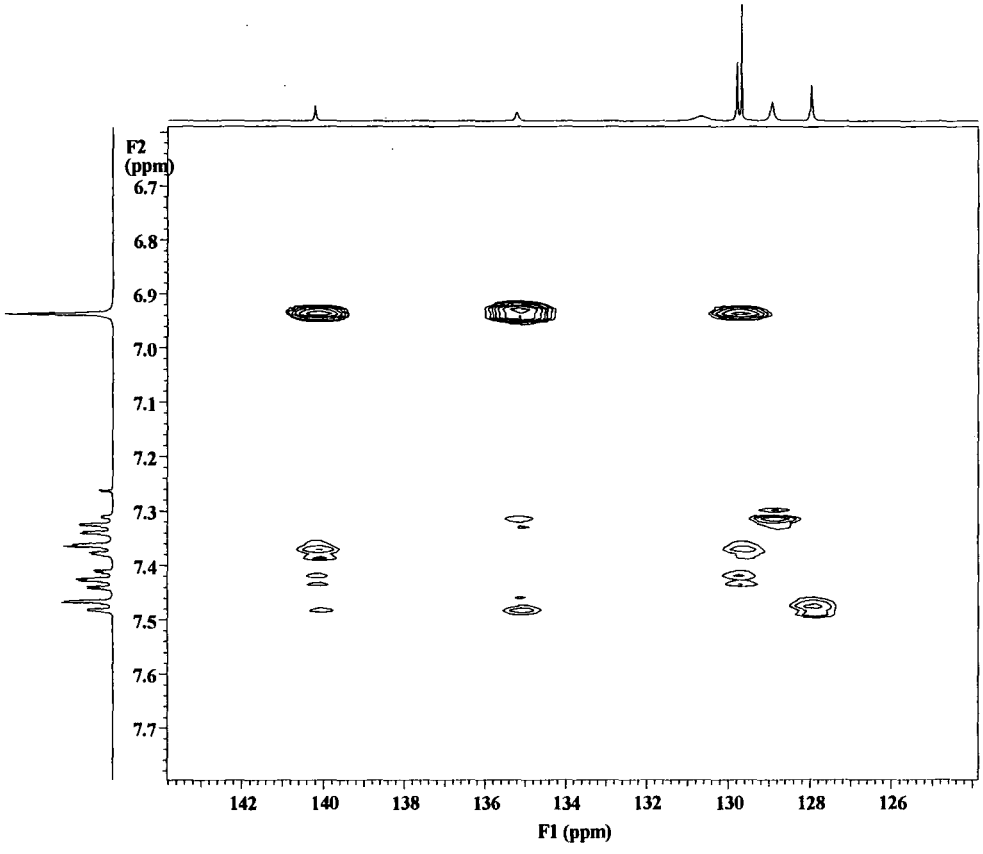

Appendix 11: HMBC spectrum of carbamazepine, in $CDCl_3$, showing the high-frequency part.

^{1}H database			^{1}H experimental	
Atom number	Chemical shift / ppm	Number of hits	Atom number	Chemical shift / ppm
NH2	5.48	1	NH2	4.82
4, 11	6.82	23	7, 8	6.94
5, 10	7.17	23	4, 11	7.33
3, 12	7.23	106	5, 10	7.37
7, 8	7.29	220	3, 12	7.43
2, 13	7.30	117	2, 13	7.47

^{13}C database			^{13}C experimental	
Atom number	Chemical shift / ppm	Number of hits	Atom number	Chemical shift / ppm
2, 13	118.4	1	4, 11	128.0
4, 11	128.2	6	2, 13	129.0
7, 8	129.2	6	3, 12	129.7
5, 10	130.5	6	5, 10	129.8
3, 12	130.8	1	7, 8	130.7
6, 9	137.1	6	6, 9	135.2
1, 14	139.3	1	1, 14	140.2
15	159.2	7	15	157.5

Appendix 12: Comparison between the experimental results and the database predictions for the assignment of ^{1}H and ^{13}C in the case of carbamazepine.

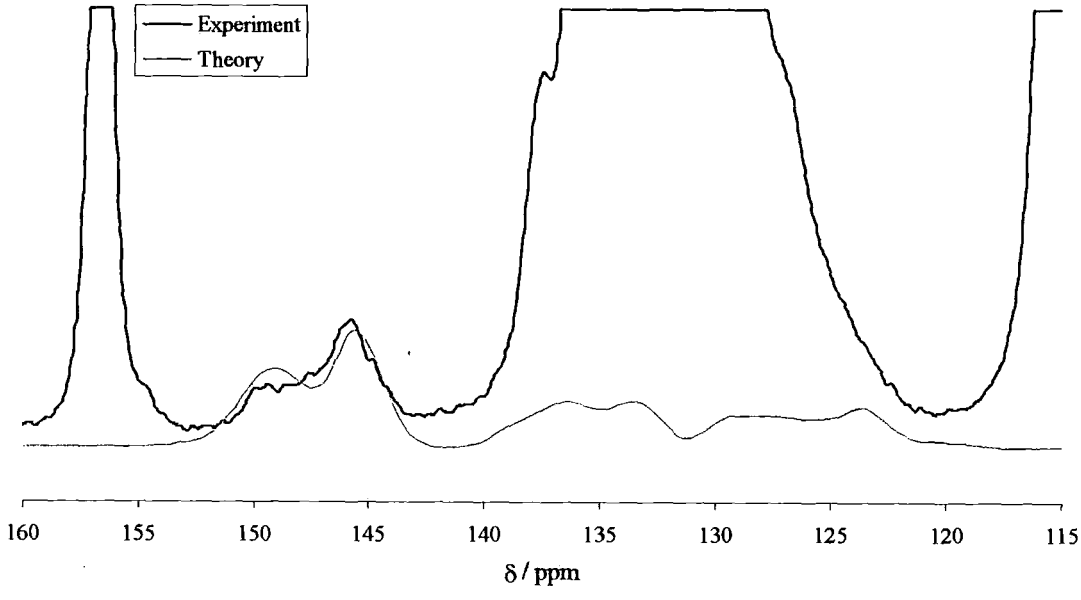

Appendix 13: Theory versus experimental for indomethacin, at 50.32 MHz, ^{13}C frequency, of C-14, J = –43 Hz and χ = –63 MHz.

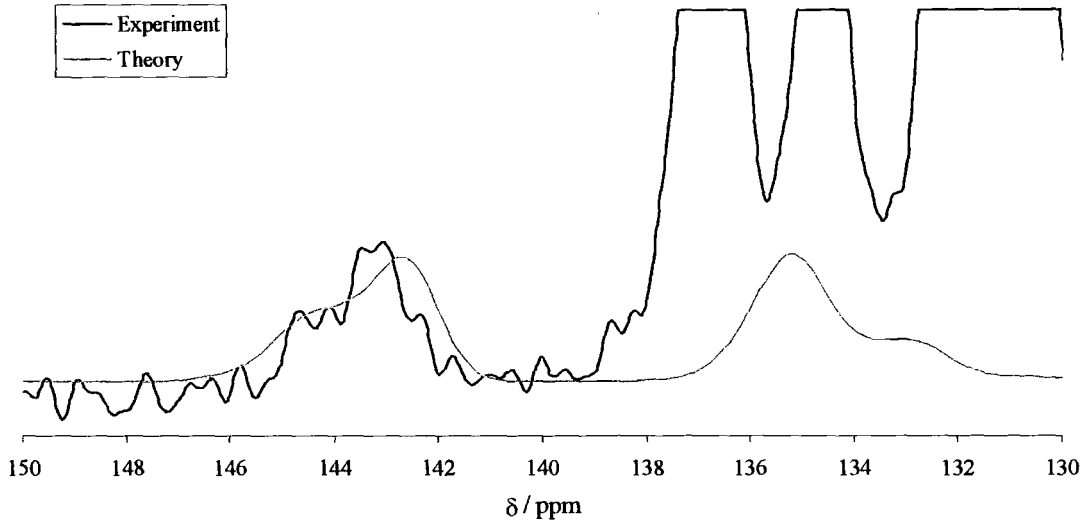

Appendix 14: Theory versus experimental for indomethacin, at 75.43 MHz, ^{13}C frequency, of C-14, J = –43 Hz and χ = –63 MHz.

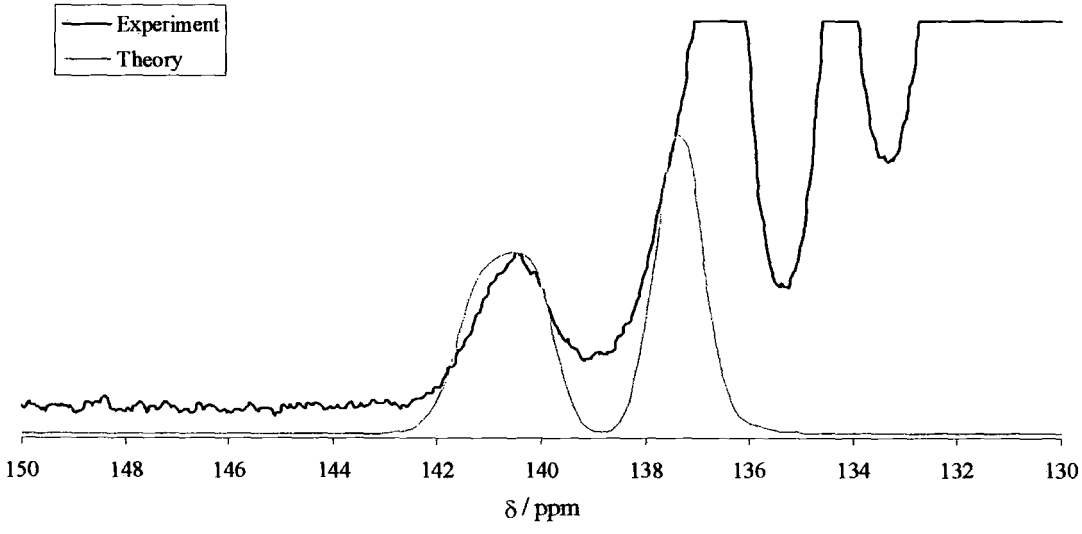

Appendix 15: Theory versus experimental for indomethacin, at 125.68 MHz, ^{13}C frequency, of C-14, J = –43 Hz and χ = –63 MHz.

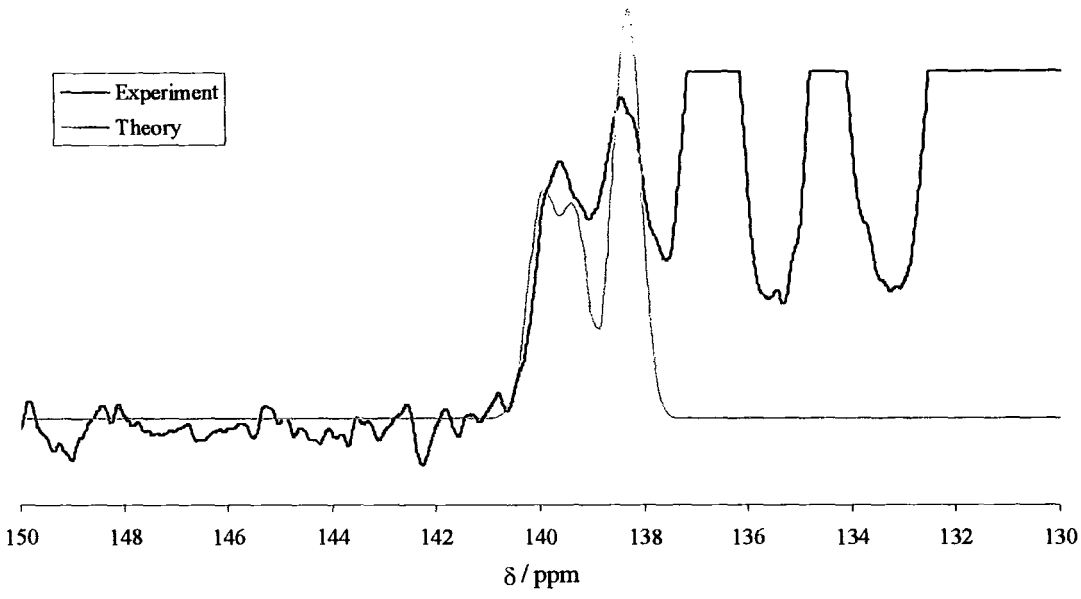

Appendix 16: Theory versus experimental for indomethacin, at 201.12 MHz, ^{13}C frequency, of C-14, J = –43 Hz and χ = –63 MHz.

Temperature / °C	T_1^H / s	$T_{1\rho}^H$ / ms
-70	0.7	850.0
-50	1.1	924
-30	1.9	323
-10	2.9	65.2
10	4.7	22
25	5.8	20.8
30	6.7	24.5
40	8.1	39.2
50	9	60.8
60	11.5	97.4
80	12.5	214.6

Appendix 17: T_1^H and $T_{1\rho}^H$ raw data obtained as a function of temperature for crystalline indomethacin.

Temperature / °C	T_1^H / s
-70	12.7
-50	15.3
-30	18.0
-10	20.9
10	24.9
25	26.0
30	26.7
40	26.9
50	27.9
60	29.1
70	29.6
80	29.1
100	30.2

Appendix 18: T_1^H and $T_{1\rho}^H$ raw data obtained as a function of temperature for crystalline nifedipine. At each temperature $T_{1\rho}^H$ was too long to be measured.

Temperature / °C	T_1^H / s	$T_{1\rho}^H$ / ms
-70	404.6	Too long
-40	331.3	Too long
-10	340.5	Too long
10	438.7	Too long
25	348.1	Too long
40	311.6	Too long
55	355.7	Too long
75	407.4	726.7
95	412.8	173.6

Appendix 19: T_1^H and $T_{1\rho}^H$ raw data obtained as a function of temperature for crystalline carbamazepine.

300 MHz		
Temperature / °C	T_1^H / s	$T_{1\rho}^H$ / ms
-70	1.6	64
-50	2.1	57
-30	3.0	52
-10	4.3	46
10	6.2	42
22	7.8	41
30	8.6	40
40	9.3	37
50	7.9	24
60	7.9	8.8
80	6.1	1.2

200 MHz		
Temperature / °C	T_1^H / s	$T_{1\rho}^H$ / ms
-70	0.9	86.2
-50	1.0	69.7
-30	1.1	56.9
-10	1.5	46.3
10	2.1	39.1
22	2.6	36.1
30	2.8	34.1
40	2.9	28.5
50	2.8	19.6
60	2.6	8.9
80	1.3	3.0

300 MHz		
Temperature / °C	T_1^H / s	$T_{1\rho}^H$ / ms
-70	1.59	72.1
-60	1.77	70
-50	2.09	66.9
-40	2.47	62.7
-30	3.01	58.3
-20	3.66	54.2
-10	4.52	50.2
0	5.48	47.8
10	6.53	45.5
20	7.59	44.6
30	8.81	43.7
40	9.24	37
45	8.26	29.8
50	7.9	22.3
60	7.93	7.5
70	7.44	1.9
75	7.07	1.3
80	6.45	1.2
90	5.23	1.6
100	3.48	3.2

200 MHz		
Temperature / °C	T_1^H / s	$T_{1\rho}^H$ / ms
-70	0.5	121
-50	0.8	91.2
-30	1.1	76.3
0	2	57.6
20	3.1	51.2
30	3.7	51.1
40	3.6	37.1
50	3.2	23.6
60	3.3	9.8
80	2.3	1.2
90	1.6	1.1
100	1.2	2.9

Appendix 20: T_1^H and $T_{1\rho}^H$ raw data obtained as a function of temperature for amorphous indomethacin. The colours are the same as for the plots.

300 MHz	
Temperature / °C	T_1^H / s
-70	8.79
-50	10.8
-30	12.3
-10	13.7
10	16.4
20	18.7
30	20.2
40	21.7
50	19.2
60	17.1
70	14.1

200 MHz	
Temperature / °C	T_1^H / s
-70	4.3
-50	5.7
-30	6.7
-10	7.7
15	8.8
25	10.1
30	10.6
40	10.6
50	9.5
60	8.4

300 MHz	
Temperature / °C	T_1^H / s
-60	10.5
-20	17.8
0	20.9
20	24.4
30	26.2
40	25.2
60	17.7

Appendix 21: T_1^H raw data obtained as a function of temperature for amorphous nifedipine. The colours are the same as for the plots.

300 MHz	
Temperature / °C	$T_{1\rho}^{H}$ / ms
-60	161
-40	148
-20	142
0	135
10	139
20	145
30	129
40	98
50	39
60	9.0
65	4.1

200 MHz	
Temperature / °C	$T_{1\rho}^{H}$ / ms
-70	136.8
-50	116.8
-30	114.3
-10	92.9
10	97.2
22	79.1
30	76.0
40	54.9
50	28.9
60	9.8

300 MHz	
Temperature / °C	$T_{1\rho}^{H}$ / ms
-60	138
-20	130
0	123
20	126
30	124

200 MHz	
Temperature / °C	$T_{1\rho}^{H}$ / ms
-70	359.5
-40	223.3
-10	216.8
20	148.1
30	101.2
40	73.6
50	35.7
60	10.8

Appendix 22: $T_{1\rho}^{H}$ raw data obtained as a function of temperature for amorphous nifedipine. The colours are the same as for the plots.

200 MHz		
Temperature / °C	T_1^H / s	$T_{1\rho}^H$ / ms
-70	7.6	951.3
-30	5.6	286.9
10	6.7	88.6
25	6.6	60.0
35	6.9	45.9
45	7.3	29.8
55	7.4	16.7
65	6.7	7.9
75	5.9	3.3
85	4.9	2.9
105	-	5.6

200 MHz		
Temperature / °C	T_1^H / s	$T_{1\rho}^H$ / ms
-70	9.4	754.3
-30	7.0	292.3
10	7.5	91.0
25	7.5	56.4
35	7.9	42.5
45	8.3	28.5
55	8.3	16.4
65	7.9	7.7
75	7.1	3.0
85	5.3	3.6
105	-	7.2

Appendix 23: T_1^H and $T_{1\rho}^H$ raw data obtained as a function of temperature for amorphous carbamazepine. The colours are the same as for the plots.

Temperature / °C	T_1^H / s	$T_{1\rho}^H$ / ms
-20	5.7	6.2
-10	5.1	6.5
0	4.4	7.3
10	3.9	9.6
20	3.5	11.2
30	2.1	14.3
40	2.1	14.1
50	2.1	20.6
60	2.4	19.9
70	2.7	21.8
80	3.2	22
90	3.8	21.8
100	4.2	18.7
110	5.0	15.4
120	5.6	13.8
130	6.2	11.7
140	7.0	10.3

Appendix 24: T_1^H and $T_{1\rho}^H$ raw data obtained as a function of temperature for PVP on its own[2].

[2] D. C. Apperley. GlaxoWellcome - Amorphous drug project, Unpublished.

300 MHz		
Temperature / °C	T_1^H / s	$T_{1\rho}^H$ / ms
-20	3.2	21.1
-10	3.2	18.8
0	3.4	17.5
10	3.6	15.8
20	3.9	16.0
30	3.5	15.9
40	3.6	16.0
50	3.8	16.2
60	4.2	15.5
70	5.2	16.1
80	6.6	14.5
90	6.8	10.2
100	6.9	6.1
110	7.4	2.6
120	7.3	1.5
130	6.4	1.2
140	5.3	-

200 MHz		
Temperature / °C	T_1^H / s	$T_{1\rho}^H$ / ms
-70	1.8	107.3
-40	2.3	80.6
-10	3.0	59.1
15	4.1	47.7
40	5.0	40.9
65	6.0	38.3
85	6.1	25.1
100	5.9	12.6
110	5.4	4.7
120	5.1	2.2
140	4.0	0.9

200 MHz		
Temperature / °C	T_1^H / s	$T_{1\rho}^H$ / ms
-70	1.8	97.6
-30	2.4	63.4
10	3.5	41.5
40	4.4	35.8
65	5.6	34.3
85	6.0	24.8
100	5.8	13.0
110	5.4	6.8
120	5.3	2.5
140	3.7	0.9

Appendix 25: T_1^H and $T_{1\rho}^H$ raw data obtained as a function of temperature for the PVP/indomethacin co-melt. The colours are the same as for the plots.

300 MHz		
Temperature / °C	T_1^H / s	$T_{1\rho}^H$ / ms
-20	4.0	29.9
-10	3.9	27.1
0	4.0	25.9
10	4.0	25.9
20	4.4	26.5
30	3.8	27.9
40	3.7	30.4
50	4.0	31.9
60	4.5	26.6
70	4.8	19.9
80	4.9	13.1
90	4.6	6.9
100	4.9	4.3
110	5.3	2.8
120	5.9	2.1
130	5.4	2.2
140	4.2	3.2

200 MHz		
Temperature / °C	T_1^H / s	$T_{1\rho}^H$ / ms
-70	3.3	96.0
-40	3.0	82.9
0	3.5	71.8
40	4.4	62.0
65	5.4	51.3
85	5.8	30.3
100	5.5	10.2
110	5.2	5.7
120	4.9	2.8
140	3.7	1.0

200 MHz		
Temperature / °C	T_1^H / s	$T_{1\rho}^H$ / ms
-70	3.1	93.5
-30	2.9	75.7
10	3.7	62.6
40	4.2	56.3
65	5.4	47.2
85	5.6	27.3
100	5.1	9.1
110	4.7	3.5
120	4.4	1.9
140	3.1	1.0

Appendix 26: T_1^H and $T_{1\rho}^H$ raw data obtained as a function of temperature for the PVP/nifedipine co-melt. The colours are the same as for the plots.

200 MHz		
Temperature / °C	T_1^H / s	$T_{1\rho}^H$ / ms
-70	6.2	248.3
-30	4.9	134.7
10	5.3	59.4
40	6.2	31.5
65	9.0	20.6
85	10.3	12.2
100	9.3	7.6
110	7.8	5.1
120	6.4	2.3
140	3.9	1.1

200 MHz		
Temperature / °C	T_1^H / s	$T_{1\rho}^H$ / ms
-70	5.8	121.6
-30	4.8	69.5
10	5.2	33.2
40	5.7	23.4
65	7.6	17.9
85	7.8	11.2
100	7.3	5.0
110	6.4	2.8
120	5.7	1.7
140	3.6	0.9

Appendix 27: T_1^H and $T_{1\rho}^H$ raw data obtained as a function of temperature for the PVP/carbamazepine co-melt. The colours are the same as for the plots.

Appendix 28: Glibenclamide

Three different samples of glibenclamide, figure 2, have been given, by James Patterson. One was a crystalline sample, whilst the other two were prepared in order to make them amorphous, i.e. by milling and by quench-cooling. It was needed to find out which method of amorphisation was the most efficient for this compound. The ^{13}C SSNMR spectra of each of the three samples was acquired and the result is shown in figure 3.

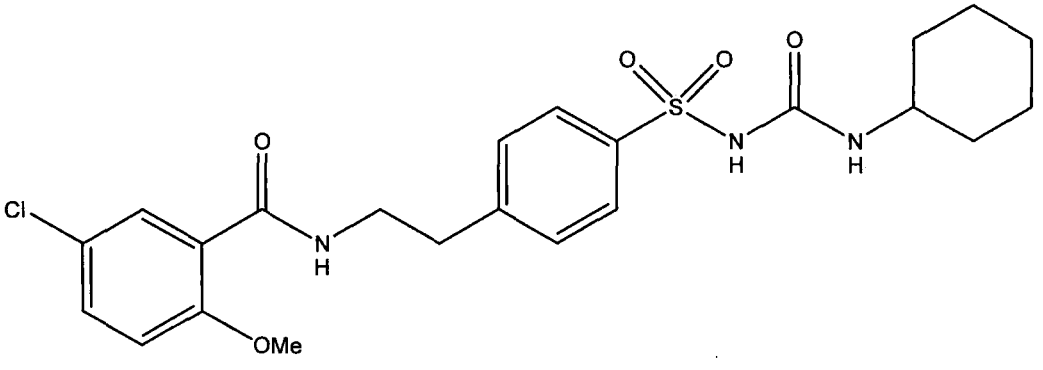

Figure 2: Glibenclamide.

It is clearly visible from figure 3 that both methods gave an amorphous compound. However, the milling technique seemed to give a sample that is not as amorphous as the quench-cooled technique. This showed that for this specific compound it would be better to use the quench-cooling technique in order to obtain an amorphous sample.

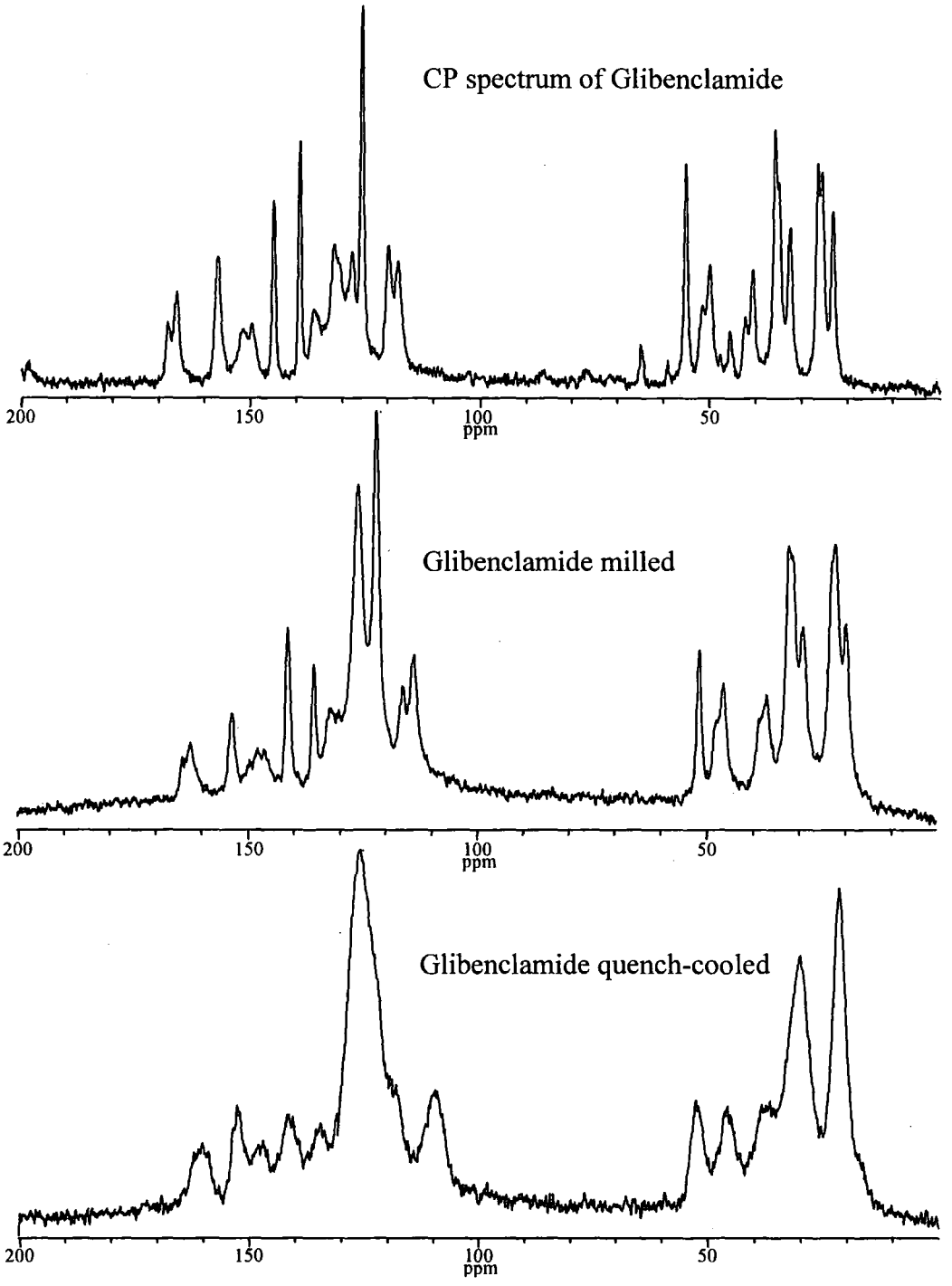

Figure 3: ^{13}C CPMAS of glibenclamide obtained at 50.32 MHz, ^{13}C frequency.

Appendix 29: Talks, posters and publication

Talks and posters:

4th July 2002:	Group meeting involving personnel form GSK and staff members form University of London School of Pharmacy.
September 2002:	Participant in the Anglo-French Meeting on Magnetic Resonance Spectroscopy conference in Southampton.
22nd September 2003:	Talk on my Ph.D. project at GSK, Stevenage. **Title:** The study of relaxation times of amorphous Indomethacin and Nifedipine using solid-state NMR.
23rd September 2003:	Group meeting involving personnel form GSK and staff members form University of London School of Pharmacy.
25th June 2004:	Final year departmental talk in the Chemistry department at Durham University. **Title:** The study of relaxation times of amorphous Indomethacin and Nifedipine using solid-state NMR.
14th July 2004:	Presentation of my Ph. D. project at GSK, Harlow. **Title:** The study of relaxation times of amorphous Indomethacin and Nifedipine using solid-state NMR.
September 2004:	Poster presentation at the Anglo-German Magnetic Resonance Spectroscopy conference in Aachen, Germany. **Poster title**: Probing the mobility of pharmaceutical systems using solid-state NMR relaxation times

Article published:

D. C. Apperley, A. H. Forster, R. Fournier, R. K. Harris, P. Hodgkinson, R. W. Lancaster and T. Rades. Characterisation of indomethacin and nifedipine using variable-temperature solid-state NMR. *Magn. Res. Chem.*. **43**: 881-892 (2005).